



UvA-DARE (Digital Academic Repository)

Neuroblastoma

Crossing borders in targeted therapy

Bate-Eya, L.T.

Publication date

2017

Document Version

Final published version

License

Other

[Link to publication](#)

Citation for published version (APA):

Bate-Eya, L. T. (2017). *Neuroblastoma: Crossing borders in targeted therapy*. [Thesis, fully internal, Universiteit van Amsterdam].

General rights

It is not permitted to download or to forward/distribute the text or part of it without the consent of the author(s) and/or copyright holder(s), other than for strictly personal, individual use, unless the work is under an open content license (like Creative Commons).

Disclaimer/Complaints regulations

If you believe that digital publication of certain material infringes any of your rights or (privacy) interests, please let the Library know, stating your reasons. In case of a legitimate complaint, the Library will make the material inaccessible and/or remove it from the website. Please Ask the Library: <https://uba.uva.nl/en/contact>, or a letter to: Library of the University of Amsterdam, Secretariat, Singel 425, 1012 WP Amsterdam, The Netherlands. You will be contacted as soon as possible.

BC12

organoids

NEUROBLASTOMA: CROSSING BORDERS IN TARGETED THERAPY

Laurel Tabé Bate-Eya

EH12

NEUROBLASTOMA: CROSSING BORDERS IN TARGETED THERAPY

Laurel Tabe Bate-Eya

ISBN: 978-94-6299-631-1
Cover design & layout: Design Your Thesis | designyourthesis.com
Printing: Ridderprint | ridderprint.nl

Copyright © 2017 Laurel Tabe Bate-Eya. No part of this dissertation may be reproduced or transmitted in any form or by any means without written permission from the author.

NEUROBLASTOMA: CROSSING BORDERS IN TARGETED THERAPY

ACADEMISCH PROEFSCHRIFT

ter verkrijging van de graad van doctor
aan de Universiteit van Amsterdam
op gezag van de Rector Magnificus
prof. dr. ir. K.I.J. Maex
ten overstaan van een door het College voor Promoties ingestelde commissie,
in het openbaar te verdedigen in de Agnietenkapel
op woensdag 06 September 2017, te 14:00 uur

door

Laurel Tabe Bate-Eya
geboren te Yaounde, Kameroen

PROMOTIECOMMISSIE:

Promotor(es):	Prof. dr. H.N.Caron	AMC-UvA
Copromotor(es):	Dr. J.J. Molenaar Dr. M.E.M. Dolman	AMC-UvA AMC-UvA
Overige leden:	Prof. dr. J.P. Medema Prof. dr. E.F. Eldering Prof. dr. Carel Van Noesel Prof. dr. Frank Speleman Prof. dr. Monique Den Boer Dr. Jason Shohet	AMC-UvA AMC-UvA AMC-UvA Ghent University Hospital, Belgium Erasmus University Rotterdam Texas Children's Cancer Center, USA

Faculteit der Geneeskunde

TABLE OF CONTENTS

Chapter 1.	Introduction	7
Chapter 2.	Newly-derived neuroblastoma cell lines propagated in serum-free media. recapitulate the genotype and phenotype of primary neuroblastoma tumors. <i>European Journal of Cancer, 2014.</i>	39
Chapter 3.	EZH2 plays an important role in neuroblastoma cell survival independent of its histone methyltransferase activity. <i>European Journal of Cancer, 2017.</i>	73
Chapter 4.	High efficacy of the BCL2 inhibitor venetoclax (ABT199) in neuroblastoma and rational for combination with MCL1 inhibition. <i>Oncotarget, 2016.</i>	99
Chapter 5.	High-throughput screening identifies idasanutlin as a re-sensitizing drug for venetoclax-resistant neuroblastoma cells. <i>Submitted.</i>	137
Chapter 6.	A systematic review on targeting BCL2 in pediatric solid tumors. Manuscript in preparation.	173
Chapter 7.	Discussion	199
Appendices.	English summary	217
	Nederlandse samenvatting	221
	Acknowledgements	225
	Curriculum Vitae	229
	Portfolio	231
	Publication List	233



CHAPTER 1

INTRODUCTION

INTRODUCTION

Cancer research involves the study of deregulated pathways and the use of a wide range of molecular biology techniques and tumor material in order to discover new therapeutic strategies. In this thesis, we describe the isolation and generation of new neuroblastoma cell lines from patient-derived tumor tissues and their future potential in neuroblastoma research. Additionally, we exploited the functional role of EZH2 in neuroblastoma and the therapeutic potential of the BCL2-specific inhibitor venetoclax (ABT199) including strategies to overcome resistance. The current introduction gives a synopsis of the pathology and genomic landscape of neuroblastoma, the currently used treatment protocol, fundamental model systems used in neuroblastoma research and deregulated pathways that can be utilized for the development of novel treatment strategies.

1. NEUROBLASTOMA PATHOLOGY

Neuroblastoma is a solid tumor that arises from the sympathoadrenal system of the adrenal gland during early neural crest formation (1) (**Figure 1**). Histologically, these tumors are composed of undifferentiated neuroectodermal cells or neuroblasts that appear as small round blue cells (2, 3). Advances in clinical and translational research reveal that neuroblastic tumors can be classified according to the differentiated state of the cells, with the ganglioneuroblastomas composed of more differentiated neuroblasts surrounded by Schwannian stroma and ganglioneuromas composed of Schwann cells with differentiated cells of ganglionic lineage (4). Neuroblastomas are the most aggressive neuroblastic tumors and can be classified into four stages: stage 1, 2 and 3 neuroblastomas presenting loco-regional tumors with or without lymph node involvement and stage 4 neuroblastomas present tumors with distant metastases. There is one additional subgroup of neuroblastoma tumors (4S), characterized by minimal dissemination to the skin and bone marrow and spontaneous regression (5, 6). Primary anatomical locations of neuroblastoma are in the adrenal medulla, organ of zuckerkind, and the sympathetic nervous system of the neck and mediastinum and retroperitoneum. The metastatic pattern of neuroblastoma usually involves the bone, bone marrow, lymph nodes and skin (7-10).

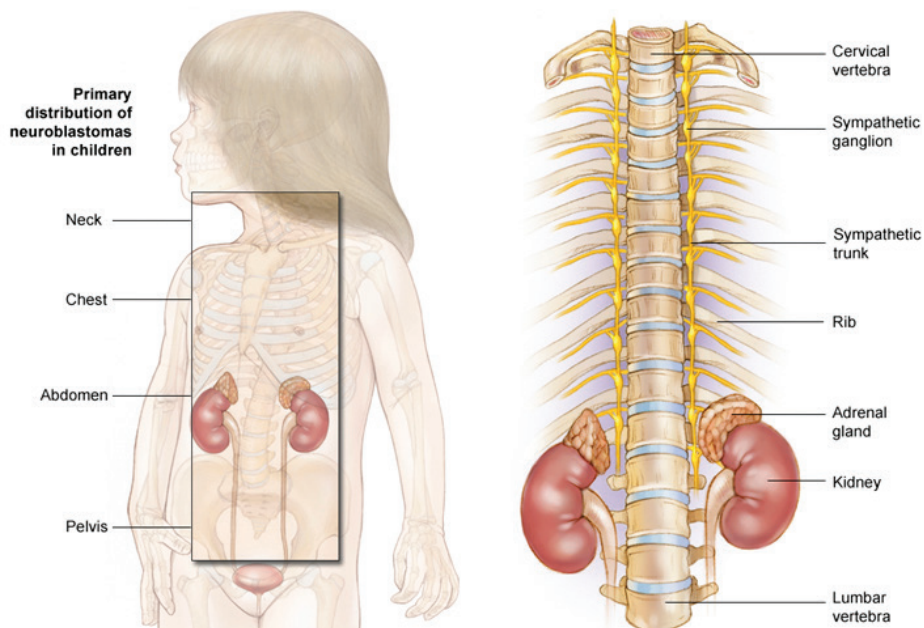


Figure 1: Anatomical representation of the sympatho-adrenal system and neuroblastoma metastatic sites by the American Society of Clinical Oncology.

1.1. The genomic landscape of neuroblastoma.

Several genomic aberrations have been identified in neuroblastoma, such as aberrations in the ploidy status (11). Near-triploidy presented with whole chromosome gains and losses is usually associated with a better prognosis and lower stage of the disease. Ploidy status in neuroblastoma is of prognostic significance in infants of less than 1 year while its prognostic relevance is lost in patients older than 1 year of age.

Partial chromosome gains and losses are frequently observed in neuroblastoma, of which 17q gain and 1p and 11q losses are the most notable. Gain of chromosome 17q occurs in more than 50% of all neuroblastoma tumors and is most frequently observed in high stage tumors. Unbalanced gain of 17q frequently occurs as a translocation between chromosome 1 and 17. Different breakpoint regions of chromosome 17q are observed but a preferential gain in the 17q22 arm results in a dosage effect of genes in this region such as *BIRC5* (survivin) and *PPM1D* (protein phosphatase 1D) (12).

Deletions in chromosomes 1p and 11q are also associated with a worse prognosis. Loss of 1p occurs in 30-35% of all neuroblastoma tumors and is thought to be a tumor-

promoting event because known tumor suppressor genes *CAMTA1*, *CHD5*, *KIF1B*, *CASZ1* and *miR-34a* are located on this region (13-16). In addition, 1p loss is often associated with amplification of the oncoprotein *MYCN*. Loss of 11q was predominantly observed in non-*MYCN* amplified neuroblastoma patients and was correlated to decreased survival in these group of patients (17).

Amplification of *MYCN* (located on chromosome 2) is one of the most notable genomic events in neuroblastoma. It is observed in 22% of all neuroblastoma patients and strongly correlates with a poor prognosis (18, 19). *MYC* oncoproteins (c-*MYC*, N-*MYC*, L-*MYC*, S and B-*MYC*) are basic helix-loop-helix leucine zipper (b-HLH-Zip) transcription factors (20). The DNA binding and transcription factor roles *MYCN* requires its dimerization with Max, a small b-HLH-Zip protein leading to the activation of genes involved in cellular processes such as cell cycle arrest, migration and apoptosis (21, 22).

Amplification of the *MDM2* proto-oncogene located on chromosome 12 has been described in 2% of neuroblastomas (23-25). *MDM2* is an E3 ubiquitin ligase responsible for the degradation of the master transcriptional regulator *TP53* (p53) by catalyzing its ubiquitylation and subsequent proteasomal degradation upon binding. p53 is a well-known tumor suppressor involved in cell cycle arrest, DNA repair and apoptosis (26-29).

Recently, chromothripsis has been identified in about 18% of the neuroblastoma tumors (30). Chromothripsis is a genomic event involving the local shredding and subsequent random reassembly of chromosomes, resulting in the loss of tumor suppressor genes and amplification of oncoproteins leading to tumor-promoting events (31, 32). The mechanisms causing chromothripsis are unknown, but advances in gene sequencing have demonstrated that these mechanisms might involve the segregation and reassembly of a single chromatid from a micronucleus (33, 34).

Somatic and single nucleotide mutations have been identified in a number of genes in neuroblastoma by whole genome and exome sequencing. The anaplastic leukemia kinase gene (*ALK*) has been identified as one of the driving oncogenes involved in familial neuroblastoma (35, 36). *ALK* is a protein tyrosine kinase receptor which through the phosphorylation activities of its kinase domain activates a variety of downstream signaling pathways involved in oncogenesis. In addition to activating somatic and germline mutations (F1174L and R1275Q), copy number gains of this gene have been observed in neuroblastoma (37, 38). Targeted inhibition of *ALK* with small molecule inhibitors crizotinib and alectinib has shown promise in a variety of

tumor types, including neuroblastoma (39-41). Somatic mutations have also been described for *PTPN11* (activating mutations in 2.9% of the neuroblastoma patients) and *ATRX* (inactivating mutations in 2.5% of the neuroblastoma patients) while germline mutations have been described in the *PHOX2B* gene (missense mutations and whole allele deletions) (30, 42).

1.2. Current treatment regimen and prognosis of neuroblastoma.

Treatment of neuroblastoma is based on the Dutch Childhood Oncology Group (DCOG) risk stratification scheme, using the INSS stage, MYCN status, tumor differentiation grade, chromosome 11q status and DNA ploidy to determine which treatment neuroblastoma patients will receive (**Figure 2**).

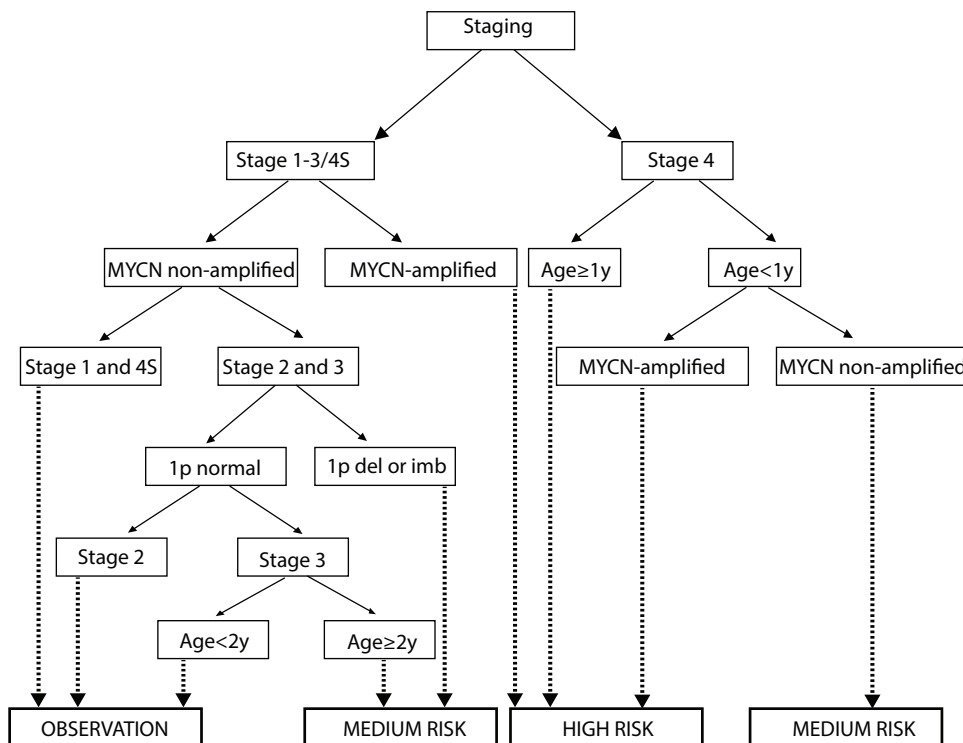


Figure 2. Risk stratification of neuroblastoma tumors according to the DCOG NBL 2009 trial.

Figure 3 shows the treatment regimen for high risk neuroblastoma patients. In the DCOG protocol, treatment of high risk neuroblastoma patients is started with 2 upfront courses of radiolabeled ^{131}I -MIBG. Radiolabeled MIBG is a neurotransmitter-like substance that can be used for treatment (^{131}I) or for diagnostic (^{123}I) purposes (43-45). Following MIBG treatment, high risk patients receive 6 cycles of N5 chemotherapy (cisplatin, vindesine and etoposide) and N6 chemotherapy (ifosfamide, vincristine, dacarbazine and doxorubicin). When necessary, tumor debulking is performed to minimize the amount of tumor left after treatment with N5/6 chemotherapy cycles. Next, myelosuppressive high dose chemotherapy (etoposide and melphalan) is given, followed by autologous stem cell transplantation and retinoic acid treatment is then carried out in 6 cycles with a short break and then 3 additional cycles. Medium risk patients receive similar treatment (i.e. without upfront ^{131}I -MIBG courses), while for the low risk patients a wait and see approach is applied.

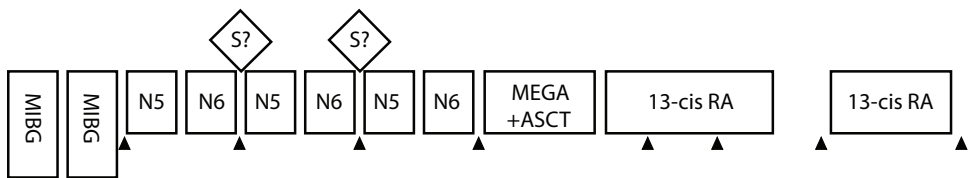


Figure 3: Overview of the DCOG NBL2009 treatment protocol of high risk neuroblastoma patients (S= surgery, N5/6= chemotherapy cycles, MIBG= MIBG treatment, MEGA+ASCT= myeloablative high dose chemotherapy with autologous stem cell transplantation, 13-cis-RA=13-cis-retinoic acid).

Despite of the intensive multimodality therapy, high risk neuroblastoma patients have an overall survival chance of only <50% (46). It is thus imperative to test new targeted therapies that might improve the survival rate patients diagnosed with high risk neuroblastoma. Pre-clinical evaluation of new therapies in adequate *in vitro* and *in vivo* model systems closely mimicking the clinical situation is essential to facilitate the eventually necessary pre-clinical to clinical translation.

2. *IN VITRO* AND *IN VIVO* SYSTEMS FOR NEUROBLASTOMA BIOLOGY.

Most tumor cells exist within a 3D microenvironment comprised of surrounding stromal and immune cell infiltrates. However, upon excision of tumor material, tumor-derived cells are frequently cultured and maintained in a 2D culture system. It has

been shown in neuroblastoma and other solid tumors that cell lines cultured under 2D conditions fail to adequately recapitulate the expression profiles of the corresponding tumors from which they were derived (47-50). Tissue-specific and cell-cell interactions are lost upon culturing of cells under 2D conditions. Key cellular events such as cell proliferation, migration and apoptosis are frequently based on cellular context and the common consensus is that mimicking cell-cell and cell-extracellular matrix interactions in 3D culture can better portray tumor-specific conditions (51). Additionally, cell lines maintained under 2D conditions are cultured with medium not containing growth factors present within the tumor microenvironment. Hence, there is a need to develop specially formulated medium enriched with growth factors found in the tumor microenvironment (52). For neuroblastoma as well as other types of solid tumors, long-term culturing of cells in 2D culture conditions leads to the acquisition of non-tumor-specific mutations, rendering these cell lines unsuitable for cell based assays (53, 54). This has led to the generation of so-called “tumor-initiating cells (TICs)” or “organoids”, i.e. short-term tumor-derived cells maintained in culture under 3D conditions.

Organoids can be defined as an *in vitro* cluster of cells derived exclusively from primary tissues, embryonic stem cells or immature pluripotent stem cells and capable of self-renewal properties with the ability to exhibit similar functional roles as its organ of origin (55, 56). Most organoid culture systems lack basement membrane and extracellular matrix components that constitute the normal tissue architecture. In order to facilitate the self-renewal and self-organizing properties of these structures, organoids are most often cultured in rigid matrices that closely resemble the components of the extracellular matrix (57). In order to maintain the 3D architecture of neuroblastoma, TIC lines or organoids are cultured on reconstituted rat extracellular matrix (matrigel) or 1% methylcellulose solution. Because of the limited knowledge of the growth factors and lineage commitment factors required by cells of the neuronal lineage, establishment of the optimal conditions for 3D culturing of neuroblastoma cells remains challenging. Currently, neuroblastoma TIC lines and organoids are cultured using neuronal stem cell medium supplemented with EGF and FGF which are important components necessary for neuronal cell maintenance and survival (58). Under these conditions, neuroblastoma cells have been shown to recapitulate the genotype and phenotype of the primary tumors from which they are derived (49, 52, 59, 60).

The ability to culture self-renewing organoids provides model systems that can be used for multiple research applications as well as translational research. Organoids

provide relevant *in vitro* platforms to study tissue homeostasis and the onset of disease in tissues. Introducing well-known driver mutations in *APC*, *KRAS*, *TP53* and *SMAD4* by CRISPR/Cas9 DNA editing in organoids derived from healthy intestinal tissues resulted in their transformation into organoids mimicking the genomic and signaling profile of colorectal tumors. After implantation in mice, mutated organoids formed tumors with genomic properties near identical to human colorectal cancers (61). For solid tumors, high-throughput drug screens in 3D culture models yielded the discovery of new therapeutic targets that were not found in 2D culture models (62-66).

As already shortly addressed above, organoids are also used for the development of more representative *in vivo* models. Organoids are injected in immune-compromised mice at two main locations: 1) subcutaneous (i.e. directly under the dermis), or 2) orthotopic (i.e. at their site of origin). Alternative models are patient-derived tumor xenograft (PDX) models whereby the patient-derived tumor material is directly engrafted into immune-compromised mice (67, 68). Organoid- and patient-derived xenograft models have served as robust model systems for efficacy testing of novel targeted inhibitors. The shift from *in vitro* 2D culture systems to 3D organoids and organoid- and patient-derived xenograft models has ushered in a new era of better predicting and understanding the effects of drug responses in patients.

In this thesis, we describe the generation and propagation of patient-derived neuroblastoma TIC lines. We show that neuroblastoma TIC lines retain the phenotypic and genotypic characteristics of the primary tumors from which they are derived, with excellent sphere forming potential. The above topic will be more extensively discussed in **chapter 2**.

3. DEREGULATED PATHWAYS IN NEUROBLASTOMA

3.1. Targeting the apoptotic pathway

Apoptosis or programmed cell death is a cellular process whereby activation leads to DNA shredding, cytoplasmic fragmentation, membrane reorganization and cell death without lysis of surrounding cells (69). The balance between cell viability and apoptosis plays an important role in maintaining normal cell homeostasis. Alterations in the apoptotic pathway has been shown to promote neoplastic transformation as well as resistance to therapy (70, 71). The apoptotic pathway consists of the extrinsic and intrinsic apoptotic pathway **Figure 4**. The main players of the extrinsic apoptotic pathway are the tumor

necrosis factor (TNF) superfamily of receptors and TNF-related apoptosis inducing ligand (TRAIL) (72). TRAIL binds to two types of receptors: death receptors that can activate apoptosis and decoy receptors that can prevent apoptosis from occurring by functioning as gatekeepers. Activation of the extrinsic apoptotic pathway occurs upon TRAIL binding to TNF receptors leading to their oligomerization and subsequent recruitment of FAS-associated protein with death domain (FADD) to their death domains. FADD in turn recruits initiator caspase-8 or caspase-10 via its death effector domain (DED), which is then cleaved and activated within the death-inducing signaling complex (DISC). Activated initiator caspases cleave and activate effector caspase-3, resulting in DNA fragmentation by DNase endonucleases, nuclear disorganization, cytoplasmic condensation, cellular shrinkage and, eventually, cell death (73, 74).

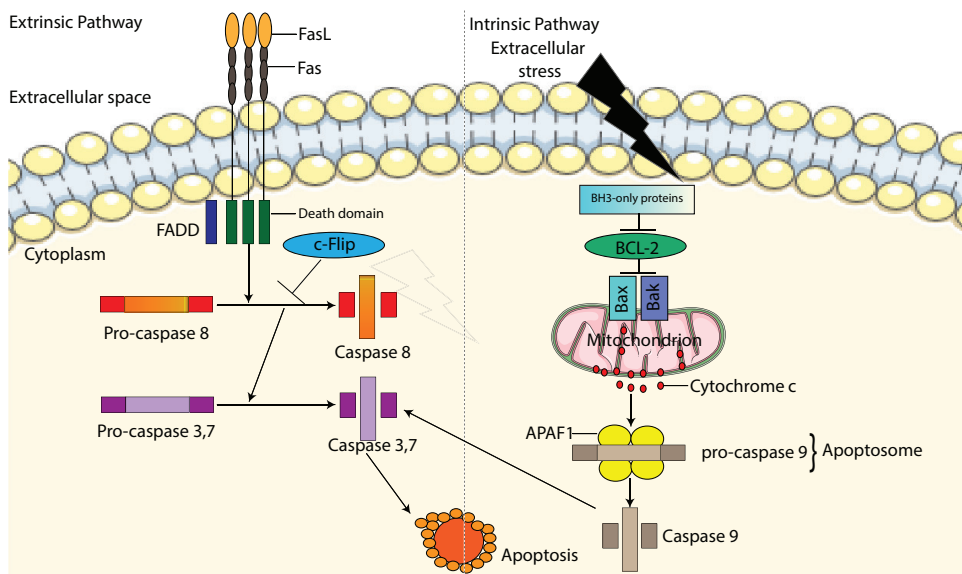


Figure 4: Schematic representation of the extrinsic and intrinsic apoptotic pathway.

In numerous tumors, resistance to TRAIL-mediated apoptosis has been shown to be attributed to downregulation of death receptors, CASP8 inactivation and overexpression of anti-apoptotic proteins such as the caspase 8 and FADD-like apoptosis regulator (CFLAR) or c-FLIP (75-77). The observation that in most high stage neuroblastomas CASP8 is inactivated due to hypermethylation or deletion of the gene provides rational for targeting the extrinsic apoptotic pathway in these tumors (78, 79). Non-small cell

lung carcinoma (NSCLC) patients showed partial or complete responses in phase I and II clinical trials upon treatment with recombinant human Apo2 ligand/TRAILZ (dulanermin). Combination studies of TRAIL with chemotherapeutics are currently being carried out to assess the feasibility of improving the response rate of these patients to TRAIL (NCT00092924). In neuroblastoma cell lines, restoration of caspase-8 levels by combination treatment with soluble TRAIL ligands and demethylating agents triggered apoptosis. Sensitization of neuroblastoma cell lines to TRAIL was shown to be effective upon additional activation of the intrinsic apoptotic pathway (80, 81). These findings suggest that combined activation of both the extrinsic and intrinsic apoptotic pathway might be beneficial in neuroblastoma patients with inactivating events in both pathways.

The B-cell lymphoma (BCL2) family of proteins are key players in the intrinsic apoptotic cascade. It consists of the anti-apoptotic proteins BCL2, BCL-extra-large (BCL-X_L), myeloid cell leukaemia sequence 1 (MCL1), BCL-2-like protein 2 (BCL-W) and BCL2 related protein A1 (A1) (82), the multi-domain pro-apoptotic proteins BCL2-associated X (BAX), BCL2 homologous antagonist/killer (BAK) and BCL2 related ovarian killer (BOK) and the BH3-only pro-apoptotic proteins BCL2-like protein 11 (BIM), BH3 interacting domain death agonist (BID) and BCL2-antagonist of cell death (BAD)(83). Activation of the intrinsic apoptotic pathway occurs primarily at the outer mitochondrial membrane. Apoptosis is induced by external stimuli such as DNA damage caused by chemotherapy or radiation or by growth factor withdrawal, resulting in the displacement of pro-apoptotic proteins (primarily BIM, Bid or Bad) from anti-apoptotic members. Displaced pro-apoptotic proteins causes oligomerization of BAX/BAK, leading to the formation of pores on the surface of the mitochondria. Cytochrome c, Second mitochondria-derived activator of caspases/ direct IAP binding protein with low PI (SMAC/DIABLO), HtrA Serine peptidase 2 (HtrA2/Omi), apoptosis-inducing factor (AIF) and endonuclease G are then released from the mitochondria into the cytosol. Cytochrome c together with the apoptotic protease activating factor 1 (Apaf1) forms the apoptosome. The apoptosome is responsible for the recruitment and cleavage of effector caspases such as caspase-3 and -9, leading to cell-mediated apoptosis (84). Regulators of apoptosis Smac/DIABLO and HtrA2/Omi play various roles in the inactivation of inhibitors of apoptosis (IAPs), while AIF and endonuclease G are involved in chromatin condensation and DNA fragmentation (85, 86). IAPs bind to effector caspases preventing their activation and subsequent induction of apoptosis (87). In humans, eight family members of these proteins have been identified: neuronal apoptosis inhibitory protein (BIRC1), cellular IAP1 (c-IAP₁ or

BIRC2), c-IAP₂ (or BIRC3), X-chromosome-linked IAP (XIAP or BIRC4), survivin (TIAP or BIRC5), Bruce (BIRC6), Livin (BIRC7) and IAP-like protein 2 (BIRC8) (88).

In numerous malignancies, inactivating genomic events in the intrinsic apoptotic pathway have been observed, including loss of *BAX* or *BAK* and overexpression of *BIRC5* or the anti-apoptotic BCL2 family member proteins (89, 90). *BIRC5* is located on chromosome 17q, which is frequently gained in neuroblastoma tumors. Inhibition of *BIRC5* with small molecule inhibitor YM155 lead to a strong apoptotic response and complete tumor regression in neuroblastoma xenograft mouse models (90), underscoring the potential of *BIRC5* as a therapeutic target for neuroblastoma treatment. The anti-apoptotic protein BCL2 is also highly expressed in the majority of all neuroblastoma patients (91-93). Previous studies have shown that BCL2 knockdown in BCL2 high-expressing neuroblastoma cell lines causes a strong apoptotic response. Thus, targeting this pathway with small molecule inhibitors might prove useful in the treatment of neuroblastoma patients with high BCL2 expression (91).

Earlier attempts to target the intrinsic apoptotic pathway were primarily through the use of antisense oligonucleotides specifically targeting BCL2 protein expression. The first agent which was specifically developed to target BCL2 protein expression was the antisense oligonucleotide oblimersen (94, 95). Oblimersen showed great promise during pre-clinical development, but its clinical development was halted due to off-target effects observed in phase III trials. Off-target effects were mainly due to the induction of apoptosis via other mechanisms than BCL2 (96-98).

Several compounds such as histone deacetylase (HDAC) inhibitors, sodium butyrate and depsipeptide were discovered to directly regulate the expression of the anti-apoptotic BCL2 family proteins BCL2, BCL-X_L and MCL1 in lymphoid malignancy cell lines (99, 100). Other agents such as the cyclin-dependent kinase (CDK) inhibitor flavopiridol inhibited apoptosis specifically by MCL1 downregulation (101). However, the specificity of these compounds is limited compared to small molecules which directly interact with the anti-apoptotic BCL2 family proteins, hence the need for such compounds.

Under normal physiological conditions, a group of BH3-only proteins can directly bind to and activate BAX and BAK, leading to activation of the intrinsic apoptotic pathway (82). The term “primed for cell death” was coined to describe the state whereby activator proteins in this group such as BIM, Bid and Puma can bind to anti-apoptotic proteins BCL2, MCL1 etc., preventing BAX and BAK1 oligomerization and hence apoptosis (93).

Based on this hypothesis, a group of small molecule inhibitors (BH3 mimetics) were developed. These small molecule inhibitors directly bind to the hydrophobic groove of the BH3 domain of the anti-apoptotic family proteins, displacing the BH3-only proteins triggering apoptosis. Gossypol (AT-101, Ascenta), a phenolic pigment, was one of the first compounds that showed significant inhibitory effects on BCL2, BCL-X_L and MCL1 (102-104). AT-101 binds to BCL2, BCL-X_L and MCL1 at low micromolar concentrations and is currently in phase II clinical trial for chronic lymphocytic leukemia (CLL; in combination with rituximab) and hormone refractory prostate cancer (in combination with docetaxel) (105-107). Because in a phase I/II clinical trial for prostate cancer dose-limiting gastrointestinal toxicity was observed, the gossypol analog apogossypol was developed. Apogossypol exhibited a stronger binding affinity to BCL2, BCL-X_L and MCL1 (0.32, 0.48 and 0.18 μM) and the systemic toxicities observed with gossypol were notably decreased (108).

Obatoclox (GX15-070) is a small molecule inhibitor that was developed as a hydrophobic pan-BCL2 family inhibitor (109). Studies performed in acute myeloid leukemia (AML) cell lines showed that the compound displays low binding affinities to BCL2, BCL-X_L, BCL-W and MCL1 (3.5, 3, 2.9 and 5 μmol/L, respectively). *In vitro* pre-clinical evaluation of the compound in AML cell lines showed moderate responses, which could be attributed to partial BIM displacement and activation of BAX and BAK. Additionally, G₂-arrest was observed in the cell lines which might be due to possible off-target effects of the compound (110). Phase I clinical trials in hematological malignancies showed only 4% partial responses and one complete remission after obatoclox treatment. Low response rates in clinical trials led to the discontinuation of further development of the compound that has now an orphan status (111).

ABT-737 (Abbott Laboratories) is a small molecule inhibitor that binds to the anti-apoptotic proteins BCL2, BCL-X_L, MCL1, A1 and BCLW ((K_i=0.001, 0.078, 0.03, 0.46 and 0.197 nmol/L) (100) displacing the pro-apoptotic BH3-only proteins, triggering BAX and BAK oligomerization ultimately inducing apoptosis in cancer cells (112). Thus, cell lines with high BCL2, MCL1, BCL-X_L and BCL-W expression were most sensitive to the compound than cell lines with low expression. Various studies have shown that ABT-737 in combination with radiation and chemotherapeutic agents increased the apoptotic response of CLL cell lines and xenografts (113, 114). Pre-clinical evaluation of ABT-737 in combination with chemotherapeutics also showed promising results for AML, multiple myeloma (MM), small cell lung cancer (SCLC) and acute lymphoblastic

leukemia (ALL) (115-117). Because ABT-737 was not suitable as an oral agent, the orally bioavailable analog ABT-263 (navitoclax) was developed (118). Similar to ABT-737, navitoclax exhibits high binding affinities to BCL2, BCL-X_L and BCL-W ($K_i=0.044$, 0.055 and 7nmol/L, respectively) (119). *In vitro* pre-clinical evaluation showed that navitoclax selectively caused a strong apoptotic response in neuroblastoma cell lines with high BCL2 expression levels. At the *in vivo* level, navitoclax delayed the onset of tumor formation and induced almost complete regression of established tumors in a neuroblastoma BCL2 high-expressing xenograft mouse model (91). In a phase I/II clinical trial for patients with relapsed and refractory CLL and Hodgkin's lymphoma, overall response rates (ORRs) of, respectively, 22% and 35% were observed with a progression free survival of about 25 months (120, 121). However, the clinical use of navitoclax was associated with dose-dependent thrombocytopenia, caused by the on-target inhibition of BCL-X_L in the platelets (122).

Due to the toxic side effects of navitoclax in early clinical trials, it was crucial to develop a BCL2-specific inhibitor. ABT-199 (venetoclax) binds over 50 times more potent to BCL2 ($K_i < 1$ nmol/L) than to anti-apoptotic BCL2 family members BCL-X_L, BCL-W and MCL1 ($K_i \sim 50$, 245 and >444 nmol/L, respectively) (123). Like navitoclax, *in vitro* pre-clinical studies showed that neuroblastoma cell lines with high BCL2 and BIM/BCL2 complex levels responded more potently to venetoclax than low-expressing lines. In mice, venetoclax strongly inhibited the growth of BCL2 high-expressing neuroblastoma xenografts, but complete tumor remission was not observed (124, 125). Resistance to venetoclax could be attributed to upregulation of MCL1, which then prevents the occurrence of apoptosis by sequestration of BIM displaced from BCL2. MCL1-mediated resistance could be effectively abrogated upon treatment of BCL2 high-expressing cell lines with venetoclax in combination with MCL1 specific inhibitors as well as Aurora kinase inhibitors that act mainly by downregulating MCL1 protein levels (124). Additional studies in ALL and CML have shown that phosphatidylinositol -3 kinase (PI3K), serine/threonine kinase 1 (AKT), mammalian target of rapamycin (mTOR) and cyclin-dependent kinase (CDK) inhibitors also successfully abrogated venetoclax resistance by directly regulating MCL1 expression (126). In hematological malignancies, combining venetoclax with the Bruton's tyrosine kinase (BTK) inhibitor ibrutinib or the anti-CD20 monoclonal antibody rituximab gave excellent responses both *in vitro* and *in vivo* (123, 127). Clinical trials combining venetoclax with the MEK inhibitor cobimetinib are currently ongoing in hematological malignancies (NCT02670044). In hematological malignancies, it has been observed that resistance to venetoclax can also occur because missense mutations

in the BH3 domain of BCL2 prevent binding of the inhibitor. Strategies to circumvent this type of resistance mechanism are still subject to further investigation (128). A dose-escalation phase I study showed that 79% of chronic lymphocytic leukemia (CLL) or small lymphocytic lymphoma (SLL) patients demonstrated a favorable response to the compound with 22% of the patients exhibiting a complete remission (127). The current thesis describes the preclinical evaluation of the BCL2-specific inhibitor venetoclax in neuroblastoma, including mechanisms causing neuroblastoma resistance to venetoclax and combination strategies to prevent this. Based on these results, a clinical trial will be conducted in neuroblastoma patients to determine the response rates to venetoclax treatment.

3.2. The clinical relevance of targeting the EZH2 pathway.

Epigenetics can be described as the study of factors that exert gene control without modification of DNA sequences (129). Epigenetics processes play an important role in normal cellular functions in development as well as in disease initiation and progression. Epigenetic modulation of a gene often results in the differential expression of the modulated gene. Several epigenetics processes have been identified: methylation, acetylation, sumoylation, phosphorylation and ubiquitylation (130). The most studied epigenetic modifications are DNA methylation and chromatin or histone modifications, of which the latter will be discussed in-depth in this thesis. DNA methylation is a process whereby methyl groups are added to the DNA (131) in regions whereby a cytosine nucleotide is located adjacent to a guanine nucleotide (known as CpG sites) (132). The methylation of CpG sites is carried out by enzymes known as DNA methyl transferases (DNMT) (133, 134). Addition of a methyl group leads to DNA modification and interaction of the transcription machinery of the gene with the DNA. As stated above, DNA methylation often occurs at CpG sites in normal cells. However, there are stretches of DNA within CpG-rich regions that are normally non-methylated. These are known as CpG islands and are located near the promoter regions of genes (135, 136). In cancer cells, CpG island methylation can be modified and this phenomenon has been identified as an early tumor promoting event (137). Several DNA demethylating agents have been developed and pre-clinically tested for the treatment of DNA methylation driven tumors. These inhibitors are capable of reactivating genes silenced by DNA methylation. 5-azacytidine and 5-aza-2'-deoxycytidine are the two pre-clinically most extensively tested and validated DNA demethylating agents and have shown promising results in numerous tumor types (138).

Histones are a family of proteins which together with DNA condense to form chromatin (139). Modifications of histones mainly occur via methylation, acetylation or phosphorylation and might result in either gene activation or silencing (130). Acetylation is a process whereby acetyl groups are added to lysine amino acids present in histones. Lysine acetylation usually results in gene activation, while methylation of lysine residues causes gene silencing (140, 141). Methylation of histones occurs primarily on lysine and arginine side chains. Methylation and acetylation of histone tails at lysine is mediated by histone methyl and acetyltransferases (142, 143). Histone methyltransferases are a SET (SU[VAR]3-9, Enhancer of Zeste and Trithorax) containing group of enzymes that together with a group of genes form the polycomb repressor complex (PRC).

Polycomb repressor genes play a key role in cell fate determination, cell cycle regulation and hematopoiesis. These genes encode a group of proteins that form two distinct complexes: polycomb repressor complex 1 and 2 (PRC1 and PRC2) (144). Polycomb repressor group proteins are transcriptional repressors that act via methylation of the histone tails of genes leading to gene silencing. The enhancer of zeste homologue 2 (EZH2) together with suppressor of zeste 12 (SUZ12) and embryonic ectoderm development (EED) form part of the PRC2 complex (141, 145, 146). SUZ12 functions by binding to and stabilizing EZH2 within the PRC2 complex. Additionally, SUZ12 enhances PRC2 activity via recruitment of RbApb48, which in turn enhances EZH2 histone methyltransferase activity (147-150). EED via its carboxy-terminal domain binds to the histone tails of histone 3 leading to the activation of the histone methyltransferase activity of the PRC2 complex (151). EZH2 consists of a catalytic SET domain, through which methyl groups are transferred to histone 3 di-methylated at lysine 27, resulting in tri-methylated histone 3 (H3K27me3) and subsequently gene silencing (152-154) **(Figure 5)**.

EZH2 is overexpressed in numerous cancer types and plays a crucial role in cancer cell proliferation and survival (155-158). Several oncoproteins such as MYC mediate EZH2 overexpression by downregulating miR-26a and miR26b, which are negative regulators of EZH2 (159, 160). Cell cycle regulators such as E2F can also regulate EZH2 expression via the pRB-E2F pathway (160, 161). In diffuse B-cell lymphomas, it has been observed that Y641 and A677G somatic point mutations in the SET transactivation domain of EZH2 result in enhanced stability and histone methyltransferase activity of the gene (162). EZH2 overexpression in neuroblastoma was correlated to increased hypermethylation and silencing of tumor suppressor genes *CASZ1*, *RUNX3*, *NGFR3* and *CLU* (163, 164).

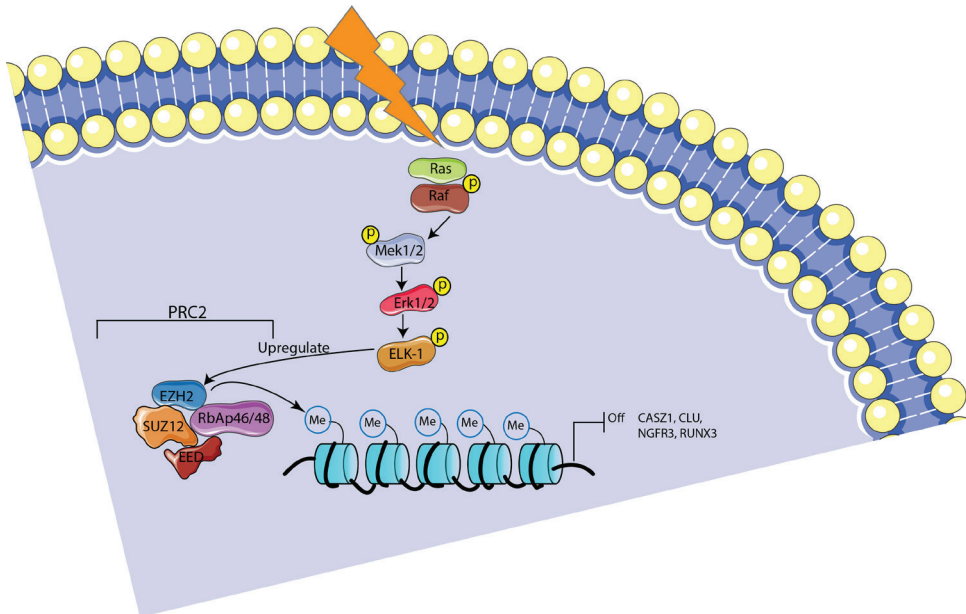


Figure 5: Schematic representation of the histone methyltransferase activity of EZH2 and the transcriptional repression of known target genes.

Because tumor promoting events are often associated with increased histone methyltransferase activity of EZH2, several small molecule histone methyltransferase inhibitors were developed. 3-Deazaneplanocin (DZNep), a first line histone methyltransferase inhibitor, was reported to cause inhibition of H3K27me₃ as well as H4K20me₃ (165-167). Treatment of neuroblastoma cell lines expressing high EZH2 levels with DZNep resulted in a strong apoptotic response. At the *in vivo* level, almost complete tumor regression was observed upon treatment with the inhibitor. Molecular analysis on neuroblastoma cell lines and xenografts treated with DZNep revealed upregulation of genes that are normally silenced by EZH2 (163). DZNep was shown to be an *s*-adenosyl homocysteine hydrolase inhibitor, indirectly also inhibiting other histone methyltransferases. Because this resulted in possible side-effects, further development of the compound was discontinued (168). This led to the development of the two new EZH2-specific methyltransferase inhibitors GSK126 and EPZ6438. *In vitro* pre-clinical evaluation of both histone methyltransferase inhibitors showed potent responses in diffuse B-cell lymphoma (DBCL) cell lines harbouring the Y641 activating mutation. A strong cell cycle arrest and apoptotic phenotype was observed upon treatment of these cells with both compounds. At the *in vivo* level, complete tumor regression was

observed upon treatment with GSK126 and EPZ6438 (169-171). The *in vitro* and *in vivo* responses observed in DBCL suggests that patients harbouring the Y641 mutation might benefit from treatment with these inhibitors.

In this thesis, we described the local gain and overexpression of *EZH2* in neuroblastoma. We attempted to study and elucidate the histone methyltransferase functions of *EZH2* in neuroblastoma using small molecule inhibitors. We report on a histone methyltransferase independent function of *EZH2* in neuroblastoma and the relevance of targeted inhibition of the *EZH2* protein as a whole in neuroblastoma.

REFERENCES

1. Brodeur GM. Neuroblastoma: biological insights into a clinical enigma. *Nat Rev Cancer* 2003;3(3):203-16.
2. Goto S, Umehara S, Gerbing RB, Stram DO, Brodeur GM, Seeger RC, et al. Histopathology (International Neuroblastoma Pathology Classification) and MYCN status in patients with peripheral neuroblastic tumors: a report from the Children's Cancer Group. *Cancer* 2001;92(10):2699-708.
3. Shimada H, Ambros IM, Dehner LP, Hata J, Joshi VV, Roald B. Terminology and morphologic criteria of neuroblastic tumors: recommendations by the International Neuroblastoma Pathology Committee. *Cancer* 1999;86(2):349-63.
4. Umehara S, Nakagawa A, Matthay KK, Lukens JN, Seeger RC, Stram DO, et al. Histopathology defines prognostic subsets of ganglioneuroblastoma, nodular. *Cancer* 2000;89(5):1150-61.
5. Shimada H, Ambros IM, Dehner LP, Hata J, Joshi VV, Roald B, et al. The International Neuroblastoma Pathology Classification (the Shimada system). *Cancer* 1999;86(2):364-72.
6. Burgues O, Navarro S, Noguera R, Pellin A, Ruiz A, Castel V, et al. Prognostic value of the International Neuroblastoma Pathology Classification in Neuroblastoma (Schwannian stroma-poor) and comparison with other prognostic factors: a study of 182 cases from the Spanish Neuroblastoma Registry. *Virchows Arch* 2006;449(4):410-20.
7. Hero B, Simon T, Horz S, Berthold F. Metastatic neuroblastoma in infancy: what does the pattern of metastases contribute to prognosis? *Med Pediatr Oncol* 2000;35(6):683-7.
8. Morgenstern DA, London WB, Stephens D, Volchenboum SL, Hero B, Di Cataldo A, et al. Metastatic neuroblastoma confined to distant lymph nodes (stage 4N) predicts outcome in patients with stage 4 disease: A study from the International Neuroblastoma Risk Group Database. *J Clin Oncol* 2014;32(12):1228-35.
9. Taggart DR, London WB, Schmidt ML, DuBois SG, Monclair TF, Nakagawara A, et al. Prognostic value of the stage 4S metastatic pattern and tumor biology in patients with metastatic neuroblastoma diagnosed between birth and 18 months of age. *J Clin Oncol* 2011;29(33):4358-64.
10. Russell HV, Golding LA, Suell MN, Nuchtern JG, Strother DR. The role of bone marrow evaluation in the staging of patients with otherwise localized, low-risk neuroblastoma. *Pediatr Blood Cancer* 2005;45(7):916-9.
11. Brodeur GM, Green AA, Hayes FA, Williams KJ, Williams DL, Tsiatis AA. Cytogenetic features of human neuroblastomas and cell lines. *Cancer Res* 1981;41(11 Pt 1):4678-86.
12. Bown N, Cotterill S, Lastowska M, O'Neill S, Pearson AD, Plantaz D, et al. Gain of chromosome arm 17q and adverse outcome in patients with neuroblastoma. *N Engl J Med* 1999;340(25):1954-61.
13. Bagchi A, Mills AA. The quest for the 1p36 tumor suppressor. *Cancer Res* 2008;68(8):2551-6.

14. Henrich KO, Schwab M, Westermann F. 1p36 tumor suppression--a matter of dosage? *Cancer Res* 2012;72(23):6079-88.
15. Guo C, White PS, Weiss MJ, Hogarty MD, Thompson PM, Stram DO, et al. Allelic deletion at 11q23 is common in MYCN single copy neuroblastomas. *Oncogene* 1999;18(35):4948-57.
16. Stallings RL, Howard J, Dunlop A, Mullarkey M, McDermott M, Breatnach F, et al. Are gains of chromosomal regions 7q and 11p important abnormalities in neuroblastoma? *Cancer Genet Cytogenet* 2003;140(2):133-7.
17. Attiyeh EF, London WB, Mosse YP, Wang Q, Winter C, Khazi D, et al. Chromosome 1p and 11q deletions and outcome in neuroblastoma. *N Engl J Med* 2005;353(21):2243-53.
18. Bordow SB, Norris MD, Haber PS, Marshall GM, Haber M. Prognostic significance of MYCN oncogene expression in childhood neuroblastoma. *J Clin Oncol* 1998;16(10):3286-94.
19. Katzenstein HM, Bowman LC, Brodeur GM, Thorner PS, Joshi VV, Smith EI, et al. Prognostic significance of age, MYCN oncogene amplification, tumor cell ploidy, and histology in 110 infants with stage D(S) neuroblastoma: the pediatric oncology group experience--a pediatric oncology group study. *J Clin Oncol* 1998;16(6):2007-17.
20. Kato GJ, Wechsler DS, Dang CV. DNA binding by the Myc oncoproteins. *Cancer Treat Res* 1992;63:313-25.
21. Fisher F, Crouch DH, Jayaraman PS, Clark W, Gillespie DA, Goding CR. Transcription activation by Myc and Max: flanking sequences target activation to a subset of CACGTG motifs in vivo. *Embo j* 1993;12(13):5075-82.
22. Nilsson JA, Cleveland JL. Myc pathways provoking cell suicide and cancer. *Oncogene* 2003;22(56):9007-21.
23. Inomistova MV, Svergun NM, Khranovska NM, Skachkova OV, Gorbach OI, Klymnyuk GI. Prognostic significance of MDM2 gene expression in childhood neuroblastoma. *Exp Oncol* 2015;37(2):111-5.
24. Chen Z, Lin Y, Barbieri E, Burlingame S, Hicks J, Ludwig A, et al. Mdm2 deficiency suppresses MYCN-Driven neuroblastoma tumorigenesis in vivo. *Neoplasia* 2009;11(8):753-62.
25. Imamura J, Bartram CR, Berthold F, Harms D, Nakamura H, Koeffler HP. Mutation of the p53 gene in neuroblastoma and its relationship with N-myc amplification. *Cancer Res* 1993;53(17):4053-8.
26. Nag S, Qin J, Srivenugopal KS, Wang M, Zhang R. The MDM2-p53 pathway revisited. *J Biomed Res* 2013;27(4):254-71.
27. Rozan LM, El-Deiry WS. p53 downstream target genes and tumor suppression: a classical view in evolution. *Cell Death Differ* 2007;14(1):3-9.
28. Sax JK, El-Deiry WS. p53 downstream targets and chemosensitivity. *Cell Death Differ* 2003;10(4):413-7.
29. Wei CL, Wu Q, Vega VB, Chiu KP, Ng P, Zhang T, et al. A global map of p53 transcription-factor binding sites in the human genome. *Cell* 2006;124(1):207-19.

30. Molenaar JJ, Koster J, Zwijnenburg DA, van Sluis P, Valentijn LJ, van der Ploeg I, et al. Sequencing of neuroblastoma identifies chromothripsis and defects in neurogenesis genes. *Nature* 2012;483(7391):589-93.
31. Furgason JM, Koncar RF, Michelhaugh SK, Sarkar FH, Mittal S, Sloan AE, et al. Whole genome sequence analysis links chromothripsis to EGFR, MDM2, MDM4, and CDK4 amplification in glioblastoma. *Oncoscience* 2015;2(7):618-28.
32. McEvoy J, Nagahawatte P, Finkelstein D, Richards-Yutz J, Valentine M, Ma J, et al. RB1 gene inactivation by chromothripsis in human retinoblastoma. *Oncotarget* 2014;5(2):438-50.
33. Stevens JB, Abdallah BY, Liu G, Ye CJ, Horne SD, Wang G, et al. Diverse system stresses: common mechanisms of chromosome fragmentation. *Cell Death Dis* 2011;2:e178.
34. Storchova Z, Kloosterman WP. The genomic characteristics and cellular origin of chromothripsis. *Curr Opin Cell Biol* 2016;40:106-13.
35. Janoueix-Lerosey I, Lequin D, Brugieres L, Ribeiro A, de Pontual L, Combaret V, et al. Somatic and germline activating mutations of the ALK kinase receptor in neuroblastoma. *Nature* 2008;455(7215):967-70.
36. Mosse YP, Laudenslager M, Longo L, Cole KA, Wood A, Attiyeh EF, et al. Identification of ALK as a major familial neuroblastoma predisposition gene. *Nature* 2008;455(7215):930-5.
37. Ogawa S, Takita J, Sanada M, Hayashi Y. Oncogenic mutations of ALK in neuroblastoma. *Cancer Sci* 2011;102(2):302-8.
38. Chen Y, Takita J, Choi YL, Kato M, Ohira M, Sanada M, et al. Oncogenic mutations of ALK kinase in neuroblastoma. *Nature* 2008;455(7215):971-4.
39. Li S, Qi X, Huang Y, Liu D, Zhou F, Zhou C. Ceritinib (LDK378): a potent alternative to crizotinib for ALK-rearranged non-small-cell lung cancer. *Clin Lung Cancer* 2015;16(2):86-91.
40. Friboulet L, Li N, Katayama R, Lee CC, Gainor JF, Crystal AS, et al. The ALK inhibitor ceritinib overcomes crizotinib resistance in non-small cell lung cancer. *Cancer Discov* 2014;4(6):662-73.
41. Zhang YC, Zhou Q, Wu YL. Efficacy of crizotinib in first-line treatment of adults with ALK-positive advanced NSCLC. *Expert Opin Pharmacother* 2016;17(12):1693-701.
42. Trochet D, Bourdeaut F, Janoueix-Lerosey I, Deville A, de Pontual L, Schleiermacher G, et al. Germline mutations of the paired-like homeobox 2B (PHOX2B) gene in neuroblastoma. *Am J Hum Genet* 2004;74(4):761-4.
43. Wiseman GA, Kvoles LK. Therapy of neuroendocrine tumors with radiolabeled MIBG and somatostatin analogues. *Semin Nucl Med* 1995;25(3):272-8.
44. DuBois SG, Matthay KK. Radiolabeled metaiodobenzylguanidine for the treatment of neuroblastoma. *Nucl Med Biol* 2008;35 Suppl 1:S35-48.
45. Defachelles AS, Cougnenc O, Carpentier P. [Radio iodized metaiodobenzylguanidine (MIBG) in the treatment of neuroblastoma: modalities and indications]. *Bull Cancer* 2011;98(5):559-69.

46. Cohn SL, Pearson AD, London WB, Monclair T, Ambros PF, Brodeur GM, et al. The International Neuroblastoma Risk Group (INRG) classification system: an INRG Task Force report. *J Clin Oncol* 2009;27(2):289-97.
47. Tian XF, Heng BC, Ge Z, Lu K, Rufaihah AJ, Fan VT, et al. Comparison of osteogenesis of human embryonic stem cells within 2D and 3D culture systems. *Scand J Clin Lab Invest* 2008;68(1):58-67.
48. Weigelt B, Bissell MJ. Unraveling the microenvironmental influences on the normal mammary gland and breast cancer. *Semin Cancer Biol* 2008;18(5):311-21.
49. Coulon A, Flahaut M, Muhlethaler-Mottet A, Meier R, Liberman J, Balmas-Bourloud K, et al. Functional sphere profiling reveals the complexity of neuroblastoma tumor-initiating cell model. *Neoplasia* 2011;13(10):991-1004.
50. Sun T, Jackson S, Haycock JW, MacNeil S. Culture of skin cells in 3D rather than 2D improves their ability to survive exposure to cytotoxic agents. *J Biotechnol* 2006;122(3):372-81.
51. Wakimoto H, Mohapatra G, Kanai R, Curry WT, Jr., Yip S, Nitta M, et al. Maintenance of primary tumor phenotype and genotype in glioblastoma stem cells. *Neuro Oncol* 2012;14(2):132-44.
52. Lee J, Kotliarova S, Kotliarov Y, Li A, Su Q, Donin NM, et al. Tumor stem cells derived from glioblastomas cultured in bFGF and EGF more closely mirror the phenotype and genotype of primary tumors than do serum-cultured cell lines. *Cancer Cell* 2006;9(5):391-403.
53. Kumar HR, Zhong X, Hoelz DJ, Rescorla FJ, Hickey RJ, Malkas LH, et al. Three-dimensional neuroblastoma cell culture: proteomic analysis between monolayer and multicellular tumor spheroids. *Pediatr Surg Int* 2008;24(11):1229-34.
54. De Witt Hamer PC, Van Tilborg AA, Eijk PP, Sminia P, Troost D, Van Noorden CJ, et al. The genomic profile of human malignant glioma is altered early in primary cell culture and preserved in spheroids. *Oncogene* 2008;27(14):2091-6.
55. Clevers H. Modeling Development and Disease with Organoids. *Cell* 2016;165(7):1586-97.
56. Fatehullah A, Tan SH, Barker N. Organoids as an in vitro model of human development and disease. *Nat Cell Biol* 2016;18(3):246-54.
57. Yin X, Mead BE, Safaee H, Langer R, Karp JM, Levy O. Engineering Stem Cell Organoids. *Cell Stem Cell* 2016;18(1):25-38.
58. Tropepe V, Sibilica M, Ciruna BG, Rossant J, Wagner EF, van der Kooy D. Distinct neural stem cells proliferate in response to EGF and FGF in the developing mouse telencephalon. *Dev Biol* 1999;208(1):166-88.
59. Cao L, Zhou Y, Zhai B, Liao J, Xu W, Zhang R, et al. Sphere-forming cell subpopulations with cancer stem cell properties in human hepatoma cell lines. *BMC Gastroenterol* 2011;11:71.
60. Uchida Y, Tanaka S, Aihara A, Adikrisna R, Yoshitake K, Matsumura S, et al. Analogy between sphere forming ability and stemness of human hepatoma cells. *Oncol Rep* 2010;24(5):1147-51.

61. Matano M, Date S, Shimokawa M, Takano A, Fujii M, Ohta Y, et al. Modeling colorectal cancer using CRISPR-Cas9-mediated engineering of human intestinal organoids. *Nat Med* 2015;21(3):256-62.
62. Chen YC, Ingram PN, Fouladdel S, McDermott SP, Azizi E, Wicha MS, et al. High-Throughput Single-Cell Derived Sphere Formation for Cancer Stem-Like Cell Identification and Analysis. *Sci Rep* 2016;6:27301.
63. Kunz-Schughart LA, Freyer JP, Hofstaedter F, Ebner R. The use of 3-D cultures for high-throughput screening: the multicellular spheroid model. *J Biomol Screen* 2004;9(4):273-85.
64. Weigelt B, Ghajar CM, Bissell MJ. The need for complex 3D culture models to unravel novel pathways and identify accurate biomarkers in breast cancer. *Adv Drug Deliv Rev* 2014;69-70:42-51.
65. Hongisto V, Jernstrom S, Fey V, Mpindi JP, Kleivi Sahlberg K, Kallioniemi O, et al. High-throughput 3D screening reveals differences in drug sensitivities between culture models of JIMT1 breast cancer cells. *PLoS One* 2013;8(10):e77232.
66. Howes AL, Richardson RD, Finlay D, Vuori K. 3-Dimensional culture systems for anti-cancer compound profiling and high-throughput screening reveal increases in EGFR inhibitor-mediated cytotoxicity compared to monolayer culture systems. *PLoS One* 2014;9(9):e108283.
67. Marangoni E, Poupon MF. Patient-derived tumour xenografts as models for breast cancer drug development. *Curr Opin Oncol* 2014;26(6):556-61.
68. Whittle JR, Lewis MT, Lindeman GJ, Visvader JE. Patient-derived xenograft models of breast cancer and their predictive power. *Breast Cancer Res* 2015;17:17.
69. Elmore S. Apoptosis: a review of programmed cell death. *Toxicol Pathol* 2007;35(4):495-516.
70. Pommier Y, Sordet O, Antony S, Hayward RL, Kohn KW. Apoptosis defects and chemotherapy resistance: molecular interaction maps and networks. *Oncogene* 2004;23(16):2934-49.
71. Igney FH, Krammer PH. Death and anti-death: tumour resistance to apoptosis. *Nat Rev Cancer* 2002;2(4):277-88.
72. Fulda S, Debatin KM. Extrinsic versus intrinsic apoptosis pathways in anticancer chemotherapy. *Oncogene* 2006;25(34):4798-811.
73. Johnstone RW, Frew AJ, Smyth MJ. The TRAIL apoptotic pathway in cancer onset, progression and therapy. *Nat Rev Cancer* 2008;8(10):782-98.
74. Nunez G, Benedict MA, Hu Y, Inohara N. Caspases: the proteases of the apoptotic pathway. *Oncogene* 1998;17(25):3237-45.
75. Riccioni R, Pasquini L, Mariani G, Saulle E, Rossini A, Diverio D, et al. TRAIL decoy receptors mediate resistance of acute myeloid leukemia cells to TRAIL. *Haematologica* 2005;90(5):612-24.
76. Chamuleau ME, Ossenkuppele GJ, van Rhenen A, van Dreunen L, Jirka SM, Zevenbergen A, et al. High TRAIL-R3 expression on leukemic blasts is associated with poor outcome

- and induces apoptosis-resistance which can be overcome by targeting TRAIL-R2. *Leuk Res* 2011;35(6):741-9.
77. Longley DB, Wilson TR, McEwan M, Allen WL, McDermott U, Galligan L, et al. c-FLIP inhibits chemotherapy-induced colorectal cancer cell death. *Oncogene* 2006;25(6):838-48.
 78. Casciano I, Banelli B, Croce M, De Ambrosis A, di Vinci A, Gelvi I, et al. Caspase-8 gene expression in neuroblastoma. *Ann N Y Acad Sci* 2004;1028:157-67.
 79. Fulda S, Poremba C, Berwanger B, Hacker S, Eilers M, Christiansen H, et al. Loss of caspase-8 expression does not correlate with MYCN amplification, aggressive disease, or prognosis in neuroblastoma. *Cancer Res* 2006;66(20):10016-23.
 80. Muhlethaler-Mottet A, Bourlout KB, Auderset K, Joseph JM, Gross N. Drug-mediated sensitization to TRAIL-induced apoptosis in caspase-8-complemented neuroblastoma cells proceeds via activation of intrinsic and extrinsic pathways and caspase-dependent cleavage of XIAP, Bcl-xL and RIP. *Oncogene* 2004;23(32):5415-25.
 81. Muhlethaler-Mottet A, Flahaut M, Bourlout KB, Auderset K, Meier R, Joseph JM, et al. Histone deacetylase inhibitors strongly sensitise neuroblastoma cells to TRAIL-induced apoptosis by a caspases-dependent increase of the pro- to anti-apoptotic proteins ratio. *BMC Cancer* 2006;6:214.
 82. Cory S, Adams JM. The Bcl2 family: regulators of the cellular life-or-death switch. *Nat Rev Cancer* 2002;2(9):647-56.
 83. Petros AM, Olejniczak ET, Fesik SW. Structural biology of the Bcl-2 family of proteins. *Biochim Biophys Acta* 2004;1644(2-3):83-94.
 84. Tait SW, Green DR. Mitochondria and cell death: outer membrane permeabilization and beyond. *Nat Rev Mol Cell Biol* 2010;11(9):621-32.
 85. LaCasse EC, Baird S, Korneluk RG, MacKenzie AE. The inhibitors of apoptosis (IAPs) and their emerging role in cancer. *Oncogene* 1998;17(25):3247-59.
 86. Li LY, Luo X, Wang X. Endonuclease G is an apoptotic DNase when released from mitochondria. *Nature* 2001;412(6842):95-9.
 87. Berthelet J, Dubrez L. Regulation of Apoptosis by Inhibitors of Apoptosis (IAPs). *Cells* 2013;2(1):163-87.
 88. Deveraux QL, Reed JC. IAP family proteins--suppressors of apoptosis. *Genes Dev* 1999;13(3):239-52.
 89. McCurrach ME, Connor TM, Knudson CM, Korsmeyer SJ, Lowe SW. bax-deficiency promotes drug resistance and oncogenic transformation by attenuating p53-dependent apoptosis. *Proc Natl Acad Sci U S A* 1997;94(6):2345-9.
 90. Lamers F, van der Ploeg I, Schild L, Ebus ME, Koster J, Hansen BR, et al. Knockdown of survivin (BIRC5) causes apoptosis in neuroblastoma via mitotic catastrophe. *Endocr Relat Cancer* 2011;18(6):657-68.

91. Lamers F, Schild L, den Hartog IJ, Ebus ME, Westerhout EM, Ora I, et al. Targeted BCL2 inhibition effectively inhibits neuroblastoma tumour growth. *Eur J Cancer* 2012;48(16):3093-103.
92. Lestini BJ, Goldsmith KC, Fluchel MN, Liu X, Chen NL, Goyal B, et al. Mcl1 downregulation sensitizes neuroblastoma to cytotoxic chemotherapy and small molecule Bcl2-family antagonists. *Cancer Biol Ther* 2009;8(16):1587-95.
93. Goldsmith KC, Gross M, Peirce S, Luyindula D, Liu X, Vu A, et al. Mitochondrial Bcl-2 family dynamics define therapy response and resistance in neuroblastoma. *Cancer Res* 2012;72(10):2565-77.
94. Cheson BD. Oblimersen for the treatment of patients with chronic lymphocytic leukemia. *Ther Clin Risk Manag* 2007;3(5):855-70.
95. Emi M, Kim R, Tanabe K, Uchida Y, Toge T. Targeted therapy against Bcl-2-related proteins in breast cancer cells. *Breast Cancer Res* 2005;7(6):R940-52.
96. Marcucci G, Stock W, Dai G, Klisovic RB, Liu S, Klisovic MI, et al. Phase I study of oblimersen sodium, an antisense to Bcl-2, in untreated older patients with acute myeloid leukemia: pharmacokinetics, pharmacodynamics, and clinical activity. *J Clin Oncol* 2005;23(15):3404-11.
97. O'Brien S, Moore JO, Boyd TE, Larratt LM, Skotnicki A, Koziner B, et al. Randomized phase III trial of fludarabine plus cyclophosphamide with or without oblimersen sodium (Bcl-2 antisense) in patients with relapsed or refractory chronic lymphocytic leukemia. *J Clin Oncol* 2007;25(9):1114-20.
98. Sternberg CN, Dumez H, Van Poppel H, Skoneczna I, Sella A, Daugaard G, et al. Docetaxel plus oblimersen sodium (Bcl-2 antisense oligonucleotide): an EORTC multicenter, randomized phase II study in patients with castration-resistant prostate cancer. *Ann Oncol* 2009;20(7):1264-9.
99. Cao XX, Mohuiddin I, Ece F, McConkey DJ, Smythe WR. Histone deacetylase inhibitor downregulation of bcl-xl gene expression leads to apoptotic cell death in mesothelioma. *Am J Respir Cell Mol Biol* 2001;25(5):562-8.
100. Khan SB, Maududi T, Barton K, Ayers J, Alkan S. Analysis of histone deacetylase inhibitor, depsipeptide (FR901228), effect on multiple myeloma. *Br J Haematol* 2004;125(2):156-61.
101. Rosato RR, Almenara JA, Kolla SS, Maggio SC, Coe S, Gimenez MS, et al. Mechanism and functional role of XIAP and Mcl-1 down-regulation in flavopiridol/vorinostat antileukemic interactions. *Mol Cancer Ther* 2007;6(2):692-702.
102. Oliver CL, Miranda MB, Shangary S, Land S, Wang S, Johnson DE. (-)-Gossypol acts directly on the mitochondria to overcome Bcl-2- and Bcl-X(L)-mediated apoptosis resistance. *Mol Cancer Ther* 2005;4(1):23-31.
103. Voss V, Senft C, Lang V, Ronellenfitsch MW, Steinbach JP, Seifert V, et al. The pan-Bcl-2 inhibitor (-)-gossypol triggers autophagic cell death in malignant glioma. *Mol Cancer Res* 2010;8(7):1002-16.

104. Wong FY, Liem N, Xie C, Yan FL, Wong WC, Wang L, et al. Combination therapy with gossypol reveals synergism against gemcitabine resistance in cancer cells with high BCL-2 expression. *PLoS One* 2012;7(12):e50786.
105. Volate SR, Kawasaki BT, Hurt EM, Milner JA, Kim YS, White J, et al. Gossypol induces apoptosis by activating p53 in prostate cancer cells and prostate tumor-initiating cells. *Mol Cancer Ther* 2010;9(2):461-70.
106. Liu G, Kelly WK, Wilding G, Leopold L, Brill K, Somer B. An open-label, multicenter, phase I/II study of single-agent AT-101 in men with castrate-resistant prostate cancer. *Clin Cancer Res* 2009;15(9):3172-6.
107. Balakrishnan K, Wierda WG, Keating MJ, Gandhi V. Gossypol, a BH3 mimetic, induces apoptosis in chronic lymphocytic leukemia cells. *Blood* 2008;112(5):1971-80.
108. Arnold AA, Aboukameel A, Chen J, Yang D, Wang S, Al-Katib A, et al. Preclinical studies of Apogossypolone: a new nonpeptidic pan small-molecule inhibitor of Bcl-2, Bcl-XL and Mcl-1 proteins in Follicular Small Cleaved Cell Lymphoma model. *Mol Cancer* 2008;7:20.
109. Konopleva M, Watt J, Contractor R, Tsao T, Harris D, Estrov Z, et al. Mechanisms of antileukemic activity of the novel Bcl-2 homology domain-3 mimetic GX15-070 (obatoclax). *Cancer Res* 2008;68(9):3413-20.
110. Nguyen M, Marcellus RC, Roulston A, Watson M, Serfass L, Murthy Madiraju SR, et al. Small molecule obatoclax (GX15-070) antagonizes MCL-1 and overcomes MCL-1-mediated resistance to apoptosis. *Proc Natl Acad Sci U S A* 2007;104(49):19512-7.
111. O'Brien SM, Claxton DF, Crump M, Faderl S, Kipps T, Keating MJ, et al. Phase I study of obatoclax mesylate (GX15-070), a small molecule pan-Bcl-2 family antagonist, in patients with advanced chronic lymphocytic leukemia. *Blood* 2009;113(2):299-305.
112. Oltersdorf T, Elmore SW, Shoemaker AR, Armstrong RC, Augeri DJ, Belli BA, et al. An inhibitor of Bcl-2 family proteins induces regression of solid tumours. *Nature* 2005;435(7042):677-81.
113. Konopleva M, Contractor R, Tsao T, Samudio I, Ruvolo PP, Kitada S, et al. Mechanisms of apoptosis sensitivity and resistance to the BH3 mimetic ABT-737 in acute myeloid leukemia. *Cancer Cell* 2006;10(5):375-88.
114. van Delft MF, Wei AH, Mason KD, Vandenberg CJ, Chen L, Czabotar PE, et al. The BH3 mimetic ABT-737 targets selective Bcl-2 proteins and efficiently induces apoptosis via Bak/Bax if Mcl-1 is neutralized. *Cancer Cell* 2006;10(5):389-99.
115. Tahir SK, Yang X, Anderson MG, Morgan-Lappe SE, Sarthy AV, Chen J, et al. Influence of Bcl-2 family members on the cellular response of small-cell lung cancer cell lines to ABT-737. *Cancer Res* 2007;67(3):1176-83.
116. Del Gaizo Moore V, Schlis KD, Sallan SE, Armstrong SA, Letai A. BCL-2 dependence and ABT-737 sensitivity in acute lymphoblastic leukemia. *Blood* 2008;111(4):2300-9.
117. Del Gaizo Moore V, Brown JR, Certo M, Love TM, Novina CD, Letai A. Chronic lymphocytic leukemia requires BCL2 to sequester prodeath BIM, explaining sensitivity to BCL2 antagonist ABT-737. *J Clin Invest* 2007;117(1):112-21.

118. Billard C. BH3 mimetics: status of the field and new developments. *Mol Cancer Ther* 2013;12(9):1691-700.
119. Tse C, Shoemaker AR, Adickes J, Anderson MG, Chen J, Jin S, et al. ABT-263: a potent and orally bioavailable Bcl-2 family inhibitor. *Cancer Res* 2008;68(9):3421-8.
120. Roberts AW, Seymour JF, Brown JR, Wierda WG, Kipps TJ, Khaw SL, et al. Substantial susceptibility of chronic lymphocytic leukemia to BCL2 inhibition: results of a phase I study of navitoclax in patients with relapsed or refractory disease. *J Clin Oncol* 2012;30(5):488-96.
121. Wilson WH, O'Connor OA, Czuczman MS, LaCasce AS, Gerecitano JF, Leonard JP, et al. Navitoclax, a targeted high-affinity inhibitor of BCL-2, in lymphoid malignancies: a phase 1 dose-escalation study of safety, pharmacokinetics, pharmacodynamics, and antitumour activity. *Lancet Oncol* 2010;11(12):1149-59.
122. Rudin CM, Hann CL, Garon EB, Ribeiro de Oliveira M, Bonomi PD, Camidge DR, et al. Phase II study of single-agent navitoclax (ABT-263) and biomarker correlates in patients with relapsed small cell lung cancer. *Clin Cancer Res* 2012;18(11):3163-9.
123. Souers AJ, Levenson JD, Boghaert ER, Ackler SL, Catron ND, Chen J, et al. ABT-199, a potent and selective BCL-2 inhibitor, achieves antitumor activity while sparing platelets. *Nat Med* 2013;19(2):202-8.
124. Ham J, Costa C, Sano R, Lochmann TL, Sennott EM, Patel NU, et al. Exploitation of the Apoptosis-Primed State of MYCN-Amplified Neuroblastoma to Develop a Potent and Specific Targeted Therapy Combination. *Cancer Cell* 2016;29(2):159-72.
125. Tanos R, Karmali D, Nalluri S, Goldsmith KC. Select Bcl-2 antagonism restores chemotherapy sensitivity in high-risk neuroblastoma. *BMC Cancer* 2016;16:97.
126. Choudhary GS, Al-Harbi S, Mazumder S, Hill BT, Smith MR, Bodo J, et al. MCL-1 and BCL-xL-dependent resistance to the BCL-2 inhibitor ABT-199 can be overcome by preventing PI3K/AKT/mTOR activation in lymphoid malignancies. *Cell Death Dis* 2015;6:e1593.
127. Roberts AW, Davids MS, Pagel JM, Kahl BS, Puvvada SD, Gerecitano JF, et al. Targeting BCL2 with Venetoclax in Relapsed Chronic Lymphocytic Leukemia. *N Engl J Med* 2016;374(4):311-22.
128. Fresquet V, Rieger M, Carolis C, Garcia-Barchino MJ, Martinez-Climent JA. Acquired mutations in BCL2 family proteins conferring resistance to the BH3 mimetic ABT-199 in lymphoma. *Blood* 2014;123(26):4111-9.
129. Arimondo PB, Egger G, Tost J. Epigenetics. *Biochimie* 2012;94(11):2191-2.
130. Lennartsson A, Ekwall K. Histone modification patterns and epigenetic codes. *Biochim Biophys Acta* 2009;1790(9):863-8.
131. Robertson KD. DNA methylation and chromatin - unraveling the tangled web. *Oncogene* 2002;21(35):5361-79.
132. Bird AP. CpG-rich islands and the function of DNA methylation. *Nature* 1986;321(6067):209-13.

133. Leonhardt H, Page AW, Weier HU, Bestor TH. A targeting sequence directs DNA methyltransferase to sites of DNA replication in mammalian nuclei. *Cell* 1992;71(5):865-73.
134. Okano M, Bell DW, Haber DA, Li E. DNA methyltransferases Dnmt3a and Dnmt3b are essential for de novo methylation and mammalian development. *Cell* 1999;99(3):247-57.
135. Shen L, Kondo Y, Guo Y, Zhang J, Zhang L, Ahmed S, et al. Genome-wide profiling of DNA methylation reveals a class of normally methylated CpG island promoters. *PLoS Genet* 2007;3(10):2023-36.
136. Eckhardt F, Lewin J, Cortese R, Rakyan VK, Attwood J, Burger M, et al. DNA methylation profiling of human chromosomes 6, 20 and 22. *Nat Genet* 2006;38(12):1378-85.
137. Esteller M. CpG island hypermethylation and tumor suppressor genes: a booming present, a brighter future. *Oncogene* 2002;21(35):5427-40.
138. Mani S, Herceg Z. DNA demethylating agents and epigenetic therapy of cancer. *Adv Genet* 2010;70:327-40.
139. Bannister AJ, Kouzarides T. Regulation of chromatin by histone modifications. *Cell Res* 2011;21(3):381-95.
140. Rice JC, Allis CD. Histone methylation versus histone acetylation: new insights into epigenetic regulation. *Curr Opin Cell Biol* 2001;13(3):263-73.
141. Kirmizis A, Bartley SM, Kuzmichev A, Margueron R, Reinberg D, Green R, et al. Silencing of human polycomb target genes is associated with methylation of histone H3 Lys 27. *Genes Dev* 2004;18(13):1592-605.
142. Jacob Y, Stroud H, Leblanc C, Feng S, Zhuo L, Caro E, et al. Regulation of heterochromatic DNA replication by histone H3 lysine 27 methyltransferases. *Nature* 2010;466(7309):987-91.
143. Legube G, Trouche D. Regulating histone acetyltransferases and deacetylases. *EMBO Rep* 2003;4(10):944-7.
144. Margueron R, Reinberg D. The Polycomb complex PRC2 and its mark in life. *Nature* 2011;469(7330):343-9.
145. Xu C, Bian C, Yang W, Galka M, Ouyang H, Chen C, et al. Binding of different histone marks differentially regulates the activity and specificity of polycomb repressive complex 2 (PRC2). *Proc Natl Acad Sci U S A* 2010;107(45):19266-71.
146. O'Meara MM, Simon JA. Inner workings and regulatory inputs that control Polycomb repressive complex 2. *Chromosoma* 2012;121(3):221-34.
147. Cao R, Zhang Y. SUZ12 is required for both the histone methyltransferase activity and the silencing function of the EED-EZH2 complex. *Mol Cell* 2004;15(1):57-67.
148. Rai AN, Vargas ML, Wang L, Andersen EF, Miller EL, Simon JA. Elements of the polycomb repressor SU(Z)12 needed for histone H3-K27 methylation, the interface with E(Z), and in vivo function. *Mol Cell Biol* 2013;33(24):4844-56.
149. Pasini D, Bracken AP, Jensen MR, Lazzerini Denchi E, Helin K. Suz12 is essential for mouse development and for EZH2 histone methyltransferase activity. *Embo j* 2004;23(20):4061-71.

150. Lee SC, Miller S, Hyland C, Kauppi M, Lebois M, Di Rago L, et al. Polycomb repressive complex 2 component Suz12 is required for hematopoietic stem cell function and lymphopoiesis. *Blood* 2015;126(2):167-75.
151. Margueron R, Justin N, Ohno K, Sharpe ML, Son J, Drury WJ, 3rd, et al. Role of the polycomb protein EED in the propagation of repressive histone marks. *Nature* 2009;461(7265):762-7.
152. Cao R, Zhang Y. The functions of E(Z)/EZH2-mediated methylation of lysine 27 in histone H3. *Curr Opin Genet Dev* 2004;14(2):155-64.
153. Stepanik VA, Harte PJ. A mutation in the E(Z) methyltransferase that increases trimethylation of histone H3 lysine 27 and causes inappropriate silencing of active Polycomb target genes. *Dev Biol* 2012;364(2):249-58.
154. Burmeister T. EZH2: a pleiotropic protein. *Blood* 2016;128(7):888-9.
155. Cardoso C, Mignon C, Hetet G, Grandchamps B, Fontes M, Colleaux L. The human EZH2 gene: genomic organisation and revised mapping in 7q35 within the critical region for malignant myeloid disorders. *Eur J Hum Genet* 2000;8(3):174-80.
156. Liu YL, Gao X, Jiang Y, Zhang G, Sun ZC, Cui BB, et al. Expression and clinicopathological significance of EED, SUZ12 and EZH2 mRNA in colorectal cancer. *J Cancer Res Clin Oncol* 2015;141(4):661-9.
157. Varambally S, Dhanasekaran SM, Zhou M, Barrette TR, Kumar-Sinha C, Sanda MG, et al. The polycomb group protein EZH2 is involved in progression of prostate cancer. *Nature* 2002;419(6907):624-9.
158. Kleer CG, Cao Q, Varambally S, Shen R, Ota I, Tomlins SA, et al. EZH2 is a marker of aggressive breast cancer and promotes neoplastic transformation of breast epithelial cells. *Proc Natl Acad Sci U S A* 2003;100(20):11606-11.
159. Friedman JM, Liang G, Liu CC, Wolff EM, Tsai YC, Ye W, et al. The putative tumor suppressor microRNA-101 modulates the cancer epigenome by repressing the polycomb group protein EZH2. *Cancer Res* 2009;69(6):2623-9.
160. Bracken AP, Pasini D, Capra M, Prosperini E, Colli E, Helin K. EZH2 is downstream of the pRB-E2F pathway, essential for proliferation and amplified in cancer. *Embo j* 2003;22(20):5323-35.
161. Sander S, Bullinger L, Klapproth K, Fiedler K, Kestler HA, Barth TF, et al. MYC stimulates EZH2 expression by repression of its negative regulator miR-26a. *Blood* 2008;112(10):4202-12.
162. Bodor C, Grossmann V, Popov N, Okosun J, O'Riain C, Tan K, et al. EZH2 mutations are frequent and represent an early event in follicular lymphoma. *Blood* 2013;122(18):3165-8.
163. Wang C, Liu Z, Woo CW, Li Z, Wang L, Wei JS, et al. EZH2 Mediates epigenetic silencing of neuroblastoma suppressor genes CASZ1, CLU, RUNX3, and NGFR. *Cancer Res* 2012;72(1):315-24.
164. Henrich KO, Bender S, Saadati M, Dreidax D, Gartlgruber M, Shao C, et al. Integrative Genome-Scale Analysis Identifies Epigenetic Mechanisms of Transcriptional Deregulation in Unfavorable Neuroblastomas. *Cancer Res* 2016;76(18):5523-37.

165. Girard N, Bazille C, Lhuissier E, Benateau H, Llombart-Bosch A, Boumediene K, et al. 3-Deazaneplanocin A (DZNep), an inhibitor of the histone methyltransferase EZH2, induces apoptosis and reduces cell migration in chondrosarcoma cells. *PLoS One* 2014;9(5):e98176.
166. Miranda TB, Cortez CC, Yoo CB, Liang G, Abe M, Kelly TK, et al. DZNep is a global histone methylation inhibitor that reactivates developmental genes not silenced by DNA methylation. *Mol Cancer Ther* 2009;8(6):1579-88.
167. Hibino S, Saito Y, Muramatsu T, Otani A, Kasai Y, Kimura M, et al. Inhibitors of enhancer of zeste homolog 2 (EZH2) activate tumor-suppressor microRNAs in human cancer cells. *Oncogenesis* 2014;3:e104.
168. Knutson SK, Warholic NM, Wigle TJ, Klaus CR, Allain CJ, Raimondi A, et al. Durable tumor regression in genetically altered malignant rhabdoid tumors by inhibition of methyltransferase EZH2. *Proc Natl Acad Sci U S A* 2013;110(19):7922-7.
169. McCabe MT, Ott HM, Ganji G, Korenchuk S, Thompson C, Van Aller GS, et al. EZH2 inhibition as a therapeutic strategy for lymphoma with EZH2-activating mutations. *Nature* 2012;492(7427):108-12.
170. Knutson SK, Kawano S, Minoshima Y, Warholic NM, Huang KC, Xiao Y, et al. Selective inhibition of EZH2 by EPZ-6438 leads to potent antitumor activity in EZH2-mutant non-Hodgkin lymphoma. *Mol Cancer Ther* 2014;13(4):842-54.
171. Knutson SK, Wigle TJ, Warholic NM, Sneeringer CJ, Allain CJ, Klaus CR, et al. A selective inhibitor of EZH2 blocks H3K27 methylation and kills mutant lymphoma cells. *Nat Chem Biol* 2012;8(11):890-6.



CHAPTER 2

NEWLY-DERIVED NEUROBLASTOMA CELL LINES PROPAGATED IN SERUM-FREE MEDIUM RECAPITULATE THE GENOTYPE AND PHENOTYPE OF PRIMARY NEUROBLASTOMA TUMOURS.

Authors: Laurel T. Bate-Eya^a, Marli E. Ebus^a, Jan Koster^a, Ilona J.M. den Hartog^a, Danny A. Zwijnenburg^a, Linda Schild^a, Ida van der Ploeg^a, M. E.(Emmy) M. Dolman^a, Huib N. Caron^b, Rogier Versteeg^a, Jan J. Molenaar^{a*}.

^a Department of Oncogenomics, Academic Medical Center, University of Amsterdam, Meibergdreef 15, PO BOX 22700, 1105 AZ Amsterdam, The Netherlands

^b Department of Paediatric Oncology, Academic Medical Center, University of Amsterdam, Meibergdreef 15, PO BOX 22700, 1105 AZ Amsterdam, The Netherlands

European Journal of Cancer (2014)

ABSTRACT.

Recently protocols have been devised for the culturing of cell lines from fresh tumors under serum-free conditions in defined neural stem cell medium. These cells, frequently called Tumor Initiating Cells (TICs) closely retained characteristics of the tumors of origin. We report the isolation of 8 newly-derived neuroblastoma TICs from 6 primary neuroblastoma tumors and 2 bone-marrow metastases. The primary tumors from which these TICs were generated have previously been fully typed by Whole Genome Sequencing (WGS). Array CGH analysis showed that TIC cell lines retained essential characteristics of the primary tumors and exhibited typical neuroblastoma chromosomal aberrations such as MYCN amplification, gain of chromosome 17q and deletion of 1p36. Protein analysis showed expression for neuroblastoma markers MYCN, NCAM, CHGA, DBH and TH while haematopoietic markers CD19 and CD11b were absent. We analysed the growth characteristics and confirmed tumor-forming potential using sphere-forming assays, subcutaneous and orthotopic injection of these cells into immune-compromised mice. Affymetrix mRNA expression profiling of TIC line xenografts showed an expression pattern more closely mimicking primary tumors compared to xenografts from classical cell lines. This establishes that these neuroblastoma TICs cultured under serum-free conditions are relevant and useful neuroblastoma tumor models.

1. INTRODUCTION

Neuroblastoma is a neuroendocrine tumor that arises from the peripheral sympathetic nervous system¹. INSS stage 1 and 2 tumors display excellent prognosis while stage 3 and 4 tumors have poor clinical outcome with a survival rate of 30%²⁻⁵. Neuroblastoma can genomically be characterised by aberrations such as gain of chromosome 17q, partial loss of chromosome 1p or 11q and MYCN amplification⁶. MYCN amplification occurs in about 20% of tumors and strongly correlates with poor prognosis⁷⁻⁸. Gain of 17q is the most frequent genomic abnormality which is present in over 90% of high grade neuroblastomas⁹.

Cancer cell lines have been regarded as valid systems to study cancer biology. Nevertheless, these cell systems are cultured in non-physiological conditions and maintained for many years allowing considerable artificial adaptation. The genetic makeup and phenotypic characteristics of these cells can thus differ substantially from their original tumors¹⁰⁻¹¹. In recent years, protocols have been devised to culture cells from fresh tumors in serum-free conditions in neural stem cell medium¹²⁻¹³. Such cells retained much of the characteristics of the original tumors and were able to initiate tumors in immuno-compromise mice. They were therefore frequently called Tumor Initiating Cells (TICs), a terminology that we use in this paper to refer to cells cultured by these protocols. TICs isolated from neuroblastoma have recently been reported, but the origin of these cells has been under debate¹⁴⁻¹⁷.

Here we report the unambiguous establishment of TIC cell lines from neuroblastoma. These TICs reflect the primary tumors based on the genotype and phenotype and are not contaminated with cells from the haematopoietic lineage. We also show xenografts of neuroblastoma TICs recapitulate the genotype of primary neuroblastoma and showed similar mRNA expression compared to primary tumors as opposed to xenografts from classical neuroblastoma cell lines.

2. MATERIALS AND METHODS.

2.1. Patients, isolation and culture of neuroblastoma TICs.

Freshly resected human neuroblastoma tissue was obtained directly at surgery. Primary neuroblastoma cells were derived by mechanical disaggregation followed by enzymatic digestion of sheared tumor tissues with Liberase DH (500µl/25ml) (Roche)

for 45mins. Digests were passed through a 40µM cell strainer (BD Biosciences) and cells were cultured in TIC total medium containing DMEM/ F12 (GIBCO) supplemented with 40ng/ml bFGF, 20ng/ml EGF, 1X B27supplement (GIBCO) and 500U/ml of penicillin/streptomycin, 1000mg/ml glucose and 110mg/ml pyruvate. Neuroblastoma TICs were designated by "AMC" (Academic Medical Centre), the name of the research institute, followed by the patient number and in case of TIC lines the letter "T" or "B" was added (T indicating that the TIC cell line was derived from the primary tumors and B from bone marrow metastases).

2.2 Array CGH analysis

aCGH was performed by hybridizing 100ng genomic DNA to a 180K platform (Agilent Technologies). DNA was labelled by random priming with CY5-dCTP and CY3-dCTP respectively and hybridized at 65°C for about 17h. The chips were scanned on an Agilent G2565BA DNA microarray Agilent scanner. Digital analysis was performed with the R2 bioinformatics platform (<http://r2.amc.nl>).

2.3 mRNA expression profiling and Principal component analysis

RNA was extracted from tumors and cell lines with TRIzol (Invitrogen, Carlsbad, CA) following the manufacturer's protocols. RNA concentration and quality were determined using the RNA 6000 Nano assay on the Agilent 2100 Bioanalyzer (Agilent Technologies). Fragmentation of cRNA, hybridization to hg-u133 plus 2.0, microarrays and scanning were carried out according to the manufacturers protocol (Affymetrix inc. Santa Barbara, CA). The mRNA gene expression data were normalized with the MAS5.0 algorithm within the GCOS program of Affymetrix Inc. Target intensity was set to 100. All data were analyzed using the R2 genomic analysis and visualization platform (<http://r2.amc.nl>).

2.4 Animal experimentation

Athymic NMRI-*nu/nu* and NOD-CB17-Prkdcscid/NCrHsd were subcutaneously injected with 1×10^6 , $2,5 \times 10^6$ and 5×10^6 cells of the TIC lines. The size of the tumors was recorded for a period of about 3 months after which tumors were formalin fixed and paraffin sections routinely analysed by haematoxylin-eosin staining. Tumor pieces were serially xenotransplanted into mice recipients for up to 14 passages. Orthotopic injection of luciferase 2 expressing AMC711T and AMC691B cells was also performed. Briefly, 1×10^6 , $2,5 \times 10^6$ and 5×10^6 cells were injected into the fat tissue surrounding the adrenal glands of NMRI *nu/nu*. Tumor take was evaluated after a period of 3 months by exponential increase of the intensity of luciferase signal within the mice using a highly-cooled CCD camera.

3. RESULTS

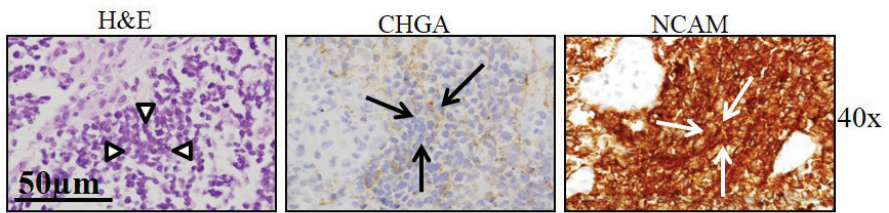
3.1 Clinical and genomic characteristics of patients tumors

Tumor material was obtained from six stages 4 neuroblastoma patients aged 15-115 months. Primary tumors were typed by H&E and by immunohistochemistry staining for NCAM, CHGA and Syp (Figure 1A and B and Supplementary Figure 1). All primary tumors were positive for nuclear imaging using MIBG I127 and all patients were positive for urine catecholamines. aCGH analysis showed *MYCN* amplification in four out of six tumors and multiple other aberrations at chromosomes 1p36, 11q and 17q. *ALK* mutation status of the primary tumors and neuroblastoma TIC cell lines was also reported (Table 1). These primary tumors were previously characterized using whole genome sequencing as described by Molenaar *et. al*¹⁸ and the data is available at the European Genome-phenome Archive under the accession code EGAS00001000222.

Patient	INSS Stage	Age at diagnostics (months)	Gender	Site	MYCN amplification	ALK mutation status	Chromosomal aberrations	Cell line
N691	4	73	F	Adrenal	Yes	No	1p36 Loss 11q Normal 17q Gain	AMC691T AMC691B
N700	4	115	F	Adrenal	Yes	No	1p36 Loss 11q Normal 17q Normal	AMC700T AMC700B
N711	4	15	M	Abdominal side chain	Yes	No	1p36 Loss 11q Normal 17q Gain	AMC711T
N717	4	18	M	Adrenal	Yes	No	1p36 Loss 11q Normal 17q Gain	AMC717T
N753	4	25	M	Abdominal side chain	No	No	1p36 Normal 11q Loss 17q Gain	AMC753T
N772	4	36	M	Adrenal	No	No	1p36 Normal 11q Loss 17q Gain	AMC772T

Table 1. Clinical and genomic characteristics of patient tumours.

A



B

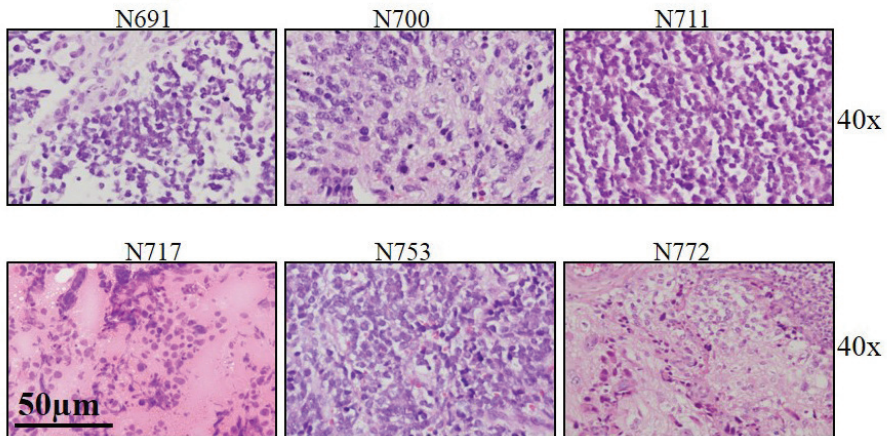


Figure 1: H&E, CHGA and NCAM staining in human neuroblastoma tissue specimens. (A) H&E staining and immunohistochemistry for CHGA and NCAM was performed for patient N691. Neuroblastoma cells in the H&E staining were indicated with white arrowheads. Cells staining positive for CHGA are indicated with black arrows and NCAM with white arrows. (B) H&E staining in N691, N700, N711, N717, N753 and N772.

3.2 Neuroblastoma TICs express neuroblastoma markers and harbour neuroblastoma specific chromosomal aberrations.

Chemically dissociated cells obtained from primary neuroblastoma tumours could be isolated and cultured in serum free media containing bFGF and EGF under conditions used for TIC culture¹²⁻¹³. To verify that the newly-derived TIC lines are indeed neuroblastoma cells, Western blot analysis with specific neuroblastoma markers was performed on TICs and compared to 4 established classical neuroblastoma cell lines (Figure 2A). All TICs expressed MYCN including the two MYCN single copy cell lines. Also, NCAM was expressed albeit at varying levels. AMC691T did not express the neuroblastoma markers CHGA, DBH and TH, whereas AMC691B did express these 3 proteins. This indicates the heterogeneity in neuroblastoma tumours. To exclude that neuroblastoma TICs were contaminated with haematopoietic cells, protein expression of two haematopoietic markers CD19 and CD11b was assessed in all TIC lines. Lymphocytes served as positive controls.

In addition we performed FACS analysis with the same two haematopoietic markers CD19 and CD11b. First AMC691B was spiked with CD19 positive lymphocytes to determine the sensitivity of this method. Flow cytometry analysis revealed that the limit of detection of contamination of TIC cell lines with hematopoietic cells was observed at 1:100 (Supplementary Figure 2C). Subsequent FACS analysis of all neuroblastoma TICs showed that these were negative for CD19 and CD11b (Supplementary Figure 2D and 2E) as previously shown by Western blot in Figure 2A. We therefore concluded that the neuroblastoma TICs are not contaminated with haematopoietic cells.

The origin of neuroblastoma TICs was verified by comparing the aCGH profile of the primary tumour with the aCGH profiles of neuroblastoma TICs (Figure 2B). Chromosome 17q aberrations were most frequently seen. Copy number increases were observed in MYCN amplified TIC cell lines as well as their respective parent tumours (Supplementary Figure 2A). The identical position of the chromosomal breakpoints of the TICs cell lines and original tumours showed that the TICs were derived from the neuroblastoma tumours. In 5 out of 8 TICs a limited number of chromosomal aberrations were not identical with those in the primary tumours. A loss of chromosome 11q and gain of 1q appeared only in AMC691T and loss of 19p only in AMC691B. Gains of parts of 1p31 and 17q were observed in AMC700T and AMC700B. AMC717T had gains in parts of chromosome 1 and 8q and did not have a 1p deletion, whereas the primary tumour did show 1p deletion. AMC772T had unique gains in chromosome 12 and 14.

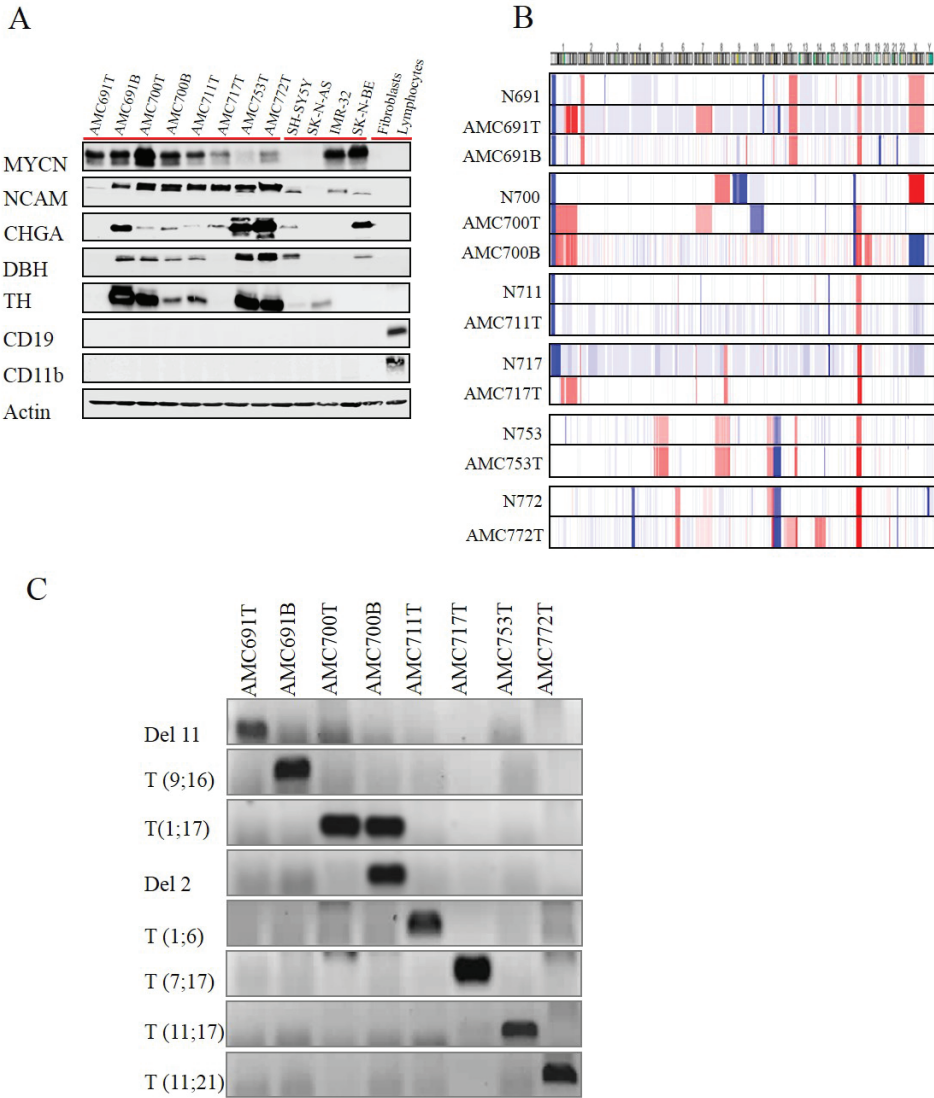


Figure 2: Genomic, protein characterization and DNA typing of neuroblastoma TIC cell lines. (A) Western blot analysis of various neuroblastoma markers MYCN, NCAM, CHGA, DBH and TH and haematopoietic markers CD19 and CD11b in neuroblastoma TIC lines (n=8), classical neuroblastoma cells (n=4), fibroblasts (n=1) and lymphocytes (n=1). Lymphocytes isolated from whole blood served as positive controls for CD19 and CD11b. B-actin was used as a loading control. (B) aCGH profiles comparing primary tumors and neuroblastoma TIC lines. Chromosome gains and losses were detected using the R2 software with blue indicating loss and red indicating gain. (C) Identification of unique breakpoints in neuroblastoma TIC cell lines by breakpoint PCR. Deletions in chromosome 11 were validated for AMC691T, t(9;16) for AMC691B, t(1;17)(AMC700T and AMC700B), deletion chromosome 2 (AMC700B), t(1;6)(AMC711T), t(7;17)(AMC717T), t(11;17)(AMC753T) and t(11;21)(AMC772T).

There were no major differences between the genomic profiles of N711 and N753 and their corresponding TIC lines AMC711T and AMC753T. The discrepancies in the genomic profiles between the tumours and TIC lines most likely indicate the presence of different sub-clones within primary tumours.

3.3 Typing of TIC lines by unique chromosomal breakpoints and short tandem repeat analysis

Correct identification of cell lines is essential and therefore, we performed two typing procedures for the TIC lines. The structural defects identified by aCGH (Figure 2B) allow identification of unique breakpoints in each sample. Based on WGS data (Supplementary Figure 2B), unique breakpoints were identified by JunctionDiff using the Complete Genomics Analysis suite software and were validated by breakpoint PCR with primers specifically designed for each of these breakpoints (Figure 2C and Supplementary Table 1). For AMC700T no unique breakpoint could be identified compared to AMC700B. To allow typing of these two TIC lines a breakpoint for AMC700T and B and a breakpoint unique for AMC700B were included.

Short tandem repeat profiling of cells has previously been described as a method permitting the unambiguous identification of cell lines¹⁹⁻²¹. This method was used to obtain the DNA fingerprints of the 8 neuroblastoma TICs using probes for 16 short tandem repeat markers (Supplementary Table 2). All TIC cell lines showed a distinct DNA fingerprint with the exception of the pair AMC691T and AMC691B, and the pair AMC700T and AMC700B which were derived from the primary tumour and bone marrow metastasis of the same patients.

3.4 Neuroblastoma TIC lines have distinct phenotypic characteristics and exhibit tumour sphere-forming capacity.

Upon isolation from the primary tumour mass and bone marrow aspirates, neuroblastoma TICs were cultured in serum-free medium supplemented with bFGF and EGF. Significant phenotypic differences between the neuroblastoma TICs were observed ranging from the adherent phenotype (AMC691T, AMC691B and AMC700T), to semi-attached (AMC700B and AMC711T) and spheroids (AMC717T, AMC753T and AMC772T) (Figure 3A). All neuroblastoma TICs exhibited different proliferative capacities with doubling times ranging from 76 hrs (AMC700T) to 204 hrs (AMC772T) (Figure 3B). In order to explore the *in vitro* tumourigenic potential of neuroblastoma TICs cells, we determined their ability to form tumour spheres from single cells under ultra-low attachment

conditions in 1% methylcellulose. All neuroblastoma TICs formed spheres within 30 days (Figure 3C). Sphere-forming potential varied among the TIC lines with AMC691B and AMC711T having the highest sphere-forming capacity as shown in Figure 3D.

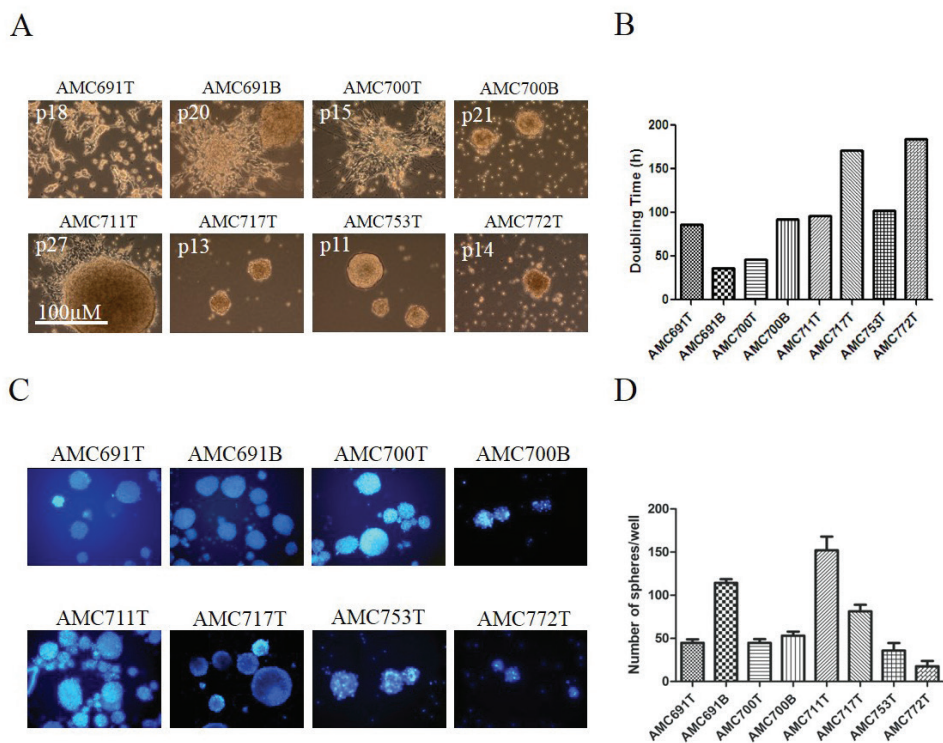


Figure 3: *In vitro* characterization of neuroblastoma TICs cell lines. (A) Light microscopy images of TICs cell lines AMC691T, AMC691B, AMC700T, AMC700B, AMC711T, AMC717T, AMC753T and AMC772T. (B) Doubling times of TICs cell lines as determined by MTT assays. The y-axis values represent the doubling time in hours of each cell line. (C) Fluorescent microscopy images of TIC cell line spheres stained with DAPI in 1% methylcellulose. (D) Sphere forming frequency of each TIC cell lines. An average of 2500 cells was seeded in each well and the number of spheres was estimated for on average 6 wells per cell line. The y-axis represents the number of spheres for on average n=6 wells.

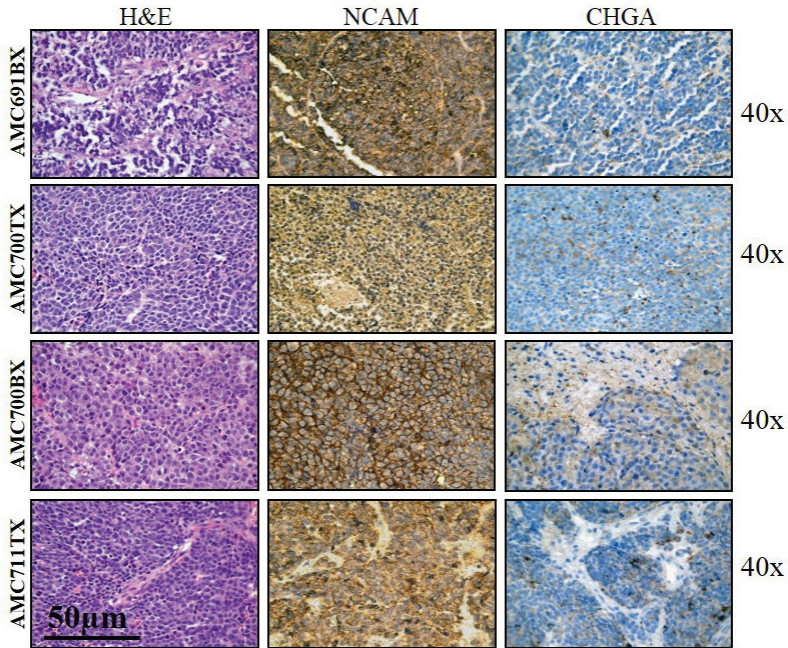
3.5 Neuroblastoma TICs form tumours in mice and recapitulate the genotype of primary neuroblastoma tumours.

We used subcutaneous and orthotopic adrenal mouse models for evaluating tumour formation of all TICs cell lines. Subcutaneous engraftment was primarily performed in NMRI *nu/nu* mice. For TIC lines that showed low tumour take rates, additional xenografting was performed in NOD-SCID mice. All cell lines were tumourigenic in NMRI *nu/nu* and/or NOD-SCID mice, except AMC 691T and AMC753T (Supplementary Table 3). H&E staining and immunohistochemistry showed that these tumours consisted of small round blue immature neuroblasts and were positive for neuroblastoma markers NCAM, CHGA and Syp (Fig. 4A and supplementary Figure 3A). Serial passaging of small tumour pieces in secondary and tertiary mice recipients was performed to improve the tumour take rate of the TICs. This markedly increased the rate of engraftment and early onset of tumour formation (Figure 4B) (Supplementary Figure 3B).

In addition, we performed orthotopic xenografting to validate that TIC lines can form tumours in the microenvironment where neuroblastoma tumour initiation normally occurs. Injection of luc2 expressing AMC711T in the adrenals of immune compromised mice resulted in an increase of luciferase activity and corresponding tumour growth (Supplementary Figure 3C).

Xenografts from cancer cells have been reported to retain the genomic aberrations of parent tumours²²⁻²⁹. In order to confirm the origin of the xenografts from the neuroblastoma TICs, AMC691BX, AMC700TX and AMC711TX aCGH profiles of xenografts were compared with the primary tumour and neuroblastoma TIC lines. Genomic aberrations of the TIC xenografts clearly resembled the aberrations of the primary tumours and TIC lines from which they were derived (Figure 4C). A limited number of genomic aberrations were unique and most likely reflect clonal variation between the bulk of the TIC line and the sub-population from which the xenografts formed.

A



B

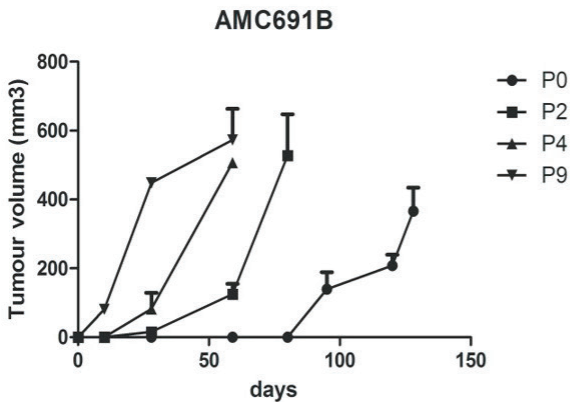
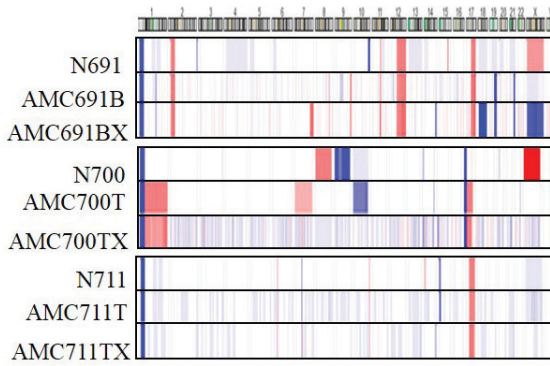


Figure 4: *In vivo* characterization of neuroblastoma TIC cell lines. (A) H&E, NCAM and CHGA staining of neuroblastoma tumors in mice was carried out on p6-p10 of serially passaged mice tumors. (B) Serial xenotransplantation of mice tumor pieces of AMC691B into secondary and tertiary recipients was performed to improve tumor engraftment. The y-axis represents tumor volume in mm³

C



D

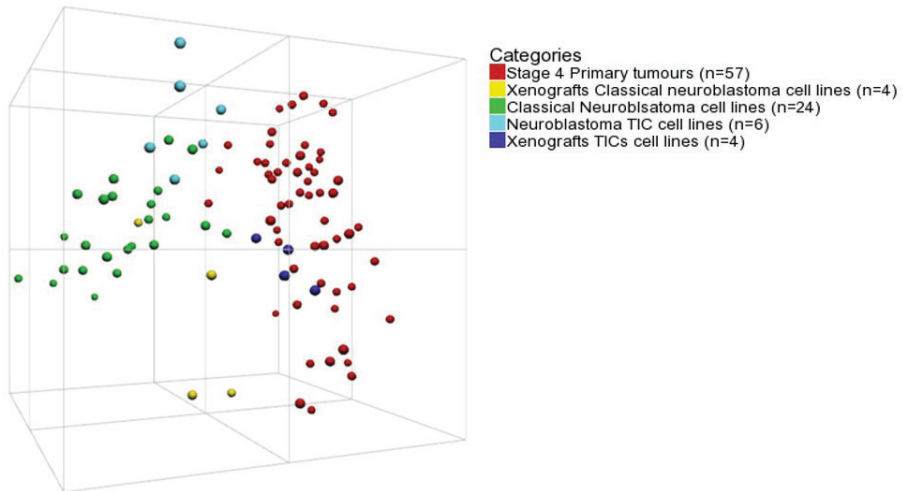


Figure 4: *In vivo* characterization of neuroblastoma TIC cell lines. (C) aCGH profiles of primary tumors, neuroblastoma TIC cell lines and mice xenografts were compared for similarities and differences in genomic aberrations. The in-house R2 software was used to generate the aCGH profile heat map. Blue and red in the heat map represents chromosomes losses and gains respectively. (D) Principal component analysis of 57 stage 4 primary tumors, 6 neuroblastoma TIC cell lines, 24 classical neuroblastoma cells, xenografts from 4 neuroblastoma TIC cell lines AMC691B, AMC700T, AMC700B and AMC711T and xenografts from 4 classical neuroblastoma cells SH-SY5Y, SK-N-AS, IMR-32 and SK-N-BE. Colours of the balls indicate the origin of the samples. PCA was performed in 3 major components.

3.6 Transcriptional analyses reveal a close relationship in the gene expression profiles of primary neuroblastoma tumours and neuroblastoma TIC xenografts

We subsequently investigated whether the phenotypes of xenografts derived from TIC lines better reflected primary tumours as compared to xenografts derived from classical neuroblastoma cell lines. Gene expression profiles of the TIC cell lines (n=6), of neuroblastoma xenografts derived from TIC lines (n=4) and xenografts derived from classical cell lines (n=4) were compared to previously generated profiles of classical cell lines (n=24) and stage 4 primary tumours (n=57). Unsupervised principal component analysis of all samples showed that xenografts from classical neuroblastoma cells clustered further away from primary tumours than neuroblastoma TIC xenografts. The only exception was a xenograft from the classical neuroblastoma cell line SH-SY5Y (Figure 4D and Supplementary Figure 4D). In addition, an unsupervised Euclidian distance-based hierarchical clustering using 500 highest standard deviation containing genes in all samples revealed 2 clusters with distinct gene expression patterns. Neuroblastoma TIC xenografts clustered within the group of primary tumours (Supplementary Figure 3E) while almost all classical cell line xenografts clustered together with the cell line population. All cell lines had the tendency to cluster away from the primary tumours irrespective of whether they were TICs or classical neuroblastoma cells. These results suggest that xenografts from neuroblastoma TICs retained the gene expression profiles of the primary neuroblastoma tumours.

4. DISCUSSION

In this study, we isolated and cultured 8 neuroblastoma TICs from primary neuroblastoma tumors and bone marrow metastases in serum-free medium supplemented with bFGF and EGF. We use the terminology of tumor initiating cells (TICs) to refer to our cell lines although we have not studied stem cell properties of these cell lines in depth. Nevertheless, we will continue to call these cell lines TICs as they were established with the protocols and techniques previously used to establish TIC lines for glioblastoma³⁰⁻³¹. In this paper we aim to report the full phenotyping and genotyping of these cell cultures. We could confirm the origin of neuroblastoma TICs isolated in this study by western blot analysis of neuroblastoma markers and aCGH profiling. Neuroblastoma TICs were positive for known neuroblastoma markers and negative for the haematopoietic markers CD19 and CD11b, excluding contamination with cells of the haematopoietic lineage. There was no clear pattern of expression of neuroblastoma markers between the TICs derived from the primary tumors and bone marrow derived TICs. For example, AMC691T lacks expression of many neuroendocrine markers while AMC691B does express these markers. In AMC700B the TH and DBH markers show marked lower expression compared to the corresponding tumor derived TIC line. Thus the existence of different phenotypes of neuroblastoma cells is not restricted to certain niches.

aCGH profiling confirmed that the TICs were indeed derived from their parent tumors. The neuroblastoma TICs showed key genomic aberrations found in the primary tumors such as 17q gain and MYCN amplification. However, the TICs also contained unique chromosomal aberrations that were not detected in their tumors of origin. Loss of chromosome 11q was found in AMC691T and not in AMC691B and the corresponding primary tumor. Gain of chromosome 17q was present both in AMC700T and AMC700B and not in the primary tumor. This suggests that highly recurrent genomic aberrations as 17q gain and 11q loss can also appear as late events in sub-clones of neuroblastoma. This could have implications for targeted drug development strategies that aim at genes located at these chromosomal locations. *In vitro* tumorigenicity of TICs is defined by their ability to form spheres in suspension culture³²⁻³⁵. AMC711T and AMC691B showed high sphere forming capacity and xenografted with high efficacy while AMC691T and AMC753T did not form tumors in nude mice and had low sphere-forming capacity. The absence of tumor-forming potential *in vivo* of two of our eight TIC lines is in contrast with the previously described potential of TIC cells to form tumors *in vivo*³⁶⁻³⁷. This could relate to specific characteristics of these sub-clones which is a subject of further studies. PCA

and Euclidian distance clustering showed that the xenografts from neuroblastoma TICs clustered more with the primary neuroblastoma tumors as opposed to xenografts from classical cell lines. This suggested that the TIC cells more closely resemble the primary tumors compared to classical cell lines. In conclusion, we think that neuroblastoma TICs isolated in this study closely resemble the human neuroblastoma biology and are therefore useful additions to model systems for the study of neuroblastoma tumor biology and targeted drug development.

REFERENCES

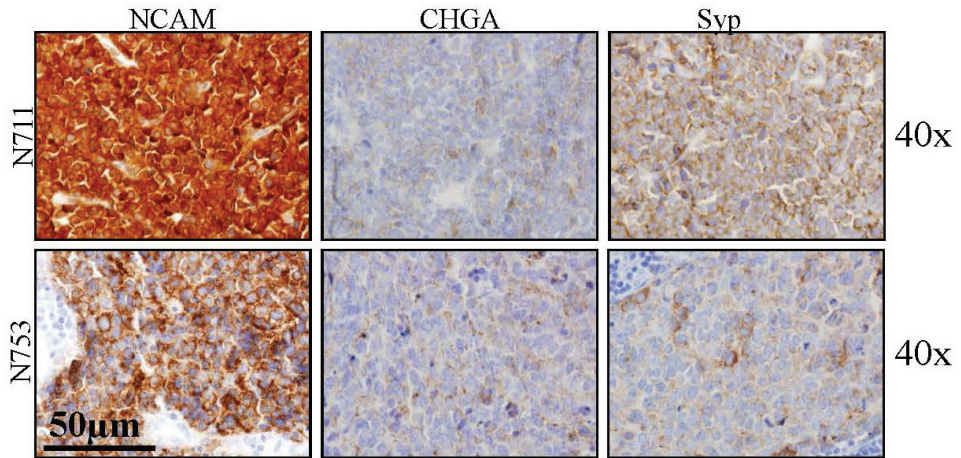
1. Brodeur GM. Neuroblastoma: biological insights into a clinical enigma. *Nat Rev Cancer*. 2003; 3: 203-16
2. Brodeur GM, Green AA, Hayes FA, *et al*. Cytogenetic features of human neuroblastomas and cell lines. *Cancer Res*. 1981; **41**: 4678-86.
3. Brown N, Cotterill S, Lastkowska M, *et al*. Gain of chromosome arm 17q and adverse outcome in patients with neuroblastoma. *N Engl J Med*. 1999; 340: 1954-1961.
4. White PS, Maris JM, Beltinger C, *et al*. A region of consistent deletion in neuroblastoma maps within human chromosome 1p36.2-36.3. *Proc Natl Acad Sci U S A*. 1995; 92: 5520-4.
5. Martinsson T, Sjöberg RM, Hedborg F, *et al*. Deletion of chromosome 1p loci and microsatellite instability in neuroblastomas analysed with short-tandem repeat polymorphisms. *Cancer Res*. 1995; 55: 5681-6.
6. Guo C, White PS, Weiss MJ, *et al*. Allelic deletion at 11q23 is common in MYCN single copy neuroblastomas. *Oncogene*. 1999; 18: 4948-57.
7. Plantaz D, Vandesompele J, Van Roy N, *et al*. Comparative genomic hybridization (CGH) analysis of stage 4 neuroblastoma reveals high frequency of 11q deletion in tumors lacking MYCN amplification. *Int J Cancer*. 2001. 91: 680-6.
8. Spitz R, Oberthuer A, Zapatka M, *et al*. Oligonucleotide array-based comparative genomic hybridization (aCGH) of 90 neuroblastomas reveal aberration patterns closely associated with relapse pattern and outcome. *Genes Chromosomes and Cancer*. 2006; **45**: 390-403.
9. Meddeb M, Danglot G, Chudoba I, *et al*. Additional copies of a 25 Mb chromosomal region originating from 17q23.1-17qter are present in 90% of high-grade neuroblastomas. *Genes Chrom Cancer*. 1996; **17**: 156-165.
10. Li A, Walling J, Kotliarov Y, *et al*. Genomic changes and gene expression profiles reveal that established glioma cell lines are poor representatives of primary human gliomas. *Mol Cancer Res*. 2008; **6**: 21-30.
11. Greshock J, Nathanson K, Martin A *et al*. Cancer cell lines as genetic models of their parent histology: analysis based on array comparative genomic hybridization. *Cancer Res*. 2007; **67**:3594-3600.
12. Ponti D, Costa A, Zaffaroni N *et al*. Isolation and In vitro propagation of Tumorigenic Breast Cancer Cells with Stem/Progenitor Cell Properties. *Cancer Res*.2005; **65**: 5506-5511.
13. Ricci-Vitiani L, Lombardi DG, Pilozzi E *et al*. Identification and Expansion of Human colon-cancer initiating cells.2007; **445**:111-115.
14. Hansford LM, McKee AE, Zhang L, *et al*. Neuroblastoma cells isolated from bone marrow metastases contain a naturally enriched tumor-initiating cell. *Cancer Res*. 2007; 67:11234-11243.

15. Mohlin S, Pietras A, Wigerup C, *et al.* Tumor-initiating cells in childhood neuroblastoma. *Cancer Res.* 2012; 72:821-2.
16. Hansford LM, Kaplan DR. Tumor-initiating cells in childhood neuroblastoma response. *Cancer Res.* 2012; 72: 823-824.
17. Coulon A, Flahaut M, Mühlethaler-Mottet A, *et al.* Functional sphere profiling reveal the complexity of neuroblastoma tumor-initiating cell model. *Neoplasia.* 2011;13: 991-1004.
18. Molenaar JJ, Koster J, Zwijnenburg DA *et al.* Sequencing of neuroblastoma identifies chromothripsis and defects in neuritogenesis genes. *Nature.* 2012; 483: 589-593.
19. Ciulla TA, Sklar RM, Hauser SL. A simple method for DNA purification from peripheral blood. *Anal Biochem.* 1988; **174**: 485-8.
20. Parson W, Kirchebner R, Mühlmann R, *et al.* Cancer cell line identification by short tandem repeat profiling: power and limitations. *Faseb J.* 2005; **19**: 434-6.
21. Masters JR, Thomson JA, Daly-Burns B, *et al.* Short tandem repeat profiles provides an international standard reference standard for human cell lines. *Proc Natl Acad Sci U S A.* 2001; **98**: 8012-17.
22. Clappier E, Gerby B, Sigaux F, *et al.* Clonal selection in xenografted human T cell acute lymphoblastic leukaemia recapitulates gain of malignancy and relapse. *J Exp Med.* 2011; 208:653-661.
23. Marangoni E, Vincent-Salomon A, Auger N, *et al.* A new model of patient tumor-derived breast cancer xenografts for preclinical assays. *Cancer Res.* 2007; 13: 3989-3998.
24. Reyat F, Guyader C, Decraene C, *et al.* Molecular profiling of patient-derived breast cancer xenografts. *Breast Cancer Research.* 2012; 14: 11-14.
25. Priolo C, Agostini M, Vena N, *et al.* Establishment and genomic characterization of mouse xenografts of human primary prostate tumors. *The American Journal of Pathology.* 2010; **176**:1901-1913.
26. Voortman J, Lee J, Killian JK, *et al.* Array comparative genomic hybridization-based characterization of genetic alterations in pulmonary neuroendocrine tumors. *PNAS.* 2010; **107**:13040-13045.
27. Wakimoto H, Mohapatra G, Kanai R, *et al.* Maintenance of primary tumor phenotype and genotype in glioblastoma stem cells. *Neuro-Oncology.* 2011; **14**:132-144.
28. Abdel-Rahman WM, Katsura K, Rens W, *et al.* Spectral Karyotyping suggest additional subsets of colorectal cancers characterized by pattern of chromosome rearrangement. *PNAS.* 2001; **98**:2538-2543.
29. Zhang S, Balch C, Chan MW, *et al.* Identification and characterization of ovarian cancer-initiating cells from primary human tumors. *Cancer Res.* 2008; 68:4311-4320.
30. Fael Al-Mayhany TM, Ball SLR, Zhao J, *et al.* An efficient method for the derivation and propagation of glioblastoma cell Lines that conserves the molecular profile of their original tumors. *J Neurosci Methods.* 2009; 176: 192-9.

Newly-derived neuroblastoma cell lines propagated in serum-free medium recapitulate the genotype and phenotype of primary neuroblastoma tumours

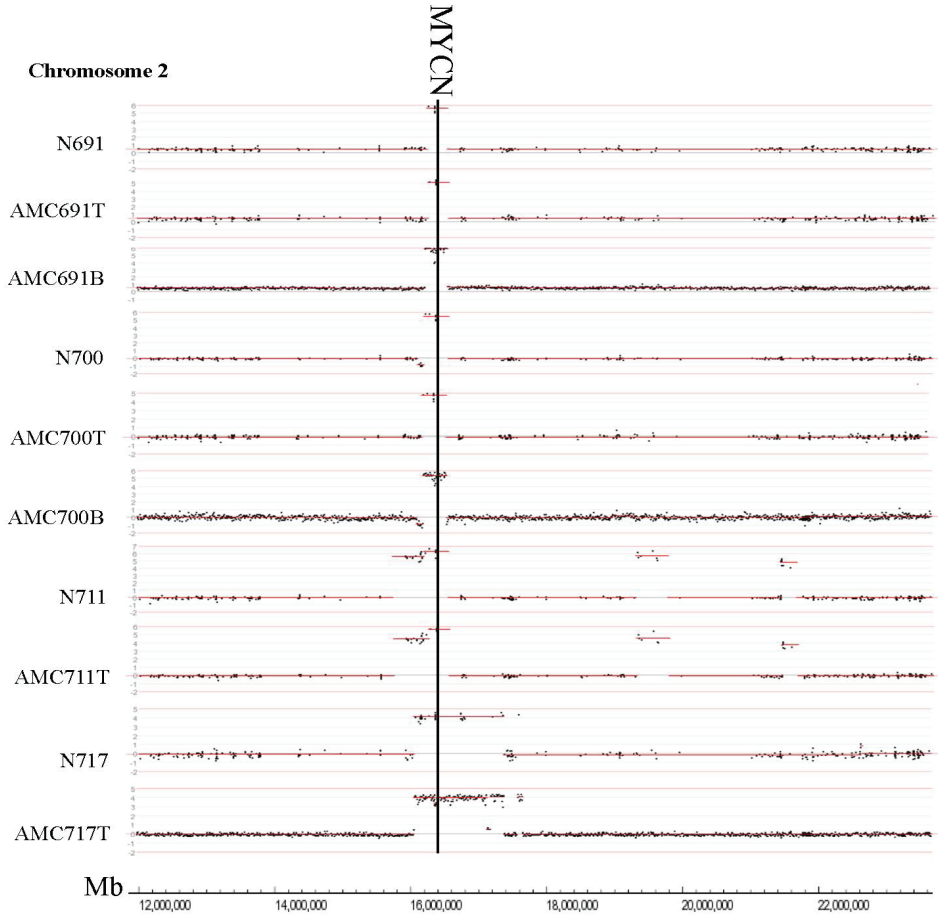
31. Lee J, Kotliarova S, Kotliarova Y, *et al.* Tumor stem cells derived from glioblastomas cultured in bFGF and EGF more closely mirror the phenotype and genotype of primary tumors than do serum-cultured cell lines. *Cancer Cell.* 2006; 9: 391-403.
32. Pastrana E, Silva-Vargas V, Doestch F. Eyes wide open: a critical review of the sphere-formation as an assay for stem cells. *Cell Stem Cell.* 2011; 8:486-498.
33. Hirschhaeuse F, Menne H, Dittfeld C, *et al.* Multicellular tumor spheroids: An underestimated tool is catching up again. *Journal of Biotechnology.* 2010; 148:3-15.
34. Dontu G, Abdallah WM, Foley JM, *et al.* In vitro propagation and transcriptional profiling of human mammary stem/progenitor cells. *Genes Dev.* 2003; 15:1253-70.
35. De Witt Hamer PC, Van Tilborg AAG, Eijk PP *et al.* The genomic profil of malignant human glioma is altered early in primary cell culture and preserved in spheroids. *Oncogene.* 2008; **27**: 2091-2096.
36. Nakanishi T, Chumsri S, Khakpour N, *et al.* Side-population cells in luminal-type breast cancer have tumor-initiating cell properties, and are regulated by HER2 expression and signalling. *BJC.* 2010; **102**:815-826.
37. Lui JC, Deng T, Rajwinder S, *et al.* Identification of tumorsphere and tumor-initiating cells in Her2/Neu-induced mammary tumors.2007; **67**:8671-8681.

SUPPLEMENTARY INFORMATION



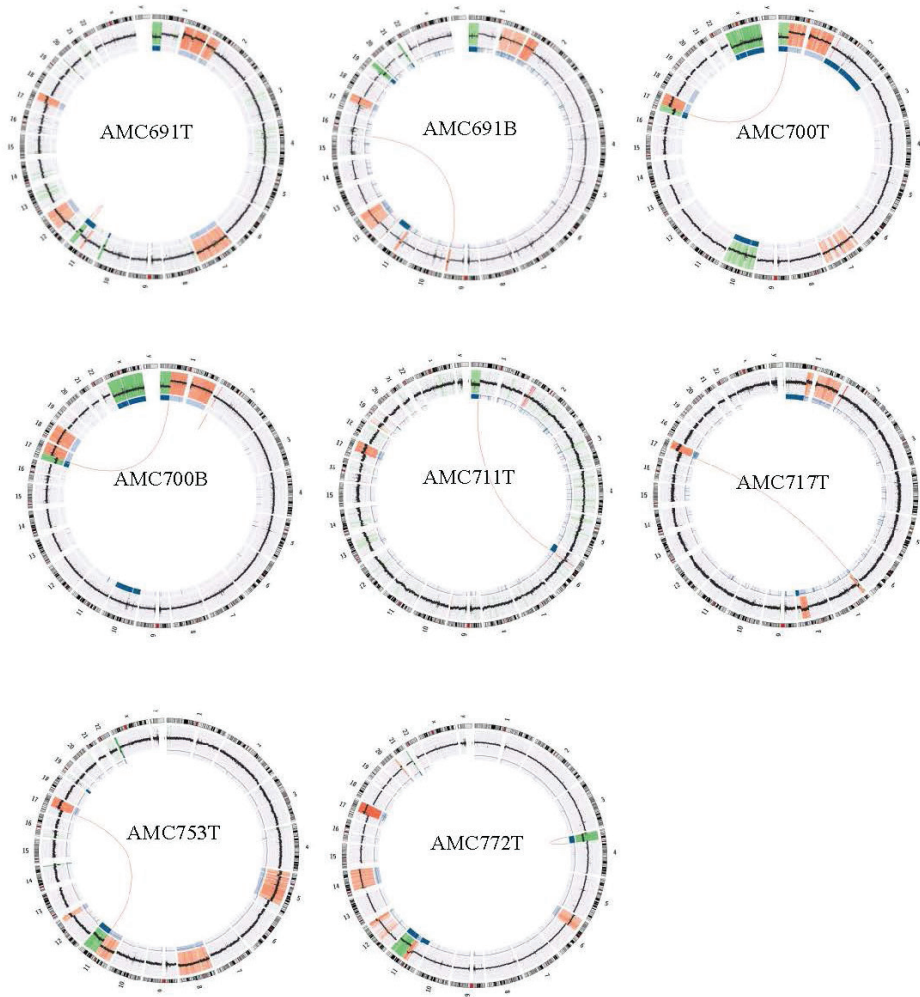
Supplementary Figure 1: IHC staining of human neuroblastoma tumor specimens. Immunohistochemistry was performed for NCAM, CHGA and Syp for patient N711 and N753.

A

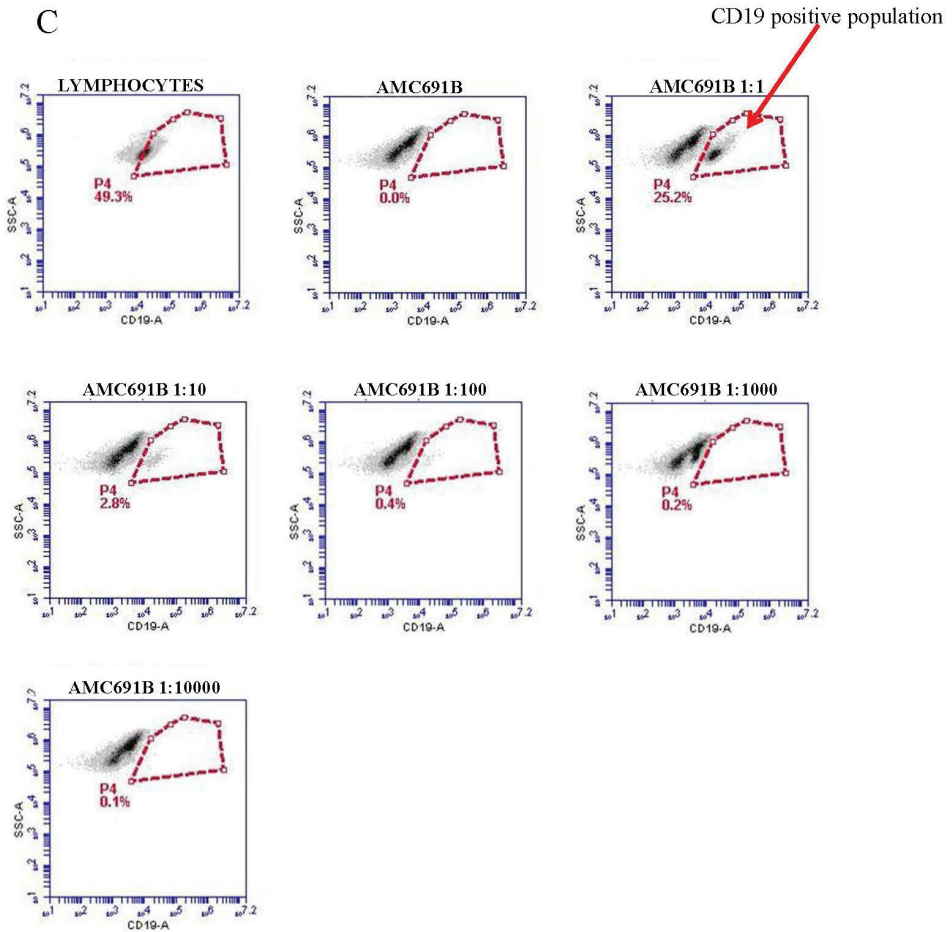


Supplementary Figure 2: MYCN amplification, identification of unique chromosomal breakpoints of neuroblastoma TIC cell lines and flow cytometry analysis of hematopoietic cell surface markers on neuroblastoma TIC cell lines. (A) Zoom in on chromosome 2 bearing the MYCN amplified region in MYCN amplified primary tumors and TIC cell lines. Black line indicates regions of MYCN copy number gains.

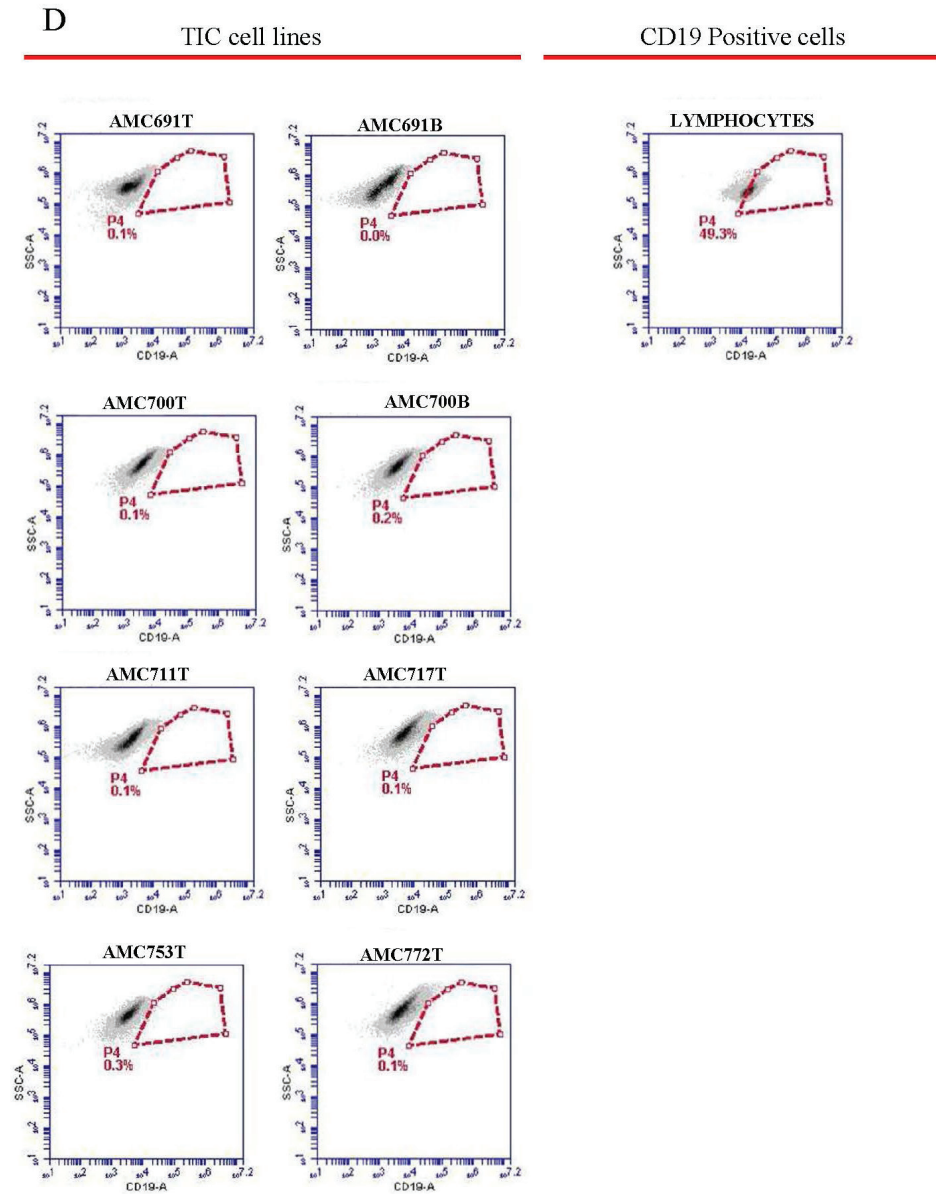
B



Supplementary Figure 2: MYCN amplification, identification of unique chromosomal breakpoints of neuroblastoma TIC cell lines and flow cytometry analysis of hematopoietic cell surface markers on neuroblastoma TIC cell lines. (B) Circos plots of neuroblastoma TICs cell lines with breakpoint regions validated highlighted in red.

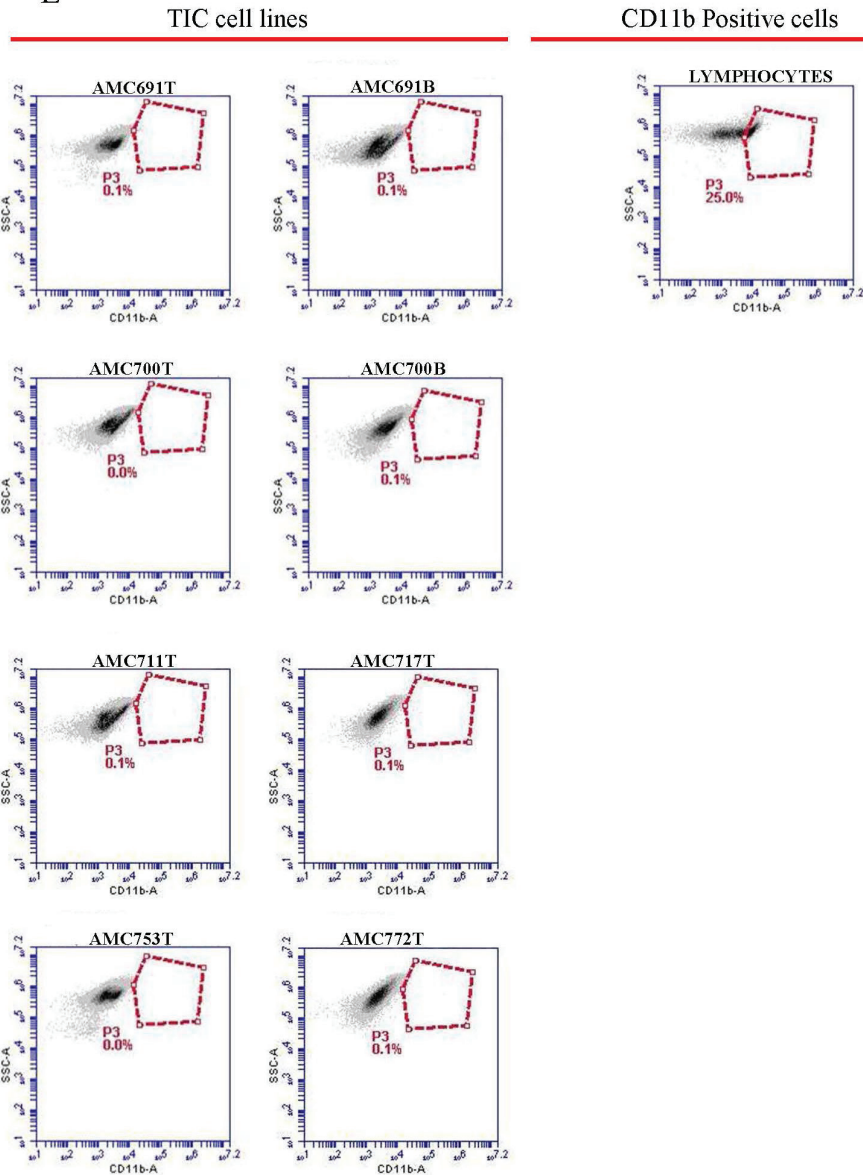


Supplementary Figure 2: MYCN amplification, identification of unique chromosomal breakpoints of neuroblastoma TIC cell lines and flow cytometry analysis of hematopoietic cell surface markers on neuroblastoma TIC cell lines. (C) Flow cytometry analysis of AMC691B spiked with CD19 positive lymphocytes with spiking concentration ranges 1:1, 1:10, 1:100, 1:1000 and 1:10000.



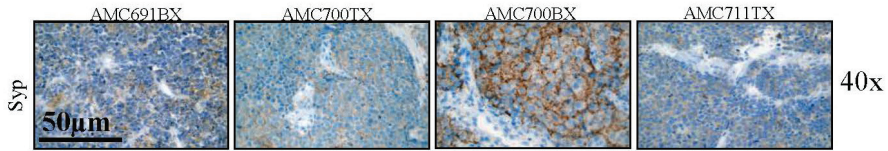
Supplementary Figure 2: MYCN amplification, identification of unique chromosomal breakpoints of neuroblastoma TIC cell lines and flow cytometry analysis of hematopoietic cell surface markers on neuroblastoma TIC cell lines. (D) Flow cytometry analysis of the level of expression of CD19 cell surface markers on TIC cell lines. CD19 lymphocytes served as positive controls.

E

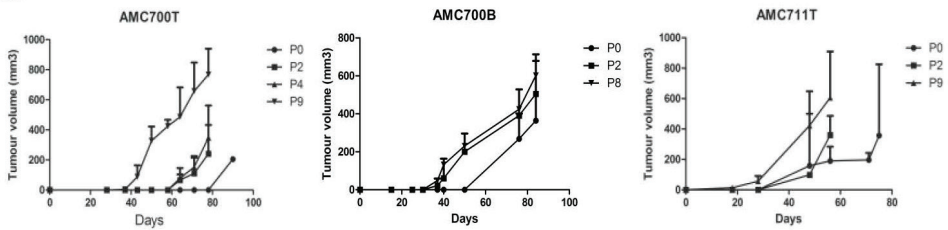


Supplementary Figure 2: MYCN amplification, identification of unique chromosomal breakpoints of neuroblastoma TIC cell lines and flow cytometry analysis of hematopoietic cell surface markers on neuroblastoma TIC cell lines. (E). Flow cytometry analysis of the level of expression of CD11b cell surface marker on TIC cell lines. CD11b lymphocytes served as positive controls.

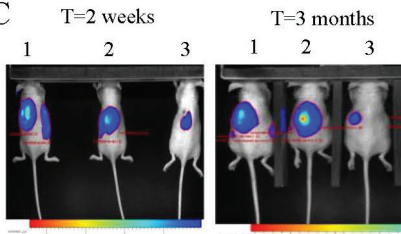
A



B



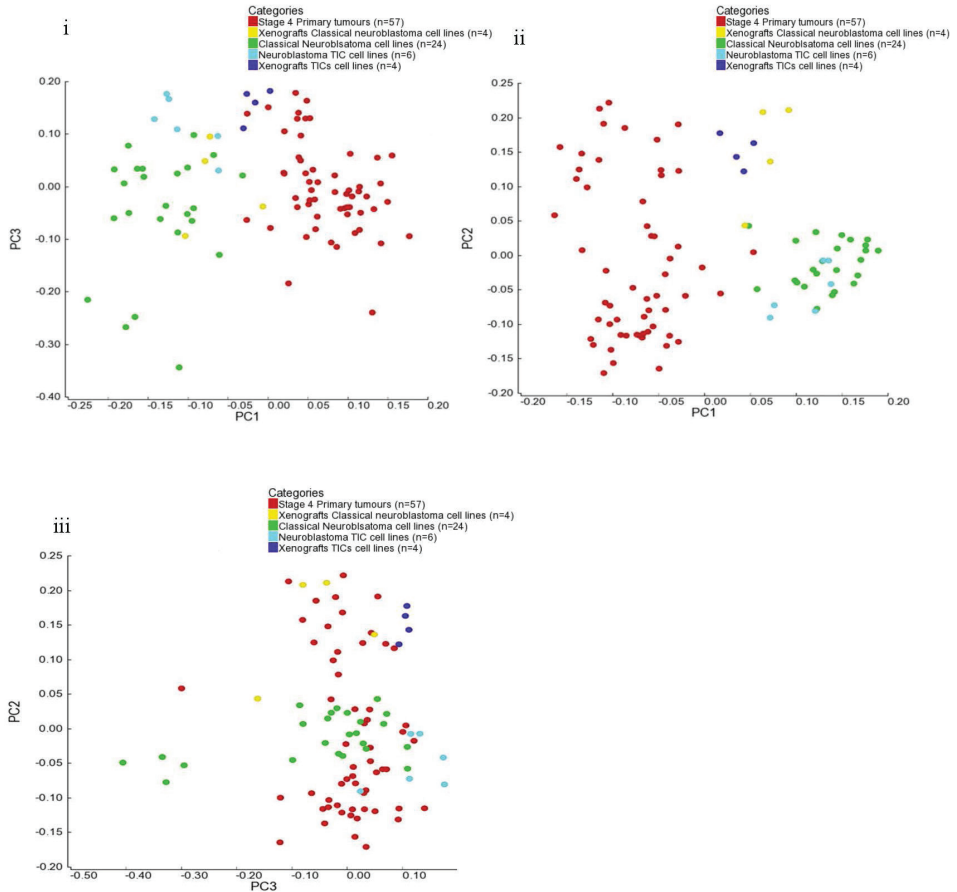
C



Supplementary Figure 3: *In vivo* growth properties and characterization of neuroblastoma TIC mice xenografts. (A) Immunohistochemistry was performed for Syp for neuroblastomas from AMC691BX, AMC700TX, AMC700BX and AMC711TX. (B) Serial xeno-transplantation of mice tumor pieces of AMC700TX, AMC700BX and AMC711TX into secondary and tertiary recipients was performed to improve tumor engraftment. The y-axis represents tumor volume in mm³. (C) Intensity of luc2 AMC711T cells in adrenal glands of mice viewed with a CCD camera.

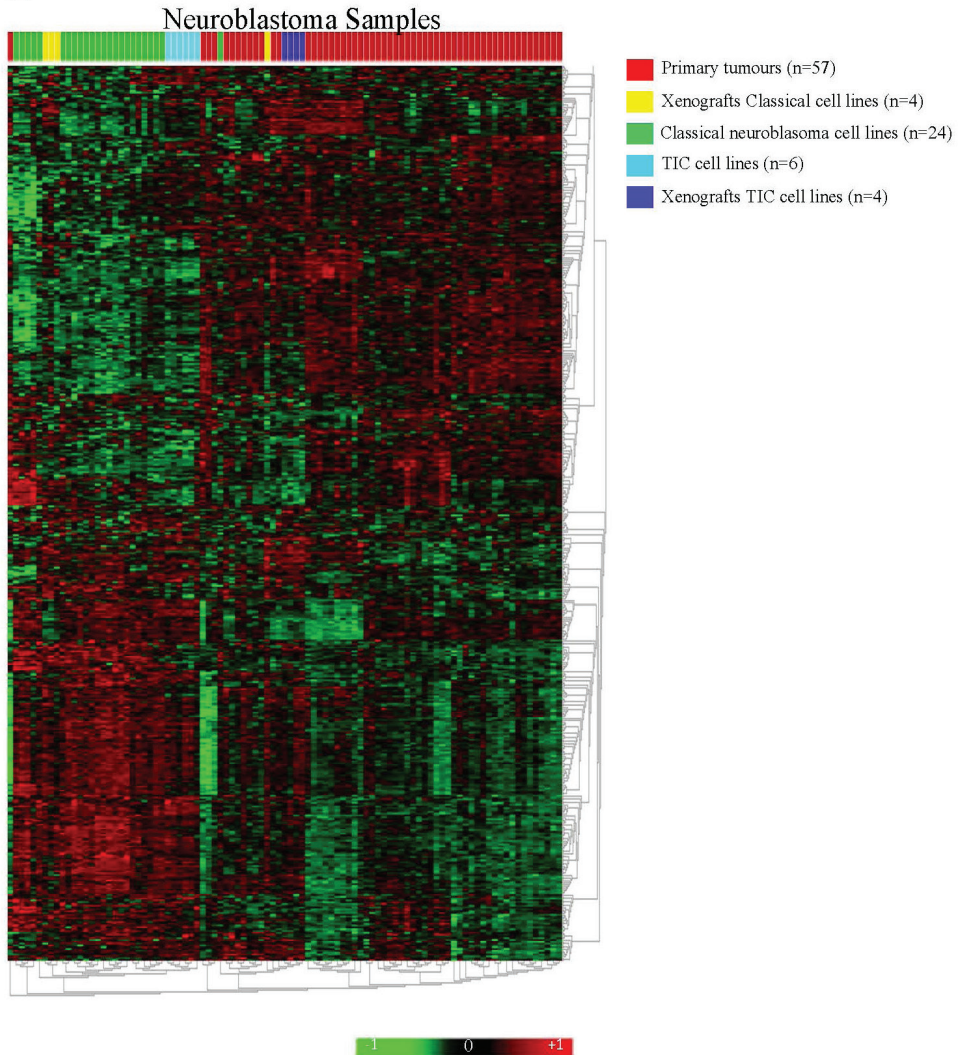
Newly-derived neuroblastoma cell lines propagated in serum-free medium recapitulate the genotype and phenotype of primary neuroblastoma tumours

D



Supplementary Figure 3: *In vivo* growth properties and characterization of neuroblastoma TIC mice xenografts. (D) Principal component analysis of 57 stage 4 neuroblastoma tumors, xenografts from classical cell lines and xenografts from TIC cell lines (n=8) in three different components; PC2:PC1, PC3:PC1 and PC2:PC3(i-iii).

E



Supplementary Figure 3: *In vivo* growth properties and characterization of neuroblastoma TIC mice xenografts. (E) Euclidian distance cluster analysis of *in vivo* TICs and Classical neuroblastoma cell line xenografts (n=8), stage 4 primary neuroblastoma samples (n=57), neuroblastoma TIC cell lines (n=6) and classical neuroblastoma cells (n=24). The expression level of a given gene is indicated in red.

Newly-derived neuroblastoma cell lines propagated in serum-free medium recapitulate the genotype and phenotype of primary neuroblastoma tumours

Cell line	Breakpoint	Nucleotide sequence	Product size
AMC691T	Deletion chromosome 11	5'-TCCCTTATAAGATGACCATCCC-3' 5'-CCAATTAAGGCAAAGATTGG-3'	199bp
AMC691B	Translocation (9;16)	5'-GTTAGCCTTGGTCACGGAG-3' 5'-GGAGGCTGAGTCTCGGTGT-3'	194bp
AMC700T AMC700B	Translocation (1;17)	5'-TGCTCAAACACCAATACATGC-3' 5'-TGAGAATCGAGGTCTCAGCA-3'	244bp
AMC700B	Deletion chromosome 2	5'-GAAGTTGGGTGGAGGAGTCA-3' 5'-TGGTTAGACTGGGATTGTTC-3'	160bp
AMC711T	Translocation (1;6)	5'-CCTGGGCAACAAAGTGAGAC-3' 5'-TCCTTCTCCTCACTCCTCCA-3'	204bp
AMC717T	Translocation (7;17)	5'-CAGCACCTCTCCTGAAACAA-3' 5'-CTTTTCTCCACAGCCTCACC-3'	164bp
AMC753T	Translocation (11;17)	5'-TAGTGAGCACCAGGCGATTG-3' 5'-CTGCGGTCTGTTCTCAACAT-3'	197bp
AMC772T	Translocation (11;21)	5'TAAAGATGTCCAACCAGGGC-3' 5'-GCTCAGTCTCCCTCACCT-3'	189bp

Supplementary Table 1: Primer sequences used for breakpoint identification and chromosomal location of each breakpoint in each cell line.

	D3S1358	TH01	D21S11	D18S51	PentaE	D5S818	D13S317	D7S820	D169S539	CSF1PO	PentaD	Amel	Vwa	D8S1179	TPOX	FGA
AMC691T	14,15	7,9,3	29,31,2	14,18	7,13	10,11	9,14	9,12	9	10,11	12,13	X	18,19	16	8	21,22
AMC691B	14,15	7,9,3	29,31,2	14,18	7,13	10,11	9,14	9,12	9	10,11	12	X	18,19	16	8	21,22
AMC700T	14,17	7,9,3	29,31	12,16	13,17	10,12	11,12	8,10	9,11	12	10,11	X	14,15	12,16	8	18,20
AMC700B	14,17	7,9,3	29,31	12,16	13,17	10,12	11,12	8,10	9,11	12	10,11	X	14,15	12,16	8	18,20
AMC711T	16,17	7,9,3	31,2,32,3	14,18	7,12	12,13	11,12	8,9	11,12	10,11	10,13	X,Y	17,18	13,14	8	20,22
AMC717T	15,16	6,9,3	16,18	11,18	11,18	11	11,13	8,9	9,13	11,12	13,14	X,Y	16,18	11,14	8,9	20,21
AMC753T	11,18	9,9,3	28,31,2	14,18	17,20	12,13	12	11	10,11	11,12	13	X,Y	14,18	10,15	10,12	20,23
AMC772T	16,19	9,3	28	12,13	14,15	12	12,14	8,10	12,13	10,12	9	X,Y	16,17	10,13	8,10	19,23

Supplementary Table 2: Allelic determinants of neuroblastoma TIC cell lines relative to a reference DNA sample.

Newly-derived neuroblastoma cell lines propagated in serum-free medium recapitulate the genotype and phenotype of primary neuroblastoma tumours

Cell line	Subcutaneous (% engrafted)	Orthotopic (% engrafted)
NMRI nu/nu		
AMC691T	0	ND
AMC691B	60	ND
AMC700T	41	ND
AMC700B	33	ND
AMC711T	67	ND
AMC717T	ND	ND
AMC753T	0	ND
AMC772T	ND	ND
NOD-SCIDS		
AMC691T	0	ND
AMC691B	ND	66
AMC700T	75	ND
AMC700B	66	ND
AMC711T	ND	ND
AMC717T	33	ND
AMC753T	0	ND
AMC772T	100	80

Supplementary Table 3: Overview of xenografting procedures and tumor take rates of all TIC lines in NMRI *nu/nu* and NOD-SCID mice.

SUPPLEMENTARY MATERIALS AND METHODS

1. Protein isolation and western blot and FACS analysis

Cell lysates were resuspended in laemmli lysis buffer (25ml H₂O, 5ml 1M Tris /HCl pH 6.8, 10ml 100% Glycerol, 10ml 20% SDS, with bromophenol blue) containing protease inhibitors. Lysates 15µg per lane were applied to SDS-PAGE. Immunoblotting of antibodies specific for Chromogranin A (1:10000 Abcam), Neural Cell Adhesion Molecule (1:10000 Millipore), Dopamine Beta Hydroxylase (1:1000 Cell Signalling), Tyrosine Hydroxylase (1:1000 Santa Cruz), CD11b (1:20000 Abcam), CD19 (1:1000 Dako), MYCN (1:5000 BD Pharmingen) and B-actin (1:5000 Abcam) were detected using HRP-conjugated anti-mouse or anti-rabbit Abs (Amersham) and Licor 800 mouse and rabbit secondary antibodies and visualized using the Odyssey LI-COR system (LI-COR BIOSCIENCES GmbH) and the Image Quant LAS 4000 mini system (GE Healthcare).

For FACS analysis, neuroblastoma TIC cell lines were harvested and rendered single celled using the Neurocult Chemical Dissociation Kit (Stem Cell Technologies). Cells were washed with FACS staining buffer (1% BSA, 0.5mM EDTA in PBS) and stained with CD11b (10µl BD Bioscience) and CD19 (2,5µl Abcam) and incubated at 4°C in the dark for 20 minutes. FACS analysis was carried out immediately using a BDAccuri flow cytometer (BD Biosciences).

2. Immunohistochemistry

Immunohistochemistry was performed on 4µM paraffin-embedded sections heated in an antigen retrieval solution (citrate buffer pH 6.0). Endogenous peroxidase activity was inhibited by incubation with 30% hydrogen peroxide (20 min, RT) and the non-specific sites blocked with PBS/BSA 0, 25% (10 mins, RT). CHGA (Abcam, USA) and NCAM (Abcam, USA) were detected by incubating tissue sections overnight at 4°C with primary antibodies. Sections were washed with TBS and incubated with anti-mouse or anti-rabbit immunoglobulins/horse rabbit peroxidase for 30 min at room temperature (DPVR-55HRP, DPVM-55HRP, Counterstaining of the slides was performed with haematoxylin and antibodies were detected using a DAB detection system (Ventana, USA).

3. Microsatellite typing and breakpoint PCR

DNA was harvested from primary neuroblastoma cell lines by the chloroform/isopropanol method as previously described¹⁸. Microsatellite typing was performed

Newly-derived neuroblastoma cell lines propagated in serum-free medium recapitulate the genotype and phenotype of primary neuroblastoma tumours

with 10ng of DNA using the PowerPlex 16 system (Promega Corp) and results were analysed using the GeneMapper software (Applied Biosystems). The following Loci were amplified; Penta E, D18S51, D21S11, TH01, D3S1358, FGA, TPOX, D8S1179, vWA, Amelogenin, Penta D, CSF1P0, D16S539, D7S820, D13S317 and D5S818.

For breakpoint PCR, 10ng genomic DNA was used as templates for the amplification of breakpoint regions with 5ng of primers specific for each breakpoint PCR conditions were as follows: initial DNA denaturation for 3 minutes 95°C followed by 35 cycles consisting of 30 seconds of denaturation at 94°C, 30 seconds annealing at 58°C and 30 seconds of primer extension at 72°C. 10µl of PCR reactions were analysed by agarose gel electrophoresis (1% agarose) followed by ethidium bromide staining.

4. Sphere forming assays

For neurosphere culture, 2500 primary NB cells were seeded in ultra-low attachment 24 well plates (Corning) in 1% methylcellulose and spheres were counted as soon as they reached 25-200µM in diameter.

5. Data analysis

Segmentation by DNA copy using the bioconductor package was performed in-house before generation of a heat map for chromosome gains and losses. A copy number gain was defined as a 2log ratio >0,5 and a copy number loss was defined as a 2log ratio <0,5.

For the generation of WGS data, the somatic structural variants were compared between the TIC cell lines and the lymphocytes from the patients using the JunctionDiff and the Junction2Event tool from CGA tools. The somatic events were filtered based on the following criteria: events noted as artefacts, footprints less than 70 bases, smaller than 10 discordant mate pairs, under-represented repeats and present in a set of v2.0 baseline genomes.

WGS data for the primary tumours is deposited in the European Genome-phenome Archive and available under accession number EGAS00001000222.

PCA was performed in R based on mRNA expression data normalized with a MAS5.0 software and visualized with the R2 software program.



CHAPTER 3

ENHANCER OF ZESTE HOMOLOGUE 2 PLAYS AN IMPORTANT ROLE IN NEUROBLASTOMA CELL SURVIVAL INDEPENDENT OF ITS HISTONE METHYLTRANSFERASE ACTIVITY.

Authors: Laurel T. Bate-Eya¹, Hincó J. Gierman²,
Marli E. Ebus¹, Jan Koster³, Huib N. Caron², Rogier Versteeg³,
M. Emmy M. Dolman¹ and Jan J. Molenaar¹

¹Department of Translational Medicine, Prinses Máxima Center for Pediatric Oncology, Utrecht, ²Department of Pediatric Oncology, Emma Kinderziekenhuis, and ³Departments of Oncogenomics Academic Medical Center, University of Amsterdam, Amsterdam, the Netherlands.

European Journal of Cancer (2017)

ABSTRACT

Neuroblastoma is predominantly characterized by chromosomal rearrangements. Next to MYCN amplification, chromosome 7 and 17q gains are frequently observed. We identified a neuroblastoma patient with a regional 7q36 gain, encompassing the enhancer of zeste homologue 2 (EZH2) gene. EZH2 is the histone methyltransferase of lysine 27 of histone H3 (H3K27me3) that forms the catalytic subunit of the polycomb repressive complex 2 (PRC2). H3K27me3 is commonly associated with the silencing of genes involved in cellular processes such as cell cycle regulation, cellular differentiation and cancer. High EZH2 expression correlated with poor prognosis and overall survival independent of MYCN amplification status.

Unexpectedly, treatment of three EZH2-high expressing neuroblastoma cell lines (IMR32, CHP134 and NMB), with EZH2-specific inhibitors (GSK126 and EPZ6438) resulted in only a slight G1 arrest, despite maximum histone methyltransferase activity inhibition. Furthermore, colony formation in cell lines treated with the inhibitors was reduced only at concentrations much higher than necessary for complete inhibition of EZH2 histone methyltransferase activity.

Knockdown of the complete protein with three independent shRNAs resulted in a strong apoptotic response and decreased cyclin D1 levels. This apoptotic response could be rescued by overexpressing EZH2 Δ SET, a truncated form of wild-type EZH2 lacking the SET transactivation domain necessary for histone methyltransferase activity.

Our findings suggest that high EZH2 expression, at least in neuroblastoma, has a survival function independent of its methyltransferase activity. This important finding highlights the need for studies on EZH2 beyond its methyltransferase function and the requirement for compounds that will target EZH2 as a complete protein.

INTRODUCTION

Overexpression of the Enhancer of zeste homologue 2 (EZH2) gene has been associated with tumourigenicity in numerous solid tumour types (1-7) and gain-of-function point mutations in the catalytically active SET domain of EZH2 has been recognized in B-cell and T-cell lymphomas(8-16). Genetic loss-of-function studies have demonstrated a crucial role of EZH2 in the establishment of cell fate decisions in the skin, heart and mammary glands(17). EZH2 together with suppressor of zeste 12 (SUZ12) and embryonic ectoderm development (EED) forms part of the Polycomb repressive complex 2 (PRC2), which mediates the silencing of genes by trimethylation of lysine 27 on histone H3 (H3K27me3) (18, 19). This H3k27me3 mark has been found in genes that play a key role in cellular processes such as cell differentiation, cell cycle regulation and oncogenesis (20-22). However, recent studies suggest that EZH2 directly binds to the promoter regions of certain genes and acts as a transcriptional co-activator independent of its histone methyltransferase enzymatic activity (23-25).

Neuroblastoma is a neuroendocrine tumour that arises from the peripheral nervous system (26). It is the most commonly diagnosed extracranial solid cancer in children, accounting for approximately 15% of all pediatric cancer deaths (27, 28). Chromosome 17q gain, partial loss of chromosome 1p or 11q and MYCN amplification are frequently observed genetic aberrations in neuroblastoma tumours (29). EZH2 is located on chromosome 7q35 and frequent gains of whole chromosome 7 have been observed in neuroblastoma (30, 31). A functional role for EZH2 in neuroblastoma was reported whereas EZH2 caused histone hypermethylation in the promoter regions of known tumour suppressor genes CASZ1, CLU, RUNX3 and NGFR resulting in the silencing and downregulation of these genes (32). In the current study, we show that pharmacological inhibition of EZH2 histone methyltransferase activity (33-36) only causes limited inhibitory effects on cell cycle progression, while silencing of the whole protein causes a strong apoptotic phenotype. We overcame apoptosis caused by EZH2 silencing by overexpressing a truncated form of wild-type EZH2 lacking histone methyltransferase activity. These findings highlight the importance of EZH2 for the survival of neuroblastoma cells independent of its histone methyltransferase activity and development of compounds that inhibit EZH2 protein as a whole might be beneficial for the treatment of neuroblastoma patients with high EZH2 expression.

2. MATERIALS AND METHODS

2.1. Patient samples, RNA isolation and profiling.

RNA was extracted from 88 tumours with TRIzol (Invitrogen, Carlsbad, CA) following the manufacturer's protocols. RNA concentration and quality were determined using the RNA 6000 Nano assay on the Agilent 2100 Bioanalyzer (Agilent Technologies). Fragmentation of cRNA, hybridization to Human Genome U133 Plus 2.0, microarrays and scanning were carried out according to the manufacturers protocol (Affymetrix inc. Santa Barbara, CA). mRNA gene expression data were normalized with the MAS5.0 algorithm within the GCOS program of Affymetrix Inc. Target intensity was set to 100. All data were analyzed using the bioinformatics platform R2 (<http://r2.amc.nl>). As a reference dataset, an RNAseq data set of 498 neuroblastoma tumors was used. Data was derived from GEO database under number gse 62564(37).

2.2 Array CGH analysis.

Array CGH was performed by hybridizing 100 ng genomic DNA to a 180K platform (Agilent Technologies). DNA was labelled by random priming with CY5-dCTP and CY3-dCTP respectively and hybridized at 65°C for about 17 h. Chips were scanned on an Agilent G2565BA DNA microarray Agilent scanner. Data processing was performed using the bioinformatics platform R2. Circular binary segmentation (CGHcall package in R) was used for scoring the regions of gain, amplification and deletion. Testing for elevated EZH2 expression of tumours with 7q gain versus no gain tumours was determined using a one-tailed Student's t-test for equal variance.

2.3. Cell culture and compound exposure assays.

Classical human neuroblastoma cell lines and neuroblastoma tumour-initiating cell (TIC) lines were cultured as previously described (38). Cell culture protocols are described in detail in the Supplementary Materials and Methods.

Neuroblastoma cell lines were seeded in triplicate in 6-well plates using the most optimal confluency for each cell line. Cells were incubated overnight and treated with 1 nmol/L to 100 µmol/L GSK126 or EPZ6438. Control samples were treated with 0.5% DMSO. After 72 h, cells were transferred to 96-well plates (classical cell lines) or 48-well plates (TIC lines) and incubated with the compounds for another 72 h. Cell viability was determined prior to and after 144 h treatment using the 3-(4,5-dimethylthiazol-2-yl)-2,5-diphenyltetrazolium bromide (MTT) colorimetric assay (39). Half maximal effective

concentration (IC_{50}) values were derived from dose-response curves. IC_{50} values at 144 h were calculated by determining the GSK126 or EPZ6438 concentrations needed to achieve a 50% reduction in cell viability observed for DMSO-treated cells at 144 h (set at 100%) using the GraphPad Prism software.

2.4. Western blotting.

Cells were lysed using Laemmli buffer (i.e. H_2O /glycerol/20% sodium dodecyl sulfate (SDS)/1 M Tris-HCl (pH 6.8) 5:2:2:1 (v/v/v/v)) containing protease inhibitors. Equal protein amounts (i.e. 40 μ g) were separated by SDS- polyacrylamide gel electrophoresis (SDS-PAGE). The following primary antibodies were used: rabbit anti-human EZH2 (Clone 4905) monoclonal antibody (1:10,000, Cell Signaling Technology), rabbit anti-human tri-methyl histone lysine 27 (clone C3B6B11) monoclonal antibody (1:1,000, Cell Signaling Technology), rabbit anti-human total H3 (Clone 9715) polyclonal polyclonal (1:1,000, Cell Signaling Technology), rabbit anti-human PARP (Clone 9542S) monoclonal antibody (1:1,000, Cell Signaling Technology), mouse anti-human cyclin D1 monoclonal antibody (1:1,000, Thermo Scientific) and mouse anti-human β -actin (clone AC-15) monoclonal antibody (1:5,000, Abcam). Horseradish peroxidase (HRP)-conjugated goat anti-rabbit (clone NA9340V) and goat anti-mouse (clone NXA931) secondary antibodies (1:10,000 GE Healthcare) were used prior to visualization with the Image Quant LAS 4000 mini system (GE Healthcare). (Amersham) IRDye 800CW goat anti-rabbit and goat anti-mouse secondary antibodies (1:5,000, Li-COR) were used prior to visualization on the Li-COR Odyssey.

2.5. FACS analysis.

Neuroblastoma cell lines IMR32, CHP134 and NMB were seeded in triplicates in 6-cm plates and incubated overnight. Cells were then treated for 72 h with 0.01% DMSO (control), GSK126 (62.5 nmol/L - 2 μ mol/L) or EPZ6438 (62.5 nmol/L - 2 μ mol/L). Floating and adherent cells were subsequently harvested for FACS analysis to determine the cell-cycle distribution and the apoptotic subG1 fraction. See Supplementary Materials and Methods for a detailed protocol.

2.6. Colony forming assays.

IMR32, CHP134 and NMB (5×10^3 cells per well) were resuspended in 500 μ L DMEM containing 0.4% low melting point agar and seeded in duplicate in 24-wells plates coated overnight with 1% low melting point agar in DMEM containing 4% serum. GSK126 and EPZ6438 were diluted to final concentration ranges of 32.5 nM - 2 μ M in 0.4%

low melting point soft agar and added to the corresponding wells. Control wells were treated with 0.1% DMSO in 0.4% low melting point soft agar. Colonies were allowed to form for 14 d and stained with 5 mg/mL MTT dissolved in 4% serum containing DMEM. Number of colonies were scored by the Image J quantification software (U.S. National Institute of Health).

2.7. Cell Transduction

IMR32, CHP134 and NMB were seeded onto 6-cm dishes (2×10^5 cells in 5 mL culture medium) and incubated overnight. Next, cells were transduced with non-targeting shRNA (AACAAAGATGAAGAGCACCAA; negative control), EZH2 shRNA specifically targeting the coding sequence and the 3'UTR region of the gene (TRCN0000040073, TRCN0000040074, TRCN0000040076, TRCN0000293738 and TRCN0000286227) using the pLenti VI system or with EZH2 Δ SET (which was donated by Dr. Marian Martínez-Balbás at the Department of Molecular Genomics of the Barcelona Molecular Biology Institute, Spain) using the pInd system according to the manufacturers protocol (Sigma Aldrich). After 72 h overexpression and knockdown, cells were harvested for FACS and Western blot analysis as described above.

3. RESULTS

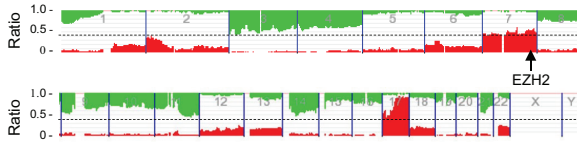
3.1. Gain of 7q36 correlates to EZH2 over-expression in neuroblastoma.

Evaluation of the frequency distribution of all chromosomal gains and losses in 87 neuroblastoma showed that most frequent gains occur in chromosomes 17 and 7 (Fig. 1A). The gain of chromosome 7 mostly involved the complete chromosome, however we identified 1 neuroblastoma tumour with a 785 kb regional gain, forming a SRO harbouring only 10 genes located at chromosome 7q36 (Fig. 1B) including EZH2. Affymetrix mRNA expression profiling of the same neuroblastoma tumour series showed that the tumour with the regional gain harbouring EZH2 on 7q36 had the highest EZH2 gene expression (Fig. 1C). Neuroblastoma tumours harbouring increased chromosome 7 copy number and also shows significant higher expression of EZH2 than tumours with no gain in chromosome 7 ($P = 5.6 \times 10^{-3}$) (Fig. 1D). These results suggest that the gain on DNA level contributed to EZH2 overexpression. Next we analyzed EZH2 Affymetrix mRNA expression data of 2,448 tumour samples representing 13 different tumour types and 504 samples of 9 types of normal tissues. Average EZH2 mRNA levels in neuroblastoma were significantly higher than the average EZH2 mRNA expression levels found in

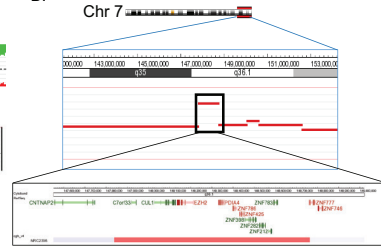
multiple other tumour types ($P=1.9 \times 10^{-22}$) and normal tissues ($P=3.9 \times 10^{-7}$) (Fig. 1E). In order to establish the clinical relevance of EZH2 in neuroblastoma, we analysed whether EZH2 expression correlates to prognosis in the 88 neuroblastoma series. Kaplan-Meier analysis of overall survival shows that EZH2 expression is significantly associated with poor prognosis ($P=3.7 \times 10^{-04}$) (Fig. 1F). These results were confirmed in a publicly available cohort of 493 tumours ($P=1.5 \times 10^{-05}$) (Supplementary Fig. 1D). Previous studies have shown a correlation between MYCN amplification and EZH2 status which we could confirm in the larger cohort ($p=0.41$ and 1.5×10^{-05}) (Supplementary Fig. 1F). Independent of MYCN amplification EZH2 expression was still correlated to a poor prognosis in non-MYCN-amplified tumors ($p=5.2 \times 10^{-05}$) (Supplementary Fig. 1E). However, EZH2 should not be considered as an independent prognostic factor in neuroblastoma. Together, these analyses show that EZH2 is highly expressed in neuroblastoma compared to other tumour types and normal tissues. Our data also suggests that gain of chromosome 7 contributes to overexpression of the gene.

Chapter 3

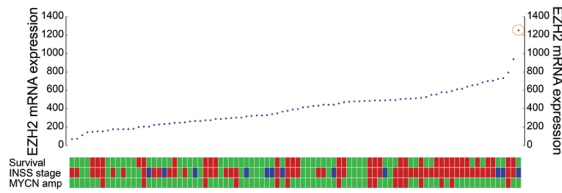
A.



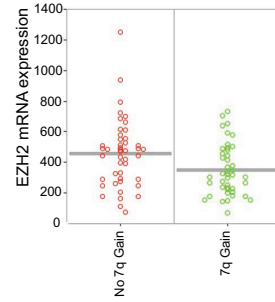
B.



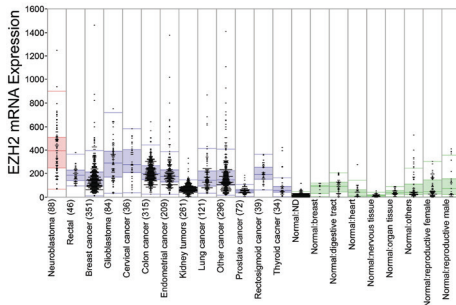
C.



D.



E.



F.

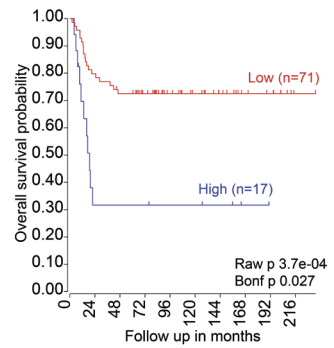


Figure 1. Array CGH and mRNA expression analysis of EZH2 in neuroblastoma tumours. (A) Summary of CGH analysis of 87 neuroblastoma tumours showing the frequency of gains (red) and losses (green) per chromosome (horizontal). The y-axis indicates the overall gains and losses per region. The arrow indicates the EZH2 gene locus. (B) Close-up view of CGH analysis of the neuroblastoma tumour N167T with a local gain of the EZH2 locus. A cytogenetic map of the chromosome 7 is shown above with a blue box indicating the region shown below. CGH log-fold ratios are shown per probe (gray; no significant gain or loss; black significant gain or loss). The red line indicates the moving average over 5 probes. Below; chromosomal position in Mb and cytogenetic map. The blue box indicates the gained region of 785 kb encompassing EZH2. Below; a zoom-in of the gained region harbouring the EZH2 locus showing 10 genes including EZH2 in this region. (C) Overview of EZH2 mRNA expression levels measured by Affymetrix 133 plus 2.0 array analysis in 88 neuroblastoma tumours. Tumours are ranked by EZH2 expression (y-axis). The x-axis shows Survival (green: alive >5yrs red: death), INSS stage (light green: stage 1; dark green: stage 2; orange: stage 3; red: stage 4; blue: stage 4s) and MYCN amplification (red: ≥ 8 copies of MYCN; green: < 8 copies of MYCN; gray: not informative). The circle indicates tumour N167T with local gain of EZH2. (D) EZH2 Affymetrix 133 plus 2.0 array mRNA expression levels in 87 neuroblastoma tumours (y-axis). Tumours were grouped according to CGH data for chromosome arm 7q as gain (red) or no gain (green) ($P = 5.6 \times 10^{-3}$). A copy number gain was defined as a $2\log$ ratio > 0.5 and a copy number loss was defined as a $2\log$ ratio < -0.5 . (E) Combined box-dot plot of EZH2 Affymetrix 133 plus 2.0 array mRNA expression levels in 12 cancer datasets (blue), 1 neuroblastoma dataset (red) and normal tissues (green) divided in adrenal gland, central nervous system (CNS) tissues and non-CNS tissues. In a combined box-dot-plot every dot represents one sample. The number of tumour samples is given between brackets. The colored boxes represent the area between the 25th and the 75th percentile with a line indicating the median. (F) Kaplan-Meier analysis for overall survival of neuroblastoma patients divided into high and low EZH2 expression groups for all neuroblastoma patients ($n = 88$). Significance is denoted as P -value (p) and Bonferroni corrected P -value (bonf p).

3.2. Inhibition of the histone methyltransferase activity of EZH2 results in a slight G-1 arrest in neuroblastoma.

In order to explore the functional relevance of the histone methyltransferase activity of EZH2 in neuroblastoma, we first established the fitted IC_{50} values of 14 neuroblastoma cell lines treated with two EZH2 specific histone methyltransferase inhibitors EPZ6438 and GSK126 (Table 1 and Supplementary Fig. 1A).

Neuroblastoma cell lines IMR32 and CHP134 responded most potently to EPZ6438 with IC_{50} values in the nanomolar range (i.e. 570 and 670 nmol/L respectively) IMR32 responded most potently to GSK126 (i.e. $IC_{50} = 740$ nmol/L). Although IMR32 and CHP134 do express relatively high levels of EZH2 (Supplementary Fig 1B.), the IC_{50} values of EPZ6438 and GSK126 in the complete neuroblastoma cell line panel did not correlate with EZH2 mRNA expression levels (Supplementary Fig. 1C).

Cell lines	EPZ6438 ($\mu\text{mol/L}$)	GSK126 ($\mu\text{mol/L}$)
IMR32	0.6	0.7
CHP134	0.7	1.1
AMC691B	0.9	4.9
SKNAS	1.1	1.9
AMC106	1.5	1.6
AMC700B	2.1	1.5
AMC772T	2.3	1.1
KCNR	2.5	5.9
NMB	2.6	3.3
SHEP2	3.8	2.7
CAN	3.9	1.1
AMC700T	5.4	1.2
N206	7.4	1.1
AMC691T	8.3	8.0

Table 1. IC₅₀ values of GSK126 and EPZ6438 for neuroblastoma cell lines.

To study the correlation between the phenotype after treatment with EPZ6438 and GSK126 and the histone methyltransferase activity of EZH2, neuroblastoma cell lines IMR32, CHP134 (with low IC₅₀ values) and NMB (with highest expression of EZH2) were treated with increasing concentrations of both compounds and harvested for protein analysis. Treatment with low nanomolar concentrations of EPZ6438 (i.e. 62.5 nmol/L) and high nanomolar concentrations of GSK126 (i.e. 500 nmol/L) was sufficient to almost completely inhibit the methyltransferase activity of EZH2, as was shown by the downregulation of H3K27me3 (Fig. 2A). Strikingly, phenotypically the cells did not show obvious differences under the light microscope, even if cells were treated with high concentrations of the EZH2 inhibitors (supplementary figure 2A). To study the phenotype in more detail we performed flow cytometry for analysis of the cell cycle distribution and apoptotic sub G1 fraction after treatment with 125 nmol/L or 1 $\mu\text{mol/L}$ EPZ6438 and GSK126. A slight increase in the fraction of cells in G1 phase was observed, but only after treatment with the highest dose of both compounds (Fig. 2B and Supplementary Fig. 2B). The minimal phenotypic effects obtained with micromolar concentrations of EPZ6438 and GSK126 were in sharp contrast with the strong inhibition of the EZH2 histone methyltransferase activity obtained with nanomolar concentrations of EPZ6438 and GSK126. We therefore hypothesized that the effect of inhibiting the histone methyltransferase activity on cell viability occurs only after prolonged treatment

of the cell lines with either EPZ6438 or GSK126. Therefore, we performed colony forming assays for 14 days on the three cell lines treated with concentrations whereby target specific inhibition of H3K27me3 is known to occur (125 nmol/L-1 μ mol/L). In line with the effects on G1 arrest, the strongest inhibitory effect on colony formation was obtained after treatment with EPZ6438 and GSK126 only at concentrations much higher than necessary for complete EZH2 histone methyltransferase activity inhibition (i.e. 1 μ mol/L) (Fig. 2C).

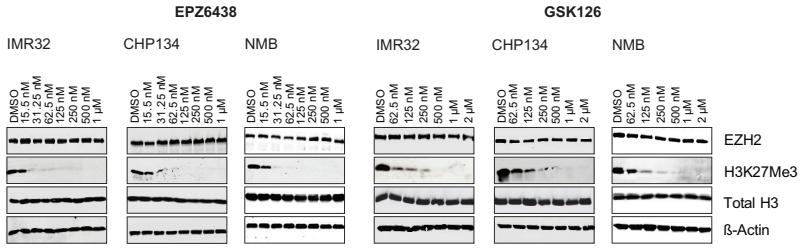
Taken together, these results indicate that, even though EZH2 is known to silence tumour suppressor gene activity through its methyltransferase activity, EZH2 might have other functionally relevant roles, independent of its histone methyltransferase activity, in neuroblastoma.

3.3. Downregulation of EZH2 causes a strong apoptotic response independent of the EZH2 histone methyl transferase activity.

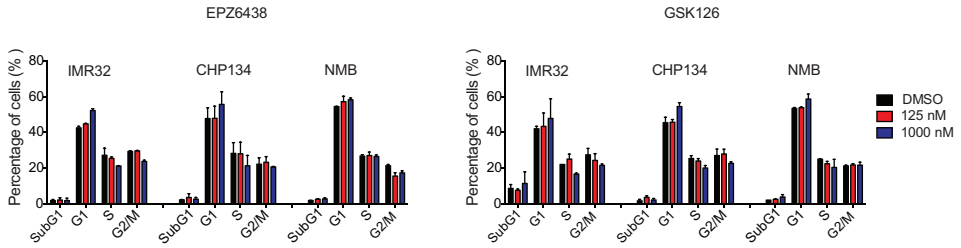
It has previously been reported that the oncogenic role of EZH2 in diffuse B-cell lymphoma and prostate cancer can be independent of its histone methyltransferase activity (23-25). To investigate this for neuroblastoma, we first performed knockdown experiments (T=72h) targeting wild-type EZH2 with three independent shRNA's in the three EZH2 high expressing cells and studied its effect on the cell viability of these cells. Western blot analysis showed that knockdown of the complete EZH2 protein resulted in the downregulation of cyclin D1 and induction of cleaved PARP (Figure 3A). Light microscopy images showed a marked reduction in cell number and increased number of floating cells in all cell lines after EZH2 knockdown with all three shRNAs (Supplementary Fig. 3A). Subsequent cell cycle analysis using flow cytometry indicated a strong increase in the sub-G1 fraction in all three cell lines (Fig. 3B and Supplementary Fig 3B). Both PARP cleavage and sub G1 fraction were indicative for a strong apoptotic response. This was in contrast with the results using targeted compounds inhibiting the EZH2 methyltransferase activity. To determine whether the apoptotic response observed after knockdown of wild-type EZH2 was independent of EZH2 histone methyltransferase activity, we overexpressed an exogenous EZH2 mutant (EZH2 Δ SET) lacking functional histone methyltransferase activity. This was then combined with a knockdown of wild-type EZH2 using two shRNAs specifically targeting the wild-type EZH2 transcript at the 3'UTR.

Chapter 3

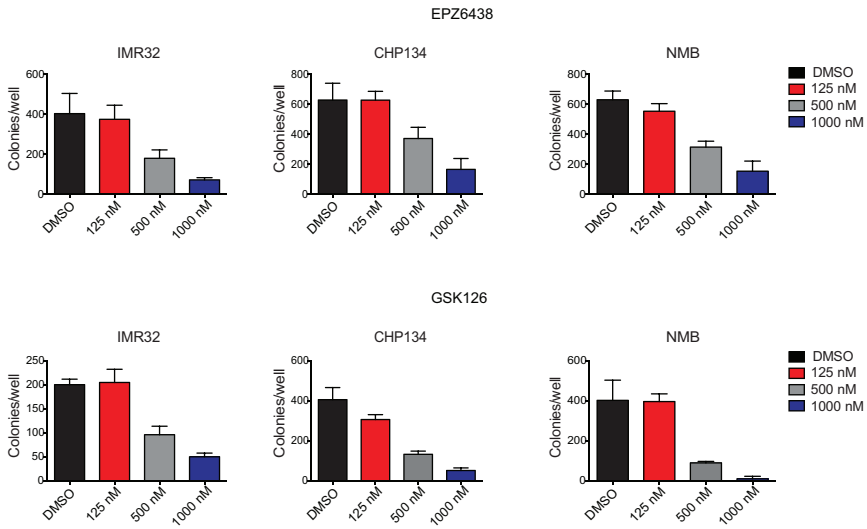
A.



B.



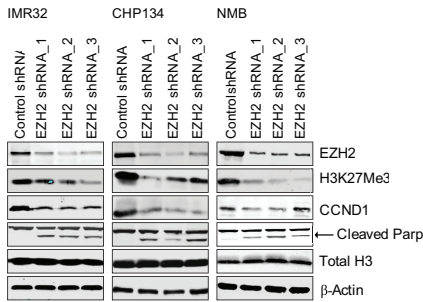
C.



In cell line CHP134 we could show a decrease in cleaved PARP (Fig. 4A) and a reduction in the apoptotic sub-G1 fraction after overexpression of the EZH2 Δ SET, indicative of a partial rescue of the apoptotic phenotype caused by knocking down wild-type EZH2 (Fig. 4B). We thereby concluded that the decrease in the amount of cleaved PARP and the sub-G1 fraction of apoptosis observed was as a result of EZH2 Δ SET taking over the functional role of EZH2 on neuroblastoma cell survival upon depletion of wild-type EZH2 by shRNAs. This highlights an important role of EZH2 in neuroblastoma cell viability independent of its histone methyltransferase activity.

Figure 2. Pharmacological inhibition of EZH2 histone (4)(4)(4)(4)(4)(4)methyltransferase activity by EPZ6438 and GSK126 (A) Western blot analysis of EZH2 high expressing cell lines IMR32, CHP134 and NMB after 72 h treatment with increasing concentrations of EPZ6438 and GSK126. Blots were incubated with EZH2, H3K27Me3 and total H3 antibodies. β -Actin served as loading control for this experiment. (B) Flow cytometric analysis of PI stained nuclei of neuroblastoma cell lines IMR32, CHP134 and NMB. The effects on the cell cycle after 144h treatment with 125 nmol/L and 1 μ mol/L of EPZ6438 and GSK126 are indicated. The data represents the mean percentage of cells \pm SD of three replicate experiments. (C) Colony forming capacity of EZH2 high expressing cell lines IMR32, CHP134 and NMB treated for 14 d with 125nmol, 500nmol and 1 μ mol/L of EPZ6438 and GSK126. The data represents the mean number of colonies per well \pm SD of two replicate wells per concentration of both compounds.

A.



B.

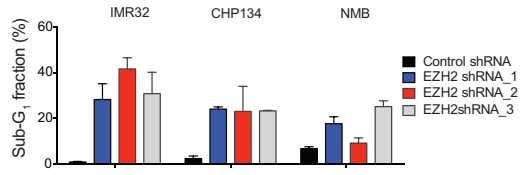


Figure 3. EZH2 knockdown by shRNA in EZH2 high expressing cell lines. (A) Western blot analysis of IMR32, CHP134 and NMB 72 h after transduction with lentivirus targeting EZH2 (i.e. EZH2 shRNA_1, EZH2 shRNA_2 and EZH2 shRNA_3) and control shRNA. Blots were incubated with EZH2, H3K27Me3, CCND1, total PARP and total H3 antibodies. β -actin served as loading control for this experiment. (B) Flow cytometric analysis of PI stained nuclei of neuroblastoma cell lines IMR32, CHP134 and NMB 96 h after lentiviral transduction with three shRNA's targeting EZH2 and a control shRNA. Data represent the mean percentages of cells in sub-G₁ \pm SD of three replicate experiments.

EZH2 plays an important role in neuroblastoma cell survival independent of its histone methyltransferase activity

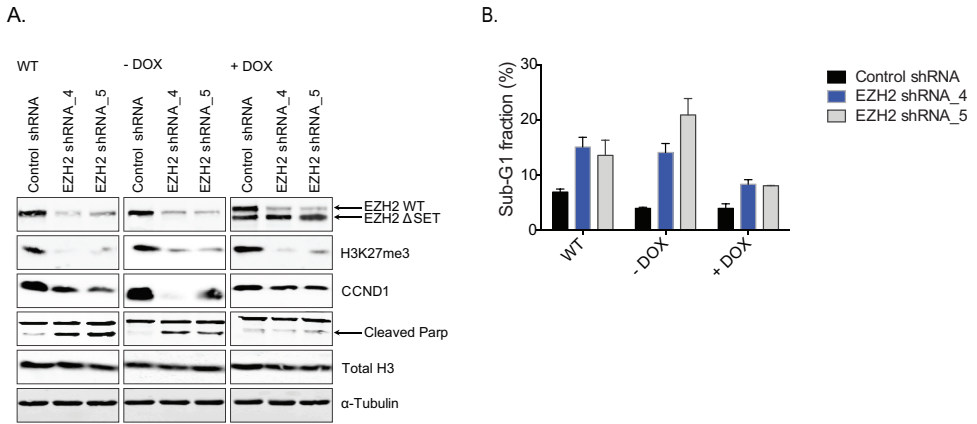


Figure 4. Overexpression of an exogenous EZH2 Δ SET mutant upon depletion of wild-type EZH2. (A) Western blot analysis showing simultaneous overexpression of an exogenous EZH2 mutant form lacking histone methyltransferase activity and knockdown of wild-type EZH2 in CHP134 72 h after transduction with two shRNA specifically targeting wild-type EZH2 (EZH2 shRNA_4 and EZH2 shRNA_5) and control shRNA. Blots were incubated with EZH2, H3K27Me3, CCND1, total PARP and total H3 antibodies. α -tubulin served as a loading control for this experiment. (B) Flow cytometric analysis of PI stained nuclei of the neuroblastoma cell line CHP134 after 72 h overexpression of an exogenous EZH2 Δ SET mutant and lentiviral transduction of CHP134 with two shRNA's targeting wild-type EZH2 and a control shRNA. Data represent the mean percentages of cells in sub-G₁ \pm SD of three replicate experiments.

4. DISCUSSION

It has previously been reported that EZH2 plays a key role in the silencing of tumour suppressor genes through methylation of H3K27me3 in the promoter region of these genes in neuroblastoma (32, 40). In this study, we show that EZH2 is aberrantly gained and overexpressed in neuroblastoma tumours and that patients with high EZH2 expression have a poor prognosis. However, this is not independent of other prognostic factors as previously reported (41). In agreement with its described function, we found that the EZH2 specific histone methyltransferase inhibitors GSK126 and EPZ6438 strongly downregulated H3k27me3 in EZH2 high expressing cell lines. Interestingly, only a slight G1-arrest of the cell cycle and a mild reduction in colony formation was observed at biologically relevant compound concentrations. A more explicit inhibition of colony formation only occurred at higher concentrations. This suggests that this is due to off-target effects of both compounds at these concentrations. However, it has recently been reported that combined inhibition of DNA methylation with a DNA demethylating agent 5-aza-2'-deoxycytidine and the EZH2 histone methyltransferase-specific inhibitor EPZ6438 re-induced the expression of tumour suppressor genes suggesting that combining DNA demethylating agents with histone methyltransferase inhibitors might be a therapeutic effective option in neuroblastoma (41).

Additionally, we observed a strong apoptotic response in neuroblastoma cells upon inhibition of the total EZH2 protein which was largely independent of EZH2 methyltransferase activity. Alternative oncogenic functions of EZH2 have been described previously. First EZH2 was shown to function as a transcriptional activator but this required an intact methyltransferase domain (24). More recent papers have shown oncogenic functions of EZH2 independent of the methyltransferase activity (23, 25). In Natural Killer/T-cell lymphoma this required an intact PRC2 complex and functioned through direct transcriptional activation of CCND1 (Cyclin D1). In our study, we could show a downregulation of CCND1 after knockdown of EZH2 which suggests involvement of a similar mechanism. In SWI/SNF mutant cancers the majority of tumours showed EZH2 dependence which required an intact PRC2 complex but was independent of EZH2 methyltransferase activity. This resulted in insensitivity to EZH2 methyltransferase activity inhibitors. Neuroblastoma might mimic these tumour types where frequent mutations in SWI/SNF genes ARID1A and ARID1B have recently been shown to occur frequently in this tumour type (42).

EZH2 plays an important role in neuroblastoma cell survival independent of its histone methyltransferase activity

Our findings of an oncogenic role of EZH2 in neuroblastoma independent of its methyltransferase activity, highlights also the need for the development and testing of therapeutics which specifically target the EZH2 protein as a whole (43).

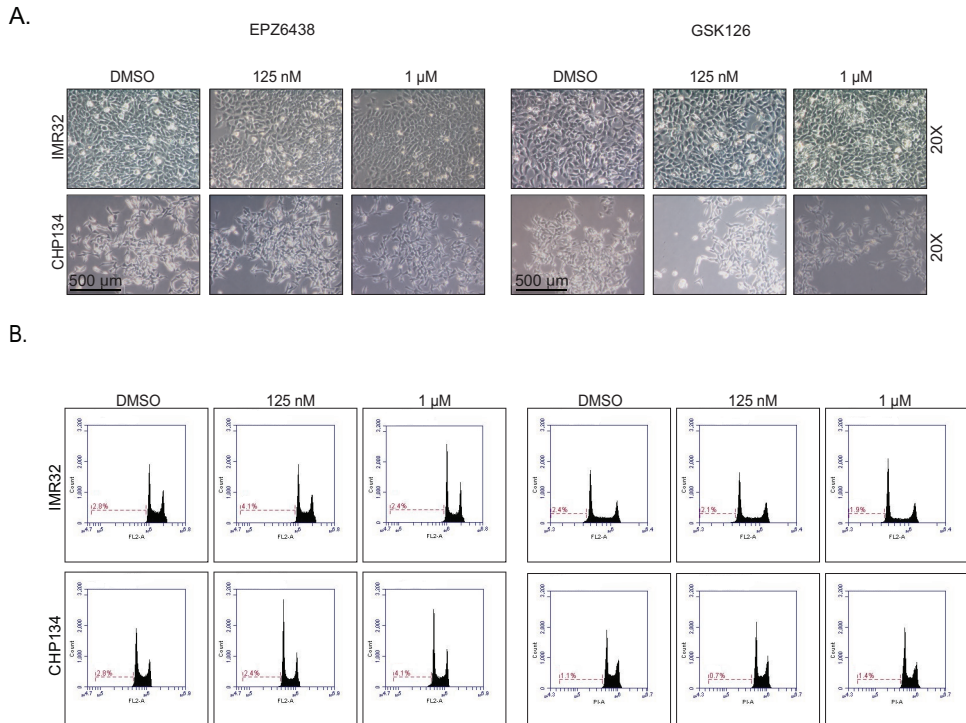
REFERENCES

1. Wu Z, Lee ST, Qiao Y, Li Z, Lee PL, Lee YJ, et al. Polycomb protein EZH2 regulates cancer cell fate decision in response to DNA damage. *Cell Death Differ* 2011;18(11):1771-9.
2. van Leenders GJ, Dukers D, Hessels D, van den Kieboom SW, Hulsbergen CA, Witjes JA, et al. Polycomb-group oncogenes EZH2, BMI1, and RING1 are overexpressed in prostate cancer with adverse pathologic and clinical features. *Eur Urol* 2007;52(2):455-63.
3. Simon JA, Lange CA. Roles of the EZH2 histone methyltransferase in cancer epigenetics. *Mutat Res* 2008;647(1-2):21-9.
4. Raaphorst FM, Meijer CJLM, Fieret E, Blokzijl T, Mommers E, Buerger H, et al. Poorly Differentiated Breast Carcinoma is Associated with Increased Expression of the Human Polycomb Group EZH2 Gene. *Neoplasia* 2003;5(6):481-488.
5. Holm K, Grabau D, Lovgren K, Aradottir S, Gruvberger-Saal S, Howlin J, et al. Global H3K27 trimethylation and EZH2 abundance in breast tumor subtypes. *Mol Oncol* 2012;6(5):494-506.
6. Chase A, Cross NC. Aberrations of EZH2 in cancer. *Clin Cancer Res* 2011;17(9):2613-8.
7. Chang CJ, Hung MC. The role of EZH2 in tumour progression. *Br J Cancer* 2012;106(2):243-7.
8. Zhang X, Zhao X, Fiskus W, Lin J, Lwin T, Rao R, et al. Coordinated silencing of MYC-mediated miR-29 by HDAC3 and EZH2 as a therapeutic target of histone modification in aggressive B-Cell lymphomas. *Cancer Cell* 2012;22(4):506-23.
9. Velichutina I, Shaknovich R, Geng H, Johnson NA, Gascoyne RD, Melnick AM, et al. EZH2-mediated epigenetic silencing in germinal center B cells contributes to proliferation and lymphomagenesis. *Blood* 2010;116(24):5247-55.
10. Sneeringer CJ, Scott MP, Kuntz KW, Knutson SK, Pollock RM, Richon VM, et al. Coordinated activities of wild-type plus mutant EZH2 drive tumor-associated hypertrimethylation of lysine 27 on histone H3 (H3K27) in human B-cell lymphomas. *Proc Natl Acad Sci U S A* 2010;107(49):20980-5.
11. McCabe MT, Graves AP, Ganji G, Diaz E, Halsey WS, Jiang Y, et al. Mutation of A677 in histone methyltransferase EZH2 in human B-cell lymphoma promotes hypertrimethylation of histone H3 on lysine 27 (H3K27). *Proc Natl Acad Sci U S A* 2012;109(8):2989-94.
12. Majer CR, Jin L, Scott MP, Knutson SK, Kuntz KW, Keilhack H, et al. A687V EZH2 is a gain-of-function mutation found in lymphoma patients. *FEBS Lett* 2012;586(19):3448-51.
13. Folkert J, van Kemenade FMR, Tjasso Blokzijl, Elly Fieret, Karien M. Hamer, David P. E. Satijn, Arie P. Otte, and Chris J. L. M. Meijer. Coexpression of BMI-1 and EZH2 polycomb-group proteins is associated with cycling cells and degree of malignancy in B-cell non-Hodgkin lymphoma. *Blood* 2001;97(12):3896-3901.
14. Ernst T, Chase AJ, Score J, Hidalgo-Curtis CE, Bryant C, Jones AV, et al. Inactivating mutations of the histone methyltransferase gene EZH2 in myeloid disorders. *Nat Genet* 2010;42(8):722-6.

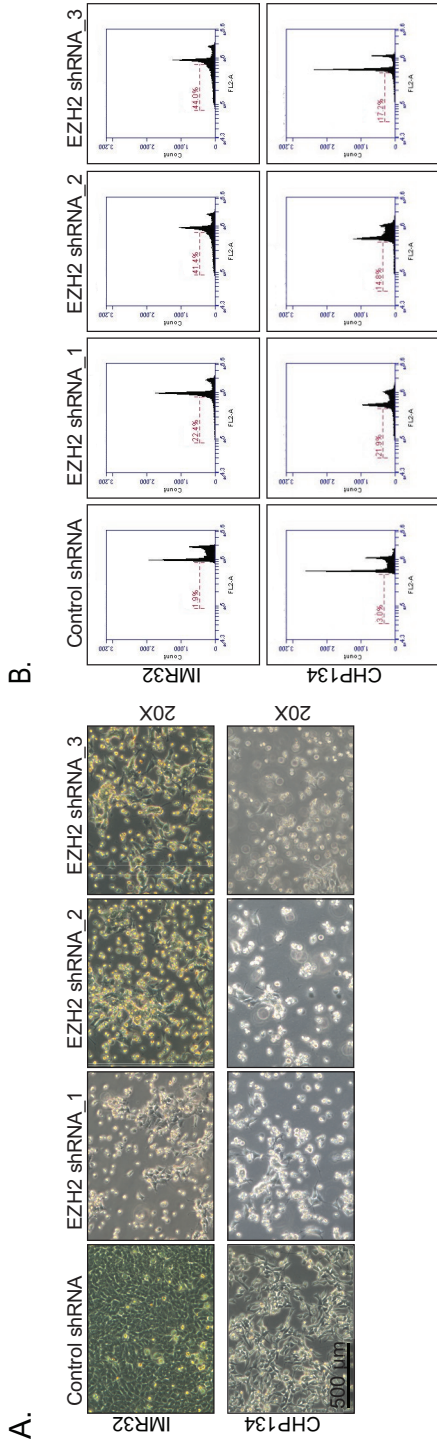
15. Dukers DF, van Galen JC, Giroth C, Jansen P, Sewalt RGAB, Otte AP, et al. Unique Polycomb Gene Expression Pattern in Hodgkin's Lymphoma and Hodgkin's Lymphoma-Derived Cell Lines. *The American Journal of Pathology* 2004;164(3):873-881.
16. Damian B, Yap JC, Tobias Berg, Matthieu Schapira, S.-W. Grace Cheng, Annie Moradian, Ryan D. Morin, Andrew J. Mungall, Barbara Meissner, Merrill Boyle, Victor E. Marquez, Marco A. Marra, Randy D. Gascoyne,, R. Keith Humphries CHA, Gregg B. Morin, and Samuel A. J. R. Aparicio. Somatic mutations at EZH2 Y641 act dominantly through a mechanism of selectively altered PRC2 catalytic activity, to increase H3K27 trimethylation. *Blood* 2011;117(8):2451-2459.
17. Cao R, Zhang Y. The functions of E(Z)/EZH2-mediated methylation of lysine 27 in histone H3. *Curr Opin Genet Dev* 2004;14(2):155-64.
18. Schuettengruber B, Chourrout D, Vervoort M, Leblanc B, Cavalli G. Genome regulation by polycomb and trithorax proteins. *Cell* 2007;128(4):735-45.
19. Di Croce L, Helin K. Transcriptional regulation by Polycomb group proteins. *Nat Struct Mol Biol* 2013;20(10):1147-55.
20. Raman JD, Mongan NP, Tickoo SK, Boorjian SA, Scherr DS, Gudas LJ. Increased expression of the polycomb group gene, EZH2, in transitional cell carcinoma of the bladder. *Clin Cancer Res* 2005;11(24 Pt 1):8570-6.
21. O'Carroll D, Erhardt S, Pagani M, Barton SC, Surani MA, Jenuwein T. The polycomb-group gene *Ezh2* is required for early mouse development. *Mol Cell Biol* 2001;21(13):4330-6.
22. Chamberlain SJ, Yee D, Magnuson T. Polycomb repressive complex 2 is dispensable for maintenance of embryonic stem cell pluripotency. *Stem Cells* 2008;26(6):1496-505.
23. Yan J NS, Tay JLS, Lin B, Koh TL, Tan J, et al. EZH2 overexpression in natural killer/T-cell lymphoma confers growth advantage independently of histone methyltransferase activity. *Blood* 2013;121(22):4512-4520.
24. Xu K, Wu ZJ, Groner AC, He HH, Cai C, Lis RT, et al. EZH2 oncogenic activity in castration-resistant prostate cancer cells is Polycomb-independent. *Science* 2012;338(6113):1465-9.
25. Kim KH, Kim W, Howard TP, Vazquez F, Tsherniak A, Wu JN, et al. SWI/SNF-mutant cancers depend on catalytic and non-catalytic activity of EZH2. *Nat Med* 2015;21(12):1491-6.
26. Brodeur GM GA, Hayes FA, Williams KJ, Williams DL, and Tsiatis AA. Cytogenic features of neuroblastoma. *Cancer Res* 1981;41(11):4678-4686.
27. Irwin MS, Park JR. Neuroblastoma: paradigm for precision medicine. *Pediatr Clin North Am* 2015;62(1):225-56.
28. Brodeur GM. Neuroblastoma: biological insights into a clinical enigma. *Nat Rev Cancer* 2003;3(3):203-16.
29. Guo C WP, Weiss MJ, Hogarty MD, Thompson PM, Stram DO, et al. Allelic deletion at 11q23 is common in MYCN single copy neuroblastomas. *Oncogene* 1999;18(35):4948-4957.

30. R.L. Stallings JH, A. Dunlop, M. Mullarkey, M. McDermott, F. Breatnach, A. O'Meara D'Acunto, C. W. Are gains of chromosomal regions 7q and 11p important abnormalities in neuroblastoma? *Cancer Genetics and Cytogenetics* 2003;150(2):133-137.
31. George RE, Attiyeh EF, Li S, Moreau LA, Neuberg D, Li C, et al. Genome-wide analysis of neuroblastomas using high-density single nucleotide polymorphism arrays. *PLoS One* 2007;2(2):1-9.
32. Wang C, Liu Z, Woo CW, Li Z, Wang L, Wei JS, et al. EZH2 Mediates epigenetic silencing of neuroblastoma suppressor genes CASZ1, CLU, RUNX3, and NGFR. *Cancer Res* 2012;72(1):315-24.
33. McCabe MT, Ott HM, Ganji G, Korenchuk S, Thompson C, Van Aller GS, et al. EZH2 inhibition as a therapeutic strategy for lymphoma with EZH2-activating mutations. *Nature* 2012;492(7427):108-12.
34. Knutson SK WN, Wigle TJ, Klaus CR, Allain CJ, Raimondi A, et al. Durable tumor regression in genetically altered malignant rhabdoid tumors by inhibition of methyltransferase EZH2. *Proc Natl Acad Sci U S A* 2013;110(19):7922-27.
35. Knutson SK, Wigle TJ, Warholc NM, Sneeringer CJ, Allain CJ, Klaus CR, et al. A selective inhibitor of EZH2 blocks H3K27 methylation and kills mutant lymphoma cells. *Nat Chem Biol* 2012;8(11):890-6.
36. Knutson SK, Kawano S, Minoshima Y, Warholc NM, Huang KC, Xiao Y, et al. Selective inhibition of EZH2 by EPZ-6438 leads to potent antitumor activity in EZH2-mutant non-Hodgkin lymphoma. *Mol Cancer Ther* 2014;13(4):842-54.
37. Peifer M, Hertwig F, Roels F, Dredax D, Gartlgruber M, Menon R, et al. Telomerase activation by genomic rearrangements in high-risk neuroblastoma. *Nature* 2015;526(7575):700-4.
38. Bate-Eya LT, Ebus ME, Koster J, den Hartog IJ, Zwijnenburg DA, Schild L, et al. Newly-derived neuroblastoma cell lines propagated in serum-free media recapitulate the genotype and phenotype of primary neuroblastoma tumours. *Eur J Cancer* 2014;50(3):628-37.
39. Twentyman PR LM. A study of some variables in a tetrazolium dye (MTT) based assay for cell growth and chemosensitivity. *Br J Cancer* 1987;56:279-85.
40. Corvetta D, Chayka O, Gherardi S, D'Acunto CW, Cantilena S, Valli E, et al. Physical interaction between MYCN oncogene and polycomb repressive complex 2 (PRC2) in neuroblastoma: functional and therapeutic implications. *J Biol Chem* 2013;288(12):8332-41.
41. Henrich KO, Bender S, Saadati M, Dredax D, Gartlgruber M, Shao C, et al. Integrative Genome-Scale Analysis Identifies Epigenetic Mechanisms of Transcriptional Dereglulation in Unfavorable Neuroblastomas. *Cancer Res* 2016;76(18):5523-37.
42. Sausen M, Leary RJ, Jones S, Wu J, Reynolds CP, Liu X, et al. Integrated genomic analyses identify ARID1A and ARID1B alterations in the childhood cancer neuroblastoma. *Nat Genet* 2013;45(1):12-7.
43. Kim W, Bird GH, Neff T, Guo G, Kerényi MA, Walensky LD, et al. Targeted disruption of the EZH2-EED complex inhibits EZH2-dependent cancer. *Nat Chem Biol* 2013;9(10):643-50.

P-value (bonf p). (E) Kaplan-Meier analysis for overall survival of neuroblastoma patients divided into high and low EZH2 expression groups for all non-MYC*N*-amplified neuroblastoma patients ($n = 401$). Significance is denoted as *P*-value (*p*) and Bonferroni corrected *P*-value (bonf p). (F) EZH2 Affymetrix 133 plus 2.0 array mRNA and RNAseq expression levels in 88 and 493 neuroblastoma tumours respectively (*y*-axis). Tumours were grouped according to MYC*N*-amplification (red) or non-MYC*N*-amplification (green) ($P = 0.41$ and 1.5×10^{-05}).



Supplementary Figure 2. (A) Light microscopy images of IMR32 and CHP134 treated for 144h with increasing concentrations of EPZ6438 and GSK126. Magnification of the images: 20X. Scale bar: 500 μ m. (B) Flow cytometric DNA content histogram of IMR32 and CHP134 showing the effect of EPZ6438 and GSK126 on the cell cycle treated for 144h with DMSO, 125 nM and 1 μ M.



Supplementary Figure 3. (A) Light microscopy images of IMR32 and CHP134 transfected for 96h with a control shRNA and 3 shRNA's specifically targeting EZH2. Magnification of the images: 20x. Scale bar: 500 μm. (B) Flow cytometric DNA content histograms of IMR32 and CHP134 transfected for 96h with a control shRNA and 3 shRNA.

SUPPLEMENTARY MATERIALS AND METHODS

1. Cell culture.

Classical human neuroblastoma cell lines were grown in Dulbecco's modified Eagle's medium (DMEM) containing 4.5 g/L D-glucose, glutamate and supplemented with 10% (v/v) foetal calf serum, 2 mM L-glutamine, 10 U/mL penicillin, 10 µg/mL streptomycin and MEM non-essential amino acids (1x). Neuroblastoma tumour-initiating cell (TIC) lines were grown in neural specific stem cell medium (400 mL DMEM GlutaMAX™-1 containing 1g/L D-glucose and pyruvate, 133 mL F12 medium, 10 mL B27, 18 ng/mL EGF, 36 ng/mL FGF, 10 U/mL penicillin and 10 µg/mL streptomycin. Cells were maintained at 37°C under 5% CO₂ in humidified air. Penicillin and streptomycin were obtained from Sigma Aldrich, EGF from Corning Life Sciences and FGF from PeproTech. Other cell culture related materials were obtained from Life Technologies.

2. FACs Analysis.

Neuroblastoma cell lines IMR32, CHP134 and NMB were seeded in triplicates in 6-cm plates and incubated overnight. Cells were then treated for 72 h with 0.01% DMSO (control) or EPZ6438 and GSK126 using concentration ranges of 62.5 nmol/L to 2 µmol/L or with control shRNA and EZH2 shRNA. Adherent cells were washed once with PBS and the PBS solutions were pooled with the supernatants. After trypsinization of the adherent cells with 0.05% trypsin/EDTA, cells were resuspended in the pooled supernatant/PBS solution. Next, cells were centrifuged (5 min; 1,500 rpm), washed by resuspension in PBS and centrifuged again (5 min; 3,000 rpm). Cells were fixed with 100% ice-cold ethanol and stained with 0.05 mg/mL propidium iodide and 0.05 mg/mL RNase A in PBS. After 1 h incubation in the dark at room temperature, cells were filtered through a 50 µm filter (BD Biosciences) and DNA contents of the nuclei were analyzed using a fluorescent activated cell sorter. A total of 20,000 nuclei per sample were counted. The cell cycle distribution and apoptotic Sub-G1 fraction were determined using the Accuri™ C6 flow cytometer with the CFlow plus software (BD Biosciences).



CHAPTER 4

HIGH EFFICACY OF THE BCL-2 INHIBITOR ABT199 (VENETOCLAX) IN BCL-2 HIGH-EXPRESSING NEUROBLASTOMA CELL LINES AND XENOGRAPTS AND RATIONAL FOR COMBINATION WITH MCL-1 INHIBITION.

Authors: Laurel T. Bate-Eya¹, Ilona J.M. den Hartog¹, Ida van der Ploeg¹,
Linda Schild¹, Jan Koster¹ Evan E. Santo¹, Ellen M. Westerhout¹,
Rogier Versteeg¹, Huib N. Caron², Jan J. Molenaar¹
and M. Emmy M. Dolman¹.

Departments of ¹Oncogenomics, and ²Pediatric Oncology,
Emma Kinderziekenhuis, Academic Medical Center,
University of Amsterdam, Amsterdam, the Netherlands.

Oncotarget (2016)

ABSTRACT

The anti-apoptotic protein B cell lymphoma/leukaemia 2 (*BCL-2*) is highly expressed in neuroblastoma and plays an important role in oncogenesis. In this study, the selective *BCL-2* inhibitor ABT199 was tested in a panel of neuroblastoma cell lines with diverse expression levels of *BCL-2* and other *BCL-2* family proteins. ABT199 caused apoptosis more potently in neuroblastoma cell lines expressing high *BCL-2* and BIM/*BCL-2* complex levels than low expressing cell lines. Effects on cell viability correlated with effects on BIM displacement from *BCL-2* and cytochrome c release from the mitochondria. ABT199 treatment of mice with neuroblastoma tumors expressing high *BCL-2* levels only resulted in growth inhibition, despite maximum BIM displacement from *BCL-2* and the induction of a strong apoptotic response. We showed that neuroblastoma cells might survive ABT199 treatment due to its acute upregulation of the anti-apoptotic *BCL-2* family protein myeloid cell leukaemia sequence 1 (*MCL-1*) and BIM sequestration by *MCL-1*. *In vitro* inhibition of *MCL-1* sensitized neuroblastoma cell lines to ABT199, confirming the pivotal role of *MCL-1* in ABT199 resistance. Our findings suggest that neuroblastoma patients with high *BCL-2* and BIM/*BCL-2* complex levels might benefit from combination treatment with ABT199 and compounds that inhibit *MCL-1* expression.

INTRODUCTION

Numerous cancer types have been associated with aberrations in genes encoding B cell lymphoma/leukaemia 2 (BCL-2) family proteins [1]. The BCL-2 family of proteins are key regulators of the intrinsic apoptotic pathway [2, 3], consisting of anti-apoptotic [e.g., BCL-2, BCL-extra large (BCL-X_L), BCL-2-like protein 2 (BCL-W) and myeloid cell leukaemia sequence 1 (MCL-1)] and pro-apoptotic members [e.g., BCL-2-like protein 11 (BIM) and BH3-interacting domain death agonist (BID)] [4-6]. Increased interactions between anti-apoptotic and pro-apoptotic proteins inhibits apoptosis by preventing mitochondrial outer membrane permeabilization by the essential effector family members BAX and BAK. Consequently, cytochrome c cannot be released into the cytosol where it activates caspase 9-induced proteolysis and cell death [7-13].

Neuroblastoma is the most commonly diagnosed extracranial solid cancer in children, accounting for approximately 15% of all pediatric cancer deaths [14]. A large subset of neuroblastoma patients has enhanced levels of the anti-apoptotic gene *BCL-2* [15, 16]. Previously, we showed that selective *BCL-2* inhibition using RNA interference caused an apoptotic response in cell lines with moderate to high *BCL-2* levels. These findings could be confirmed with the small-molecule BCL-2 family inhibitor ABT263, which inhibits the anti-apoptotic activity of BCL-2, BCL-X_L, BCL-W and MCL-1 with inhibition constant (K_i) values of 0.044, 0.055, 7 and 224 nmol/L, respectively [17]. Neuroblastoma cell lines expressing high *BCL-2* levels responded better to ABT263 treatment than low *BCL-2*-expressing cell lines. ABT263 furthermore delayed the onset of tumor formation in mice injected with high *BCL-2*-expressing neuroblastoma cells [16]. These observations supported the potential benefit of BCL-2 family inhibitors for the future treatment of high *BCL-2*-expressing neuroblastoma tumors. Unfortunately, the administration of ABT263 in phase I/II clinical studies for adult cancers was associated with dose-limiting thrombocytopenia due to concomitant inhibition of anti-apoptotic BCL-X_L, a key survival factor for circulating platelets [18-22]. Therefore, the more specific ABT263-derivative ABT199 was developed [17, 23, 24].

Compared with ABT263, ABT199 displays less activity against BCL-X_L (K_i of 48 nmol/L), BCL-W (K_i of 245 nmol/L) and MCL-1 (K_i of >444 nmol/L), while maintaining its activity against BCL-2 (K_i of <0.01 nmol/L) [17, 25]. ABT199 has shown preclinical and clinical efficacy against lymphoma, while sparing platelets [24, 26, 27]. In the current study, we explored the preclinical therapeutic potential of ABT199 for the treatment of BCL-2-dependent neuroblastoma tumors.

MATERIALS AND METHODS

Chemicals. ABT199, ABT263 and A-1210477 were purchased from Selleck Chemicals while QVD-OPH was purchased from Sigmaaldrich. For *in vivo* studies ABT199 and ABT263 were formulated in 10% ethanol/30% polyethylene glycol (PEG) 400/60% phosal 50 propylene glycol (PG) (v/v/v) in final concentrations of 10 mg/mL.

Cell culture. Classical human neuroblastoma cell lines and neuroblastoma tumor-initiating cell (TIC) lines were cultured as previously described [41, 42]. Cell culture protocols are described in detail in the Supplementary Materials and Methods.

IC₅₀ and LC₅₀. Neuroblastoma cell lines were seeded in triplicate in 96-well (classical cell lines) or 48-well (TIC lines) plates using the most optimal confluency for each cell line [42]. Cells were incubated overnight and treated with 1 nmol/L to 50 μmol/L ABT199. Control samples were treated with 0.5% DMSO. Cell viability was determined prior to and after 72-hour treatment using the 3-(4,5-dimethylthiazol-2-yl)-2,5-diphenyltetrazolium bromide (MTT) colorimetric assay [43]. Half maximal effective concentration (IC₅₀) and half lethal concentration (LC₅₀) values were derived from dose-response curves. IC₅₀ values at 72 hours were calculated by determining the ABT199 concentrations needed to achieve a 50% reduction in cell viability observed for DMSO-treated cells at 72 hours (set at 100%). LC₅₀ values at 72 hours were calculated by establishing the ABT199 concentrations needed to attain a 50% reduction in the cell viability compared to time point 0.

FACS analysis. Cells were treated with 0.1% DMSO (control) or ABT199 using concentration ranges of 7.8 nmol/L to 10 μmol/L. After 72-hour treatment, floating and adherent cells were harvested for FACS analysis to determine the cell-cycle distribution and the apoptotic sub-G₁ fraction. See Supplementary Materials and Methods for a detailed protocol.

Cell fractionation. CHP126, KCNR, SJNB12, SKNAS and SHEP2 were 24-hour treated with 0.04% DMSO (control) or 62.5 nmol/L to 10 μmol/L ABT199. Floating and adherent cells were harvested to determine cytochrome c in the cytosolic and organelle fractions. See Supplementary Materials and Methods for a detailed protocol.

In vitro western blotting. The following antibodies were used: rabbit anti-human BCL-2 (clone D55G8) monoclonal antibody (1:1,000, Cell Signaling Technology);

rabbit anti-human BCL-X_L (clone 54H6) monoclonal antibody (1:1,000, Cell Signaling Technology); rabbit anti-human MCL-1 monoclonal antibody (1:1,000, Cell Signaling Technology); rabbit anti-human BCL-W (clone 31H4) monoclonal antibody (1:1,000, Cell Signaling Technology); rabbit anti-human Noxa (clone EPR9735B) monoclonal antibody (1:1,000, Abcam); rabbit anti-human BIM (1:1,000, Cell Signaling Technology); mouse anti-human cytochrome c (clone 7H8.2C12) monoclonal antibody (1:1,000 BD pharmingen); rabbit anti-human PARP (clone 9542S) monoclonal antibody (1:1,000, Cell Signaling Technology); rabbit anti-human cleaved caspase 3 (clone 5AE17) monoclonal antibody (1:1000, Cell Signaling Technology); mouse anti-human α -tubulin (clone DM1A) monoclonal antibody (1:10,000, Cell Signaling Technology) and horseradish peroxidase (HRP)-conjugated goat anti-rabbit (clone NA9340V) and goat anti-mouse (clone NXA931) secondary antibodies (1:10,000 GE Healthcare). See Supplementary Materials and Methods for detailed protocol.

***In vitro* co-immunoprecipitation and immunoblotting.** Cell lines were seeded onto 14-cm culture dishes. For the detection of basal BIM/BCL-2 complex levels, untreated cells were harvested after 72 hours incubation at normal culture conditions. For the detection of BIM displacement from BCL-2 and BIM complexation with MCL-1 and BCL-X_L, cells were treated with 0.25% DMSO (control) or 62.5 nmol/L or 1.25 μ mol/L ABT199 at 24 hours after seeding and harvested after 24-hour treatment. Co-immunoprecipitation studies have been performed as described in detail in the Supplementary Materials and Methods.

Cell transfection. CHP126, KCNR, SJNB12 and SY5Y were seeded in 6-cm culture dishes (2×10^5 cells in 4 mL culture medium) and incubated overnight. Next, cells were transfected with non-targeting shRNA (AACAAGATGAAGAGCACCAA; negative control) or MCL-1 shRNA (TRCN0000199070 and TRCN0000005518) for the BCL-2 high-expressing cell lines using the PLenti VI system according to the manufacturers protocol (Sigma Aldrich), while SY5Y was transfected with either a Luc2 control or a TERT-on vector constitutively overexpressing the BCL-2 protein. After 72 hours, cells were transferred into 96-well plates for *in vitro* MTT assays and synergy studies (see below).

***In vitro* synergy assays.** CHP126, KCNR and SJNB12 transiently transfected with non-targeting shRNA or MCL-1 shRNA were seeded in duplicates in 96-well plates and incubated overnight. Cells were then treated with ten-fold serial dilutions of ABT199 (0–10 μ mol/L). Effects on cell viability were studied after 72-hour treatment with ABT199, using the MTT cell proliferation assay.

For synergy studies between ABT199 and the MCL-1 inhibitor A-1210477, non-transfected cells in 96-well plates were co-treated with ten-fold serial dilutions of ABT199 (0-10 $\mu\text{mol/L}$) and five-fold serial dilution of A-1210477 (0-50 $\mu\text{mol/L}$).

***In vivo* efficacy in neuroblastoma mouse models.** Female NMRI *nu/nu* mice (6-15 weeks old; 20-30 g) were obtained from Harlan and experiments were performed with permission from and according to the standards of the Dutch animal ethics committee (DAG 102776, 102830 and 102690). NMRI *nu/nu* mice with KCNR neuroblastoma xenografts of approximately 268 mm^3 were orally treated with 100 mg/kg/d ABT199 ($n = 5$), 100 mg/kg/d ABT263 ($n = 5$), or vehicle ($n = 6$) for 21 days. Tumor sizes were measured by an external caliper. See Supplementary Materials and Methods for a more detailed protocol.

***In vivo* western blotting.** Per mouse sample, 10 tumor sections of 50 μm were homogenized in 2% CHAPS buffer as previously described. Western blot detection of protein levels of BCL-2 like family members was carried out as described for *in vitro* western blotting.

***In vivo* co-immunoprecipitation.** Sections of treated and untreated KCNR tumors harvested at 4 hours after administration of the last dose were homogenized using the Ultra Turrax T25 tissue homogenizer (Janke & Kunkel) and lysed (overnight at 4 $^{\circ}\text{C}$) in 2% CHAPS buffer. Co-immunoprecipitation was carried out as described above.

***In vivo* immunohistochemistry.** The following antibodies were used: rabbit anti-human Ki-67 (clone SP6) monoclonal antibody (1:1,000, Thermo Scientific), rabbit anti-human cleaved caspase 3 (Asp175) polyclonal antibody (1:100, Cell Signaling Technology) and BrightVision horseradish peroxidase-conjugated goat anti-rabbit polyclonal secondary antibody (undiluted; 30 min; Immunologic). See Supplementary Materials and Methods for a detailed protocol.

mRNA expression profiling. RNA was extracted from tumors with TRIzol (Invitrogen, Carlsbad, CA) following the manufacturers protocols. RNA concentration and quality were determined using the RNA 6000 Nano assay on the Agilent 2100 Bioanalyzer (Agilent Technologies). Fragmentation of cRNA, hybridization to hg-u133 plus 2.0, microarrays and scanning were carried out according to the manufacturers protocol (Affymetrix Inc. Santa Barbara, CA). The mRNA gene expression data were normalized with the MAS5.0 algorithm within the GCOS program of Affymetrix Inc. Target intensity

was set to 100. All data were analyzed using the R2 genomic analysis and visualization platform (<http://r2.amc.nl>).

RESULTS

BCL-2 and BIM/BCL-2 complex levels predict sensitivity of neuroblastoma cells to ABT199.

IC_{50} and LC_{50} values of ABT199 were established for 21 classical neuroblastoma cell lines and 3 tumor-initiating cell lines (TIC) (Table 1). Cell lines CHP126, KCNR and SJNB12 responded most potently to ABT199, with IC_{50} and LC_{50} values in the nanomolar range (i.e. 10-210 and 16-338 nmol/L, respectively) versus micromolar IC_{50} and LC_{50} values (i.e. 4.9-19.3 and 6.9-32.3 μ mol/L, respectively) for the other cell lines tested. Evaluation of the BCL-2, MCL-1, BCL-X_L, BCL-W and BIM protein levels (Fig. 1A) showed significantly higher BCL-2 levels in the sensitive neuroblastoma cell lines CHP126, KCNR and SJNB12 compared with the insensitive cell lines (Fig. 1B). No significant differences in expression of the anti-apoptotic proteins MCL-1, BCL-X_L, BCL-W and the pro-apoptotic protein BIM were found between the sensitive and insensitive cell lines (Fig. 1B). The same pattern was observed when looking at the mRNA level (Supplementary Fig. S1A). Sensitive neuroblastoma cell lines expressed significantly higher *BCL-2* mRNA levels as compared to the insensitive cell lines, while no expression differences were observed for the other *BCL-2* family genes. Of note, BCL-2 protein levels better predict the sensitivity of neuroblastoma cell lines to ABT199 than *BCL-2* mRNA levels, as shown by the factor difference in average expression between the sensitive and insensitive cell lines (i.e. ~14 versus ~4). As ABT199 acts by displacing pro-apoptotic BCL-2 family members including BIM from BCL-2 [17], we also studied if levels of BIM bound to BCL-2 could be used as a predictive biomarker for sensitivity to ABT199. BCL-2 immunoprecipitation followed by immunoblotting for BIM showed that BIM/BCL-2 complex levels were indeed significantly higher in the sensitive neuroblastoma cell lines (Fig. 1B and C). Results were confirmed by reciprocal co-immunoprecipitation experiments in which BIM/BCL-2 complex levels were determined by BIM immunoprecipitation followed by BCL-2 immunoblotting (Supplementary Fig. S1A and B). We also tested if there was a correlation between ABT199 sensitivity and *MYCN* status. *MYCN*-amplified neuroblastoma cell lines responded more potently to ABT199 than *MYCN* single copy cell lines, with IC_{50} values ranging from 10 nmol/L-20 μ mol/L versus 10-18 μ mol/L, respectively (Supplementary Fig. 1C).

Cell lines	IC ₅₀ (μmol/L)	LC ₅₀ (μmol/L)
CHP126	0.010	0.016
KCNR	0.026	0.153
SJNB12	0.210	0.338
LAN5	4.90	20.50
IMR32	6.01	8.80
AMC106	6.30	6.90
LAN1	6.40	7.10
N206	7.01	8.21
TR14	7.65	11.90
SJNB6	8.20	10.33
CHP134	9.40	17.70
SJNB1	9.40	9.50
700B	9.54	16.62
SKNFI	9.79	10.97
SKNSH	11.04	13.10
700T	11.29	17.50
GIMEN	14.01	21.80
SKNAS	14.20	19.10
NMB	14.60	17.40
SKNBE	14.70	18.60
SYSY	15.32	17.71
691T	15.80	17.01
SHEP2	18.30	21.60
SJNB10	19.30	32.30

Table 1. IC₅₀ and LC₅₀ values of ABT199 for neuroblastoma cell lines.

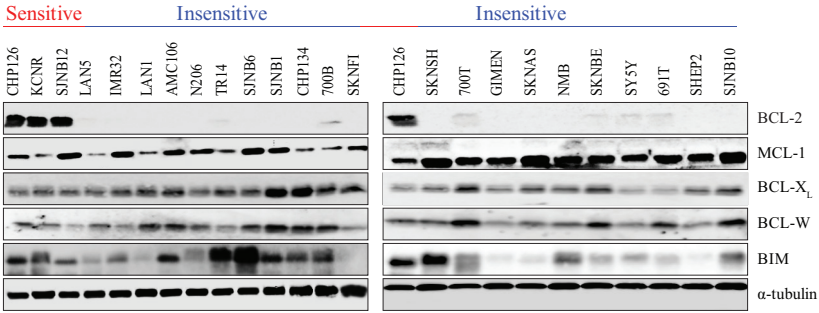
ABT199 causes cell death in BCL-2-dependent neuroblastoma cells by activation of the intrinsic apoptotic program.

High BCL-2-expressing neuroblastoma cell lines CHP126, KCNR and SJNB12 and low BCL-2-expressing cell lines SKNAS and SHEP2 were treated with increasing doses of ABT199 to study effects on apoptosis. PARP cleavage induction in the high BCL-2-expressing cell lines was already observed after treatment with only 7.5 nmol/L ABT199, while for the low BCL-2-expressing neuroblastoma cell lines PARP cleavage was only detected in

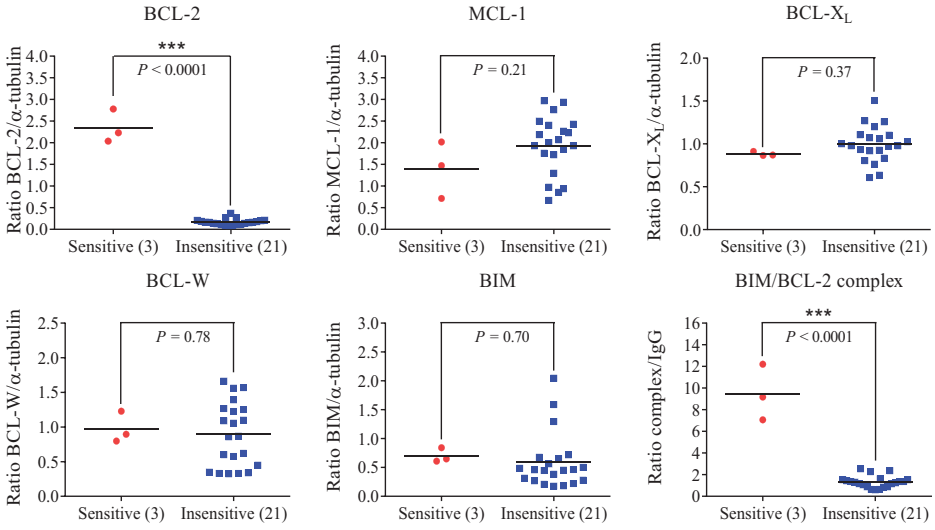
SKNAS after treatment with 10 $\mu\text{mol/L}$ ABT199 (Fig. 2A). Similar results were obtained when investigating the effects of ABT199 on cleaved caspase 3 (Supplementary Fig. S2A). Apoptotic effects of ABT199 were further validated by flow cytometry. In line with the effects on PARP and caspase 3 cleavage, ABT199 treatment of the high BCL-2-expressing neuroblastoma cell lines resulted in more pronounced increases in sub- G_1 fraction than observed for the low BCL-2-expressing cell lines (Fig. 2B and Supplementary Table S1). Treatment with only 7.5 nmol/L ABT199 resulted in increases in sub- G_1 fraction of 8% (CHP126), 13% (KCNR) and 5% (SJNB12) for the high BCL-2-expressing cell lines versus 0% (SKNAS) and 1% (SHEP2) for the low BCL-2-expressing cell lines. Effects on sub- G_1 were dose-dependent, with maximum increases observed after treatment with 10 $\mu\text{mol/L}$ ABT199 (i.e. 44%, 25% and 37% for CHP126, KCNR and SJNB12, respectively, versus 7% and 3% for SKNAS and SHEP2, respectively). Next, *in vitro* effects of ABT199 on the activation of the intrinsic apoptosis pathway were studied. As ABT199 inhibits the activity of BCL-2 by displacement of pro-apoptotic proteins, we first studied the effects of ABT199 on BIM displacement from BCL-2. Treatment of the high BCL-2-expressing neuroblastoma cell lines with 62.5 nmol/L ABT199 was already sufficient for almost complete displacement of BIM from BCL-2 (Fig. 2C). No or only moderate increases in BIM displacement were observed after treatment with higher ABT199 concentrations (i.e. 1.25 $\mu\text{mol/L}$). BCL-2-dependent activation of the intrinsic apoptotic program was further studied by evaluation of the effects of ABT199 on cytochrome c release. Dose-dependent cytochrome c release from the mitochondria into the cytoplasm was observed after ABT199 treatment of CHP126, KCNR and SJNB12 (Fig. 2D). In line with the effects on BIM displacement from BCL-2, cytochrome c release was already observed after treatment with nanomolar concentrations of ABT199. No cytochrome c release was observed after ABT199 treatment of the low BCL-2-expressing cell lines, even at the highest concentration of 10 $\mu\text{mol/L}$ (Fig. 2D). Together, these findings confirm that ABT199 causes apoptosis in BCL-2-dependent neuroblastoma cells via activation of the intrinsic apoptotic pathway. This was strengthened by the observation that the effects of ABT199 on PARP and caspase 3 cleavage and sub- G_1 fraction could be completely rescued in KCNR by combination treatment with the pan-caspase inhibitor QVD-OPH (Supplementary Fig. S2D and E).

In addition, overexpression of BCL-2 in the low BCL-2-expressing neuroblastoma cell line SY5Y resulted in a strong increase in sensitivity to SY5Y (Supplementary Fig. S2B and C). The remarkable decrease in IC_{50} value observed after BCL-2 overexpression (i.e. from 16.3 μM to 2.6 μM) shows that the effects of ABT199 obtained in CHP126, KCNR and SJNB12 are indeed caused by BCL-2 inhibition rather than off-target effects.

A.



B.



C.

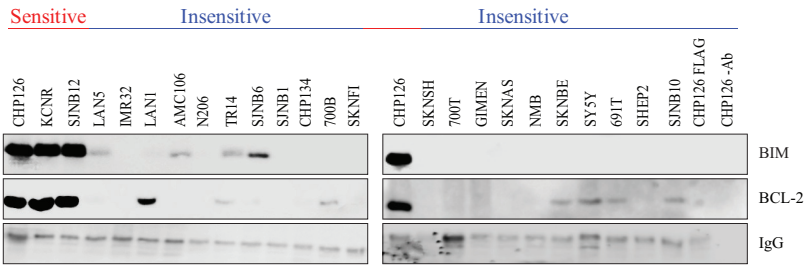
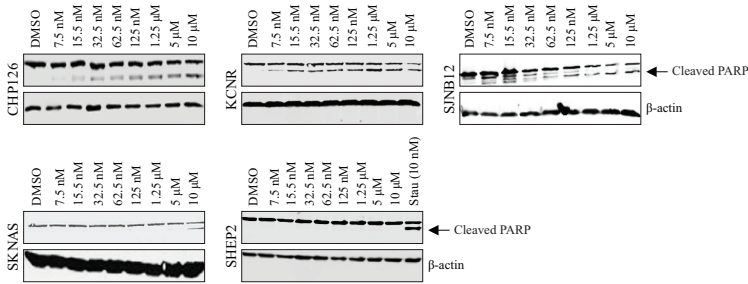


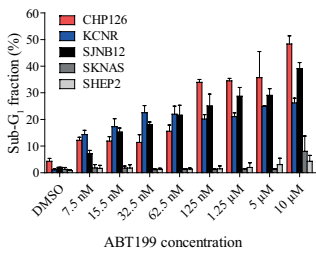
Figure 1. BCL-2 protein and BIM/BCL-2 complex levels predict sensitivity of neuroblastoma cell lines to ABT199. A, Western blot analysis of the protein expression levels of anti-apoptotic proteins BCL-2, MCL-1, BCL-X_L and BCL-W and the pro-apoptotic protein BIM in neuroblastoma cell lines. α -tubulin was used as household protein. B, Protein levels of BCL-2, MCL-1, BCL-X_L, BCL-W and BIM and BIM/BCL-2 complex levels in sensitive (i.e., CHP126, KCNR, and SJNB12) versus insensitive neuroblastoma cell lines. Protein levels shown in Fig. A were quantified by calculating the protein/ α -tubulin band intensity ratios. BIM/BCL-2 complex levels were established by anti-BCL-2 immunoprecipitation of whole cell lysates, followed by Western blotting for BIM. BIM band intensities were normalized to the IgG heavy chain of the BCL-2 antibody. Statistical differences between the sensitive and insensitive cell lines were calculated using a one-tailed (for BCL-2 and BIM/BCL-2 complex) or two-tailed unpaired Student *t* test, with *P* < 0.05 as the minimal level of significance and *P* < 0.0001 indicated as ***. Horizontal lines represent the mean of the relative intensities of the cell line panel. C, Western blot analysis of BIM/BCL-2 complex levels in 24 neuroblastoma cell lines, ordered from ABT199 sensitive (left) to ABT199 insensitive (right). The IgG heavy chain of the BCL-2 antibody served as a loading control. Total protein levels of the BCL-2-like family member proteins of the cell line panel in Figure 1A served as whole cell lysates for this experiment.

Chapter 4

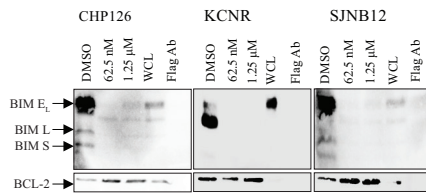
A.



B.



C.



D.

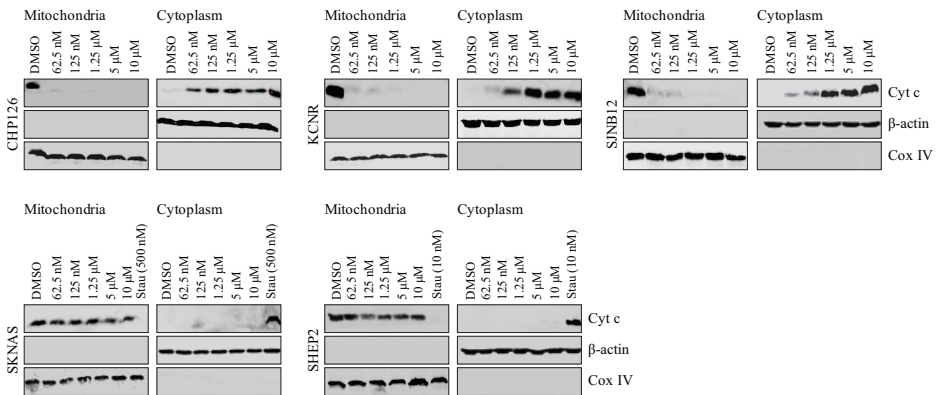


Figure 2. ABT199 induces cell death in BCL-2 dependent neuroblastoma cell lines through activation of the intrinsic apoptotic pathway. A, Western blot analysis of the *in vitro* effects of ABT199 on PARP cleavage after 72-hour treatment of sensitive neuroblastoma cell lines CHP126, KCNR and SJNB12 and insensitive cell lines SKNAS and SHEP2 with increasing ABT199 concentrations. β -actin served as loading control. As ABT199 failed to induce PARP cleavage in SHEP2, staurosporine (10 nmol/L, 24 hours; indicated as Stau) was used as a positive control for this cell line. B, FACS analysis of the *in vitro* effects on sub-G₁ induction after 72-hour treatment with increasing ABT199 concentrations. Data represent the mean percentages of cells in sub-G₁ \pm SD of three replicate experiments. C, *In vitro* effects on BIM displacement from BCL-2 after 24-hour treatment of CHP126, KCNR and SJNB12 with 62.5 nmol/L or 1.25 μ mol/L ABT199. BIM displacement was established by detecting BIM/BCL-2 complex levels by anti-BCL-2 immunoprecipitation, followed by western blotting for BIM. BCL-2 levels served as loading control. (BIM E_L = BIM extra-large, BIM L = BIM large and BIM S = BIM small) WCL= whole cell lysate. D, Western blot analysis of the *in vitro* effects of ABT199 on cytochrome c release from the mitochondria into the cytosol. Cytochrome c levels (indicated as Cyt c) in the mitochondrial and cytoplasmic cell fractions were established after 24-hour treatment of the cell lines with increasing ABT199 concentrations. COX IV and β -actin were used as loading controls for the mitochondrial and cytoplasmic fractions, respectively. As ABT199 failed to induce cytochrome c release in SKNAS and SHEP2, cell lines were 24-hour treated with 500 and 10 nmol/L staurosporine, respectively, as a positive control.

ABT199 causes apoptosis in high BCL-2-expressing neuroblastoma xenografts by BIM displacement from BCL-2.

The efficacy of ABT199 was subsequently studied *in vivo* in mice with high BCL-2-expressing KCNR neuroblastoma xenografts. Once-daily oral treatment with 100 mg/kg ABT199 for three consecutive weeks resulted in significant tumor growth inhibition relative to the vehicle treated controls (Fig. 3A). However, comparison studies in the same animal model demonstrated superior antitumor activity of ABT263 over ABT199, i.e. complete tumor regression versus tumor growth inhibition (Fig. 3A).

The difference in efficacy between ABT199 and ABT263 might be the result of the concomitant inhibition of other anti-apoptotic BCL-2 family members by ABT263 and/or incomplete BCL-2 inhibition by ABT199. We therefore studied the *in vivo* effects of ABT199 on BIM displacement from BCL-2. Co-immunoprecipitation studies at 4 h after administration of the last ABT199 dose showed almost complete release of BIM, while in the control mice BIM was still firmly complexed to BCL-2 (Fig. 3B). This indicates that sufficient high intratumoral ABT199 levels were achieved for maximum target inhibition. In line with ABT199 effects on BIM displacement from BCL-2, a strong apoptotic response was observed. Treatment with 100 mg/kg/day ABT199 caused an increase in cleaved caspase 3-positive cells (Fig. 3C and D). No clear phenotypic changes and effects on cell proliferation were observed, as shown by hematoxylin-eosin and Ki67 staining of tumor tissues, respectively (Supplementary Fig. S3A). Together, these results show that the differential efficacy between ABT199 and ABT263 is not the result of insufficient target inhibition by ABT199, but might result from simultaneous inhibition of multiple anti-apoptotic BCL-2 family members by ABT263. Discontinuation of treatment with ABT199 and ABT263 resulted in tumor growth and tumor recurrence, respectively (Supplementary Fig. S3B).

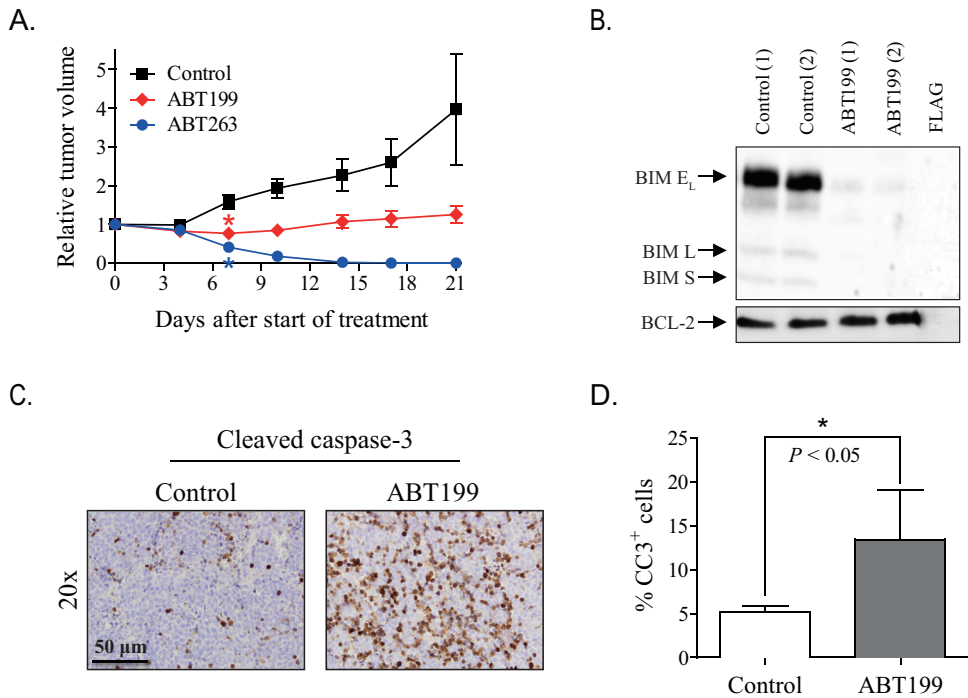


Figure 3. ABT199 and ABT263 cause apoptosis in mice with KCNR neuroblastoma xenografts expressing high levels of BCL-2 and BIM/BCL-2 complex. **A**, Inhibitory effects of ABT199 and ABT263 on the growth of KCNR neuroblastoma xenografts in mice. Relative tumor volume was calculated as the volume at the indicated day after start of treatment divided by the volume prior to treatment initiation. Data represent the mean relative tumor volume \pm SEM [Group sizes: $n = 10$ (control; 10% ethanol/30% PEG 400/60% phosal 50 PG (v/v/v)), $n = 5$ (100 mg/kg ABT199), and $n = 5$ (100 mg/kg ABT263)]. Statistical differences between treated and control groups were calculated using one-way ANOVA with Bonferroni adjustment and are indicated on the first day after treatment initiation at which a statistically different effect was observed (*). P values < 0.05 were considered significant. **B**, *In vivo* effects of ABT199 on BIM displacement from BCL-2. Effects were studied by detecting BIM/BCL-2 complex levels by anti-BCL-2 immunoprecipitation, followed by western blotting for BIM (BIM E_L = BIM extra-large, BIM L = BIM large and BIM S = BIM small). Levels of BIM/BCL-2 complex were established for $n = 2$ mice per group at 4 hours after administration of the last dose of ABT199. BCL-2 levels served as loading control. Total protein levels of the BCL-2 family members in figure 4D served as input levels for this experiment. **C**, Representative microscopic images of cleaved caspase 3 stained paraffin-embedded tumor sections of control and ABT199-treated tumor samples collected at 4 hours after administration of the last dose. Magnification of the images: 20x. Scale bar: 50 μ m. **D**, Quantification of the stimulatory effect of ABT199 on cleaved caspase 3 was performed by manual counting of the total number of cells and the number of cleaved caspase 3-positive (CC3⁺) cells in 20 microscopic fields per mouse sample at 40x magnification (30% of each field). The average percentage of CC3⁺ cells for each mouse was used to determine the effect of ABT199. Statistical differences between the control group ($n = 6$) and ABT199-treated group ($n = 2$) were calculated using a one-tailed unpaired Students t test and are indicated as * ($P < 0.05$).

MCL-1 stabilization and upregulation and BIM sequestration by MCL-1 provide rationale for combination treatment with MCL-1 inhibitors.

Upregulation and increased activity of the non-targeted anti-apoptotic BCL-2 family proteins MCL-1 and BCL-X_L have been reported as key mechanisms of resistance to BCL-2 inhibitors including ABT199 [28-33]. We observed that ABT199 treatment of the high BCL-2-expressing neuroblastoma cell lines CHP126, KCNR and SJNB12 indeed resulted in strongly increased MCL-1 levels, while the other anti-apoptotic proteins and the pro-apoptotic protein BIM were not affected (Fig. 4A). As Noxa is a negative regulator of MCL-1 [33], effects of ABT199 on Noxa protein levels were also studied. Noxa protein levels were decreased after ABT199 treatment of CHP126, KCNR and SJNB12 (Fig.4A), which might explain the increased MCL-1 levels. Real-time quantitative PCR analysis after 24-hour treatment of KCNR cells treated with increasing ABT199 concentrations showed no significant changes in *MCL-1* and *Noxa* mRNA levels (Supplementary Fig. S3C and D). *In vitro* observations were confirmed in the *in vivo* experiments using tumor materials of the ABT199-treated KCNR xenografts and control samples. MCL-1 protein levels were again strongly increased after ABT199 treatment, while Noxa was decreased (Fig. 4B). No effects of ABT199 on anti-apoptotic proteins BCL-2 and BCL-X_L and the pro-apoptotic protein BIM were observed *in vivo*. Affymetrix mRNA profiling of the *in vivo* tumor samples revealed no significant changes in *BCL-2*, *MCL-1*, *BCL-X_L* and *BIM* mRNA levels after ABT199 treatment (Supplementary Fig. S3E). The lack of effects on *MCL-1* mRNA indicates that ABT199-induced MCL-1 upregulation is caused at the protein rather than mRNA level, making the increased stabilization of MCL-1 by reduced Noxa protein levels more plausible. While also not statistically significant, *in vivo* *Noxa* mRNA levels appeared to be lower after ABT199 treatment. Next, the *in vitro* sequestration of released BIM by other anti-apoptotic proteins was studied. After 24-hour treatment of neuroblastoma cell lines CHP126, KCNR and SJNB12 with nanomolar concentrations ABT199, shifting of BIM from BCL-2 to the anti-apoptotic protein MCL-1 was observed while no sequestration of released BIM by the anti-apoptotic protein BCL-X_L was observed (Fig. 4C and Supplementary Fig. S2F). BIM displacement from BCL-2 to MCL-1 also occurred *in vivo* (Fig. 4D), confirming the pivotal role of MCL-1 in the biological mechanism by which neuroblastoma cells can escape from ABT199-induced apoptosis.

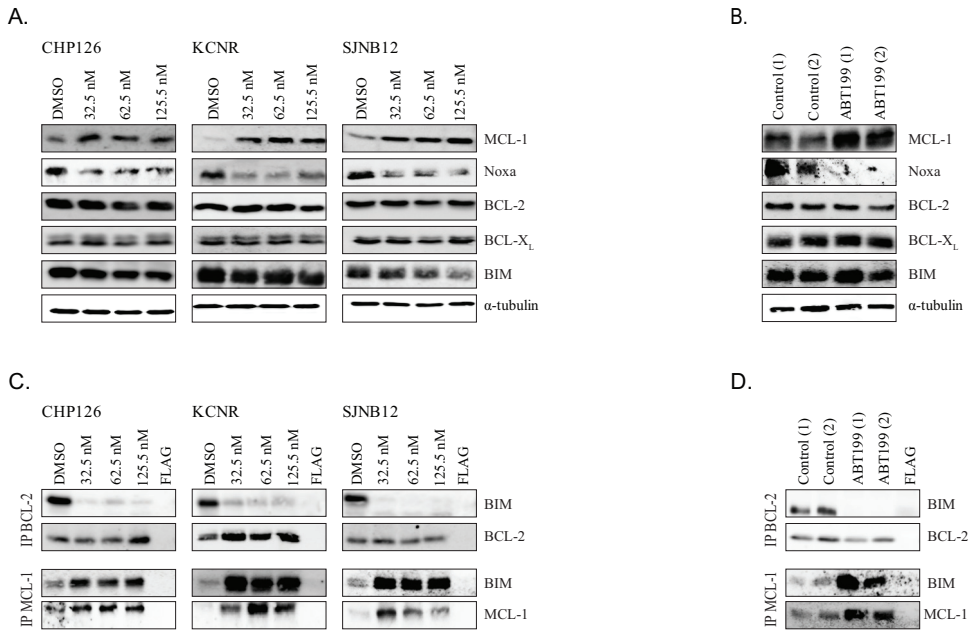


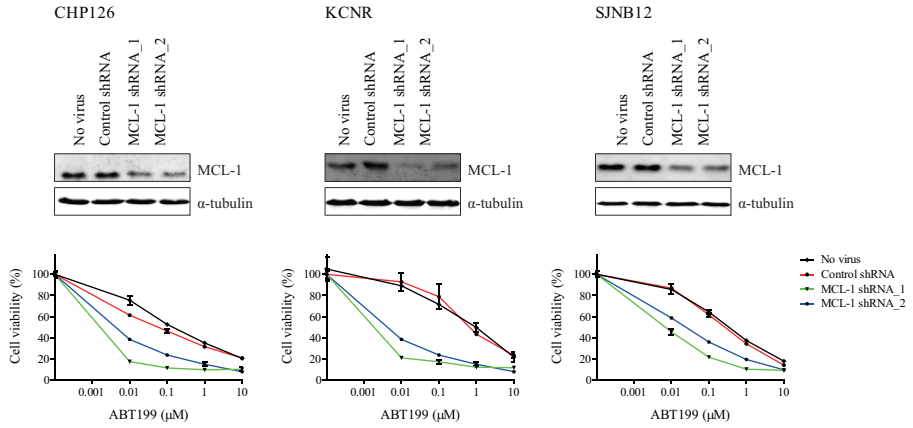
Figure 4. ABT199 causes MCL-1 upregulation and Noxa downregulation, leading to increased sequestration of released BIM from BCL-2. *A*, *In vitro* effects of ABT199 on total protein levels of MCL-1, Noxa, BCL-2, BCL-X_L and BIM in CHP126, KCNR and SJNB12 after 24-hour treatment with increasing doses. Effects were determined by western blot analysis using α-tubulin as a loading control. *B*, *In vivo* effects of ABT199 on total protein levels of MCL-1, Noxa, BCL-2, BCL-X_L and BIM. Mice with KCNR neuroblastoma xenografts were daily treated with vehicle or 100 mg/kg ABT199 for 3 consecutive weeks. Tumor samples were collected at 4 hours after administration of the last dose and analyzed by western blot analysis. α-tubulin served as a loading control. *C*, *In vitro* effects of ABT199 on BIM/BCL-2, and BIM/MCL-1 complex levels in CHP126, SJNB12 and KCNR after 24-hour treatment with increasing doses. BIM/BCL-2 and BIM/MCL-1 complex levels were established by immunoprecipitation of BCL-2 and MCL-1 followed by western blot analysis of BIM. Immunoprecipitated levels of BCL-2 and MCL-1 were used as loading controls. *D*, *In vivo* effects of ABT199 on BIM/BCL-2 and BIM/MCL-1 complex levels. Tumor samples ($n = 2$ per group) were collected after 3 weeks treatment with vehicle or 100 mg/kg/day ABT199, at 4 hours after administration of the last dose. BIM/BCL-2 and BIM/MCL-1 complex levels were subsequently determined as described above.

To further demonstrate the importance of MCL-1 in neuroblastoma resistance to ABT199, combined effects of MCL-1 knockdown and ABT199 on cell viability were studied. MCL-1 knockdown in CHP126, KCNR and SJNB12 using two different shRNAs sensitized the neuroblastoma cell lines to ABT199 treatment (Fig. 5A). Effects of MCL-1 inhibition on the sensitivity of neuroblastoma cell lines CHP126, KCNR and SJNB12 to ABT199 were additionally studied using the selective MCL-1 inhibitor A-1210477. Combined treatment of CHP126, KCNR and SJNB12 with ABT199 and A-1210477 caused additive to slightly synergistic inhibitory effects on cell viability (Fig. 5B and Table 2). In line with the effects on cell viability, combination treatment of KCNR with ABT199 and A-1210477 resulted in a significantly larger increase in sub-G₁ fraction than treatment with either of the inhibitors alone (Fig. 5C). BCL-2/BIM co-immunoprecipitation studies confirmed the occurrence of BIM displacement from BCL-2 after treatment with ABT199 alone or in combination with A-1210477. In a similar manner, MCL-1/BIM co-immunoprecipitation studies showed that the increased binding of BIM to MCL-1 observed after monotherapy with ABT199 was prevented by combination treatment with A-1210477 (Fig. 5D). Taken together, these results demonstrate that the efficacy of ABT199 can be potentiated by preventing sequestration of released BIM by MCL-1.

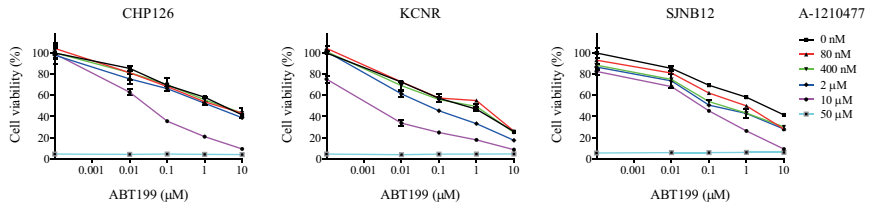
Figure 5. MCL-1 inhibition sensitizes high BCL-2 and BIM/BCL-2-expressing neuroblastoma cells to ABT199. *A*, *In vitro* effects of MCL-1 knockdown on the sensitivity of neuroblastoma cell lines CHP126, KCNR and SJNB12 to ABT199. Cells were 72-hour transfected with non-targeting control shRNA or MCL-1 shRNA (i.e., MCL-1 shRNA_1 or MCL-1 shRNA_2) prior to treatment with DMSO (control) or indicated ABT199 concentrations. Cell viability was assessed after 72-hour treatment using the MTT colorimetric assay. For each cell line, the viability of non-transfected cells treated with DMSO was set to 100%. *B*, *In vitro* effects of the small molecule MCL-1 inhibitor A-1210477 on the sensitivity of CHP126, KCNR and SJNB12 to ABT199. Cells were co-treated with 0-10 $\mu\text{mol/L}$ ABT199 and 0-50 $\mu\text{mol/L}$ A-1210477. Effects on cell viability were established after 72-hour treatment using the MTT colorimetric assay. For each cell line, the viability of untreated cells was set to 100%. *C*, FACs analysis of KCNR after 72-hour treatment with 10 $\mu\text{mol/L}$ ABT199 alone or in combination with 10 $\mu\text{mol/L}$ A-1210477. Data represent the mean percentages of cells in sub-G₁ \pm SD of three replicate experiments. *D*, *In vitro* effects on BIM displacement from BCL-2 and MCL-1 after 24-hour treatment of KCNR with 10 $\mu\text{mol/L}$ of ABT199 or 10 $\mu\text{mol/L}$ of A-1210477 and a combination of both compounds. BIM displacement was established by detecting BIM/BCL-2 and BIM/MCL-1 complex levels by anti-BCL-2 and anti-MCL-1 immunoprecipitation, followed by western blotting for BIM. BCL-2 and MCL-1 levels served as loading control.

High efficacy of the BCL2 inhibitor venetoclax (ABT199) in neuroblastoma and rational for combination with MCL1 inhibition

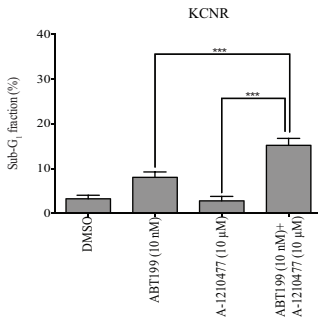
A.



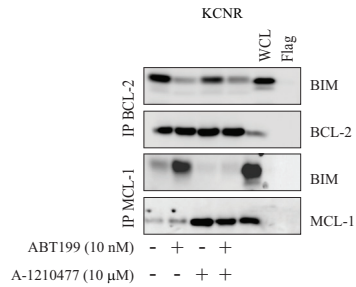
B.



C.



D.



	CHP126	KCNR	SJNB12
A-1210477	++++ (0.18)	+++ (0.28)	+ (0.74)

Table 2. Synergy between BCL-2 inhibitor ABT199 and MCL-1 inhibitor A-1210477 in high BCL-2-expressing neuroblastoma cell lines. Combination indices (between brackets) were determined according to Chou and Talalay [44]2,3...n is the velocity of reaction in the simultaneous presence of n inhibitors, v_i is the velocity observed in the presence of each individual inhibitor, and v_0 is the velocity in the absence of inhibition. The derivation is based on the assumption that each enzyme species can combine with no more than one of the inhibitors (i.e. the inhibitors are mutually exclusive).

DISCUSSION

Based on previously performed preclinical studies [16], BCL-2 inhibitor ABT263 was considered to have high potential for testing in neuroblastoma patients. Unfortunately, the clinical implementation of ABT263 was hampered because of dose-limiting thrombocytopenia due to concomitant inhibition of the anti-apoptotic protein BCL-X_L. The current manuscript describes the preclinical evaluation of the novel selective BCL-2 inhibitor ABT199. In line with previous results obtained with ABT263, neuroblastoma cell lines expressing high *BCL-2* mRNA levels responded more potently to ABT199 than low *BCL-2*-expressing cell lines, with an over 90-fold difference in average LC₅₀ value (i.e., 0.17 μ M versus 15.46 μ M, respectively). *In vitro* efficacy studies furthermore showed that BCL-2 protein and BIM/BCL-2 complex levels are better predictive biomarkers for ABT199 sensitivity than *BCL-2* mRNA levels. Although less strong, MYCN amplification status was also observed to be a predictive biomarker for sensitivity to ABT199.

The current manuscript describes the first side-by-side *in vivo* comparison of ABT199 with ABT263 for solid cancer treatment. Although ABT199 induced a strong apoptotic response, comparison of the efficacy of equal doses of ABT199 and ABT263 in mice with KCNR neuroblastoma xenografts expressing high levels of BCL-2 showed superior antitumor activity for ABT263. As maximum BIM displacement from BCL-2 was observed after ABT199 treatment, the most plausible explanation for the superior efficacy of ABT263 is its additional activity against anti-apoptotic proteins BCL-X_L and BCL-W. Results indicate that the simultaneous inhibition of multiple anti-apoptotic proteins is more effective for treatment of BCL-2-dependent neuroblastoma than inhibition of BCL-2 alone.

The importance of inhibiting multiple anti-apoptotic proteins is strengthened by the observations that *in vitro* and *in vivo* treatment with ABT199 resulted in upregulation of the anti-apoptotic protein MCL-1 and sequestration of released BIM by MCL-1. Upregulation of non-targeted anti-apoptotic BCL-2 family proteins taking over the function of BCL-2 has earlier been described as one of the key mechanisms of tumor resistance to BCL-2 inhibitors including ABT199 [28-32, 34]. Long-term ABT199 treatment of non-Hodgkin lymphoma cells resulted in upregulated levels of anti-apoptotic proteins MCL-1 and BCL-X_L that sequestered BIM [29]. No changes in the expression and activity of BCL-X_L were observed after ABT199 treatment, indicating that MCL-1 plays a more important role in neuroblastoma resistance to ABT199 than BCL-X_L.

MCL-1 upregulation after ABT199 treatment could be explained by Noxa downregulation and MCL-1 stabilization by BIM. Binding of Noxa to MCL-1 triggers Mule-mediated ubiquitination and proteasomal degradation of the anti-apoptotic protein, resulting in decreased MCL-1 levels [33, 35-40]. We observed that Noxa was downregulated after *in vitro* and *in vivo* treatment with ABT199, which has not been reported for BCL-2 inhibitors before. Since complexation of BIM with MCL-1 stabilizes MCL-1 independent of Noxa [33], BIM displacement from BCL-2 to MCL-1 after ABT199 treatment might also contribute to upregulated MCL-1 levels.

Combining *MCL-1* knockdown with ABT199 treatment resulted in synergistic cell growth inhibition. Potentiating effects of MCL-1 inhibition were confirmed with the small molecule MCL-1 inhibitor A-1210477, but combined effects of ABT199 and A-1210477 were additive rather than synergistic. The less potentiating effects obtained with A-1210477 might be due to the incomplete displacement of BIM from MCL-1, which has been described before. In addition, MCL-1 might have other functions independent of its role in apoptosis such as maintenance of mitochondrial integrity and deregulation of mitochondrial integrity by *MCL-1* knockdown in combination with BCL-2 inhibitors might have a more lethal effect on neuroblastoma cells than inhibition of the pro-apoptotic function of MCL-1 alone. Of interest is the observation that several compounds in use or development for cancer treatment also cause MCL-1 inhibition (e.g., CDK inhibitors, MEK inhibitors and PI3K/mTOR inhibitors [24, 28, 29]. Specific combination studies with these types of compounds should be considered.

For the clinical use of ABT199 it is important to identify pharmacodynamic biomarkers for efficacy. In line with previously published results for ABT199 [17], our study demonstrated that BIM displacement from BCL-2 and cytochrome c release from the

mitochondria can be utilized as target-specific efficacy biomarkers for ABT199. *In vitro* dose-dependent stimulatory effects on PARP- and caspase 3 cleavage and the *in vivo* observed cleaved caspase 3 induction after ABT199 treatment furthermore indicate that both apoptotic markers are potential non-target specific biomarkers for ABT199 efficacy. Additional studies are required to validate the dose-dependency of all potential biomarkers *in vivo*.

Taken together, the results presented in this study strongly suggest that children with neuroblastoma tumors expressing high levels of BCL-2 and BIM/BCL-2 complex might benefit from combined treatment with ABT199 and compounds that inhibit MCL-1.

REFERENCES

1. Yip KW and Reed JC. Bcl-2 family proteins and cancer. *Oncogene*. 2008; 27(50): 6398-6406.
2. Czabotar PE, Lessene G, Strasser A and Adams JM. Control of apoptosis by the BCL-2 protein family: implications for physiology and therapy. *Nat Rev Mol Cell Biol*. 2014; 15(1): 49-63.
3. Iqbal J, Neppalli VT, Wright G, Dave BJ, Horsman DE, Rosenwald A, Lynch J, Hans CP, Weisenburger DD, Greiner TC, Gascoyne RD, Campo E, Ott G, Muller-Hermelink HK, Delabie J, Jaffe ES, et al. BCL2 expression is a prognostic marker for the activated B-cell-like type of diffuse large B-cell lymphoma. *J Clin Oncol*. 2006; 24(6): 961-968.
4. Chipuk JE, Moldoveanu T, Llambi F, Parsons MJ and Green DR. The BCL-2 family reunion. *Mol Cell*. 2010; 37(3): 299-310.
5. Green DR and Kroemer G. The pathophysiology of mitochondrial cell death. *Science*. 2004; 305(5684): 626-629.
6. Llambi F, Moldoveanu T, Tait SW, Bouchier-Hayes L, Temirov J, McCormick LL, Dillon CP and Green DR. A unified model of mammalian BCL-2 protein family interactions at the mitochondria. *Mol Cell*. 2011; 44(4): 517-531.
7. Davids MS and Letai A. Targeting the B-cell lymphoma/leukemia 2 family in cancer. *J Clin Oncol*. 2012; 30(25): 3127-3135.
8. Hu W and Kavanagh JJ. Anticancer therapy targeting the apoptotic pathway. *Lancet Oncol*. 2003; 4(12): 721-729.
9. Korsmeyer SJ, Wei MC, Saito M, Weiler S, Oh KJ and Schlesinger PH. Pro-apoptotic cascade activates BID, which oligomerizes BAK or BAX into pores that result in the release of cytochrome c. *Cell Death Differ*. 2000; 7(12): 1166-1173.
10. Saelens X, Festjens N, Vande Walle L, van Gurp M, van Loo G and Vandenberghe P. Toxic proteins released from mitochondria in cell death. *Oncogene*. 2004; 23(16): 2861-2874.
11. Sun XM, MacFarlane M, Zhuang J, Wolf BB, Green DR and Cohen GM. Distinct caspase cascades are initiated in receptor-mediated and chemical-induced apoptosis. *J Biol Chem*. 1999; 274(8): 5053-5060.
12. Tait SW and Green DR. Mitochondria and cell death: outer membrane permeabilization and beyond. *Nat Rev Mol Cell Biol*. 2010; 11(9): 621-632.
13. Wei MC, Lindsten T, Mootha VK, Weiler S, Gross A, Ashiya M, Thompson CB and Korsmeyer SJ. tBID, a membrane-targeted death ligand, oligomerizes BAK to release cytochrome c. *Genes Dev*. 2000; 14(16): 2060-2071.
14. Irwin MS and Park JR. Neuroblastoma: paradigm for precision medicine. *Pediatr Clin North Am*. 2015; 62(1): 225-256.
15. Goldsmith KC, Gross M, Peirce S, Luyindula D, Liu X, Vu A, Sliozberg M, Guo R, Zhao H, Reynolds CP and Hogarty MD. Mitochondrial Bcl-2 family dynamics define therapy response and resistance in neuroblastoma. *Cancer Res*. 2012; 72(10): 2565-2577.

16. Lamers F, Schild L, den Hartog IJ, Ebus ME, Westerhout EM, Ora I, Koster J, Versteeg R, Caron HN and Molenaar JJ. Targeted BCL2 inhibition effectively inhibits neuroblastoma tumor growth. *Eur J Cancer*. 2012; 48(16): 3093-3103.
17. Souers AJ, Levenson JD, Boghaert ER, Ackler SL, Catron ND, Chen J, Dayton BD, Ding H, Enschede SH, Fairbrother WJ, Huang DC, Hymowitz SG, Jin S, Khaw SL, Kovar PJ, Lam LT, et al. ABT-199, a potent and selective BCL-2 inhibitor, achieves antitumor activity while sparing platelets. *Nat Med*. 2013; 19(2): 202-208.
18. Mason KD, Carpinelli MR, Fletcher JI, Collinge JE, Hilton AA, Ellis S, Kelly PN, Ekert PG, Metcalf D, Roberts AW, Huang DC and Kile BT. Programmed anuclear cell death delimits platelet life span. *Cell*. 2007; 128(6): 1173-1186.
19. Roberts AW, Seymour JF, Brown JR, Wierda WG, Kipps TJ, Khaw SL, Carney DA, He SZ, Huang DC, Xiong H, Cui Y, Busman TA, McKeegan EM, Krivoshik AP, Enschede SH and Humerickhouse R. Substantial susceptibility of chronic lymphocytic leukemia to BCL2 inhibition: results of a phase I study of navitoclax in patients with relapsed or refractory disease. *J Clin Oncol*. 2011; 30(5): 488-496.
20. Rudin CM, Hann CL, Garon EB, Ribeiro de Oliveira M, Bonomi PD, Camidge DR, Chu Q, Giaccone G, Khaira D, Ramalingam SS, Ranson MR, Dive C, McKeegan EM, Chyla BJ, Dowell BL, Chakravarty A, et al. Phase II study of single-agent navitoclax (ABT-263) and biomarker correlates in patients with relapsed small cell lung cancer. *Clin Cancer Res*. 2012; 18(11): 3163-3169.
21. Wilson WH, O'Connor OA, Czuczman MS, LaCasce AS, Gerecitano JF, Leonard JP, Tulpule A, Dunleavy K, Xiong H, Chiu YL, Cui Y, Busman T, Elmore SW, Rosenberg SH, Krivoshik AP, Enschede SH, et al. Navitoclax, a targeted high-affinity inhibitor of BCL-2, in lymphoid malignancies: a phase 1 dose-escalation study of safety, pharmacokinetics, pharmacodynamics, and antitumor activity. *Lancet Oncol*. 2010; 11(12): 1149-1159.
22. Zhang H, Nimmer PM, Tahir SK, Chen J, Fryer RM, Hahn KR, Iciek LA, Morgan SJ, Nasarre MC, Nelson R, Preusser LC, Reinhart GA, Smith ML, Rosenberg SH, Elmore SW and Tse C. Bcl-2 family proteins are essential for platelet survival. *Cell Death Differ*. 2007; 14(5): 943-951.
23. Pan R, Hogdal LJ, Benito JM, Bucci D, Han L, Borthakur G, Cortes J, DeAngelo DJ, Debose L, Mu H, Dohner H, Gaidzik VI, Galinsky I, Golfman LS, Haferlach T, Harutyunyan KG, et al. Selective BCL-2 inhibition by ABT-199 causes on-target cell death in acute myeloid leukemia. *Cancer Discov*. 2014; 4(3): 362-375.
24. Vandenberg CJ and Cory S. ABT-199, a new Bcl-2-specific BH3 mimetic, has in vivo efficacy against aggressive Myc-driven mouse lymphomas without provoking thrombocytopenia. *Blood*. 2013; 121(12): 2285-2288.
25. Choo EF, Boggs J, Zhu C, Lubach JW, Catron ND, Jenkins G, Souers AJ and Voorman R. The role of lymphatic transport on the systemic bioavailability of the Bcl-2 protein family inhibitors navitoclax (ABT-263) and ABT-199. *Drug Metab Dispos*. 2013; 42(2): 207-212.
26. Davids MS and Letai A. ABT-199: taking dead aim at BCL-2. *Cancer Cell*. 2013; 23(2): 139-141.

27. Touzeau C, Dousset C, Le Gouill S, Sampath D, Levenson JD, Souers AJ, Maiga S, Bene MC, Moreau P, Pellat-Deceunynck C and Amiot M. The Bcl-2 specific BH3 mimetic ABT-199: a promising targeted therapy for t(11;14) multiple myeloma. *Leukemia*. 2014; 28(1): 210-212.
28. Chen S, Dai Y, Harada H, Dent P and Grant S. Mcl-1 down-regulation potentiates ABT-737 lethality by cooperatively inducing Bak activation and Bax translocation. *Cancer Res*. 2007; 67(2): 782-791.
29. Choudhary GS, Al-Harbi S, Mazumder S, Hill BT, Smith MR, Bodo J, Hsi ED and Almasan A. MCL-1 and BCL-xL-dependent resistance to the BCL-2 inhibitor ABT-199 can be overcome by preventing PI3K/AKT/mTOR activation in lymphoid malignancies. *Cell Death Dis*. 2015; 6: e1593.
30. Lestini BJ, Goldsmith KC, Fluchel MN, Liu X, Chen NL, Goyal B, Pawel BR and Hogarty MD. Mcl1 downregulation sensitizes neuroblastoma to cytotoxic chemotherapy and small molecule Bcl2-family antagonists. *Cancer Biol Ther*. 2009; 8(16): 1587-1595.
31. Mazumder S, Choudhary GS, Al-Harbi S and Almasan A. Mcl-1 Phosphorylation defines ABT-737 resistance that can be overcome by increased NOXA expression in leukemic B cells. *Cancer Res*. 2012; 72(12): 3069-3079.
32. Wang B, Ni Z, Dai X, Qin L, Li X, Xu L, Lian J and He F. The Bcl-2/xL inhibitor ABT-263 increases the stability of Mcl-1 mRNA and protein in hepatocellular carcinoma cells. *Mol Cancer*. 2014; 13: 98.
33. Czabotar PE, Lee EF, van Delft MF, Day CL, Smith BJ, Huang DC, Fairlie WD, Hinds MG and Colman PM. Structural insights into the degradation of Mcl-1 induced by BH3 domains. *Proc Natl Acad Sci U S A*. 2007; 104(15): 6217-6222.
34. Yecies D, Carlson NE, Deng J and Letai A. Acquired resistance to ABT-737 in lymphoma cells that up-regulate MCL-1 and BFL-1. *Blood*. 2010; 115(16): 3304-3313.
35. Gomez-Bougie P, Menoret E, Juin P, Dousset C, Pellat-Deceunynck C and Amiot M. Noxa controls Mule-dependent Mcl-1 ubiquitination through the regulation of the Mcl-1/USP9X interaction. *Biochem Biophys Res Commun*. 2011; 413(3): 460-464.
36. Gomez-Bougie P, Wulleme-Toumi S, Menoret E, Trichet V, Robillard N, Philippe M, Bataille R and Amiot M. Noxa up-regulation and Mcl-1 cleavage are associated to apoptosis induction by bortezomib in multiple myeloma. *Cancer Res*. 2007; 67(11): 5418-5424.
37. Hauck P, Chao BH, Litz J and Krystal GW. Alterations in the Noxa/Mcl-1 axis determine sensitivity of small cell lung cancer to the BH3 mimetic ABT-737. *Mol Cancer Ther*. 2009; 8(4): 883-892.
38. Nakajima W, Hicks MA, Tanaka N, Krystal GW and Harada H. Noxa determines localization and stability of MCL-1 and consequently ABT-737 sensitivity in small cell lung cancer. *Cell Death Dis*. 2014; 5: e1052.
39. Pang X, Zhang J, Lopez H, Wang Y, Li W, O'Neill KL, Evans JJ, George NM, Long J, Chen Y and Luo X. The carboxyl-terminal tail of Noxa protein regulates the stability of Noxa and Mcl-1. *J Biol Chem*. 2014; 289(25): 17802-17811.

40. Yan J, Zhong N, Liu G, Chen K, Liu X, Su L and Singhal S. Usp9x- and Noxa-mediated Mcl-1 downregulation contributes to pemetrexed-induced apoptosis in human non-small-cell lung cancer cells. *Cell Death Dis.* 2014; 5: e1316.
41. Bate-Eya LT, Ebus ME, Koster J, den Hartog IJ, Zwijnenburg DA, Schild L, van der Ploeg I, Dolman ME, Caron HN, Versteeg R and Molenaar JJ. Newly-derived neuroblastoma cell lines propagated in serum-free media recapitulate the genotype and phenotype of primary neuroblastoma tumors. *Eur J Cancer.* 2014; 50(3): 628-637.
42. Dolman ME, Poon E, Ebus ME, den Hartog IJ, van Noesel CJ, Jamin Y, Hallsworth AM, Robinson SP, Petrie K, Sparidans RW, Kok RJ, Versteeg R, Caron HN, Chesler L and Molenaar JJ. Cyclin-dependent kinase inhibitor AT7519 as a potential drug for MYCN-dependent neuroblastoma. *Clin Cancer Res.* 2015.
43. Twentyman PR and Luscombe M. A study of some variables in a tetrazolium dye (MTT) based assay for cell growth and chemosensitivity. *Br J Cancer.* 1987; 56(3): 279-285.
44. Chou TC, Talalay P. A simple generalized equation for the analysis of multiple inhibitions of Michaelis-Menten kinetic systems. *J Biol Chem* 1977;(252):6438-42.

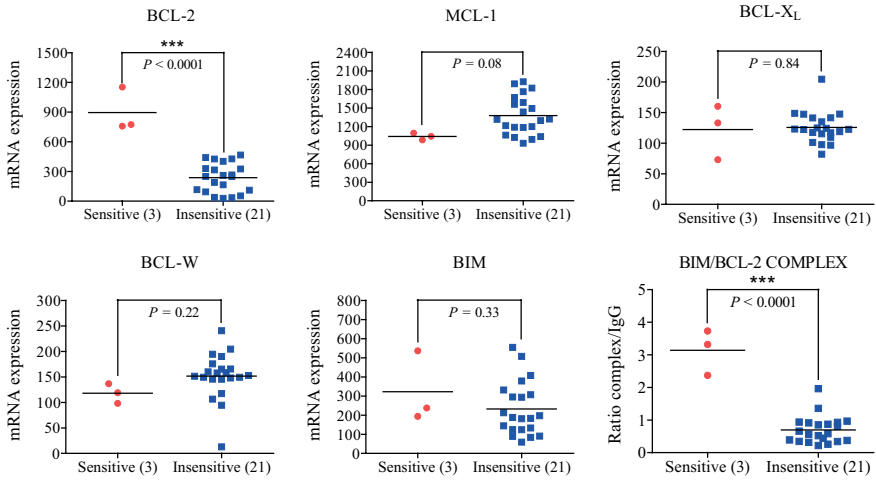
SUPPLEMENTARY INFORMATION

	ABT199 concentration	Sub-G ₁ (%)	G ₁ (%)	S (%)	G ₂ (%)
CHP126	0 nmol/L	4.3±1.1	58.9±3.6	19.6±2.2	19.4±3.8
	7.5 nmol/L	12.2±1.2	58.1±5.3	13.6±2.7	14.6±1.6
	15.5 nmol/L	11.9±1.6	57.3±3.1	14.5±1.6	17.6±1.4
	32.5 nmol/L	11.3±2.8	59.8±2.1	14.1±0.4	15.1±1.1
	62.5 nmol/L	15.6±2.3	56.6±2.1	13.8±2.4	15.6±1.9
	125 nmol/L	33.9±1.1	51.1±5.6	9.5±5.4	7.2±3.6
	1.25 µmol/L	34.5±0.9	46.3±7.1	9.8±3.4	9.1±2.7
	5 µmol/L	35.7±9.8	45.2±7.5	9.9±0.9	9.3±1.9
	10 µmol/L	48.3±3.1	39.3±1.4	7.3±0.9	6.6±0.7
KCNR	0 nmol/L	1.1± 0.5	58.7±0.9	21.5±0.8	18.3±0.9
	7.5 nmol/L	14.4±1.6	55.1±2.9	19.4±1.9	11.4±2.4
	15.5 nmol/L	17.3±3.0	49.9±0.5	21.2±0.02	12.1±3.5
	32.5 nmol/L	22.5±2.7	47.7±1.6	18.7±1.6	10.6±1.5
	62.5 nmol/L	22.0±2.9	49.7±1.1	17.8±0.3	9.8±0.04
	125 nmol/L	20.2±1.6	53.9±2.2	17.0±3.4	9.4±0.5
	1.25 µmol/L	21.1±1.3	52.5±6.4	17.2±4.1	10.5±3.3
	5 µmol/L	24.9±0.4	48.5±0.6	16.5±1.2	9.2±0.3
	10 µmol/L	26.3±1.8	46.1±0.8	17.6±0.5	9.8±0.1
SJNB12	0 nmol/L	2.0±0.01	70.3±0.6	8.1±5.9	19.2±8.8
	7.5 nmol/L	7.2±1.2	63.5±2.1	5.0±0.4	24.3±0.5
	15.5 nmol/L	15.3±1.5	57.4±0.9	5.3±1.6	21.7±0.6
	32.5 nmol/L	18.0±1.1	57.2±1.7	4.6±1.9	20.0±2.8
	62.5 nmol/L	21.7±3.6	54.8±3.8	6.7±1.1	17.2±0.3
	125 nmol/L	25.1±4.4	52.4±4.8	6.6±0.9	15.9±1.2
	1.25 µmol/L	28.8±3.3	49.3±4.6	7±1.2	15.6±1.3
	5 µmol/L	29.1±2.5	48.9±2.7	7.5±0.7	15.7±2.1
	10 µmol/L	39.1±2.3	45.1±1.2	4.6±1.7	11.3±1.7
SKNAS	0 nmol/L	1.3±0.6	59.4±6.3	17.9±1.6	21.4±4.3
	7.5 nmol/L	1.8±1.2	58.2±2.1	18.9±0.5	19.3±1.7
	15.5 nmol/L	1.7±0.7	58.3±4.1	19.9±1.1	20.9±4.6
	32.5 nmol/L	1.1±0.4	59.1±3.7	19.1±0.3	20.1±3.1
	62.5 nmol/L	1.3±0.2	60.1±3.3	19.6±0.2	19.3±3.4
	125 nmol/L	1.2±0.1	59.6±1.1	20.1±1.1	18.4±1.6
	1.25 µmol/L	1.3±0.2	58.7±1.2	19.5±1.2	18.7±2.6
	5 µmol/L	1.4±0.09	58.8±2.6	21.6±2.6	17.4±0.6
	10 µmol/L	8.1±5.6	59.7±4.9	15.3±4.9	16.5±4.7
SHEP2	0 nmol/L	0.8±0.4	75.6±2.1	13.7±2.4	10.7±3.6
	7.5 nmol/L	1.6±1.1	74.6±0.9	11.7±0.9	12.1±2.9
	15.5 nmol/L	1.7±1.2	76.1±3.7	12.0±0.8	12.1±3.2
	32.5 nmol/L	1.3±0.3	75.7±2.3	11.3±1.3	12.6±1.3
	62.5 nmol/L	1.4±0.4	77.1±1.5	10.4±1.2	11.6±1.8
	125 nmol/L	1.4±1.1	77.9±2.6	11.0±1.6	10.4±3.3
	1.25 µmol/L	1.9±1.8	75.4±2.9	10.3±1.9	11.9±3.6
	5 µmol/L	3.6±2.4	72.1±2.8	12.8±0.4	12.1±2.3
	10 µmol/L	4.3±2.2	70.8±4.4	12.6±1.1	11.1±3.9

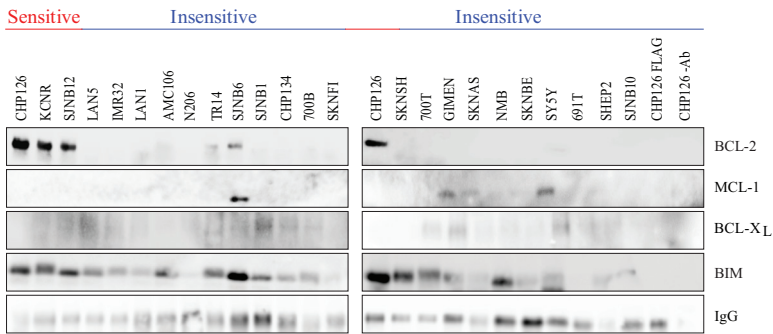
Supplementary Table 1. *In vitro* effects on sub-G₁ induction and cell cycle progression in neuroblastoma cell lines expressing high BCL-2 and BIM/BCL-2 complex levels (i.e., CHP126, KCNR and SJNB12) versus low expressing neuroblastoma cell lines (i.e., SKNAS and SHEP2) after 72 h treatment with ABT199. Values represent the average percentage of cells in sub-G₁, G₁, S and G₂ +/- SD.

Chapter 4

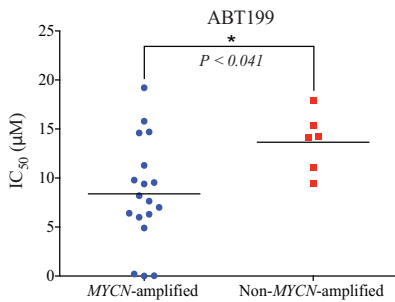
A.



B.



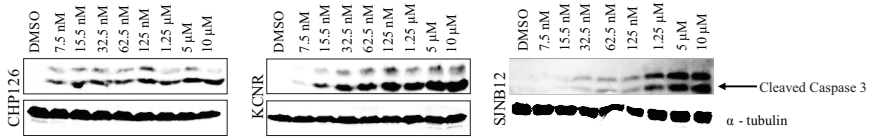
C.



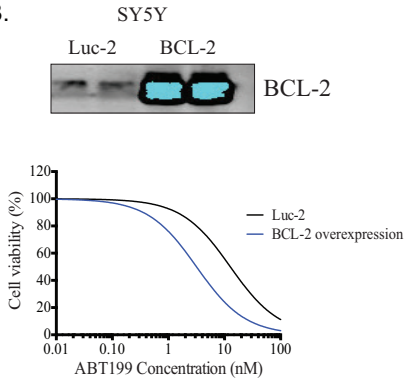
Supplementary Figure 1. *BCL-2* mRNA levels, protein levels of BCL-2/BIM complex and *MYCN* amplification status predict sensitivity to ABT199. A, mRNA expression levels of *BCL-2*, *MCL-1*, *BCL-X_L*, *BCL-W* and *BIM* and BCL-2/BIM protein complex levels in sensitive (i.e., CHP126, KCNR, and SJNB12) versus insensitive neuroblastoma cell lines. *BCL-2*, *MCL-1*, *BCL-X_L*, *BCL-W* and *BIM* mRNA levels have been established using the R2 bioinformatics platform (<http://r2.amc.nl>), which contains Affymetrix mRNA expression data of all cell lines studied in the current manuscript. BCL-2/BIM complex levels were established by anti-BIM immunoprecipitation of whole cell lysates, followed by western blotting for BCL-2. BCL-2 band intensities were normalized to the IgG heavy chain of the BIM antibody. Statistical differences between the sensitive and insensitive cell lines were calculated using a one-tailed (for *BCL-2* mRNA and BIM/BCL-2 protein complex) or two-tailed unpaired Student *t* test, with $P < 0.05$ as the minimal level of significance and $P < 0.0001$ indicated as ***. Horizontal lines represent the mean of the mRNA expression of the BCL-2 family proteins and the BCL-2/BIM complex levels of the cell line panel. B, BCL-2/BIM, MCL-1/BIM and BCL-X_L/BIM complex levels in 24 neuroblastoma cell lines, ordered from ABT199 sensitive (left) to ABT199 insensitive (right). Complex levels were established by anti-BIM immunoprecipitation of whole cell lysates, followed by western blotting for BCL-2 and MCL-1. The IgG heavy chain of the BIM antibody served as a loading control. Total protein levels of the BCL-2-like family member proteins of the cell line panel in Figure 1A served as whole cell lysates for this experiment. C, IC₅₀ of *MYCN* amplified versus non-*MYCN* amplified cell lines treated with ABT199. IC₅₀ curves were obtained by MTT assays after 72-hour treatment of the cell lines with ABT199 and IC₅₀ values were calculated by the fitted-method using the Graphpad Prism software. Statistical differences in sensitivity to ABT199 between the *MYCN* and non-*MYCN* amplified cell lines were calculated using a one-tailed Student *t* test, with $P < 0.05$ as the minimal level of significance and $P < 0.0001$ indicated as ***.

Chapter 4

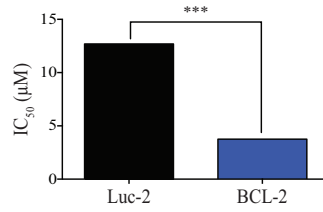
A.



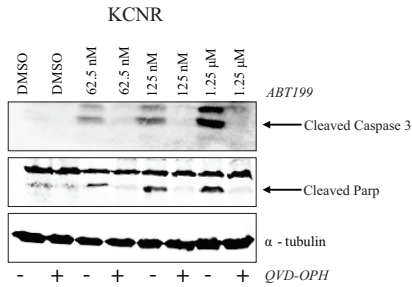
B.



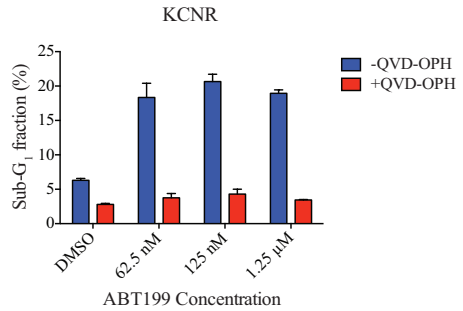
C.



D.

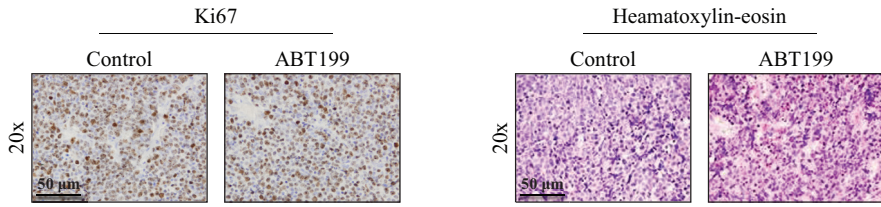


E.

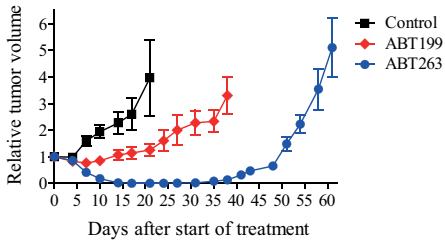


Supplementary Figure 2. ABT199 inhibits BCL-2 and causes apoptosis by induction of the intrinsic apoptotic pathway which can be rescued with caspase inhibitors. A, Western blot analysis of the *in vitro* effects of ABT199 on caspase 3 cleavage after 72-hour treatment of sensitive cell lines CHP126, KCNR and SJNB12 with increasing ABT199 concentrations. Alpha-tubulin served as loading control. B, Western blot analysis of the level of overexpression of BCL-2 in a BCL-2 low-expressing cell line SY5Y compared to an SY5Y cell lines expressing the Luc2 control construct and IC₅₀ curves comparing the sensitivity of a BCL-2 low expressing cell lines SY5Y overexpressing BCL-2 in blue compared to an SY5Y line overexpressing a luciferase 2 construct in black. Cell viability was measured after 72-hour treatment of the cell lines with ABT199. The data are the mean of three replicate wells. C, Bar graphs comparing the IC₅₀ values between SY5Y cells expressing the Luc2 construct and SY5Y overexpressing BCL-2. Data represents one experiment. D, Western blot analysis on the *in vitro* effects of the inhibition of caspase 3 and PARP cleavage after 4-hour treatment with the pan-caspase 3 inhibitor QVD-OPH and 24-hour treatment with the BCL-2 inhibitor ABT199 in the BCL-2 high expressing cell line KCNR. Alpha-tubulin served as loading control. E, FACS analysis of the *in vitro* effects on sub-G₁ induction after 4-hour treatment of KCNR with the pan-caspase inhibitor QVD-OPH and 24-hour treatment with increasing ABT199 concentrations. Data represent the mean percentages of cells in sub-G₁ ± SD of three replicate experiments.

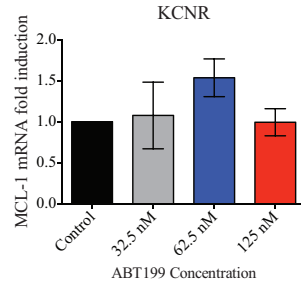
A.



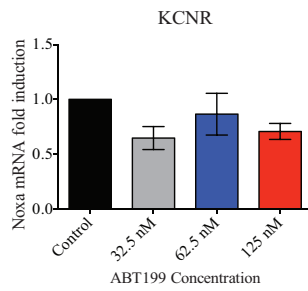
B.



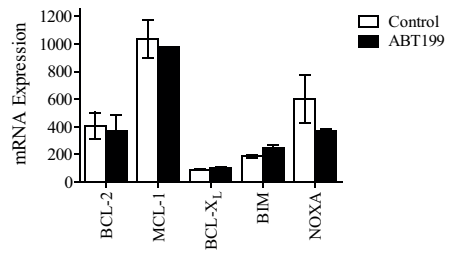
C.



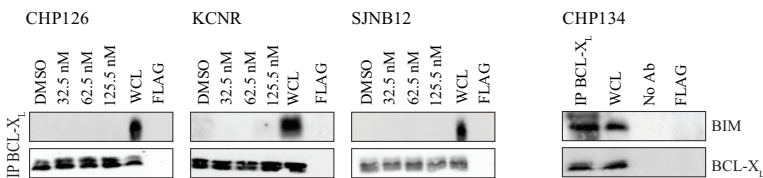
D.



E.



F.



Supplementary Figure 3. ABT199 and ABT263 elicit anticancer activity in mice with KCNR neuroblastoma xenografts expressing high BCL-2 and BIM/BCL-2 complex levels. Mice with KCNR xenografts of approximately 268 mm³ were daily treated with vehicle (control), 100 mg/kg ABT199 or 100 mg/kg ABT263 for 3 consecutive weeks. A, Representative microscopic images of Ki67 and heamatoxylin-eosin stained paraffin-embedded sections of control tumors versus tumors treated with ABT199. Tumor materials were collected at 4 hours after administration of the last dose. ABT199 effects on cell proliferation and phenotypic changes caused by ABT199 were studied by immunohistochemistry analysis of Ki67 and conventional heamatoxylin-eosin staining, respectively. Magnification of the images: 20x. Scale bar: 50 μm. B, Long-term effects of ABT199 and ABT263 on the growth of KCNR neuroblastoma xenografts after three weeks treatment. Relative tumor volume was calculated as the volume at the indicated day after start of treatment divided by the volume prior to treatment initiation. Data represent the mean relative tumor volume ± SEM. [Group sizes at the start of treatment: *n* = 10 (control), *n* = 5 (ABT199), and *n* = 5 (ABT263)]. C, D, Effects on *in vitro* mRNA levels of *MCL-1* and *NOXA* in the BCL-2 high expressing cell line KCNR treated for 24-hour with increasing concentrations of ABT199. *MCL-1* and *NOXA* fold change was analyzed by real-time quantitative-PCR. RNA levels of the control treated samples were set to 1 for analysis. Data represent average mRNA expression values ± SD. E, ABT199 effects on *in vivo* mRNA levels of *BCL-2*, *MCL-1*, *BCL-X_L*, *BIM* and *NOXA*. Tumor materials of control and ABT199-treated KCNR xenografts (*n* = 2 per group) were collected at 4 hours after administration of the last dose and analyzed by Affymetrix mRNA profiling. Data represent average mRNA expression values ± SEM. F, *In vitro* effects of ABT199 on BIM/BCL-X_L complex levels in CHP126, SJNB12 and KCNR after 24-hour treatment with increasing doses. BIM/BCL-X_L complex levels were established by immunoprecipitation of BCL-X_L followed by Western blot analysis of BIM. Immunoprecipitated levels of BCL-X_L were used as loading controls. As no BIM/BCL-X_L complex could be detected in the cell lines tested, neuroblastoma cell line CHP134 was included as a positive control for BIM/BCL-X_L complex.

MATERIALS AND METHODS

Cell culture. Classical human neuroblastoma cell lines were grown in Dulbecco's modified Eagle's medium (DMEM) containing 4.5 g/L D-glucose, glutamate and supplemented with 10% (v/v) foetal calf serum, 2 mmol/L L-glutamine, 10 U/mL penicillin, 10 µg/mL streptomycin and MEM non-essential amino acids (1x). Neuroblastoma tumor-initiating cell (TIC) lines were grown in neural specific stem cell medium (400 mL DMEM GlutaMAX™-1 containing 1g/L D-glucose and pyruvate, 133 mL F12 medium, 10 mL B27, 18 ng/mL EGF, 36 ng/mL FGF, 10 U/mL penicillin and 10 µg/mL streptomycin. Cells were maintained at 37°C under 5% CO₂ in humidified air. Penicillin and streptomycin were obtained from Sigma Aldrich, EGF from Corning Life Sciences and FGF from PeproTech. Other cell culture related materials were obtained from Life Technologies.

***In vitro* FACS analysis.** High BCL-2-expressing neuroblastoma cell lines CHP126, KCNR, and SJNB12 and low BCL-2-expressing cell lines SKNAS and SHEP2 were seeded in triplicate onto 6-cm plates and incubated overnight. Cells were then 72-hour treated with 0.1% DMSO (control) or ABT199 using concentration ranges of 7.8 nmol/L to 10 µmol/L. Supernatants containing floating cells were collected from the culture dishes. Adherent cells were washed once with PBS and PBS solutions were pooled with the supernatants. After trypsinization of the adherent cells with 0.05% trypsin/EDTA, cells were resuspended in the pooled supernatant/PBS solution. Next, cells were centrifuged (5 min; 1,500 rpm), washed by resuspension in PBS and centrifuged again (5 min; 3,000 rpm). Cells were fixed with 100% ice-cold ethanol, stained with 0.05 mg/mL propidium iodide and supplemented with 0.05 mg/mL RNase A in PBS. After 1-hour incubation in the dark at room temperature (RT), cells were filtered through a 50 µm filter (BD Biosciences) and DNA contents of the nuclei were analyzed using a fluorescence-activated cell sorter. A total of 20,000 nuclei per sample were counted. The cell cycle distribution and apoptotic Sub-G₁ fraction were determined using the BD Accuri™ C6 flow cytometer with the CFlow plus software (BD Biosciences).

Cell fractionation. CHP126, KCNR, SJNB12, SKNAS and SHEP2 were seeded onto 14-cm culture dishes and incubated overnight. Cell lines were then 24-hour treated with 0.04% DMSO (control) or 62.5 nmol/L to 10 µmol/L ABT199. Supernatants containing floating cells were collected from the culture dishes. Adherent cells were washed once with PBS and the PBS solutions were pooled with the supernatants. After trypsinization of the adherent cells with 0.05% trypsin/EDTA, cells were resuspended in the pooled supernatant/PBS solution. Next, cells were centrifuged (5 min; 1,500 rpm), twice washed

by resuspension in PBS and centrifuged again (5 min; 1,500 rpm). Cytosolic and organelle fractions were subsequently separated using the ProteoExtract® Subcellular Proteome Extraction Kit according to the manufacturers protocol (Calbiochem, 539790). Cell fractions were used for cytochrome c detection by western blot analysis (see below).

***In vitro* western blotting.** Cells were seeded onto 9- or 14-cm dishes and treated with DMSO (control) or up to 10 µmol/L ABT199. Treated cells were harvested at indicated time points and lysed using Laemmli buffer [i.e., H₂O/glycerol/20% sodium dodecyl sulfate (SDS)/1 M Tris-HCl (pH 6.8) 5:2:2:1 (v/v/v/v)]. Lysates were homogenized by hydrodynamic shearing through a 23 G needle, followed by 10 min incubation at 50°C. Protein concentrations were determined using the Bio-Rad DC Protein Assay (Bio-Rad, Venendaal, the Netherlands).

Equal protein amounts (40 µg) were diluted in 5x reducing sampling buffer (i.e., Laemmli buffer/β-mercaptoethanol 3:1 (v/v) with bromophenol blue sodium salt). Diluted samples were boiled for 5 min at 95°C and centrifuged (1,500 rpm 5 min). Proteins were separated by SDS-polyacrylamide gel electrophoresis on 12% Mini-Protean® Tris-glycine extended (TGX) precast gels (Bio-Rad) and transferred on hybond nitrocellulose membranes (0.45 µm) by 1.5-hour wet blotting (200 mA; 4°C). Transfer buffer consisted of 20% (v/v) methanol, 3.025 g/L Tris and 14.4 g/L glycine in demineralized water. Membranes were blocked in 2% ECL Prime™ blocking agent (GE Healthcare) in PBS with 0.1% (v/v) Tween-20 (= blocking buffer) for 1-hour at RT. After blocking, membranes were incubated with the primary (overnight; 4°C) and secondary (1-hour; RT) antibodies in blocking buffer and scanned using the Image Quant LAS 4000 detection system (GE Healthcare Life Science).

***In vitro* co-immunoprecipitation and immunoblotting.** For all samples, total cell lysates were prepared in 2% CHAPS buffer (i.e., 1 mol/L HEPES, 150 mmol/L NaCl, 5 mmol/L EDTA, 5% sodium glycerol phosphate (w/v) and 2% (w/v) CHAPS). Equal protein amounts (1 mg) were added to antibody-matrix complex Protein A-Agarose beads (Roche) for 24 hours at 4°C. Immunoprecipitated proteins were released from the matrix using RIPA buffer (1x) and analyzed by western blot analysis as described above, with minor modifications. MCL-1 detection has been performed using mouse anti-human MCL-1 (clone RC13) monoclonal antibody (Merck Millipore). Other antibodies were similar to the antibodies used for *in vitro* western blotting and all antibodies have been used in a 1:100 dilution. Flag control samples were immunoprecipitated with an anti-Flag rabbit DYDDDDK tag antibody (clone 2368) (1:100 Cell Signaling Technology).

***In vivo* efficacy in neuroblastoma mouse models.** Female NMRI *nu/nu* mice (6-15 weeks old; 20-30 g) were subcutaneously injected with $1-5 \times 10^6$ cells/flank of KCNR. The size of the tumors was recorded twice weekly and when the tumors reached a size of approximately 1,000 mm³, tumor pieces were serially xenotransplanted in recipient mice. Formalin-fixed and paraffin-embedded sections of the serially xenotransplanted tumors were routinely checked by hematoxylin-eosin staining. For the efficacy studies, recipient mice with KCNR neuroblastoma xenografts of approximately 268 mm³ were orally treated with 100 mg/kg/d ABT199 (n = 5), 100 mg/kg/d ABT263 (n = 5), or vehicle (n = 6) for 21 days. Tumor sizes were measured by an external caliper.

***In vivo* immunohistochemistry.** Paraffin-embedded sections of 4 μm were deparaffinized in xylene and hydrated in a series of alcohol baths. Endogenous peroxidase activity was inactivated by 10 minutes incubation with 0.3% (v/v) hydrogen peroxide in methanol. After rinsing in running tap water (5 min), tumor sections were pre-treated with 10.1 mmol/L Tris/EDTA buffer pH 9.1 (10 min; wet autoclaving). Sections were rinsed in Tris buffered saline (TBS) pH 7.8 (5 min) and 1-hour incubated with the primary antibodies. Anti-Ki67- and anti-cleaved caspase 3 antibodies were diluted in ScyTek Antibody Diluent (ScyTek Laboratories). Sections were washed with TBS (3x 2 min), incubated with the secondary antibody, rinsed again in TBS and incubated using the 3,3-diaminobenzidine (DAB) + Substrate Chromogen System (10 min; Dako, Heverlee, Belgium). Nuclei were stained by successively rinsing with running tap water, counterstaining with hematoxylin and rinsing again with running tap water. Sections were dehydrated in an ascending graded series of ethanol baths and xylene and mounted with Pertex and coverslip. Prior to visualization with an Olympus BX51 Microscope and DP70 Digital Camera System, sections were overnight incubated at 50°C. All incubations were performed at RT, unless indicated otherwise.

RNA isolation and real-time quantitative PCR. RNA was isolated using the Trizol-chloroform method from the KCNR cell line treated for 24-hour with 32.5-125 nmol/L concentrations of ABT199. 1 μg of mRNA was reversed transcribed using the Taqman reverse transcription kit and amplified using the SYBR Green Master Mix (Applied Biosystems, N808234) and examined on a MyiQ Real-time PCR systems (Bio-Rad). Quantitative, real-time PCR was performed using the following specific primers: *MCL-1* 5'-ATGCTTCGGAAACTGGACAT-3'(forward) and 5'-TCCTGATGCCACCTTCTAGG-3'(reverse); *Noxa* 5'-TGGAAGTCGAGTGTGCTACTCAA-3' (forward) and 5'-CAGAAGA

High efficacy of the BCL2 inhibitor venetoclax (ABT199) in neuroblastoma
and rational for combination with MCL1 inhibition

GTTTGGATATCAGATTCAGA-3' (reverse) and *B-Actin* 5'-AGAAAATCTGGCACCACACC-3'
(forward) and 5'-AGAGGCGTACAGGGATAGCA-3' (reverse).



CHAPTER 5

HIGH-THROUGHPUT SCREENING IDENTIFIES IDASANUTLIN AS A RE-SENSITIZING DRUG FOR VENETOCLAX-RESISTANT NEUROBLASTOMA CELLS.

Authors: Laurel T. Bate-Eya¹, Nil A. Schubert¹, Lindy K. Alles¹, Bianca Koopmans¹, Daphne Lelieveld², David A. Egan², Mark Kerstjens³, Ronald W. Stam¹, Jan Koster⁴, Huib N. Caron⁵, Jan J. Molenaar¹, and M. Emmy M. Dolman¹.

¹Princess Máxima Center for Pediatric Oncology, Utrecht, the Netherlands. ²Department of Cell Biology, University Medical Center Utrecht (UMCU), Utrecht, the Netherlands. ³Department of Pediatric Oncology/Hematology, Erasmus MC-Sophia Childrens's Hospital, Rotterdam, the Netherlands. Departments of ⁴Oncogenomics, and ⁵Pediatric Oncology, Emma Kinderziekenhuis, Academic Medical Center, University of Amsterdam, Amsterdam, the Netherlands.

Submitted

TRANSLATIONAL RELEVANCE

High BCL-2 expression has been observed in neuroblastoma tumors compared to other malignant tumors and normal tissues. Previous preclinical studies using the BCL-2-specific inhibitor venetoclax showed superior activity in neuroblastoma tumors with high BCL-2 and BIM/BCL-2 complex levels. However, eventually resistance occurred as is seen with most targeted compounds with high specificity.

The current study describes the identification of drugs capable of re-sensitizing venetoclax-resistant neuroblastoma cell lines to venetoclax. Long-term continuous exposure of BCL-2-dependent neuroblastoma cell lines to high venetoclax concentrations resulted in venetoclax-resistance. A compound-wide screen with targeted compounds in (pre-) clinical development and cytostatics used in neuroblastoma treatment identified idasanutlin as the strongest re-sensitizer for venetoclax in venetoclax-resistant BCL-2-dependent neuroblastoma cells. Re-sensitization by idasanutlin could be attributed to p53-mediated upregulation of BAX, resulting in re-activation of the intrinsic apoptotic pathway. *In vivo* combination studies with venetoclax and idasanutlin showed superior efficacy over single-agent treatments, with significant regression of BCL-2-dependent neuroblastoma xenografts.

Taken together, our findings suggest that BCL-2 high-expressing neuroblastoma patients might benefit from combination treatment of venetoclax with the MDM2 inhibitor idasanutlin.

ABSTRACT

Purpose: The anti-apoptotic protein B cell lymphoma/leukaemia 2 (*BCL-2*) is highly expressed in neuroblastoma. In previous preclinical studies, we have shown that the *BCL-2* specific inhibitor venetoclax causes a strong apoptotic phenotype in *BCL-2*-dependent neuroblastoma cells. However, *in vivo* treatment with venetoclax showed partial resistance. In the current manuscript, we describe the identification of re-sensitizing drugs for venetoclax-resistant *BCL-2*-dependent neuroblastoma.

Experimental Design: Non-resistant and venetoclax-resistant neuroblastoma cell lines in the absence and presence of venetoclax were exposed to a 209-compound library to identify compounds that were more effective in the venetoclax-resistant cell lines in the presence of venetoclax.

Results: Long-term continuous exposure of *BCL-2*-dependent neuroblastoma cell lines SJNB12 and KCNR to high venetoclax concentrations resulted in >50 times less sensitivity to venetoclax, as shown by differences in IC_{50} values. Resistance to venetoclax was caused by the increased expression of myeloid cell leukaemia sequence 1 (*MCL-1*) and sequestration of BIM released from *BCL-2* by *MCL-1*. High-throughput drug screening identified idasanutlin as a re-sensitizing drug for venetoclax-resistant neuroblastoma cells, as shown by the 1.5-20-fold higher activity of idasanutlin in the venetoclax-resistant cells under venetoclax pressure compared to the non-resistant cells. Idasanutlin caused BAX-mediated apoptosis in venetoclax-resistant neuroblastoma cells in the presence of venetoclax, while causing p21-mediated growth arrest in the non-resistant cells and venetoclax-resistant cells in the absence of venetoclax. *In vivo* combination treatment of mice with *BCL-2*-dependent neuroblastoma tumors with venetoclax and idasanutlin showed superior efficacy over single-agent treatments, with significant tumor regression.

Conclusions: This study suggests that patients with *BCL-2*-dependent neuroblastoma tumors might benefit from combined treatment with venetoclax and the re-sensitizing drug idasanutlin.

INTRODUCTION

Aberrations in genes encoding B cell lymphoma/leukaemia 2 (BCL-2) family proteins have been observed in numerous cancer types (1). The intrinsic apoptotic pathway consists of the anti-apoptotic BCL-2 family members (2, 3), [e.g., BCL-2, BCL-extra-large (BCL-X_L), BCL-2-like protein 2 (BCL-W) and myeloid cell leukaemia sequence 1 (MCL-1)]. These anti-apoptotic proteins prevent apoptosis from occurring by sequestering their BH3-only counterparts [e.g., BCL-2-like protein 11 (BIM), p53 upregulated modulator of apoptosis (PUMA), NOXA and BH3 interacting domain death agonist (BID)]. Displacement of the pro-apoptotic proteins during cellular stress activates the pro-apoptotic proteins BAX (BCL-2-associated X protein) and BAK (BCL-2 antagonist/killer 1) (4-6). Oligomerization of BAX/BAK causes mitochondrial outer membrane permeabilization, followed by cytochrome c release into the cytosol and activation of caspase-3-induced proteolysis and cell death (7-13).

Neuroblastomas are pediatric solid tumors that arise from the sympathetic nervous system. Despite extensive treatment regimens these tumors still account for approximately 15% of all pediatric cancer deaths (14). A large subset of neuroblastoma tumors express enhanced levels of the anti-apoptotic gene *BCL-2* (15, 16). Mitochondrial profiling of neuroblastoma cell lines expressing high BCL-2 level reveal a BH3 profile which predicts sensitivity to BCL-2 antagonists *in vitro*. BCL-2-dependent cell lines in which BIM was bound to the BH3 domain of BCL-2 were shown to respond potently to the BCL-2 inhibitor navitoclax, while neuroblastoma cell lines with an MCL-1 profile were deemed resistant to the compound (15). In previous studies, it was shown that navitoclax induced a strong apoptotic response in BCL-2-dependent neuroblastoma cell lines (16). Unfortunately, the clinical use of navitoclax was associated with dose-limiting thrombocytopenia due to concomitant targeting of BCL-X_L. Therefore, the BCL-2-specific inhibitor venetoclax was developed. *In vitro* studies have shown that also venetoclax caused strong apoptosis in BCL-2-dependent neuroblastoma cells through BIM displacement from BCL-2 and cytochrome c release from the mitochondria into the cytoplasm (17, 18). These findings could be confirmed *in vivo* in a BCL-2-dependent neuroblastoma xenograft mouse model. However, partial resistance to venetoclax was observed, which could be attributed to MCL-1 upregulation and sequestration of BIM displaced from BCL-2 by MCL-1. Combined inhibition of MCL-1 and BCL-2 abrogated the partial resistance observed in BCL-2 high-expressing cells treated with venetoclax. However, MCL-1 inhibitors are still in early preclinical development and combination

treatment of patients with MCL-1 and BCL-2 inhibitors have been reported to cause myelo-suppressive related side effects.

In the current study, we therefore aimed at identifying strategies to re-sensitize venetoclax-resistant neuroblastoma tumor cells to ventoclax.

MATERIALS AND METHODS

Chemicals. The Sequoia anti-neoplastic library containing 157 approved drugs used in cancer treatment and the SCREEN-WELL® epigenetics library containing 43 epigenetic compounds were purchased from Sequoia Research Products (Pangbourne, UK) and Enzo Life Sciences (Farmingdale, USA), respectively. Other targeted inhibitors used in the current study were purchased from Selleck Chemicals while the regularly used cytostatics in neuroblastoma treatment were purchased from Sigma Aldrich. Both compound libraries were reformatted to a single 384-well plate at a concentration of 200 μ M in DMSO. Venetoclax (ABT199), navitoclax, AT7519, JQ1, ceritinib, ribociclib, idasanutlin (RG7388), trametinib and YM155 were added to the reformatted library plate. For *in vivo* studies, venetoclax was formulated in 10% ethanol/30% polyethylene glycol (PEG) 400/60% phosal 50 propylene glycol (PG) (v/v/v) in final concentrations of 10 mg/ml. Idasanutlin was formulated in 2% hydroxypropyl cellulose/0.1% polysorbate 80/0.09% methyl paraben/0.01% propyl paraben in final concentrations of 15mg/ml.

Cell culture. Human neuroblastoma cell lines SJNB12 and KCNR were cultured as previously described (19). Cell culture protocols are described in detail in the Supplementary Materials and Methods.

Generation of venetoclax-resistant neuroblastoma cell lines. Neuroblastoma cell lines SJNB12 and KCNR were made resistant to venetoclax by long-term continuous exposure to venetoclax doses equal to the IC₈₅ concentrations for both cell lines (i.e. 2.75 μ mol/L for SJNB12 and 7.5 μ mol/L for KCNR). Venetoclax-containing medium was refreshed twice a week. This was done by allowing the cells to recover for 24-hours in normal culture medium, prior to venetoclax addition. Venetoclax resistance was confirmed by investigating differences in venetoclax dose-response curves and venetoclax-induced sub-G₁ accumulation between resistant and non-resistant cell lines after 72-hour treatment (see below).

BCL-2 DNA sequence analysis. Genomic DNA from non-resistant SJNB12 and KCNR cells and venetoclax-resistant SJNB12 and KCNR cells under venetoclax pressure (i.e. 2.75 $\mu\text{mol/L}$ for SJNB12 and 7.5 $\mu\text{mol/L}$ for KCNR) was obtained using the chloroform-isopropanol method. DNA was then purified using a QIAamp DNA Mini Kit (Qiagen), PCR amplified with Taq polymerase (Invitrogen), and sequenced in the ABI PRISM 3730 sequencer (Applied Biosystems). Primers used for the gene sequence analysis are: Exon 1: Forward primer: GTCCAAGAATGCAAAGCACA, Reverse primer: GAACGCTTTGTGGAGAGGAG. Exon 2: Forward primer: GCAGGATGCCTCTTTCTCTG, Reverse primer: AGCCTGCAGCTTTGTTTCAT.

mRNA expression profiling. RNA was extracted from non-resistant SJNB12 and KCNR cells and venetoclax-resistant SJNB12 and KCNR cells in the presence of venetoclax using TRIzol (Invitrogen, Carlsbad, CA) following the manufacturers protocols. RNA concentration and quality were determined using the RNA 6000 Nano assay on the Agilent 2100 Bioanalyzer (Agilent Technologies). Fragmentation of cRNA, hybridization to Human Genome U133 plus 2.0, microarrays and scanning were carried out according to the manufacturers protocol (Affymetrix inc. Santa Barbara, CA). The mRNA gene expression data were normalized with the MAS5.0 algorithm within the GCOS program of Affymetrix Inc. Target intensity was set to 100. All data were analyzed using the R2 genomic analysis and visualization platform (<http://r2.amc.nl>).

High-throughput drug screening and hit selection. Non-resistant and venetoclax-resistant SJNB12 and KCNR neuroblastoma cell lines were seeded in 384-well plates (i.e. 10000 cells/well for SJNB12 lines and 8000 cells/well for KCNR lines). Resistant cell lines were plated both without venetoclax and in the presence of venetoclax doses equal the IC_{85} for the matching non-resistant cell lines (i.e. 2.75 $\mu\text{mol/L}$ for SJNB12 and 7.5 $\mu\text{mol/L}$ for KCNR). Cells were incubated overnight and treated with 10 nmol/L, 100 nmol/L and 1 $\mu\text{mol/L}$ of the compounds on the library plate using the Sciclone ALH 3000 liquid handling robot (Perkin Elmer). Control samples were treated with DMSO. Cell viability was determined prior to and after 72-hour treatment using the 3-(4,5-dimethylthiazol-2-yl)-2,5-diphenyltetrazolium bromide (MTT) colorimetric assay. The cell viability of DMSO-treated cells was set to 100%. For each compound, the sum of the % viable cells observed after treatment with 10 nM, 100 nM and 1 μM was calculated for the non-resistant cells, venetoclax-resistant cells and venetoclax-resistant cells under venetoclax pressure. Compounds for which the sum of the percentages viable cells was lower for the venetoclax-resistant cells under venetoclax pressure than for the non-resistant

cells were considered re-sensitizing compounds. Hit selection was performed by taking the 40 top re-sensitizing compounds and subsequently excluding non-targeted compounds (except for the regularly used cytostatics in neuroblastoma treatment) and targeted compounds for which treatment with the highest tested concentration (i.e. 1 μ M) resulted in $\geq 20\%$ viable cells.

Validation re-sensitizing effects of compounds. Non-resistant and venetoclax-resistant SJNB12 and KCNR neuroblastoma cell lines were seeded in quadruplicate as described above. After overnight incubation, non-resistant SJNB12 and KCNR cells, venetoclax-resistant SJNB12 and KCNR cells and venetoclax-resistant SJNB12 and KCNR cells in the presence of venetoclax were treated with 8 concentrations of each compound and control samples were treated with DMSO using the Combi-Bulk Tecan HP D300 Digital Dispenser (Hewlett-Packard). Half maximal effective concentration (IC_{50}) values were derived from dose-response curves. IC_{50} values at 72 hours were calculated by determining the compound concentrations needed to achieve a 50% reduction in cell viability observed for DMSO-treated cells at 72 hours (set at 100%).

FACS analysis. To confirm the generation of venetoclax-resistant SJNB12 and KCNR cells, non-resistant and venetoclax-resistant cells were treated with 0.1% DMSO (control) or venetoclax using concentration ranges of 7.8 nmol/L to 10 μ mol/L. To study the effects of idasanutlin on sub- G_1 induction, non-resistant SJNB12 and KCNR cells, venetoclax-resistant SJNB12 and KCNR cells and venetoclax-resistant SJNB12 and KCNR cells in the presence of venetoclax were treated with 0.05% DMSO (control) or 25 nmol/L to 1 μ mol/L idasanutlin. After 72-hour treatment, floating and adherent cells were harvested for FACS analysis to determine the cell-cycle distribution and the apoptotic sub- G_1 fraction. See Supplementary Materials and Methods for a detailed protocol.

Western blotting. The following antibodies were used: rabbit anti-human BCL-2 (clone D55G8) monoclonal antibody (1:1,000, Cell Signaling Technology); rabbit anti-human MCL-1 monoclonal antibody (1:1,000, Cell Signaling Technology); rabbit anti-human BCL-X_L (clone 54H6) monoclonal antibody (1:1,000, Cell Signaling Technology); rabbit anti-human BCL-W (Clone 31H4) monoclonal antibody (1:1,000, Cell Signaling Technology); rabbit anti-human BIM (1:1,000, Cell Signaling Technology); rabbit anti-human PARP (Clone 9542S) monoclonal antibody (1:1,000, Cell Signaling Technology); rabbit anti-human p21 monoclonal antibody (1:1,000, Abcam); rabbit anti-human BAX polyclonal antibody (1:1,000, Cell Signaling Technology) mouse anti-human p53 monoclonal antibody (clone D0-7) (1:1,000, Neomarkers), rabbit anti-human MDM2

polyclonal antibody (clone N-20) (1:1,000, Santa Cruz Biotechnology), mouse anti-human α -tubulin (clone DM1A) monoclonal antibody (1:10,000, Cell Signaling Technology) and horseradish peroxidase (HRP)-conjugated goat anti-rabbit (clone NA9340V) and goat anti-mouse (clone NXA931) secondary antibodies (1:10,000 GE Healthcare). See Supplementary Materials and Methods for detailed protocol.

***In vitro* co-immunoprecipitation and immunoblotting.** Non-resistant SJNB12 and KCNR cells, venetoclax-resistant SJNB12 and KCNR cells and/or venetoclax-resistant SJNB12 and KCNR cells in the presence of venetoclax were seeded onto T75 flasks. For the detection of BIM displacement from BCL-2 and BIM complexation with MCL-1 in the non-resistant cell lines and venetoclax-resistant cell lines, cells were harvested at normal culture conditions or treated with idasanutlin. For all samples, total cell lysates were prepared in 2% Chaps buffer (i.e., 1 mol/L HEPES, 150 mmol/L NaCl, 5 mmol/L EDTA, 5% sodium glycerol phosphate (w/v) and 2% (w/v) Chaps). Equal protein amounts (1 mg) were added to antibody-matrix complex Protein A-Agarose beads (Roche) for 24 hours at 4°C. Immunoprecipitated proteins were released from the matrix using RIPA buffer (1x) and analyzed by Western blot analysis as described above, with minor modifications. MCL-1 detection has been performed using mouse anti-human MCL-1 (clone RC13) monoclonal antibody (Merck Millipore). Other antibodies were similar to the antibodies used for *in vitro* Western blotting and all antibodies have been used in a 1:100 dilution. Flag control samples were immunoprecipitated with an anti-Flag rabbit DYDDDDK tag antibody (clone 2368) (1:100 Cell Signaling Technology).

***In vivo* combination studies in neuroblastoma mouse models.** Female NMRI *nu/nu* mice (6-15 weeks old; 20-30 g) were obtained from Charles River Laboratories and experiments were performed with permission from and according to the standards of the Dutch animal ethics committee (DAG 103059, 102776, 102830 and 102690). NMRI *nu/nu* mice were subcutaneously injected with $1 \cdot 5 \times 10^6$ cells/flank of KCNR. The size of the tumors was recorded twice weekly and when the tumors reached a size of approximately 1,000 mm³, tumor pieces were serially xenotransplanted in recipient mice. Formalin-fixed and paraffin-embedded sections of the serially xenotransplanted tumors were routinely checked by hematoxylin-eosin staining and treatment started when the tumors of recipient mice with KCNR neuroblastoma xenografts reached an approximate size of about 268 mm³. Mice were randomly divided into five groups for the following treatment regimens: (1) three weeks treatment with vehicles venetoclax and idasanutlin (n=5), (2) three weeks treatment with 100 mg/kg/d venetoclax (n=6), (3)

three weeks treatment with 25 mg/kg/d idasanutlin (n=7), (4) three weeks combination treatment with 100 mg/kg/d venetoclax and 25 mg/kg/d idasanutlin (n=7) and (5) one week single treatment with 100 mg/kg/d venetoclax followed by two weeks combination treatment with venetoclax and 25 mg/kg/d idasanutlin (n=6). Compounds were administered orally and tumor sizes were measured by an external caliper.

***In vivo* western blotting.** Ten tumor sections of 50 μm were homogenized in 2% Chaps buffer as previously described. Western blot detection of protein levels of BAX was carried out as described for *in vitro* Western blotting.

***In vivo* co-immunoprecipitation.** Sections of treated and untreated KCNR tumors harvested at 4 hours after administration of the last dose were homogenized using the Ultra Turrax T25 tissue homogenizer (Janke & Kunkel) and lysed (overnight at 4 °C) in 2% Chaps buffer. Co-immunoprecipitation was carried out as described above.

RESULTS

Long-term continuous exposure of BCL-2-dependent neuroblastoma cells to high venetoclax concentrations results in MCL-1-mediated resistance

Normally sensitive BCL-2-dependent neuroblastoma cell lines SJNB12 and KCNR were made venetoclax-resistant by continuous exposure to high venetoclax doses equal to the IC_{85} concentrations for both cell lines (2.75 $\mu\text{mol/L}$ for SJNB12 and 7.5 $\mu\text{mol/L}$ for KCNR). After 3 months continuous exposure, SJNB12 and KCNR cell lines under venetoclax pressure divided as fast as the non-resistant cell lines. Resistance of SJNB12 and KCNR to venetoclax was first confirmed by differences in venetoclax dose-response curves (Fig. 1A), with 51 and 191 times higher IC_{50} values and 12 and 22 times higher LC_{50} values for resistant versus non-resistant SJNB12 and KCNR cell lines, respectively (Table 1). In addition, apoptotic responses in resistant cell lines were only observed for SJNB12 upon treatment with micromolar concentrations of venetoclax (i.e. $\geq 5 \mu\text{mol/L}$), while for both non-resistant cell lines nanomolar concentrations of venetoclax (i.e. 7.5 nmol/L) were already sufficient to induce a ≥ 2 -fold induction in sub- G_1 (Fig. 1B).

Sequencing of venetoclax-resistant neuroblastoma cell lines showed no mutations in the BH3 domain of BCL-2 (data not shown). Gene expression profiling (Affymetrix U133 plus 2.0 Arrays) of non-resistant KCNR cells and venetoclax-resistant KCNR cells under venetoclax pressure showed significantly increased *MCL-1* gene levels in the resistant

cells (Fig. 1C). This was in line with the increased MCL-1 protein levels observed in the resistant KCNR cells under venetoclax pressure (Fig. 1D). Also for SJNB12 MCL-1 protein was found to be higher expressed in the resistant cells under venetoclax pressure than in the non-resistant cells. Although at the gene level no significant changes were observed for the other anti-apoptotic BCL-2 family genes *BCL-2*, *BCL-X_L* and *BCL-W* between non-resistant and venetoclax-resistant KCNR cells, BCL-X_L protein levels were higher in the resistant KCNR cells under venetoclax pressure. BCL-2 immunoprecipitation followed by immunoblotting for BIM confirmed (almost) complete displacement of BIM from BCL-2 in resistant SJNB12 and KCNR cells under venetoclax pressure (Fig. 1E). In line with earlier observations for venetoclax treated BCL-2-dependent neuroblastoma cells, analysis of BIM/MCL-1 complex levels showed that released BIM from BCL-2 was sequestered by MCL-1 in the venetoclax-resistant cell lines. These results confirm that MCL-1 also plays an important role in resistance caused by long-term continuous treatment of BCL-2 dependent neuroblastoma cells with venetoclax.

High-throughput screening identifies idasanutlin as re-sensitizing agent for venetoclax-resistant neuroblastoma cells

As the aim of the current study was to identify compounds that re-sensitize venetoclax-resistant neuroblastoma cells to venetoclax, we first performed a high-throughput drug screen. Non-resistant SJNB12 and KCNR cells, venetoclax-resistant SJNB12 and KCNR cells and venetoclax-resistant SJNB12 and KCNR neuroblastoma cells in the presence of venetoclax were included in the screen. Cells were treated for 72 hours with a chemical library (10 nmol/L, 100 nmol/L and 1 μ mol/L) containing 157 approved drugs used in cancer treatment, 43 epigenetic compounds and 9 targeted compounds in (pre-)clinical development for neuroblastoma treatment. Compounds that were more effective in the resistant cell lines under venetoclax pressure than in the non-resistant cell lines were considered re-sensitizing drugs. Hit selection was performed by selecting the 40 top re-sensitizing compounds and subsequently excluding all non-targeted compounds (except for the regularly used cytostatics in neuroblastoma treatment) and targeted compounds for which the percentage viable cells after treatment with the highest tested concentration (i.e. 1 μ mol/L) was still $\geq 20\%$. This yielded 13 and 11 hits for venetoclax-resistant SJNB12 and KCNR, respectively, of which idasanutlin (MDM2 inhibitor), omipalisib (PI3K/mTOR inhibitor), flavopiridol (CDK inhibitor) and vorinostat (HDAC inhibitor) were overlapping (Fig. 2A and B). For idasanutlin, omipalisib and flavopiridol the increase in efficacy between venetoclax-resistant cells and the non-resistant cells was larger in the presence of venetoclax, confirming the occurrence of re-sensitization

in addition to or instead of overcoming resistance. Of the overlapping hits, idasanutlin was the number 1 re-sensitizing hit for venetoclax-resistant SJNB12 and the number 8 re-sensitizing hit for venetoclax-resistant KCNR. The observation that the non-resistant cell lines were much more sensitive to BCL-2 inhibitors venetoclax and navitoclax than the venetoclax-resistant cell lines (both in the presence and absence of venetoclax), confirmed that SJNB12 and KCNR cell lines exposed to long-term venetoclax treatment were still resistant during screening.

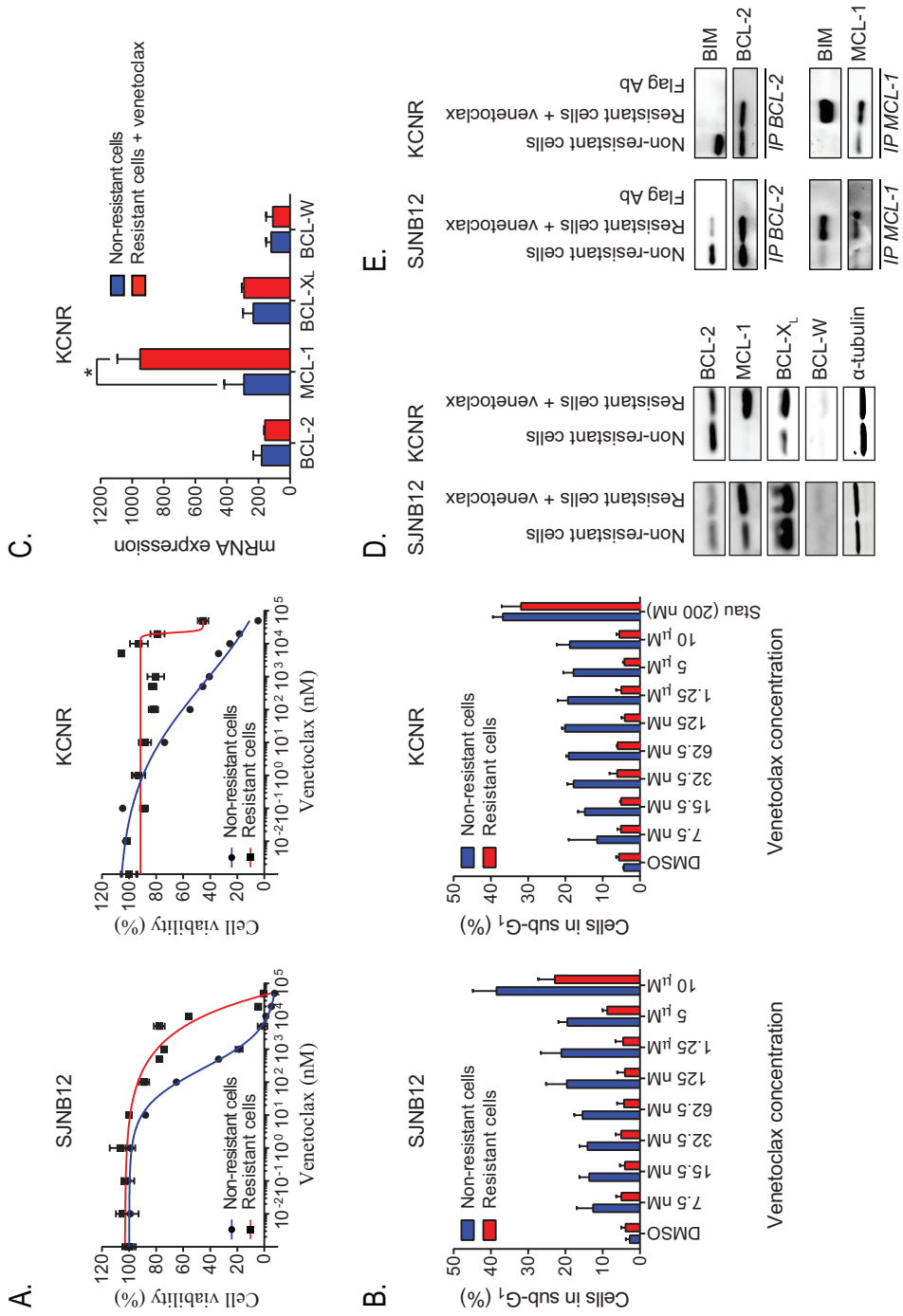
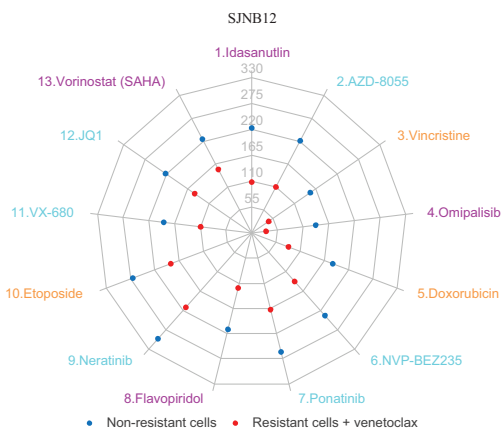
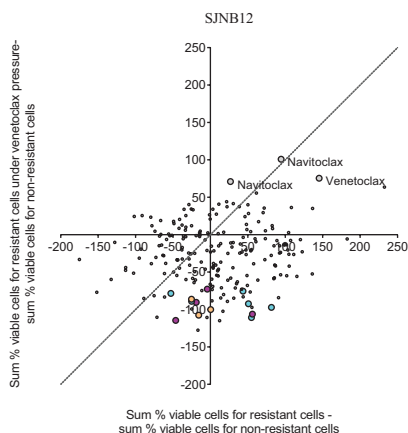


Figure 1. Long-term continuous exposure of BCL-2-dependent neuroblastoma cell lines to high venetoclax concentrations results in MCL-1-mediated venetoclax resistance. *A*, Dose-response curves of venetoclax for non-resistant (blue) versus venetoclax-resistant (red) SJNB12 and KCNR cells. Resistant neuroblastoma cell lines were generated by long-term continuous exposure of the normally sensitive SJNB12 and KCNR neuroblastoma cells to venetoclax doses equal to the IC_{50} concentrations for both cell lines (i.e. 2.75 $\mu\text{mol/L}$ for SJNB12 and 7.5 $\mu\text{mol/L}$ for KCNR). Venetoclax effects on cell viability were established at 72 hours after treatment using the MTT colorimetric assay. The cell viability of cells treated with DMSO for 72 hours was set to 100%. *B*, FACS analysis of the *in vitro* effects of venetoclax on sub- G_1 induction in non-resistant (blue) versus venetoclax-resistant (red) SJNB12 and KCNR cells. Effects on sub- G_1 induction were established after 72-hour treatment with increasing venetoclax concentrations. For venetoclax-resistant KCNR cells, staurosporine was included as a positive control. Data represent the mean percentages of cells in sub- G_1 + SD of three replicate experiments. *C*, Differences in gene expression levels of anti-apoptotic BCL-2 family members between non-resistant KCNR cells (blue) and venetoclax-resistant KCNR cells in the presence of 7.5 μM venetoclax (red). *BCL-1*, *BCL-X_L*, and *BCL-W* mRNA levels were established by Affymetrix microarray profiling. Data represent mean expression levels of triplicate samples + SD. Statistical differences between non-resistant and resistant KCNR cells in the presence of venetoclax were calculated using a one-tailed unpaired Student *t* test, with $P < 0.05$ as the minimal level of significance (indicated as *). *D*, Western blot analysis of the protein expression levels of anti-apoptotic proteins BCL-2, MCL-1, BCL-X_L and BCL-W in non-resistant SJNB12 and KCNR cells versus venetoclax-resistant SJNB12 and KCNR cells under ABT199 pressure (i.e. 2.75 $\mu\text{mol/L}$ for SJNB12 and 7.5 $\mu\text{mol/L}$ for KCNR). α -Tubulin was used as housekeeping protein. E, BIM/BCL-2 and BIM/MCL-1 complex levels in non-resistant versus venetoclax-resistant cells in the presence of venetoclax. BIM/BCL-2 and BIM/MCL-1 complex levels were established by anti-BCL-2- an anti-MCL-1 immunoprecipitation, respectively, followed by Western blotting for BIM.

Cell lines	IC_{50} ($\mu\text{mol/L}$)	LC_{50} ($\mu\text{mol/L}$)
Non-resistant KCNR cells	0.23	2.50
Venetoclax-resistant KCNR cells	44.00	55.00
Non-resistant SJNB12 cells	0.21	1.00
Venetoclax-resistant SJNB12 cells	10.80	11.70

Table 1. IC_{50} and LC_{50} values of venetoclax in non-resistant and venetoclax-resistant SJNB12 and KCNR neuroblastoma cells.

A.



B.

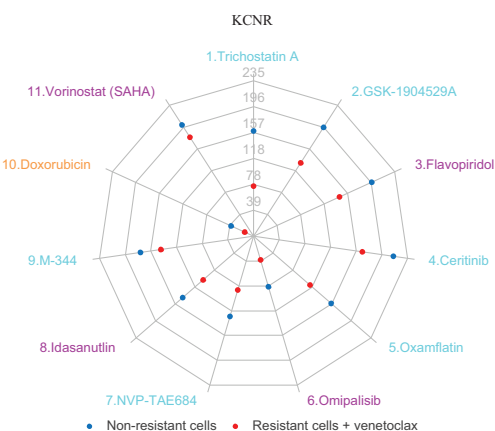
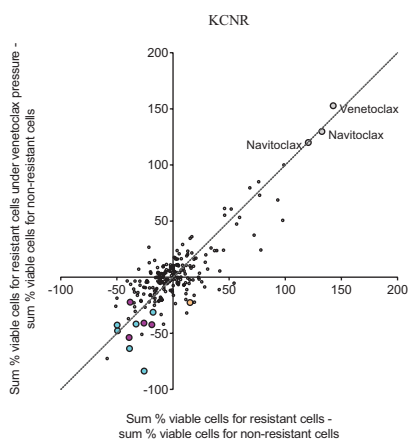


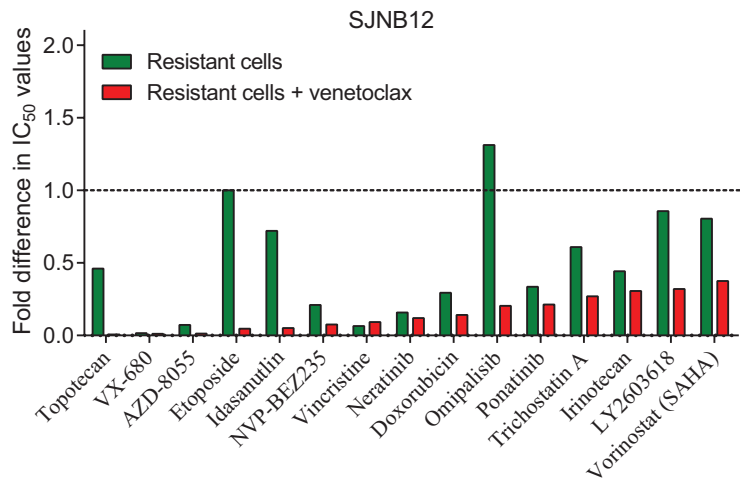
Figure 2. High-throughput screening (HTS) identifies drugs re-sensitizing neuroblastoma cells to venetoclax treatment. Non-resistant SJB12 and KCNR cells, venetoclax-resistant SJB12 and KCNR cells and venetoclax-resistant SJB12 and KCNR cells in the presence of venetoclax (i.e. 2.75 $\mu\text{mol/L}$ for SJB12 and 7.5 $\mu\text{mol/L}$ for KCNR) were treated with a 209-compound library using concentrations of 10 nmol/L, 100 nmol/L and 1 $\mu\text{mol/L}$. Effects on cell viability were established at 72 hours after treatment using the MTT colorimetric assay. The cell viability of DMSO-treated cells was set to 100%. For each compound, the sum of the % viable cells observed after treatment with 10 nmol/L, 100 nmol/L and 1 $\mu\text{mol/L}$ was calculated for the non-resistant cells, venetoclax-resistant cells and venetoclax-resistant cells under venetoclax pressure. Compounds for which the sum of the percentages viable cells was lower for the venetoclax-resistant cells under venetoclax pressure than for the non-resistant cells were considered re-sensitizing compounds. Hit selection was performed by taking the 40 top re-sensitizing compounds and subsequently excluding non-targeted compounds (except for the regularly used cytostatics in neuroblastoma treatment) and targeted compounds for which treatment with the highest tested concentration (i.e. 1 $\mu\text{mol/L}$) resulted in $\geq 20\%$ viable cells.

Graphs on the left show the difference in the sum of % viable cells between venetoclax-resistant cells and non-resistant cells (X-axis) versus the same difference between venetoclax-resistant cells under venetoclax pressure and non-resistant cells (Y-axis) for SJNB12 (A) and KCNR (B). Each dot represents a single compound and re-sensitizing hits are marked purple (hit for SJNB12 and KCNR), light blue (selective hit for SJNB12 or KCNR) or orange (regularly used cytostatic in neuroblastoma treatment). Radar charts on the right show the sum of % viable cells for the non-resistant cells versus the venetoclax-resistant cells in the presence of venetoclax obtained with the top re-sensitizing hits for SJNB12 (A) and KCNR (B), respectively. Re-sensitizing hits are numbered from most potent to least potent.

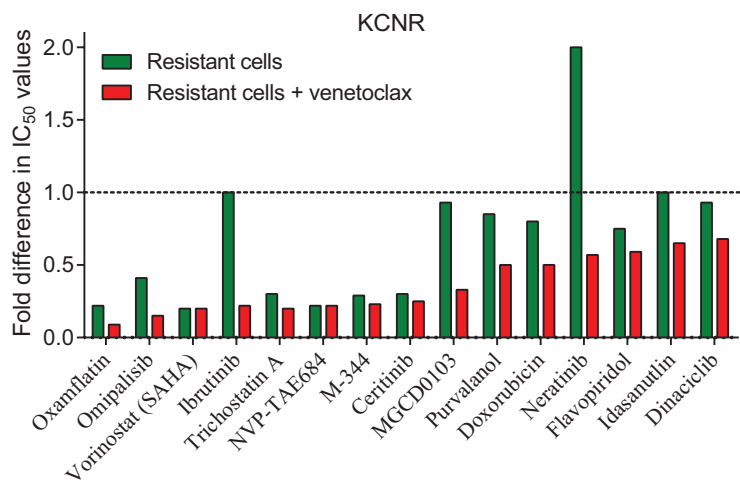
***In vitro* validation confirms re-sensitizing potential of idasanutlin**

All re-sensitizing hits from the screen were tested more extensively to validate the screening results. We also included targeted compounds for which synergy with BCL-2 inhibition has been previously described in the literature (20-28) and the regularly used cytostatics in neuroblastoma treatment (Table 2). For all compounds (i.e. 29), IC_{50} values in non-resistant SJNB12 and KCNR cells, in venetoclax-resistant SJNB12 and KCNR cells and in venetoclax-resistant SJNB12 and KCNR cells in the presence of venetoclax were determined from dose-response curves after 72 hours treatment (Supplementary Table S1). Fig. 3A and B show the top 15 of compounds with the largest fold decrease in IC_{50} value between the venetoclax-resistant cells under venetoclax pressure and the non-resistant cells for SJNB12 and KCNR, respectively. Results confirm the re-sensitizing potential of idasanutlin, with an almost 20-fold decrease in IC_{50} value for SJNB12 (i.e. 1011 versus 52 nmol/L) and a 1.5-fold decrease in IC_{50} value for KCNR (i.e. 30 versus 20 nmol/L) (Fig. 3C). For both neuroblastoma cell lines only limited differences were observed in IC_{50} values between the venetoclax-resistant cells in the absence of venetoclax and the non-resistant cells. This supports that idasanutlin re-sensitizes venetoclax-resistant neuroblastoma cells to venetoclax, rather than overcomes venetoclax resistance. In line with the screening results, omipalisib and vorinostat were also found in the top 15 list of most potent re-sensitizing drugs for venetoclax-resistant SJNB12 and KCNR neuroblastoma cells.

A.



B.



C.

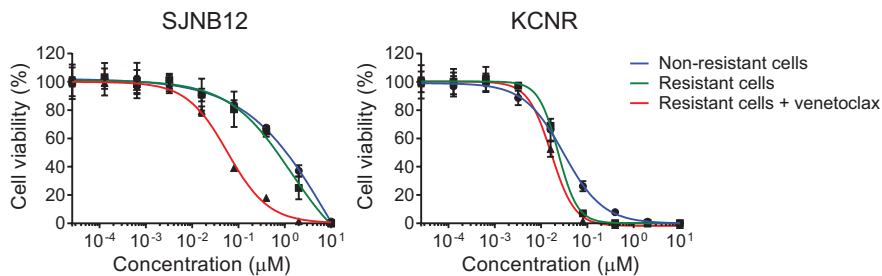


Figure 3. *In vitro* validation studies confirm re-sensitization of venetoclax-resistant neuroblastoma cells to venetoclax by idasanutlin treatment. For combined hits from the HTSs as well as targeted compounds for which synergy with BCL-2 inhibition has been described in literature and the regularly used cytostatics in neuroblastoma treatment, dose-response curves were established in non-resistant SJNB12 and KCNR cells, venetoclax-resistant SJNB12 and KCNR cells and venetoclax-resistant SJNB12 and KCNR cells under venetoclax pressure to establish IC_{50} values. A and B, Fold difference in IC_{50} values between venetoclax-resistant cells and non-resistant cells (green bars) and venetoclax-resistant cells under venetoclax pressure and non-resistant cells (red bars). Results are shown for the 15 top compounds inducing the largest difference in sensitivity between venetoclax-resistant cells under venetoclax pressure and non-resistant cells for SJNB12 (A) and KCNR (B), respectively. C, Dose-response curves of MDM2 inhibitor idasanutlin in non-resistant SJNB12 and KCNR cells (blue lines), venetoclax-resistant SJNB12 and KCNR cells (green lines) and venetoclax-resistant SJNB12 and KCNR cells in the presence of venetoclax (red lines).

Compound (Target)	Hit HTS for KCNR	Hit HTS for SJNB12	Potential hits from literature	Regularly used cytostatic in neuroblastoma treatment
AZD-8055 (mTORC1/2)		X		
Ceritinib (ALK)	X			
Cisplatin (DNA synthesis)				X
Dinaciclib (CDK1/2/5/9)			X	
Doxorubicin (DNA topoisomerase II)	X	X	X	X
Etoposide (DNA topoisomerase II)		X		X
Flavopiridol (CDK1/2/4/6/7)	X	X		
GS1101 (PI3K δ)			X	
GSK-1904529A (IGFR)	X			
Ibrutinib (BTK)			X	
Idasanutlin (MDM2)	X	X	X	
Irinotecan (DNA topoisomerase II)				X
JQ1 (BRD4 (1/2))		X	X	
LY2603618 (CHK1)			X	

Table 2. Compounds selected for more extensive *in vitro* testing of their effects on re-sensitization of venetoclax-resistant neuroblastoma cells to venetoclax. In addition to the re-sensitizing hits identified in the HTSs, we investigated the re-sensitizing effects of targeted compounds for which synergy with BCL-2 inhibition has been described in the literature as well as of the regularly used cytostatics in neuroblastoma treatment. Hit selection from the high-throughput screens (HTS) was performed by establishing the 40 top compounds more effective in the venetoclax-resistant cells under venetoclax pressure than in the non-resistant cells and subsequently excluding all non-targeted compounds (except for the regularly used cytostatics in neuroblastoma treatment) as well as targeted compounds for which the percentage viable cells after treatment with the highest tested concentration (i.e. 1 μ mol/L) was still $\geq 20\%$.

High-throughput screening identifies idasanutlin as a re-sensitizing drug for venetoclax-resistant neuroblastoma cells

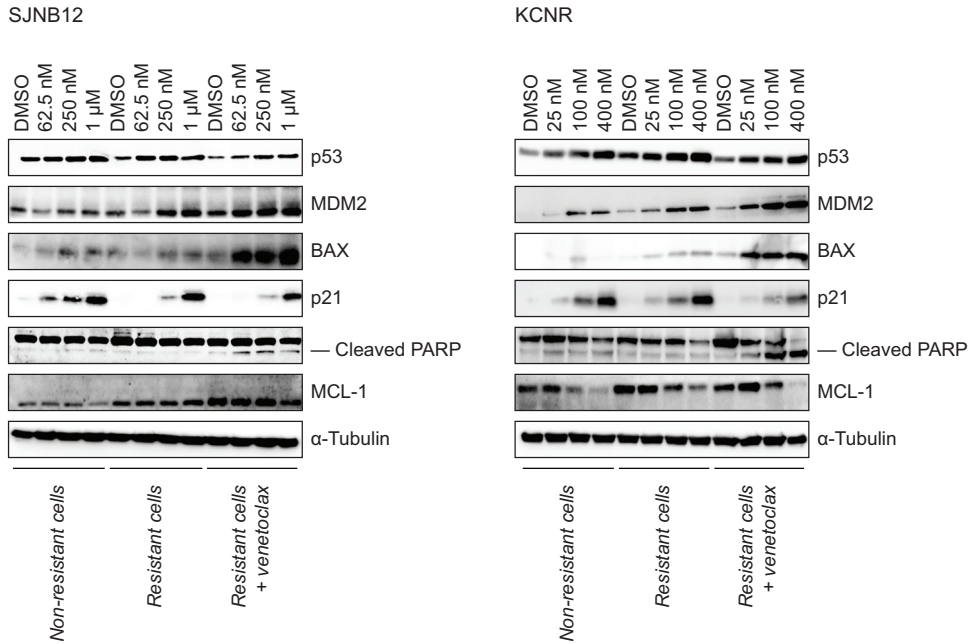
Compound (Target)	Hit HTS for KCNR	Hit HTS for SJNB12	Potential hits from literature	Regularly used cytostatic in neuroblastoma treatment
M-344 (HDAC)	X			
MGCD0103 (HDAC)			X	
Neratinib (HER2, EGFR)		X		
NVP-BEZ235 (PI3K $\alpha/\beta/\delta/\gamma$, mTORC1/2)		X	X	
NVP-TAE684 (ALK)	X			
Omipalisib (PI3K $\alpha/\beta/\delta/\gamma$, mTORC1/2)	X	X	X	
Oxamflatin (HDAC)	X			
Ponatinib (Abl, PDGFR α , VEGFR2, FGFR1, Src)		X		
Purvalanol (CDK1/2/4/5)			X	
Temozolomide (DNA alkylation)				X
Topotecan (DNA topoisomerase I)				X
Trichostatin A (HDAC)	X			
Vincristine (Microtubule polymerization)		X		X
Vorinostat (SAHA) (HDAC)	X	X	X	
VX-680 (Aurora kinase A/B/C)		X	X	

Table 2. (continued)

Idasanutlin induces growth arrest in non-resistant cells and apoptosis in venetoclax-resistant cells in the presence of venetoclax

As idasanutlin acts by inhibiting the interaction between MDM2 and the tumor suppressor p53 - thereby preventing p53 degradation by the proteasome (29, 30) we first studied idasanutlin effects on p53 and MDM2 protein levels. For SJNB12 and KCNR, idasanutlin dose-dependently increased p53 and MDM2 in the non-resistant cells as well as the venetoclax-resistant cells both in the absence and presence of venetoclax (Fig. 4A). Increased MDM2 levels could be explained by p53-mediated transcriptional activation of MDM2. Because p53 is involved in cell cycle arrest and apoptosis, we also studied idasanutlin effects on the bona fide p53 target genes p21 and BAX (31-33). Interestingly, in the non-resistant cells and venetoclax-resistant cells in the absence of venetoclax a stronger p21 upregulation was observed, while in the venetoclax-resistant SJNB12 and KCNR cells in the presence of venetoclax a stronger BAX upregulation was observed upon idasanutlin treatment. These findings correspond to a higher induction of apoptosis in the venetoclax-resistant lines under venetoclax pressure as marked by the induction in PARP cleavage and a higher sub-G₁ fraction on DNA content analysis using cytometry (Fig. 4B and Supplementary Fig. S1). These results show that idasanutlin re-sensitizes venetoclax-resistant BCL-2-dependent neuroblastoma cells to undergo apoptosis.

A.



B.

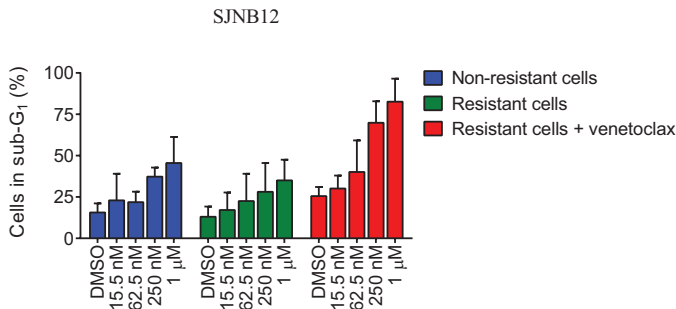


Figure 4. Idasanutlin treatment of venetoclax-resistant neuroblastoma cells in the presence of venetoclax causes BAX-mediated apoptosis. A, Western blot analysis of the *in vitro* effects of idasanutlin on p53, MDM2, BAX, p21, cleaved PARP and MCL-1 protein levels in non-resistant SJB12 (left) and KCNR (right) cells versus venetoclax-resistant SJB12 and KCNR cells and venetoclax-resistant SJB12 and KCNR cells under venetoclax pressure after 72 hours treatment. α-Tubulin was used as a loading control. B, FACS analysis of the *in vitro* effects of idasanutlin on sub-G₁ induction in non-resistant SJB12 cells (blue) versus venetoclax-resistant SJB12 cells (green) and venetoclax-resistant SJB12 cells in the presence of venetoclax (red). Effects on sub-G₁ induction were established after 72-hour treatment with increasing idasanutlin concentrations. Data represent the mean percentages of cells in sub-G₁ + SD of three replicate experiments.

Combination of venetoclax with idasanutlin shows superior efficacy in a BCL2 high-expressing xenograft model.

The efficacy of combining venetoclax with MDM2 inhibitor idasanutlin was subsequently studied *in vivo* in mice with BCL-2-dependent KCNR neuroblastoma xenografts. Direct combination treatment with venetoclax and idasanutlin for three consecutive weeks resulted in significant tumor regression (i.e. average tumor size reduction of $80\pm 21\%$) and superior efficacy over single-agent treatments. As expected, tumor reduction was also observed in the delayed combination group, though less significant compared to the group receiving the combination from the start of treatment (i.e. average tumor size reduction of $53\pm 39\%$) (Fig. 5A). The improved tumor regression observed after combination treatment with venetoclax and idasanutlin might be the result of a dual effect on the intrinsic apoptotic pathway: i.e. BIM release from BCL-2 caused by venetoclax and p53-mediated activation of the pro-apoptotic BCL-2 family protein BAX (34). While BIM was still complexed to BCL-2 in the control group, co-immunoprecipitation studies at 4 hours after administration of the last dose(s) showed (almost) complete BIM release in the venetoclax-only treated group and the group directly receiving the combination. Surprisingly, residual levels of BIM bound to BCL2 were observed in the delayed combination group. Additional Western blot analysis revealed upregulation of BAX in both combination groups as well as in the idasanutlin-only treated group (Fig 5B and C). Together, these results indicate that the significant tumor regression observed upon combination treatment with venetoclax and idasanutlin might be the result of simultaneous inhibition of BCL-2 and activation of p53-mediated induction of BAX.

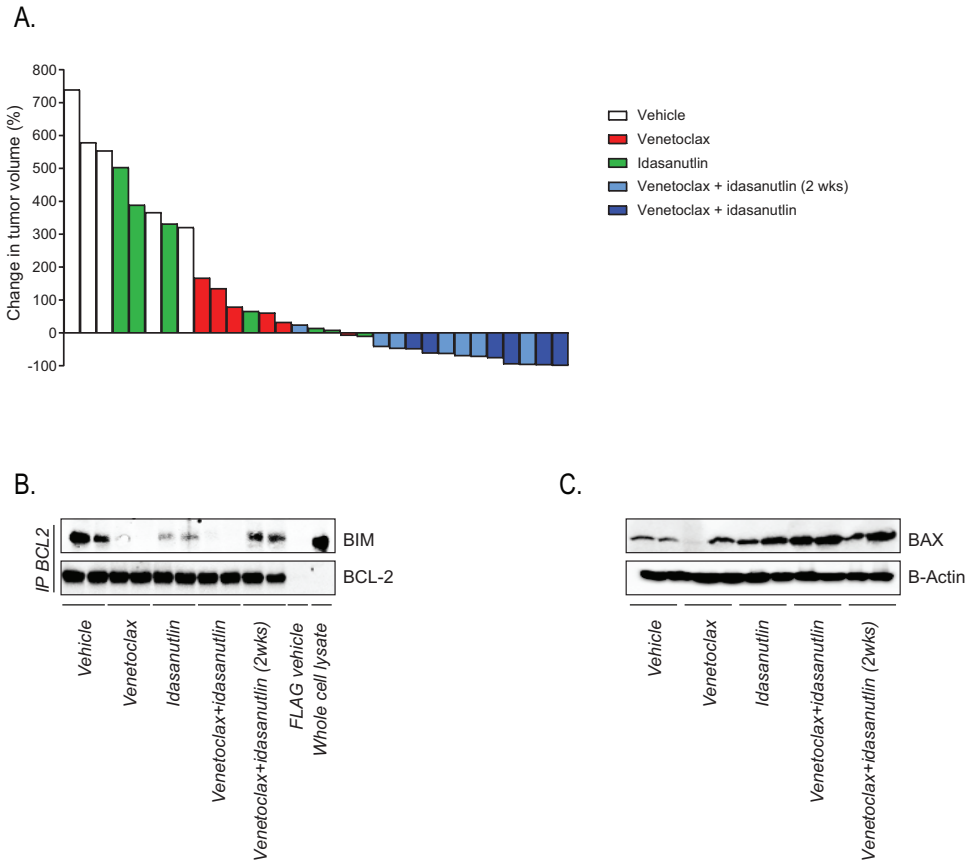


Figure 5. Combination of venetoclax with idasanutlin results in superior anticancer activity with BCL2 high-expressing neuroblastoma xenografts. **A**, Inhibitory effects of combination treatment with venetoclax and idasanutlin versus single-agent treatments on the growth of KCNR neuroblastoma xenografts. Percentages change in tumor volume at the end of treatment were calculated using the following formula: $((\text{tumor volume at the end of treatment} - \text{tumor volume at the start of treatment}) / \text{tumor volume at the start of treatment}) \times 100\%$. Mice were daily treated with: (1) vehicles venetoclax and idasanutlin, (2) 100 mg/kg/d venetoclax, (3) 25 mg/kg/d idasanutlin, (4) one week monotherapy with 100 mg/kg/d venetoclax followed by combination treatment with 25 mg/kg/d idasanutlin or (5) 100 mg/kg/d venetoclax plus 25 mg/kg/d idasanutlin. All mice were treated for a total of three consecutive weeks. **B**, *In vivo* effects on BIM displacement from BCL-2. Effects were studied by detecting BIM/BCL-2 complex levels by anti-BCL-2 immunoprecipitation, followed by Western blotting for BIM. Levels of BIM/BCL-2 complex were established for n=2 mice per group at 4 hours after administration of the last drug dose(s). BCL-2 levels served as loading control. **C**, *In vivo* effects on BAX protein levels. Effects were studied by Western blot analysis for n=2 mice per group at 4 hours after administration of the last drug dose(s). β -actin served as a loading control.

DISCUSSION

Previous preclinical studies using the BCL-2-specific inhibitor venetoclax showed superior anti-tumor activity in neuroblastoma tumors with high BCL-2 and BIM/BCL-2 complex levels (17, 18). Eventually resistance occurred as is seen with most targeted compounds with high specificity.

Several mechanisms for resistance to BCL-2 inhibitors have been described. Acquired resistance after long-term exposure of lymphoma cells to venetoclax resulted in clonal selection of cells with mutations in the BH3 domain of BCL-2, leading to decreased affinity for venetoclax (35). However, sequencing of venetoclax-resistant neuroblastoma cell lines showed no mutations in the BCL-2 BH3 domain. Alternatively, resistance to venetoclax can occur via upregulation of the anti-apoptotic BCL-2 family protein MCL-1 (17, 21, 36). We indeed observed a striking upregulation of MCL-1 in venetoclax-resistant neuroblastoma cells. Upregulated MCL-1 sequestered BIM displaced from BCL-2 by venetoclax, thereby preventing apoptosis from occurring in the resistant neuroblastoma cells.

The observation that MCL-1 upregulation is involved in preventing apoptosis in venetoclax-resistant cells, suggests the possibility to combine selective MCL-1 inhibitors with selective BCL-2 inhibitors. However, MCL-1 inhibitors are still in the early phases of development. In addition, the expected toxicity when combining two compounds with myelo-suppressive side effects might be hampering clinical development. We thus sought to identify compounds that can re-sensitize venetoclax-resistant neuroblastoma cells. Because we aimed at clinical implementation we performed a compound-wide screen with targeted compounds in clinical development and cytostatics used in the treatment of neuroblastoma patients. Targeted compounds idasanutlin, omipalisib, flavopridol and vorinostat and the cytostatic doxorubicin demonstrated superior anti-cell viability activity in venetoclax-resistant BCL-2 high expressing cell lines compared to their respective mother lines. These results confirm previous reported synergistic combinations (21-28). DNA damaging agents as doxorubicin have shown to give strong synergistic responses with venetoclax and navitoclax (16, 37). The combination with PI3K inhibitors, like omipalisib, was found in several tumor types to potentiate BCL-2 inhibition through downregulation of MCL-1 (21, 38). Finally, AURKA inhibitors were identified in neuroblastoma to combine efficiently with venetoclax (36), which we only confirmed in the SJNB12 cell line.

The synergistic combination of venetoclax with p53 reactivating, nutlin-like compounds was only reported for hematologic malignancies. We now show that, from an unbiased screening approach, idasanutlin selects as the strongest re-sensitizer for venetoclax in venetoclax-resistant neuroblastoma cells. This re-sensitization is mediated through re-activation of p53, which results in upregulation of the p53 target gene BAX. BAX then oligomerizes and forms pores in the outer membrane of the mitochondria, thereby causing cytochrome c release and apoptosis. Upregulation of BAX was only seen in venetoclax-resistant neuroblastoma cells in the presence of venetoclax and idasanutlin. This suggests that p53-mediated BAX activation by idasanutlin and BCL2 inhibition by venetoclax might result in a potent apoptotic phenotype in the venetoclax-resistant cells, which was observed in these cells. In venetoclax-resistant cells without venetoclax pressure, p53 release from MDM2 does not activate BAX but increases the expression of the p53 target gene p21. p21 is known to mediate cell cycle arrest, which we indeed observed in these cells.

In vivo studies confirmed the beneficial effects of combining BCL-2 inhibitor venetoclax with MDM2 inhibitor idasanutlin, as was shown by the remarkably improved regression of BCL-2-dependent neuroblastoma tumors. Unexpectedly, improved combined effects were more pronounced after immediate combination compared to combination after short term monotherapy with venetoclax. This could be because of the higher residual levels of BIM bound to BCL-2 observed in the delayed combination group. The underlying cause of the higher residual BIM/BCL-2 complex levels after delayed combination of venetoclax with idasanutlin is unclear. For future experiments it would be interesting to study if complete tumor regression can be achieved when directly combining venetoclax with higher doses of idasanutlin. The complete or almost complete release of BIM from BCL-2 observed after direct combination of venetoclax with idasanutlin suggests that there is no much rationale to use higher venetoclax doses.

Our results indicate idasanutlin as a potential compound for the re-sensitization of venetoclax-resistant neuroblastoma cells to venetoclax. We predict that the clinical testing of single compound venetoclax in children with neuroblastoma will induce tumor responses. Various pre-clinical studies have confirmed that neuroblastoma tumors have an expression profile that is related to high efficacy of this compound (17, 18). However, we also predict that resistance will occur in response to venetoclax treatment and therefore combination treatments should be anticipated. Our work and that of others suggest that a combination with DNA damaging agents would potentiate the efficacy of BCL-2 inhibition. A backbone therapy including cyclophosphamide or topoisomerase inhibitors would be an option for early clinical trials. Our current findings also suggest that a clinical combination of venetoclax with idasanutlin might prevent

resistance to the BCL-2 inhibitor. Preclinical studies using this combination in adults is currently ongoing (ClinicalTrials.gov Identifier: NCT02670044) and a similar combination should be further explored in neuroblastoma.

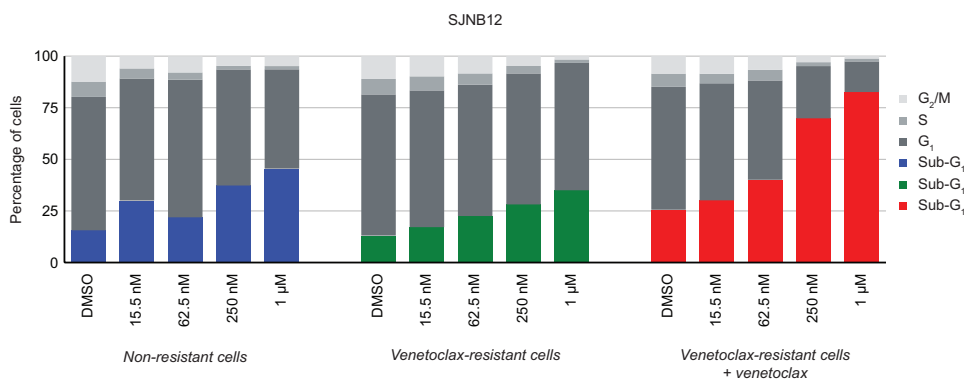
REFERENCES

1. Yip KW, Reed JC. Bcl-2 family proteins and cancer. *Oncogene* 2008;27(50):6398-406.
2. Peter E. Czabotar GL, Andreas Strasser and Jerry M. Adams. Control of apoptosis by the BCL-2 protein family: implications for physiology and therapy. *Cell Death and Autophagy* 2014;15:49-63.
3. Iqbal J, Neppalli VT, Wright G, Dave BJ, Horsman DE, Rosenwald A, et al. BCL2 expression is a prognostic marker for the activated B-cell-like type of diffuse large B-cell lymphoma. *J Clin Oncol* 2006;24(6):961-8.
4. Chipuk JE, Moldoveanu T, Llambi F, Parsons MJ, Green DR. The BCL-2 family reunion. *Mol Cell* 2010;37(3):299-310.
5. Green DR, Kroemer G. The pathophysiology of mitochondrial cell death. *Science* 2004;305(5684):626-9.
6. Llambi F, Moldoveanu T, Tait SW, Bouchier-Hayes L, Temirov J, McCormick LL, et al. A unified model of mammalian BCL-2 protein family interactions at the mitochondria. *Mol Cell* 2011;44(4):517-31.
7. Davids MS, Letai A. Targeting the B-cell lymphoma/leukemia 2 family in cancer. *J Clin Oncol* 2012;30(25):3127-35.
8. Hu W, Kavanagh JJ. Anticancer therapy targeting the apoptotic pathway. *Lancet Oncol* 2003;4(12):721-9.
9. Korsmeyer SJ, Wei MC, Saito M, Weiler S, Oh KJ, Schlesinger PH. Pro-apoptotic cascade activates BID, which oligomerizes BAK or BAX into pores that result in the release of cytochrome c. *Cell Death Differ* 2000;7(12):1166-73.
10. Saelens X, Festjens N, Vande Walle L, van Gurp M, van Loo G, Vandenabeele P. Toxic proteins released from mitochondria in cell death. *Oncogene* 2004;23(16):2861-74.
11. Sun XM, MacFarlane M, Zhuang J, Wolf BB, Green DR, Cohen GM. Distinct caspase cascades are initiated in receptor-mediated and chemical-induced apoptosis. *J Biol Chem* 1999;274(8):5053-60.
12. Tait SW, Green DR. Mitochondria and cell death: outer membrane permeabilization and beyond. *Nat Rev Mol Cell Biol* 2010;11(9):621-32.
13. Wei MC, Lindsten T, Mootha VK, Weiler S, Gross A, Ashiya M, et al. tBID, a membrane-targeted death ligand, oligomerizes BAK to release cytochrome c. *Genes Dev* 2000;14(16):2060-71.
14. Irwin MS, Park JR. Neuroblastoma: paradigm for precision medicine. *Pediatr Clin North Am* 2015;62(1):225-56.
15. Goldsmith KC, Gross M, Peirce S, Luyindula D, Liu X, Vu A, et al. Mitochondrial Bcl-2 family dynamics define therapy response and resistance in neuroblastoma. *Cancer Res* 2012;72(10):2565-77.

16. Lamers F, Schild L, den Hartog IJ, Ebus ME, Westerhout EM, Ora I, et al. Targeted BCL2 inhibition effectively inhibits neuroblastoma tumour growth. *Eur J Cancer* 2012;48(16):3093-103.
17. Bate-Eya LT, den Hartog IJ, van der Ploeg I, Schild L, Koster J, Santo EE, et al. High efficacy of the BCL-2 inhibitor ABT199 (venetoclax) in BCL-2 high-expressing neuroblastoma cell lines and xenografts and rational for combination with MCL-1 inhibition. *Oncotarget* 2016;7(19):27946-58.
18. Tanos R, Karmali D, Nalluri S, Goldsmith KC. Select Bcl-2 antagonism restores chemotherapy sensitivity in high-risk neuroblastoma. *BMC Cancer* 2016;16:97.
19. Dolman ME, Poon E, Ebus ME, den Hartog IJ, van Noesel CJ, Jamin Y, et al. Cyclin-Dependent Kinase Inhibitor AT7519 as a Potential Drug for MYCN-Dependent Neuroblastoma. *Clin Cancer Res* 2015;21(22):5100-9.
20. Lehmann C, Friess T, Birzele F, Kiialainen A, Dangl M. Superior anti-tumor activity of the MDM2 antagonist idasanutlin and the Bcl-2 inhibitor venetoclax in p53 wild-type acute myeloid leukemia models. *J Hematol Oncol* 2016;9(1):50.
21. Choudhary GS, Al-Harbi S, Mazumder S, Hill BT, Smith MR, Bodo J, et al. MCL-1 and BCL-xL-dependent resistance to the BCL-2 inhibitor ABT-199 can be overcome by preventing PI3K/AKT/mTOR activation in lymphoid malignancies. *Cell Death Dis* 2015;6:e1593.
22. Cervantes-Gomez F, Lamothe B, Woyach JA, Wierda WG, Keating MJ, Balakrishnan K, et al. Pharmacological and Protein Profiling Suggests Venetoclax (ABT-199) as Optimal Partner with Ibrutinib in Chronic Lymphocytic Leukemia. *Clin Cancer Res* 2015;21(16):3705-15.
23. Li L, Pongtornpipat P, Tiutan T, Kendrick SL, Park S, Persky DO, et al. Synergistic induction of apoptosis in high-risk DLBCL by BCL2 inhibition with ABT-199 combined with pharmacologic loss of MCL1. *Leukemia* 2015;29(8):1702-12.
24. Johnson-Farley N, Veliz J, Bhagavathi S, Bertino JR. ABT-199, a BH3 mimetic that specifically targets Bcl-2, enhances the antitumor activity of chemotherapy, bortezomib and JQ1 in "double hit" lymphoma cells. *Leuk Lymphoma* 2015;56(7):2146-52.
25. Vandenberg CJ, Cory S. ABT-199, a new Bcl-2-specific BH3 mimetic, has in vivo efficacy against aggressive Myc-driven mouse lymphomas without provoking thrombocytopenia. *Blood* 2013;121(12):2285-8.
26. Benito JM, Godfrey L, Kojima K, Hogdal L, Wunderlich M, Geng H, et al. MLL-Rearranged Acute Lymphoblastic Leukemias Activate BCL-2 through H3K79 Methylation and Are Sensitive to the BCL-2-Specific Antagonist ABT-199. *Cell Rep* 2015;13(12):2715-27.
27. Wei Y, Kadia T, Tong W, Zhang M, Jia Y, Yang H, et al. The combination of a histone deacetylase inhibitor with the Bcl-2 homology domain-3 mimetic GX15-070 has synergistic antileukemia activity by activating both apoptosis and autophagy. *Clin Cancer Res* 2010;16(15):3923-32.
28. Xie S, Jiang H, Zhai XW, Wei F, Wang SD, Ding J, et al. Antitumor action of CDK inhibitor LS-007 as a single agent and in combination with ABT-199 against human acute leukemia cells. *Acta Pharmacol Sin* 2016;37(11):1481-1489.

29. Lakoma A, Barbieri E, Agarwal S, Jackson J, Chen Z, Kim Y, et al. The MDM2 small-molecule inhibitor RG7388 leads to potent tumor inhibition in p53 wild-type neuroblastoma. *Cell Death Discov* 2015;1.
30. Chen L, Rousseau RF, Middleton SA, Nichols GL, Newell DR, Lunec J, et al. Pre-clinical evaluation of the MDM2-p53 antagonist RG7388 alone and in combination with chemotherapy in neuroblastoma. *Oncotarget* 2015;6(12):10207-21.
31. Nag S, Qin J, Srivenugopal KS, Wang M, Zhang R. The MDM2-p53 pathway revisited. *J Biomed Res* 2013;27(4):254-71.
32. Kracikova M, Akiri G, George A, Sachidanandam R, Aaronson SA. A threshold mechanism mediates p53 cell fate decision between growth arrest and apoptosis. *Cell Death and Differentiation* 2013;20(4):576-588.
33. Chipuk JE, Kuwana T, Bouchier-Hayes L, Droin NM, Newmeyer DD, Schuler M, et al. Direct activation of Bax by p53 mediates mitochondrial membrane permeabilization and apoptosis. *Science* 2004;303(5660):1010-4.
34. McCurrach ME, Connor TM, Knudson CM, Korsmeyer SJ, Lowe SW. bax-deficiency promotes drug resistance and oncogenic transformation by attenuating p53-dependent apoptosis. *Proc Natl Acad Sci U S A* 1997;94(6):2345-9.
35. Fresquet V, Rieger M, Carolis C, Garcia-Barchino MJ, Martinez-Climent JA. Acquired mutations in BCL2 family proteins conferring resistance to the BH3 mimetic ABT-199 in lymphoma. *Blood* 2014;123(26):4111-9.
36. Ham J, Costa C, Sano R, Lochmann TL, Sennott EM, Patel NU, et al. Exploitation of the Apoptosis-Primed State of MYCN-Amplified Neuroblastoma to Develop a Potent and Specific Targeted Therapy Combination. *Cancer Cell* 2016;29(2):159-72.
37. Lam LT, Zhang H, Xue J, Levenson JD, Bhathena A. Antihelminthic benzimidazoles potentiate navitoclax (ABT-263) activity by inducing Noxa-dependent apoptosis in non-small cell lung cancer (NSCLC) cell lines. *Cancer Cell Int* 2015;15(1):5.
38. Pareja F, Macleod D, Shu C, Crary JF, Canoll PD, Ross AH, et al. PI3K and Bcl-2 inhibition primes glioblastoma cells to apoptosis through downregulation of Mcl-1 and Phospho-BAD. *Mol Cancer Res* 2014;12(7):987-1001.

SUPPLEMENTARY INFORMATION



Supplementary Figure 1. Idasanutlin re-sensitizes venetoclax-resistant neuroblastoma cells to venetoclax by inducing apoptosis. FACS analysis of the *in vitro* effects of idasanutlin on the fraction of cells in G₂/M, S, G₁ and sub-G₁ in non-resistant SJNB12 cells (blue/gray) versus venetoclax-resistant SJNB12 cells (green/gray) and venetoclax-resistant SJNB12 cells in the presence of venetoclax (red/gray). Effects were established after 72-hour treatment with increasing idasanutlin concentrations. Data represent the mean percentages of cells in G₂/M, S, G₁ and sub-G₁ of three replicate experiments.

SUPPLEMENTARY TABLES

Compound (Target)	Non-resistant (nmol/L)	Resistant (nmol/L)	Resistant + venetoclax (nmol/L)	Non-resistant (nmol/L)	Resistant (nmol/L)	Resistant + venetoclax (nmol/L)
	SJNB12			KCNR		
AZD-8055 (mTORC1/2)	>10000	729	134	89	140	92
Ceritinib (ALK)	2655	2180	1041	94	28	23
Cisplatin (DNA synthesis)	>10000	>10000	5903	966	1772	1270
Dinaciclib (CDK1/2/5/9)	11	28	14	8	8	6
Doxorubicin (DNA topoisomerase II)	>10000	2940	1410	31	26	16
Etoposide (DNA topoisomerase II)	>10000	>10000	473	363	716	261
Flavopiridol (CDK1/2/4/6/7)	237	151	109	188	141	111
GS1101 (PI3K δ)	>10000	>10000	8821	>10000	>10000	>10000
GSK-1904529A (IGFR)	>10000	>10000	>10000	>10000	>10000	>10000
Ibrutinib (BTK)	6230	>10000	4735	>10000	>10000	2152
Idasanutlin (MDM2)	1011	729	52	30	30	20
Irinotecan (DNA topoisomerase II)	>10000	4430	3068	1207	1660	1161
JQ1 (BRD4 (1/2))	374	418	176	291	884	770

Supplementary Table 1. IC₅₀ values for non-resistant SJNB12 and KCNR neuroblastoma cells, venetoclax-resistant SJNB12 and KCNR cells and venetoclax-resistant SJNB12 and KCNR cells in the presence of venetoclax (i.e. 2.75 μ mol/L for SJNB12 and 7.5 μ mol/L for KCNR). Compounds tested include re-sensitizing hits identified in the high-throughput drug screens, targeted compounds for which synergy with BCL-2 inhibition has been previously described in the literature and regularly used cytostatics in neuroblastoma treatment.

Compound (Target)	Non-resistant (nmol/L)	Resistant (nmol/L)	Resistant + venetoclax (nmol/L)	Non-resistant (nmol/L)	Resistant (nmol/L)	Resistant + venetoclax (nmol/L)
	SJNB12			KCNR		
LY2603618 (CHK1)	>10000	8567	3203	808	956	959
M-344 (HDAC)	312	269	140	175	50	40
MGCD0103 (HDAC)	201	259	152	448	418	149
Neratinib (HER2, EGFR)	1772	281	212	1745	3495	998
NVP-BEZ235 (PI3K α / β / δ / γ , mTORC1/2)	618	130	47	41	320	53
NVP-TAE684 (ALK)	288	259	176	27	6	6
Omipalisib (PI3K α / β / δ / γ , mTORC1/2)	43	56	9	13	5	2
Oxamflatin (HDAC)	594	612	258	215	47	20
Ponatinib (Abl, PDGFR α , VEGFR2, FGFR1, Src)	600	201	128	516	1700	1699
Purvalanol (CDK1/2/4/5)	>10000	9231	3921	3828	3235	1933
Temozolomide (DNA alkylation)	>10000	>10000	>10000	>10000	>10000	>10000
Topotecan (DNA topoisomerase I)	6850	3160	42	32	32	29
Trichostatin A (HDAC)	497	303	134	122	32	27
Vincristine (Microtubule polymerization)	5	0.3	0.5	0.001	0.005	0.002
Vorinostat (SAHA) (HDAC)	697	561	262	490	117	94
VX-680 (Aurora kinase A/B/C)	3023	50	36	14	38	22

Supplementary Table 1. (continued)

SUPPLEMENTARY MATERIALS AND METHODS

Cell culture. Human neuroblastoma cell lines used in the current study were grown in Dulbecco's modified Eagle's medium (DMEM) containing 4.5 g/L D-glucose, glutamate and supplemented with 10% (v/v) foetal calf serum, 2 mmol/L L-glutamine, 10 U/mL penicillin, 10 µg/mL streptomycin and MEM non-essential amino acids (1x). Cells were maintained at 37°C under 5% CO₂ in humidified air. Penicillin and streptomycin were obtained from Sigma Aldrich, Other cell culture related materials were obtained from Life Technologies.

FACS analysis. Non-resistant SJNB12 and KCNR cells, venetoclax-resistant SJNB12 and KCNR cells and/or venetoclax-resistant SJNB12 and KCNR cells in the presence of venetoclax (i.e. 2.75 µmol/L for SJNB12 and 7.5 µmol/L for KCNR) were seeded onto 6-cm plates and incubated overnight. To confirm the generation of venetoclax-resistant SJNB12 and KCNR cells, non-resistant and venetoclax-resistant cells were treated with 0.1% DMSO (control) or venetoclax using concentration ranges of 7.8 nmol/L to 10 µmol/L. To study the effects of idasanutlin on sub-G₁ induction, non-resistant SJNB12 and KCNR cells, venetoclax-resistant SJNB12 and KCNR cells and venetoclax-resistant SJNB12 and KCNR cells under venetoclax pressure were treated with 0.02% DMSO (control) or 25 nmol/L to 1 µmol/L RG7388. After 72-hour treatment, supernatants containing floating cells were collected from the culture dishes. Adherent cells were washed once with PBS and PBS solutions were pooled with the supernatants. After trypsinization of the adherent cells with 0.05% trypsin/EDTA, cells were resuspended in the pooled supernatant/PBS solution. Next, cells were centrifuged (5 min; 1,500 rpm), washed by resuspension in PBS and centrifuged again (5 min; 3,000 rpm). Cells were fixed with 100% ice-cold ethanol, stained with 0.05 mg/mL propidium iodide and supplemented with 0.05 mg/mL RNase A in PBS. After 1-hour incubation in the dark at room temperature (RT), cells were filtered through a 50 µm filter (BD Biosciences) and DNA contents of the nuclei were analyzed using a fluorescence-activated cell sorter. A total of 30,000 nuclei per sample were counted. The cell cycle distribution and apoptotic Sub-G₁ fraction were determined using the BD Accuri™ C6 flow cytometer with the CFlow plus software (BD Biosciences) and the FlowJo LLC software (FlowJo LLC).

Western blotting. Non-resistant SJNB12 and KCNR cells, venetoclax-resistant SJNB12 and KCNR cells and/or venetoclax-resistant SJNB12 and KCNR cells in the presence of venetoclax (i.e. 2.75 µmol/L for SJNB12 and 7.5 µmol/L for KCNR) were seeded onto 6-cm plates and incubated overnight. To study the effects of idasanutlin on p53, MDM2,

BAX, p21, cleaved PARP and MCL-1, non-resistant cells, venetoclax-resistant cells and venetoclax-resistant cells in the presence of venetoclax were 72-hour treated with 0.02% DMSO (control) or up to 1 $\mu\text{mol/L}$ idasanutlin. For all experiments, cells were lysed using Laemmli buffer [i.e., H_2O /glycerol/20% sodium dodecyl sulfate (SDS)/1 M Tris-HCl (pH 6.8) 5:2:2:1 (v/v/v/v)]. Lysates were homogenized by hydrodynamic shearing through a 23 G needle, followed by 10 min incubation at 50°C. Protein concentrations were determined using the Bio-Rad DC Protein Assay (Bio-Rad, Veenendaal, the Netherlands).

Equal protein amounts (20 μg) were diluted in 5x reducing sampling buffer (i.e., Laemmli buffer/ β -mercaptoethanol 3:1 (v/v) with bromophenol blue sodium salt). Diluted samples were boiled for 5 min at 95°C and centrifuged (1,500 rpm 5 min). Proteins were separated by SDS-polyacrylamide gel electrophoresis on 12% Mini-Protean[®] Tris-glycine extended (TGX) precast gels (Bio-Rad) and transferred on hybond nitrocellulose membranes (0.45 μm) by 1.5-hour wet blotting (200 mA; 4°C). Transfer buffer consisted of 20% (v/v) methanol, 3.025 g/L Tris and 14.4 g/L glycine in demineralized water. Membranes were blocked in 2% ECL Prime[™] blocking agent (GE Healthcare) in PBS with 0.1% (v/v) Tween-20 (= blocking buffer) for 1 hour at RT. After blocking, membranes were incubated with the primary (overnight; 4°C) and secondary (1 hour; RT) antibodies in blocking buffer and scanned using the ChemiDoc[™] Touch Imaging detection system (Bio-Rad).



CHAPTER 6

A SYSTEMATIC REVIEW ON TARGETING BCL2 IN PEDIATRIC SOLID TUMORS.

Authors: Laurel T. Bate-Eya¹, Nil A. Schubert¹, Huib N. Caron²,
M. Emmy. M. Dolman¹ and Jan J. Molenaar¹.

¹Department of Translational Research, Princess Maxima Centre for Pediatric Oncology, Utrecht, The Netherlands, ² Department of Pediatric Oncology, Academic Medical Centre, Amsterdam, The Netherlands.

Manuscript in preparation

ABSTRACT

The aim of this study was to perform a systematic review on the pre-clinical evidence of targeting BCL2 in pediatric solid tumors. An elaborative literature search identified 3189 hits from which 74 papers were finally selected for further analysis. Papers included in this study were selected based on data on BCL2 expression patterns, *in vitro* and *in vivo* validation of the relevance of targeting BCL2, predictive biomarkers for patient stratification and efficacy of BCL2 inhibition, strategies to overcome resistance to BCL2 inhibition and clinical trials involving small molecule BCL2 inhibitors for pediatric solid tumor treatment. BCL2 protein and mRNA expression as well as BIM/BCL2 complex levels were identified as relevant predictive biomarkers for sensitivity to small molecule BCL2 inhibitors in only a few pediatric solid tumor types. BCL2 was adequately reported and highly expressed in neuroblastoma, synovial sarcoma, Ewing sarcoma, osteosarcoma and retinoblastoma and correlated with a poor survival outcome in several of these tumor types. An absence of the protein was reported in rhabdoid and inflammatory myofibroblastic tumors. ABT-199 (venetoclax) and ABT-263 (navitoclax) were the two most widely pre-clinically evaluated small molecule BCL2 inhibitors reported and were most effective in neuroblastoma model systems. The most frequently reported mechanism of resistance to BCL2 inhibitors was via MCL1 upregulation and its sequestration of BIM, preventing further apoptosis from occurring. Consequently, the primarily used strategy to overcome resistance to small molecule BCL2 inhibitors was by concomitant inhibition of MCL1.

Taken together, the current systematic review provides a resource for summarized knowledge on targeting BCL2 in pediatric solid tumors. Neuroblastoma was the pediatric solid tumor with the most validated data categories. This warrants future trials with BCL2 inhibitors to assess predictive responses in neuroblastoma patients and to investigate the clinical implementation of combination strategies to overcome resistance. Target presence was also found for limited other pediatric tumor types, but further research is essential to determine the relevance of targeting BCL2 in these tumor types (especially for synovial sarcoma, Ewing sarcoma, osteosarcoma and retinoblastoma).

INTRODUCTION

The B-cell lymphoma 2 (BCL2) protein is highly expressed in numerous adult and pediatric tumor types (1). The anti-apoptotic BCL2 family proteins BCL2, BCL-X_L (BCL2L1), MCL1, BCL-W (BCL2L2) and A1 (BCL2A1) together with its pro-apoptotic counterparts BIM (BCL2L11), BID (FP497), BAX (BCL2L4), BAK (BAK1), PUMA (BBC3) and NOXA (PMAIP1) are key players in the activation of the intrinsic apoptotic pathway (2). During cellular stress or redrawing of growth factors, activation of the intrinsic pathway is initiated upon BIM displacement from BCL2. Displaced BIM triggers the oligomerization of BAX/BAK, leading to pore formation at the outer membrane of the mitochondria. This then results into cytochrome c release from the interstitial space of the mitochondria into the cytoplasm. Cytochrome c together with apoptotic protease-activating factor I (APAF1) forms the apoptosome. The apoptosome is responsible for the recruitment and cleavage of effector caspases 3 and 9, thereby triggering apoptosis. (3). Several small molecule inhibitors targeting BCL2 have been developed and pre-clinically tested in various pediatric malignancies. ABT-263 (navitoclax) is one of the first line pan-BCL2 family of proteins inhibitors and was shown to induce a strong apoptotic phenotype at the *in vitro* level in various tumors types (4, 5). At the *in vivo* level, potent regression of tumors expressing high BCL2 levels was observed upon navitoclax treatment, demonstrating the great promise of this compound for the treatment of BCL2-dependent malignancies (3, 6-10). However, the clinical use of navitoclax was associated with dose-limiting thrombocytopenia due to the concomitant inhibition of the anti-apoptotic protein BCL-X_L (11, 12). Given the toxicity exhibited by patients treated with navitoclax at the higher doses, the BCL2-specific inhibitor ABT-199 (venetoclax) was developed and pre-clinically tested in various malignancies (13, 14). A phase I dose-escalation study of venetoclax in patients with relapsed or refractory chronic lymphocytic leukemia showed a 79% response rate, paving the way for the implementation of venetoclax in the future treatment of children with BCL2-dependent solid tumors (15). The current systematic review aims to establish an evidence-based perspective on the relevance of targeting BCL2 in pediatric solid tumors. This should facilitate the prioritization of children with solid tumors that are most likely to benefit from clinical trials with small molecule BCL2 inhibitors. Additionally, we included available knowledge related to molecular mechanisms promoting resistance to BCL2 inhibitors and combination strategies to overcome resistance. This additional information can be used to design drug combination trials for pediatric cancer patients with acquired resistance to BCL2 inhibitors.

MATERIALS AND METHODS

Guidelines for this systematic review were based on the NHS Centre for Reviews and Dissemination (1996) (<http://www.york.ac.uk/inst/crd>) and the Cochrane method for systematic reviews (<http://methodology.cochrane.org/>).

Search strategies

The online bibliographic database PubMed was chosen to extract literature (published till 18th April 2016) relevant to the subject matter of the research. Search procedures were performed using an integrative approach, using the same nine important key words for each search (**Table 1**). Specific disease names were used as the last key word. The key words “BCL2” or “BCL-2” referred to the various abbreviations of the B-cell lymphoma protein 2 used in literature. Search terms “ABT199” or “ABT-199” and “ABT263” or “ABT-263” referred to the names given to the small molecule BCL2 inhibitors for research purposes, while “venetoclax” or “navitoclax” or “obatoclax” referred to their generic names. Investigators read the abstracts of each paper and classified the papers into 3 different categories: relevant, not relevant and uncertain. For the final inclusion criteria of papers, abstracts of all papers in the uncertain category were re-read by the investigator to make a final decision on whether to include these papers.

Inclusion criteria

In order to be included in the systematic review, the paper had to contain information about at least one of the following topics: (1) BCL2 expression patterns in primary tumors (the outcome of the expression analysis should be shown in table form and $\geq 40\%$ of the study subjects should be children) and target dependency *in vitro* (BCL2 dependency should be validated *in vitro* in at least five cell lines by investigating phenotypic changes upon BCL2 knockdown), (2) target dependency *in vivo*, (3) *in vitro* efficacy of small molecule BCL2 inhibitors in at least one BCL2 high-expressing cell lines, (4) *in vivo* compound efficacy in xenograft mouse models, (5) predictive biomarkers for patient stratification and efficacy of BCL2 inhibition, (6) molecular mechanisms causing resistance to BCL2 inhibition, (7) combination strategies to improve the efficacy of BCL2 inhibitors and/or (8) phase I-III clinical trials with small molecule inhibitors targeting the BCL2 pathway in children (**Supplementary Table 1**).

Exclusion criteria

Papers were excluded when: (1) There was no evidence of *in vitro* experimental data reported in cell lines, (2) BCL2 and its small molecule inhibitors were cited without experimental data, (3) BCL2 was used as a biomarker for inhibition of apoptosis and/or (4) BCL2 expression levels in primary tumors have only been analyzed by histological staining without quantification or tabulated patient data.

Extracted information

From the included papers, the following information was extracted per pediatric tumor type: (1) the frequency of BCL2 overexpression and the correlation with survival data, (2) *in vitro* and *in vivo* responses to small molecule BCL2 inhibitors, (3) if biomarkers for sensitivity to and/or efficacy of small molecule BCL2 inhibitors were identified, (4) patient responses to BCL2 inhibitors in clinical trials, (5) genes and pathways mediating resistance to BCL2 inhibition and (6) *in vitro* and *in vivo* data on chemotherapeutics and targeted small molecule inhibitors that were successfully combined with small molecule BCL2 inhibitors. For each of the papers, color and number codes were given in order to score the papers in terms of reliability of the experimental information and the experimental setups. Color codes: red (negative experimental outcome), green (very positive experimental outcome) or yellow (inconsistent results). Number codes: 1 (excellent methodology and experimental setup), 2 (moderate experimental setup) or 3 (poor methodology and experimental setup).

RESULTS

Literature search results

This systematic review was performed in order to determine the clinical relevance of inhibiting BCL2 in pediatric solid tumor types, i.e. neuroblastoma, rhabdomyosarcoma, hepatoblastoma, Ewing sarcoma, synovial sarcoma, Wilms' tumors, ependymoma, medulloblastoma, retinoblastoma, inflammatory myofibroblastic tumors, osteosarcoma, glioblastoma multiforme, astrocytoma grade III, atypical teratoid rhabdoid tumors and malignant peripheral nerve sheath tumors. We used a series of search terms computed in the PubMed search database and identified 3189 papers. The total number of papers for each pediatric tumor type and the number of papers included in the review are given in **Table 1**. Eventually, 74 out of the 3189 papers fulfilled the in- and exclusion criteria to be included in the study. Papers included in the study were selected after appraisal

of the abstract, methodology and result sections. In order for a paper to be included for review, the methodology and result section should contain sufficient information on the number of samples used for each study. A scoring system of 1-3 and a color code of green, orange and yellow was used in order to assess whether a paper contained sufficient information based on the number of samples used for the study and the manner of reporting (**Supplementary Table 2**).

Target patterns identified in primary tumors

BCL2 expression patterns were found to be described either by RNA or protein analysis. RNA expression patterns were mostly determined by mRNA profiling of tumor materials. Protein expression analysis was performed by immunohistochemistry staining of tumor material and subsequent scoring of the number of BCL2-positive cells in each sample. Out of the 17 tumor types studied, the BCL2 expression pattern was well validated for only 5 types: neuroblastoma, synovial sarcomas, Ewing sarcoma, osteosarcoma and retinoblastoma (3, 16-22). The expression pattern of BCL2 in neuroblastoma was determined by both RNA and protein expression analysis of patient materials, while protein expression analysis was mostly reported for the other tumor types. Based on the data reported in the papers included in this study, BCL2 was found to be highly expressed in 57 and almost 100% of the neuroblastoma tumors (154 and 42 neuroblastoma tumors were scored for BCL2 expression in two different studies). In retinoblastoma, Ewing sarcoma, osteosarcoma and synovial sarcoma, BCL2 was reported to be highly expressed in, respectively, 66, 70, 84 and 100% of the tumors. Correlations between BCL2 expression and tumor stage and prognosis were also addressed in these papers. In neuroblastoma, Ewing sarcoma and osteosarcoma, there was no prognostic significance and correlation between BCL2 expression and survival in high risk patients (3, 16, 18). Synovial sarcoma patients presenting with metastatic patterns and short-term survival rates had a higher BCL2 expression pattern, despite the lack of a significant correlation between overall survival and BCL2 expression (17). In retinoblastoma patients, BCL2 expression levels correlated with poor differentiation, metastasis and high risk (19). BCL2 might serve as a biomarker of poor prognosis in synovial sarcoma and retinoblastoma and targeting this gene in tumors with high expression of the protein might prove beneficial in the long-term survival of these patients. In four of the tumors (i.e. Wilms' tumor, astrocytoma, ependymoma and rhabdomyosarcoma), the expression pattern of BCL2 was scored inconclusive because of the small sample size of patients (23-27). Expression of BCL2 was completely negative in atypical teratoid rhabdoid and inflammatory myofibroblastic tumors, while no studies were conducted reporting BCL2

expression patterns in glioblastoma, medulloblastoma, malignant peripheral nerve sheath tumors and hepatoblastoma (28).

Target validation *in vitro* and *in vivo*

Target validation *in vitro* was scored based on the phenotypic responses of cell lines to BCL2 depletion. As described in two papers, shRNA knockdown of BCL2 resulted in clear apoptotic responses in multiple BCL2-high expressing neuroblastoma cell lines (3, 16). Published *in vitro* results were clearly sufficient to validate BCL2 as a potential drug target for neuroblastoma. Due to the limited number of cell lines used, there was insufficient evidence to suggest *in vitro* BCL2 dependency in hepatoblastoma. In glioblastoma, target dependency was deemed negative because BCL2 overexpression did not potentiate the sensitivity of glioblastoma cell lines to small molecule BCL2 inhibitors. For all other pediatric tumor types addressed in the current systematic review, no literature was available reporting on the *in vitro* target dependency. *In vivo* validated tumor dependency was scored based on information about the effect of BCL2 overexpression on the tumor-forming potential of pediatric tumor cells in mouse models. In medulloblastoma, the tumor-forming potential of BCL2 was only observed upon co-expression of the protein with the *sonic hedgehog* gene. This finding suggests that the tumor-driving events of BCL2 only occur in the presence of other oncogenic partner genes in this tumor type (29). Additionally, downregulation of BCL2 by loss of function of estrogen receptor β lead to tumor reduction and increased apoptosis in medulloblastoma xenograft models (30), supporting a strong *in vivo* correlation to BCL2 dependency. There were no studies reported for BCL2 dependency *in vivo* for the rest of the tumor types (**Table 2**).

***In vitro* and *in vivo* compound efficacy**

ABT-263 or navitoclax is a first generation BH3 mimetic which showed great promise in lymphoid malignancies and non-small cell carcinoma, with strong apoptotic responses *in vitro* and complete regression of BCL2 high-expressing xenografts *in vivo* (4). However, navitoclax additionally targets BCL-W as well as BCL-X_L leading to thrombocytopenia in patients treated with the compound (11, 31). This led to the development and pre-clinical evaluation of ABT-199 (venetoclax), a BCL2-specific inhibitor with improved oral bioavailability (13). A strong apoptotic response was observed upon venetoclax treatment of BCL2-high expressing neuroblastoma cell lines, while tumor growth inhibition was observed *in vivo* (13, 32). The most commonly studied biomarkers for efficacy of small molecule BCL2 inhibitors are BIM displacement from BCL2 and

the downstream effectors of the intrinsic apoptotic pathway, i.e. cleaved PARP and caspase-3 as well as cytochrome c release from the mitochondria into the cytoplasm (32). Evaluation of each marker *in vitro* was reliably reported in 37% of the included papers (3, 6-8, 10, 14, 32-46), with *in vivo* efficacy being reported in only 9% of the papers. *In vitro* BIM displacement from BCL2, PARP cleavage and/or caspase-3 cleavage by BCL2 inhibitors navitoclax or venetoclax was reported in neuroblastoma, glioblastoma, hepatoblastoma, Ewing sarcoma, osteosarcoma, retinoblastoma and synovial sarcoma. Biomarkers for efficacy were most extensively validated in neuroblastoma. At the *in vivo* level, the efficacy of BCL2 inhibitors was determined by their effects on tumor growth reduction or inhibition, BIM displacement from BCL2 and the presence or absence of cleaved PARP and/or caspase-3. Tumor regression or growth inhibition was observed upon treatment of xenograft mouse models in neuroblastoma, glioblastoma and hepatoblastoma. Growth inhibition was strongly correlated to increased BIM displacement from BCL2 and cleaved caspase-3 (7, 10, 14, 32, 34, 37, 38). The promising pre-clinical results obtained with BH3 mimetics in these tumor types highlight the relevance of carrying out clinical trials with BCL2 inhibitors in pediatric neuroblastoma, glioblastoma and hepatoblastoma patients.

Selection biomarkers

Predictive biomarkers for sensitivity can be described as genomic, epigenetic or proteomic events that predict which patients are likely to benefit from treatment with the inhibitor of interest. Based on the *in vitro* and *in vivo* pre-clinical evaluation of small molecule BCL2 inhibitors in neuroblastoma, four predictive biomarkers for sensitivity were identified: BCL2 protein levels, BCL2 mRNA levels, BIM/BCL2 complex levels and BCL-X_L/BCL2 ratio levels (3, 14, 32). At the *in vitro* and *in vivo* levels, neuroblastoma was the only tumor whereby sensitivity to small molecule BCL2 inhibitors was shown to strongly correlate to BCL2 protein levels, BCL2 mRNA expression and BIM/BCL2 complex levels (32). No studies on the correlation of the sensitivity biomarkers to BH3 mimetics has been performed in the other solid pediatric tumor types. Currently, predictive biomarkers for sensitivity of pediatric solid tumor patients to small molecule BCL2 inhibitors have not yet been validated in a clinically relevant setting.

Resistance mechanisms and combinations

Several mechanisms inducing resistance to BCL2 inhibitors have been described. (16, 47). Missense mutations in the BH3 domain of BCL2 preventing venetoclax binding to BCL2 and subsequent BIM displacement and apoptosis induction has been reported in

various adult hematological malignancies (47). Resistance was also reported to occur due to upregulation of the anti-apoptotic BCL2 family proteins BCL-X_L and MCL1. Increased levels of both proteins were shown to sequester BIM displaced from BCL2, thereby preventing apoptosis from occurring (6, 48, 49). In neuroblastoma, rhabdomyosarcoma and glioblastoma, MCL1 upregulation and sequestration of BIM was the principal route through which resistance to BH3 mimetics occurred, while in malignant peripheral nerve sheath tumors (RMS:MPNST), upregulated BCL-X_L was the primary cause of resistance (14, 16, 32, 45, 50). Several strategies to overcome MCL1-mediated resistance mechanisms were studied and reported. Firstly, targeted downregulation of MCL1 by HDAC inhibitor vorinostat (SAHA), PI3K/mTOR inhibitors and aurora kinase inhibitors potentiated the efficacy of BCL2 inhibitors in neuroblastoma, rhabdomyosarcoma and in glioblastoma (8, 9, 14, 16, 32, 36, 50-52). Synergism between BCL2 inhibitors and chemotherapeutic and DNA damaging agents doxorubicin, cyclophosphamide, paclitaxel and 6-diazo-5-oxo-L-norleucine and the proteasome inhibitor bortezomib was also reported in both neuroblastoma and glioblastoma as well as in hepatoblastoma, synovial sarcoma, Ewing sarcoma, medulloblastoma and atypical teratoid rhabdoid tumors. (**Table 2**). The ability to overcome resistance to BH3 mimetics by combination strategies with other small molecule targeted inhibitors and chemotherapeutic agents highlights the potential benefit of combination treatment over single-agent treatment with BH3 mimetics.

Clinical trials

Despite of the extensive documentation on the clinical relevance of targeting BCL2 in pediatric solid tumor types, none of the 74 papers included in the current review reports on (ongoing) clinical trials studying small molecule BCL2 inhibitors in these patients. The set-up of a phase I dose-escalation study in neuroblastoma patients is currently being carried out and, based on the results obtained in these patients, this phase I study can serve as a platform for initiation of clinical trials in other pediatric solid tumor types with a proven track record of high BCL2 expression and BCL2 dependency (neuroblastoma, synovial sarcoma, Ewing sarcoma, osteosarcoma and retinoblastoma).

DISCUSSION

The anti-apoptotic protein BCL2 is aberrantly expressed in numerous cancer types (3, 16-22). This systematic review was performed to get a broad perspective on the clinical relevance and feasibility of targeting BCL2 for the treatment of pediatric solid tumor patients. Appraisal of the search methodology led to a selection of 74 papers which were finally included for reviewing based on the inclusion and exclusion criteria. These papers showed a diversity in methodology, data analysis and the quality of reporting. Papers included in the study were scored and ranked using color and number codes based on the methodology and experimental procedures reported in each paper. Interpretation of the expression pattern of BCL2 in the included papers showed a strong BCL2 expression pattern in several malignancies (neuroblastoma, synovial sarcoma, Ewing sarcoma, osteosarcoma and retinoblastoma). Navitoclax and venetoclax were the most extensively validated BH3 mimetics in this study(3, 6, 9, 14, 34, 35, 41, 50, 52). Several predictive biomarkers for sensitivity and efficacy have been reported for BCL2 inhibition by BH3 mimetics. The most widely validated biomarkers for sensitivity are the BCL2 protein and mRNA expression levels and the ratio of the BIM/BCL2 complex levels (32). The efficacy to BCL2 small molecule inhibitors was exclusively determined by BIM displacement from BCL2 by the compounds and activation of downstream effectors of the intrinsic apoptotic pathway such as cleaved PARP and caspase 3 (3, 14, 32). The excellent results obtained *in vitro* and *in vivo* on the pre-clinical evaluation of these compounds highlights the relevance of targeting BCL2 in pediatric solid tumors with high BCL2 expression. However, several mechanisms of resistance to BCL2 inhibition by small molecule inhibitors have been reported (47, 49). MCL1 upregulation and its sequestration of BIM displaced from BCL2 by the compounds is the most extensively studied mechanism of resistance to BCL2 small molecule inhibition (49). To date, several strategies to elucidate and overcome this resistance mechanism has been studied. Combined targeted depletion of MCL1 protein levels or inhibition of the gene function with MCL-specific inhibitors and targeted BCL2 inhibition yielded a strong synergistic effect (6, 8, 16, 32, 52). Excellent results have also been obtained upon combination studies with chemotherapeutics and BCL2 specific inhibitors (3, 10, 33, 34, 39, 41, 42, 53).

Based on the results obtained from the review process, neuroblastoma was the pediatric solid tumor type with the most sufficient data on the validation of BCL2 as a therapeutic target. Validation of *in vitro* target dependency with shRNA was an important first step in

determining the relevance of targeting this pathway in this tumor type. The subsequent pre-clinical evaluation of BH3 mimetics *in vitro* and *in vivo* yielded promising results with sensitivity to BH3 mimetics being strongly correlated to BCL2 mRNA and protein levels as well as the BIM/BCL2 complex levels. At the *in vitro* level, the strong apoptotic effects as well as tumor growth regression and inhibition linked to BIM displacement from BCL2 was a strong indicator of the exquisite efficacy of small molecule BCL2 inhibitors in neuroblastoma. The identification of MCL1 as one of the key routes through which resistance to BH3 mimetics might occur has been extensively reported and studied in neuroblastoma. The successful abrogation of this resistance mechanism by targeted downregulation of MCL1 in combination with BH3 mimetics highlights a strategy to improve neuroblastoma patient survival. Neuroblastoma patients are therefore excellent candidates for the testing of small molecule BCL2 inhibitors in a clinical setting and currently, a phase I dose-escalation study is being set-up for this tumor type.

Additional studies are needed to extensively validate biomarkers for sensitivity and efficacy of BH3 mimetics in other pediatric tumors shown to have high expression of BCL2 (i.e. synovial sarcoma, Ewing sarcoma, osteosarcoma and retinoblastoma). This systematic review also highlighted the fact there is a severe lack of knowledge on the validation of BCL2 dependency in most BCL2 high-expressing pediatric solid tumors. Based on this review, resistance to BH3 mimetics by MCL1 upregulation was the most validated resistance mechanism in pediatric solid tumors. Most combination studies laid emphasis on the targeted downregulation of MCL1. Other mechanisms of resistance to BH3 mimetics and strategies to overcome resistance need to be addressed. The ultimate goal will be the setting up of clinical trials for the testing of BH3 mimetics as a single agent and subsequently in combination with other therapeutic agents with known synergism with these compounds.

Tumor type	Search terms (Pubmed database)	Items found	Articles Included
Neuroblastoma	((BCL2 or BCL-2) or (ABT199 or ABT-199) or (ABT263 or ABT-263) or venetoclax or navitoclax or obatoclax) and neuroblastoma.	851	11
Rhabdomyosarcoma	((BCL2 or BCL-2) or (ABT199 or ABT-199) or (ABT263 or ABT-263) or venetoclax or navitoclax or obatoclax) and rhabdomyosarcoma	72	3
Synovial sarcoma	((BCL2 or BCL-2) or (ABT199 or ABT-199) or (ABT263 or ABT-263) or venetoclax or navitoclax or obatoclax) and synovial sarcoma	146	3
Ewing Sarcoma	((BCL2 or BCL-2) or (ABT199 or ABT-199) or (ABT263 or ABT-263) or venetoclax or navitoclax or obatoclax) and Ewing sarcoma	44	2
Osteosarcoma	((BCL2 or BCL-2) or (ABT199 or ABT-199) or (ABT263 or ABT-263) or venetoclax or navitoclax or obatoclax) and osteosarcoma	366	4
Wilms' tumor	((BCL2 or BCL-2) or (ABT199 or ABT-199) or (ABT263 or ABT-263) or venetoclax or navitoclax or obatoclax) and Wilms' tumor	73	2
Retinoblastoma	((BCL2 or BCL-2) or (ABT199 or ABT-199) or (ABT263 or ABT-263) or venetoclax or navitoclax or obatoclax) and retinoblastoma	511	3
Inflammatory myofibroblastic tumors	((BCL2 or BCL-2) or (ABT199 or ABT-199) or (ABT263 or ABT-263) or venetoclax or navitoclax or obatoclax) and Inflammatory myofibroblastic tumors	13	7
High grade glioma and glioblastoma multiforme	((BCL2 or BCL-2) or (ABT199 or ABT-199) or (ABT263 or ABT-263) or venetoclax or navitoclax or obatoclax) and glioblastoma multiforme	508	8
STS non-RMS:malignant peripheral nerve sheath tumors	((BCL2 or BCL-2) or (ABT199 or ABT-199) or (ABT263 or ABT-263) or venetoclax or navitoclax or obatoclax) and malignant peripheral nerve sheath tumors	33	4
Astrocytoma grade III	((BCL2 or BCL-2) or (ABT199 or ABT-199) or (ABT263 or ABT-263) or venetoclax or navitoclax or obatoclax) and astrocytoma grade III	403	4
Ependymoma	((BCL2 or BCL-2) or (ABT199 or ABT-199) or (ABT263 or ABT-263) or venetoclax or navitoclax or obatoclax) and ependymoma	14	4
Medulloblastoma	((BCL2 or BCL-2) or (ABT199 or ABT-199) or (ABT263 or ABT-263) or venetoclax or navitoclax or obatoclax) and medulloblastoma	88	6
Atypical peripheral rhabdoid tumors	((BCL2 or BCL-2) or (ABT199 or ABT-199) or (ABT263 or ABT-263) or venetoclax or navitoclax or obatoclax) and atypical teratoid rhabdoid tumors	5	3
Hepatoblastoma	((BCL2 or BCL-2) or (ABT199 or ABT-199) or (ABT263 or ABT-263) or venetoclax or navitoclax or obatoclax) and hepatoblastoma	47	6

Table 1: Search results for Medline/PubMed: 18-04-2016.

Tumor types	Expression of BCL2 patterns of high (% positive/ expression)	<i>In vitro</i> BCL2 dependency	<i>In vivo</i> BCL2 dependency	<i>In vitro</i> compound efficacy	<i>In vivo</i> compound efficacy	Biomarkers for sensitivity	Biomarkers for efficacy	Resistance mechanisms	Combination strategies	Clinical trials
Neuroblastoma	n=185 n=42 31% (16) 100% (3)	Apoptotic response (cleaved PARP, caspase-3) (3)	-	Apoptotic response (cleaved PARP, caspase-3) (3, 32, 34)	Tumor regression and growth inhibition (14, 32-34).	BCL2 protein& mRNA, BIM/ BCL2 complex levels (3, 14, 16, 32)	BIM displacement from BCL2 (32)	MCL1 upregulation (16, 32)	Chemotherapeutics (Doxorubicin, cisplatin, etoposide, cyclophosphamide) (3, 33, 34). Targeted therapy (MCL1, BET and AURKA inhibitors) (14, 32, 54)	-
Rhabdomyosarcoma	n=6 n=11 90% (55) 45% (56)	-	-	-	-	-	-	MCL1 upregulation (50)	Targeted therapy (mTOR inhibitors) (50)	-
Synovial sarcoma	n=32 100% (17)	-	-	Apoptotic response (cleaved PARP, caspase-3) (46)	-	-	-	-	Chemotherapeutics (Doxorubicin) (46)	-
Ewing Sarcoma	n=72 70% (18)	-	-	Apoptotic response (cleaved PARP, caspase-3) (57)	-	-	-	-	Targeted therapy (6-Diazo-5-oxo-L-norleucine) (57)	-
Osteosarcoma	n=202 n=49 n=29 84% (20) 43% (21) 53% (22)	-	-	Apoptotic response (cleaved PARP, caspase-3) (43)	-	-	-	-	-	-
Wilms' tumor	n=10 90% (23)	-	-	-	-	-	-	-	-	-
Retinoblastoma	n=60 66% (19)	-	-	Apoptotic response (cleaved PARP, caspase-3) (44, 58)	-	-	-	-	-	-

Table 2: Summary of results obtained from reviewed papers.

Tumor types	Expression patterns of BCL2 (% positive/high expression)	<i>In vitro</i> BCL2 dependency	<i>In vivo</i> BCL2 dependency	<i>In vitro</i> compound efficacy	<i>In vivo</i> compound efficacy	Biomarkers for sensitivity	Biomarkers for efficacy	Resistance mechanisms	Combination strategies	Clinical trials
Inflammatory myofibroblastic tumor	Negative	-	-	-	-	-	-	-	-	-
High grade glioma	-	Lack of apoptotic response upon BCL2 KD (9)	-	Apoptotic response (cleaved PARP, caspase-3) (7)	Tumor regression (7)	-	-	MCL1 upregulation (8, 36, 51, 52)	Targeted therapy (PI3K, bortezomib, YMI155, SAHA) (9, 36, 51, 52)	-
STS non-RMS;MPNST	-	-	-	-	-	-	-	BCL-X _L upregulation (48)	-	-
Astrocytoma grade III	n=21 55% (24)	-	-	-	-	-	-	-	-	-
Ependymoma	n=104 15% (25)	-	-	-	-	-	-	-	-	-
	n=31 45% (26, 27)	-	-	-	-	-	-	-	-	-
Medulloblastoma	-	-	Tumor forming potential (59)	-	-	-	-	-	Chemotherapeutics (Etoposide) (59)	-
ATRT;Rhabdoid	Negative (28)	-	-	-	-	-	-	-	Targeted therapy (Debromohymenialdisine) (60)	-
Hepatoblastoma	-	Apoptotic response (cleaved PARP, caspase-3) (39)	-	Apoptotic response (cleaved PARP, caspase-3) (40)	Tumor regression (10, 42)	-	-	-	Chemotherapeutics (Cisplatin, paclitaxel) (41, 42). Targeted inhibitors (TRAIL) (10).	-

Table 2: (continued)

	Target expression	<i>In vitro</i> target dependency	<i>In vivo</i> target dependency	<i>In vitro</i> compound efficacy	<i>In vivo</i> compound efficacy	Biomarkers for sensitivity	Biomarkers for efficacy	Resistance mechanisms	Combination strategies	Clinical • Phase 1 • Phase 2 • Phase 3
Neuroblastoma	Sufficient	Sufficient	Not tested	Sufficient	Sufficient	Sufficient	Inconclusive	Inconclusive	Inconclusive	
Rhabdomyosarcoma	Inconclusive	Not tested	Not tested	Not tested	Not tested	Not tested	Not tested	Sufficient	Sufficient	
Synovial sarcoma	Sufficient	Not tested	Not tested	Inconclusive	Not tested	Not tested	Inconclusive	Not tested	Inconclusive	
Ewing sarcoma	Sufficient	Not tested	Not tested	Inconclusive	Not tested	Not tested	Not tested	Not tested	Inconclusive	
Osteosarcoma	Sufficient	Not tested	Not tested	Inconclusive	Not tested	Not tested	Inconclusive	Not tested	Not tested	
Wilms' tumor	Inconclusive	Not tested	Not tested	Not tested	Not tested	Not tested	Not tested	Not tested	Not tested	
Retinoblastoma	Sufficient	Not tested	Not tested	Inconclusive	Not tested	Not tested	Inconclusive	Not tested	Not tested	
Inflammatory myofibroblastic tumor	Negative	Not tested	Not tested	Not tested	Not tested	Not tested	Not tested	Not tested	Not tested	
High grade glioma	Not tested	Negative	Not tested	Inconclusive	Inconclusive	Not tested	Inconclusive	Sufficient	Inconclusive	
STS-non RMS:MPNST	Not tested	Not tested	Not tested	Not tested	Not tested	Not tested	Not tested	Inconclusive	Not tested	
Astrocytoma Grade III	Inconclusive	Not tested	Not tested	Not tested	Not tested	Not tested	Not tested	Not tested	Not tested	
Ependymoma	Inconclusive	Not tested	Not tested	Not tested	Not tested	Not tested	Not tested	Not tested	Not tested	
Medulloblastoma	Not tested	Not tested	Inconclusive	Not tested	Not tested	Not tested	Not tested	Not tested	Inconclusive	
ATRT: Rhabdoid	Negative	Not tested	Not tested	Not tested	Not tested	Not tested	Not tested	Not tested	Inconclusive	
Hepatoblastoma	Not tested	Inconclusive	Not tested	Inconclusive	Inconclusive	Not tested	Inconclusive	Not tested	Sufficient	

Table 3: Target actionability literature score.

SUPPLEMENTARY INFORMATION

Module	Subcategories	Scoring	
1. Target pattern	Number of samples	1	n>25
		2	n>10<25
		3	n<10
	Type of analysis	1	Two or more different methods were used or WGS/WES
		2	qPCR, differential PCR, Southern/Northern blot, array CGH
		3	IHC, FISH
	Expression vs overexpression vs amplification	1	Well-defined amplification (>4 copies) or shown correlation between high expression and outcome
		2	Gain, overexpression
		3	Expression/immunoreactivity
1		>80% pediatric patients	
2		40-80% pediatric patients	
3		<40% pediatric patients	
2. Target validation in vitro	Knockdown/knockout	1	Different methods to induce knockdown/knockout or >3 cell lines
		2	Use of 1-3 shRNAs or siRNAs
		3	Questionable knockdown/knockout
	Confirmation and analysis of knockdown	1	Phenotypic analysis and analysis of effects of knockdown
		2	One of the two
		3	None of the two

Table S1: Scoring system PoC modules.

Module	Subcategories	Scoring	
3. Target validation in vivo	Type of in vivo model used	1	Transgenic mouse model, >2 different xenografts
		2	Xenografts with inducible genomic modification
		3	Xenografts constitutive genomic modification
	Validation of in vivo model	1	Comprehensive study of developed tumors (Characterization, mRNA expression, protein expression, etc.)
		2	Minor validation of the developed tumors
		3	No validation of the developed tumors
4. Drug efficacy in vitro	Number of cell lines	1	5 cell lines or more + at least two appropriate controls
		2	2-5 cell lines + at least one appropriate controls
		3	1 cell line and/or lack of control
	Validation of compound efficacy	1	2 or more methods are used for validation (protein expression, cell cycle distribution, apoptosis assay, etc.)
		2	1 method used for validation
		3	No validation of compound efficacy
5. Drug efficacy in vivo	Number and type of in vivo models used	1	2 or more xenograft models or one transgenic mouse model with appropriate control
		2	1 xenograft models with appropriate control
		3	1 xenograft models without appropriate control
	Validation of compound efficacy	1	2 or more methods are used for validation (protein expression, cell cycle distribution, apoptosis assay, etc.)
		2	1 methods are used for validation
		3	No validation of compound efficacy

Table S1: (continued)

Module	Subcategories	Scoring	
6. Biomarkers	Confirmation of correlation	1	Correlation molecularly confirmed in 2 or more models (e.g. silencing, overexpression, etc.)
		2	Correlation confirmed in one model
		3	Correlation not confirmed
6. Biomarkers	Number of models used to find correlation	1	>10
		2	3-10
		3	<3
7. Resistance		1	Reported resistance + comprehensive analysis + reversing/overcoming resistance
		2	Reported resistance + analysis of molecular changes underlying or due to resistance
		3	Only reporting resistance
8. Combinations	Concentrations tested	1	>4 concentrations of each compound are tested
		2	1-4 concentrations of each compound are tested
		3	1 concentration of each compound is tested
8. Combinations	Definition of synergy	1	Combination index <0.5
		2	Combination index 0.5-0.9 or >5-fold decrease in IC50
		3	Combination index 0.9-1.1 or other methods used
9. Clinical trials		1	Not applicable
		2	Not applicable
		3	Not applicable
Good methodology, convincing evidence (1)			
Reasonably good methodology (2)			
Evidence not convincing, flaws in methodology (3)			

Table S1: (continued)

Table S2: Summaries and scoring of papers included in the review study.

This table can be found at:

<https://docs.google.com/spreadsheets/d/1G8pL21BdZ4KToCdZ7zAtOXIeEwffMVD3FKdm-XDJcCw/edit?usp=sharing>

REFERENCES

1. Cory S, Adams JM. The Bcl2 family: regulators of the cellular life-or-death switch. *Nat Rev Cancer* 2002;2(9):647-56.
2. Elmore S. Apoptosis: a review of programmed cell death. *Toxicol Pathol* 2007;35(4):495-516.
3. Lamers F, Schild L, den Hartog IJ, Ebus ME, Westerhout EM, Ora I, et al. Targeted BCL2 inhibition effectively inhibits neuroblastoma tumour growth. *Eur J Cancer* 2012;48(16):3093-103.
4. Tse C, Shoemaker AR, Adickes J, Anderson MG, Chen J, Jin S, et al. ABT-263: a potent and orally bioavailable Bcl-2 family inhibitor. *Cancer Res* 2008;68(9):3421-8.
5. Kang MH, Reynolds CP. Bcl-2 inhibitors: targeting mitochondrial apoptotic pathways in cancer therapy. *Clin Cancer Res* 2009;15(4):1126-32.
6. Karpel-Massler G, Shu C, Chau L, Banu M, Halatsch ME, Westhoff MA, et al. Combined inhibition of Bcl-2/Bcl-xL and Usp9X/Bag3 overcomes apoptotic resistance in glioblastoma in vitro and in vivo. *Oncotarget* 2015;6(16):14507-21.
7. Tagscherer KE, Fassel A, Campos B, Farhadi M, Kraemer A, Bock BC, et al. Apoptosis-based treatment of glioblastomas with ABT-737, a novel small molecule inhibitor of Bcl-2 family proteins. *Oncogene* 2008;27(52):6646-56.
8. Pareja F, Macleod D, Shu C, Cray JF, Canoll PD, Ross AH, et al. PI3K and Bcl-2 inhibition primes glioblastoma cells to apoptosis through downregulation of Mcl-1 and Phospho-BAD. *Mol Cancer Res* 2014;12(7):987-1001.
9. Premkumar DR, Jane EP, DiDomenico JD, Vukmer NA, Agostino NR, Pollack IF. ABT-737 synergizes with bortezomib to induce apoptosis, mediated by Bid cleavage, Bax activation, and mitochondrial dysfunction in an Akt-dependent context in malignant human glioma cell lines. *J Pharmacol Exp Ther* 2012;341(3):859-72.
10. Lieber J, Ellerkamp V, Vogt F, Wenz J, Warmann SW, Fuchs J, et al. BH3-mimetic drugs prevent tumour onset in an orthotopic mouse model of hepatoblastoma. *Exp Cell Res* 2014;322(1):217-25.
11. Rudin CM, Hann CL, Garon EB, Ribeiro de Oliveira M, Bonomi PD, Camidge DR, et al. Phase II study of single-agent navitoclax (ABT-263) and biomarker correlates in patients with relapsed small cell lung cancer. *Clin Cancer Res* 2012;18(11):3163-9.
12. Roberts AW, Seymour JF, Brown JR, Wierda WG, Kipps TJ, Khaw SL, et al. Substantial susceptibility of chronic lymphocytic leukemia to BCL2 inhibition: results of a phase I study of navitoclax in patients with relapsed or refractory disease. *J Clin Oncol* 2012;30(5):488-96.
13. Souers AJ, Levenson JD, Boghaert ER, Ackler SL, Catron ND, Chen J, et al. ABT-199, a potent and selective BCL-2 inhibitor, achieves antitumor activity while sparing platelets. *Nat Med* 2013;19(2):202-8.

14. Ham J, Costa C, Sano R, Lochmann TL, Sennott EM, Patel NU, et al. Exploitation of the Apoptosis-Primed State of MYCN-Amplified Neuroblastoma to Develop a Potent and Specific Targeted Therapy Combination. *Cancer Cell* 2016;29(2):159-72.
15. Roberts AW, Davids MS, Pagel JM, Kahl BS, Puvvada SD, Gerecitano JF, et al. Targeting BCL2 with Venetoclax in Relapsed Chronic Lymphocytic Leukemia. *N Engl J Med* 2016;374(4):311-22.
16. Lestini BJ, Goldsmith KC, Fluchel MN, Liu X, Chen NL, Goyal B, et al. Mcl1 downregulation sensitizes neuroblastoma to cytotoxic chemotherapy and small molecule Bcl2-family antagonists. *Cancer Biol Ther* 2009;8(16):1587-95.
17. Krskova L, Kalinova M, Brizova H, Mrhalova M, Sumerauer D, Kodet R. Molecular and immunohistochemical analyses of BCL2, KI-67, and cyclin D1 expression in synovial sarcoma. *Cancer Genet Cytogenet* 2009;193(1):1-8.
18. Kavalar R, Pohar Marinsek Z, Jereb B, Cagran B, Golouh R. Prognostic value of immunohistochemistry in the Ewing's sarcoma family of tumors. *Med Sci Monit* 2009;15(8):Cr442-52.
19. Singh L, Pushker N, Saini N, Sen S, Sharma A, Bakhshi S, et al. Expression of pro-apoptotic Bax and anti-apoptotic Bcl-2 proteins in human retinoblastoma. *Clin Exp Ophthalmol* 2015;43(3):259-67.
20. Fu T, Xia C, Li Z, Wu H. Lack of association between bcl-2 expression and prognosis of osteosarcoma: a meta-analysis. *Int J Clin Exp Med* 2015;8(6):9093-9.
21. Trieb K, Sulzbacher I, Kubista B. Bcl-2 correlates with localization but not outcome in human osteosarcoma. *Oncol Lett* 2013;6(2):559-561.
22. Nedelcu T, Kubista B, Koller A, Sulzbacher I, Mosberger I, Arrich F, et al. Livin and Bcl-2 expression in high-grade osteosarcoma. *J Cancer Res Clin Oncol* 2008;134(2):237-44.
23. Re GG, Hazen-Martin DJ, El Bahtimi R, Brownlee NA, Willingham MC, Garvin AJ. Prognostic significance of Bcl-2 in Wilms' tumor and oncogenic potential of Bcl-X(L) in rare tumor cases. *Int J Cancer* 1999;84(2):192-200.
24. Daido S, Tamiya T, Ono Y, Terada K, Mizumatsu S, Ohmoto T. Expression of Bcl-2, Bcl-x, and Bax proteins in astrocytomas in relation to patient survival. *Brain Tumor Pathol* 2001;18(2):123-9.
25. Newcomb EW, Bhalla SK, Parrish CL, Hayes RL, Cohen H, Miller DC. bcl-2 protein expression in astrocytomas in relation to patient survival and p53 gene status. *Acta Neuropathol* 1997;94(4):369-75.
26. Rushing EJ, Brown DF, Hladik CL, Risser RC, Mickey BE, White CL, 3rd. Correlation of bcl-2, p53, and MIB-1 expression with ependymoma grade and subtype. *Mod Pathol* 1998;11(5):464-70.
27. Versteegen MJ, Leenstra DT, Ijlst-Keizers H, Bosch DA. Proliferation- and apoptosis-related proteins in intracranial ependymomas: an immunohistochemical analysis. *J Neurooncol* 2002;56(1):21-8.

28. Wolff JE, Brown RE, Buryanek J, Pfister S, Vats TS, Rytting ME. Preliminary experience with personalized and targeted therapy for pediatric brain tumors. *Pediatr Blood Cancer* 2012;59(1):27-33.
29. McCall TD, Pedone CA, Fults DW. Apoptosis suppression by somatic cell transfer of Bcl-2 promotes Sonic hedgehog-dependent medulloblastoma formation in mice. *Cancer Res* 2007;67(11):5179-85.
30. Cookman CJ, Belcher SM. Estrogen Receptor-beta Up-Regulates IGF1R Expression and Activity to Inhibit Apoptosis and Increase Growth of Medulloblastoma. *Endocrinology* 2015;156(7):2395-408.
31. Gandhi L, Camidge DR, Ribeiro de Oliveira M, Bonomi P, Gandara D, Khaira D, et al. Phase I study of Navitoclax (ABT-263), a novel Bcl-2 family inhibitor, in patients with small-cell lung cancer and other solid tumors. *J Clin Oncol* 2011;29(7):909-16.
32. Bate-Eya LT, den Hartog IJ, van der Ploeg I, Schild L, Koster J, Santo EE, et al. High efficacy of the BCL-2 inhibitor ABT199 (venetoclax) in BCL-2 high-expressing neuroblastoma cell lines and xenografts and rational for combination with MCL-1 inhibition. *Oncotarget* 2016;7(19):27946-58.
33. Goldsmith KC, Gross M, Peirce S, Luyindula D, Liu X, Vu A, et al. Mitochondrial Bcl-2 family dynamics define therapy response and resistance in neuroblastoma. *Cancer Res* 2012;72(10):2565-77.
34. Tanos R, Karmali D, Nalluri S, Goldsmith KC. Select Bcl-2 antagonism restores chemotherapy sensitivity in high-risk neuroblastoma. *BMC Cancer* 2016;16:97.
35. Goldsmith KC, Lestini BJ, Gross M, Ip L, Bhumbra A, Zhang X, et al. BH3 response profiles from neuroblastoma mitochondria predict activity of small molecule Bcl-2 family antagonists. *Cell Death Differ* 2010;17(5):872-82.
36. Jane EP, Premkumar DR, DiDomenico JD, Hu B, Cheng SY, Pollack IF. YM-155 potentiates the effect of ABT-737 in malignant human glioma cells via survivin and Mcl-1 downregulation in an EGFR-dependent context. *Mol Cancer Ther* 2013;12(3):326-38.
37. Yang MC, Loh JK, Li YY, Huang WS, Chou CH, Cheng JT, et al. Bcl2L12 with a BH3-like domain in regulating apoptosis and TMZ-induced autophagy: a prospective combination of ABT-737 and TMZ for treating glioma. *Int J Oncol* 2015;46(3):1304-16.
38. Vogt F, Lieber J, Dewerth A, Hoh A, Fuchs J, Armeanu-Ebinger S. BH3 mimetics reduce adhesion and migration of hepatoblastoma and hepatocellular carcinoma cells. *Exp Cell Res* 2013;319(10):1443-50.
39. Lieber J, Kirchner B, Eicher C, Warmann SW, Seitz G, Fuchs J, et al. Inhibition of Bcl-2 and Bcl-X enhances chemotherapy sensitivity in hepatoblastoma cells. *Pediatr Blood Cancer* 2010;55(6):1089-95.
40. Lieber J, Ellerkamp V, Wenz J, Kirchner B, Warmann SW, Fuchs J, et al. Apoptosis sensitizers enhance cytotoxicity in hepatoblastoma cells. *Pediatr Surg Int* 2012;28(2):149-59.

41. Lieber J, Eicher C, Wenz J, Kirchner B, Warmann SW, Fuchs J, et al. The BH3 mimetic ABT-737 increases treatment efficiency of paclitaxel against hepatoblastoma. *BMC Cancer* 2011;11:362.
42. Lieber J, Dewerth A, Wenz J, Kirchner B, Eicher C, Warmann SW, et al. Increased efficacy of CDDP in a xenograft model of hepatoblastoma using the apoptosis sensitizer ABT-737. *Oncol Rep* 2013;29(2):646-52.
43. Li Z, Yu Y, Sun S, Qi B, Wang W, Yu A. Niclosamide inhibits the proliferation of human osteosarcoma cell lines by inducing apoptosis and cell cycle arrest. *Oncol Rep* 2015;33(4):1763-8.
44. Allaman-Pillet N, Oberson A, Munier F, Schorderet DF. The Bcl-2/Bcl-XL inhibitor ABT-737 promotes death of retinoblastoma cancer cells. *Ophthalmic Genet* 2013;34(1-2):1-13.
45. Levesley J, Lusher ME, Lindsey JC, Clifford SC, Grundy R, Coyle B. RASSF1A and the BH3-only mimetic ABT-737 promote apoptosis in pediatric medulloblastoma cell lines. *Neuro Oncol* 2011;13(12):1265-76.
46. Joyner DE, Albritton KH, Bastar JD, Randall RL. G3139 antisense oligonucleotide directed against antiapoptotic Bcl-2 enhances doxorubicin cytotoxicity in the FU-SY-1 synovial sarcoma cell line. *J Orthop Res* 2006;24(3):474-80.
47. Fresquet V, Rieger M, Carolis C, Garcia-Barchino MJ, Martinez-Climent JA. Acquired mutations in BCL2 family proteins conferring resistance to the BH3 mimetic ABT-199 in lymphoma. *Blood* 2014;123(26):4111-9.
48. Lee SJ, Park HJ, Kim YH, Kim BY, Jin HS, Kim HJ, et al. Inhibition of Bcl-xL by ABT-737 enhances chemotherapy sensitivity in neurofibromatosis type 1-associated malignant peripheral nerve sheath tumor cells. *Int J Mol Med* 2012;30(2):443-50.
49. Choudhary GS, Al-Harbi S, Mazumder S, Hill BT, Smith MR, Bodo J, et al. MCL-1 and BCL-xL-dependent resistance to the BCL-2 inhibitor ABT-199 can be overcome by preventing PI3K/AKT/mTOR activation in lymphoid malignancies. *Cell Death Dis* 2015;6:e1593.
50. Preuss E, Hugle M, Reimann R, Schlecht M, Fulda S. Pan-mammalian target of rapamycin (mTOR) inhibitor AZD8055 primes rhabdomyosarcoma cells for ABT-737-induced apoptosis by down-regulating Mcl-1 protein. *J Biol Chem* 2013;288(49):35287-96.
51. Jane EP, Premkumar DR, Morales A, Foster KA, Pollack IF. Inhibition of phosphatidylinositol 3-kinase/AKT signaling by NVP-BKM120 promotes ABT-737-induced toxicity in a caspase-dependent manner through mitochondrial dysfunction and DNA damage response in established and primary cultured glioblastoma cells. *J Pharmacol Exp Ther* 2014;350(1):22-35.
52. Foster KA, Jane EP, Premkumar DR, Morales A, Pollack IF. Co-administration of ABT-737 and SAHA induces apoptosis, mediated by Noxa upregulation, Bax activation and mitochondrial dysfunction in PTEN-intact malignant human glioma cell lines. *J Neurooncol* 2014;120(3):459-72.

53. Lei XY, Zhong M, Feng LF, Zhu BY, Tang SS, Liao DF. siRNA-mediated Bcl-2 and Bcl-xl gene silencing sensitizes human hepatoblastoma cells to chemotherapeutic drugs. *Clin Exp Pharmacol Physiol* 2007;34(5-6):450-6.
54. Noujaim D, van Golen CM, van Golen KL, Grauman A, Feldman EL. N-Myc and Bcl-2 coexpression induces MMP-2 secretion and activation in human neuroblastoma cells. *Oncogene* 2002;21(29):4549-57.
55. Kiani B, Ferrell LD, Qualman S, Frankel WL. Immunohistochemical analysis of embryonal sarcoma of the liver. *Appl Immunohistochem Mol Morphol* 2006;14(2):193-7.
56. Staibano S, Franco R, Tranfa F, Mezza E, Lo Muzio L, Strianese D, et al. Orbital rhabdomyosarcoma: relationship between DNA ploidy, p53, bcl-2, MDR-1 and Ki67 (MIB1) expression and clinical behavior. *Anticancer Res* 2004;24(1):249-57.
57. Olsen RR, Mary-Sinclair MN, Yin Z, Freeman KW. Antagonizing Bcl-2 family members sensitizes neuroblastoma and Ewing's sarcoma to an inhibitor of glutamine metabolism. *PLoS One* 2015;10(1):e0116998.
58. Allaman-Pillet N, Oberson A, Schorderet DF. BIRO1, a cell-permeable BH3 peptide, promotes mitochondrial fragmentation and death of retinoblastoma cells. *Mol Cancer Res* 2015;13(1):86-97.
59. Othman RT, Kimishi I, Bradshaw TD, Storer LC, Korshunov A, Pfister SM, et al. Overcoming multiple drug resistance mechanisms in medulloblastoma. *Acta Neuropathol Commun* 2014;2:57.
60. Chiou SH, Kao CL, Chen YW, Chien CS, Hung SC, Lo JF, et al. Identification of CD133-positive radioresistant cells in atypical teratoid/rhabdoid tumor. *PLoS One* 2008;3(5):e2090.



CHAPTER 7

DISCUSSION

DISCUSSION

Neuroblastoma remains one of the deadliest forms of childhood cancers with only about 30-40% long-term survival in high-risk patients. Studies of the genomic landscape of neuroblastoma patients by whole genome sequencing (WGS) have identified only a few targetable genomic aberrations. Thus far, treatment options for these patients with more precise targeted therapies are limited. Currently, the treatment of neuroblastoma entails the use of chemotherapeutic agents with a wide range of toxic side-effects and minimal responses from the patients. Additionally, *in vitro* and *in vivo* systems to carry out pre-clinical drug studies that can be better translated to the clinical situation are still in development.

In the first part of this thesis, we reported on the isolation and establishment of *in vitro* organoid systems and TIC line xenografts models. We show that these organoids recapitulate the phenotype and genotype of the primary tumors from which they were derived. Next, we identified frequent gain and overexpression of the EZH2 gene in neuroblastoma tumors and we attempted to elucidate the clinical relevance of targeting the histone methyltransferase activity of EZH2 with small molecule inhibitors. We identified a histone methyltransferase-independent function of EZH2 in neuroblastoma. Lastly, we carried out the *in vitro* and *in vivo* pre-clinical evaluation of the BCL2-specific inhibitor venetoclax in neuroblastoma. We attempted to elucidate mechanisms of resistance to venetoclax and finally identified the small molecule MDM2 inhibitor idasanutlin as a targeted inhibitor capable of re-sensitizing venetoclax-resistant high BCL2-expressing cells.

In Chapter 2, we describe the isolation and propagation of primary neuroblastoma cells termed “tumor-initiating cells” (TICs) or organoids. The proper terminology for these cell systems is still under debate. Organoids are defined as 3D structures that arise from stem cells and are composed of organ-specific cell types (1). This terminology was first used for non-malignant cell systems. In a later stage, cells derived from patient tumors that were cultured under the same conditions were defined as ‘tumor organoids’. In this case, it is not clear if the same definition, as used for non-malignant cells, can be sustained. Tumor organoids might not have clear stem cell properties and do not have organ-specific cell types. Thus, the only characteristic that is retained is: growth in defined medium in a 3D structure. Tumor organoids and TIC lines are both short-term cultured cells derived from primary or relapsed patient tumor material that retain spheroid characteristics when cultured under non-adherent conditions. Based on this

definition, the term 'tumor organoid' can loosely be applied to define the neuroblastoma cell systems that we describe in chapter 2. But since we used the term TIC lines in the publication, we will sustain this terminology in the current thesis.

Classical cell lines cultured in 2D under serum conditions fail to recapitulate the phenotype of primary neuroblastoma tumors (2). Cluster analyses of classical cell lines with primary tumors in glioblastoma and neuroblastoma tumors have shown them to cluster far-away from primary tumors (2, 3). This result suggests that pathway activity in classical cell lines is distinctly different than that in primary tumors. Additionally, classical cell lines are thought to have acquired mutations that are not present in primary neuroblastoma tumors due to long-term propagation effects. For example, neuroblastoma cell lines have a high frequency of TP53 mutations, while these are not found in primary or relapsed neuroblastoma tumors. Thus, carrying out pre-clinical studies in such model systems might lead to false positive results in targetable pathways only activated under 2D cultured conditions and not in primary tumors.

Cell lines cultured in 3D under serum-free conditions on the other hand have been shown to more faithfully recapitulate the signaling pathway profile of the tumors from which they are derived (2). mRNA profiling and protein expression analysis of neuroblastoma TIC lines indeed suggest that the 3D grown TIC lines better reflect the phenotype of the primary tumors. For example, important neuroblastoma pathogenic markers such as dopamine beta-hydroxylase (DBH), chromogranin A (CHGA) and neural cell adhesion molecule (NCAM) were found to be highly expressed both in the primary tumors and their corresponding TIC lines. mRNA expression analysis showed that neuroblastoma TIC lines and their corresponding mice xenografts clustered together with the primary tumors from which they were derived. This suggests that neuroblastoma TIC lines might represent a better *in vitro* system than classical cell lines (3). Additionally, TIC lines exhibit a similar genomic landscape compared to their corresponding primary tumors. For example, mutations in the Ras-MAPK pathway in the form of a homozygous deletion of the NF1 allele were observed in both the primary tumors and the TIC lines that were derived from these tumors. The Ras-MAPK pathway has been shown to be an important driving genomic event in neuroblastoma relapse formation and propagation (4). Carrying out *in vitro* pre-clinical evaluation of MEK inhibitors using TIC lines from the NF1 mutated tumor might generate results which better represent the patient situation (5, 6).

The success rate of obtaining neuroblastoma cell lines cultured under 3D conditions remains poor. This is most likely due to the fact that growth factors present in the primary tumors that are important for the maintenance of neuroblastoma TIC lines are not adequately supplied in the culture medium. (7). In order to improve the culture conditions of TIC lines, a first step will be to determine essential growth factors and cell survival pathways in primary neuroblastoma tumors by profiling of these tumors. Supplementing TIC line culture medium with these growth factors might improve the efficiency of culturing these cells, while preserving their genomic and phenotypic landscape. Another strategy for optimizing the culture conditions of TIC lines can be, for example, by co-culturing these cells with tumor-derived stromal cells. Growth factors secreted by these tumor-derived stromal cells might improve the growth of these TIC lines, thereby increasing the chances of maintaining these systems *in vivo*.

Epigenetic modulation of tumor suppressor and oncogenes is one of the key tumor-promoting events in a vast number of cancers. The concept of 'epigenetics' can be described as heritable changes in gene function that cannot be explained by changes in DNA sequence (8). There are several classes of epigenetic systems. The polycomb/trithorax system, for example, is involved in histone methylation processes. In **chapter 3**, we describe a local gain and high expression of EZH2. EZH2 is one of the key components of the PRC2 complex, which belongs to the polycomb/trithorax system. High expression of EZH2 correlates with a poor prognosis in neuroblastoma (9). Thus, targeting EZH2 might be a clinically relevant strategy in neuroblastoma tumors with high EZH2 expression.

Surprisingly, we found that targeting the histone methyltransferase activity of EZH2 with small molecule histone methyltransferase inhibitors was ineffective. Despite maximum target inhibition observed at sub-micromolar concentrations of EZH2-specific histone methyltransferase inhibitors, there were only very mild phenotypic effects. Still, EZH2 inhibition might have potential in neuroblastoma. Inhibition of the EZH2 methyltransferase activity alone might lead to molecular changes that result in a mild phenotype but that sensitize these cells for other inhibitors. Thus, combination strategies of histone methyltransferase inhibitors with other compounds might result in effective responses. Potential evidence for such combinations comes from recent studies that show transcriptional repression of tumor-suppressor genes by DNA methyltransferases and PRC2-mediated histone tail modifications in high-risk neuroblastoma patients. This led to the hypothesis that tumor suppressor genes hyper-

methylyated and downregulated due to DNA methylation and histone methylation events by the PRC2 complex can be re-expressed upon combination treatment with DNA demethylating agents and EZH2-specific histone methyltransferase inhibitors (10). Combining DNA demethylating agents with the EZH2 histone methyltransferase inhibitor EPZ6438 resulted in a more pronounced re-expression of the tumor-suppressor genes compared to single agent treatment and a potent phenotypic effect of the cells. These results suggest that combining EZH2-specific histone methyltransferase inhibition with DNA demethylating agents might be effective in the future treatment of neuroblastoma. Other effective combinations of histone methyltransferase inhibitors with chemotherapeutic agents have yielded promising results in other tumor types (11).

A second alternative approach to target EZH2 will be by inhibition of its non-canonical functions. Targeted downregulation of EZH2 with shRNAs in EZH2 high-expressing neuroblastoma cell lines resulted in a strong apoptotic phenotype. This suggests that neuroblastoma cell lines might be dependent on EZH2 for their survival, independent of its methyltransferase activity (12). The apoptotic phenotype observed in neuroblastoma cell lines might be due to the downregulation of key anti-apoptotic proteins such as BCL2 and FOXM1 which are reported to be direct downstream targets of EZH2 (13). These results demonstrate the need for compounds that specifically target the non-canonical functions of EZH2 in neuroblastoma.

Resistance to apoptosis is a precursor to tumor formation and maintenance. In most cancer cell types, upregulation of key players of the extrinsic and intrinsic apoptotic pathway provide a mechanism of evasion to apoptotic cues, leading to uncontrollable proliferation of tumor cells. Hypermethylation of the promoter region of the *CASP8* gene, gain of the 17q25 locus housing the *BIRC5* gene (leading to its concomitant overexpression) and overexpression of the BCL2 protein are frequently observed anti-apoptotic events in neuroblastoma (14-16). Earlier attempts to specifically target BCL2 with the small molecule inhibitor navitoclax showed great promise *in vitro* and *in vivo*. However, due to the concomitant targeting of the anti-apoptotic proteins BCL-X_L and BCLW, thrombocytopenia was observed in patients treated with this compound (17). This led to the development of the new BCL2-specific inhibitor venetoclax (18). In **chapter 4**, we describe the pre-clinical validation of venetoclax in neuroblastoma.

First, we identified *BCL2* mRNA, BCL2 protein and BIM/BCL2 complex levels as promising candidate selection biomarkers for sensitivity to venetoclax (19). Others have suggested that MYCN levels might also hold some predictive power for determining sensitivity

to venetoclax (20), but this still needs to be clearly defined in larger series of model systems. The upcoming trial of venetoclax in neuroblastoma patients might give more insight in the predictive value of MYCN.

Despite promising *in vitro* and *in vivo* responses to the compound, resistance to venetoclax was observed. Neuroblastoma resistance to venetoclax could be attributed to upregulation of the anti-apoptotic protein MCL1. Upregulated MCL1 sequesters BIM displaced from BCL2 by venetoclax, thereby preventing further activation of downstream events in the intrinsic apoptotic pathway (19). Several strategies to overcome MCL1-mediated resistance to venetoclax have been explored. Firstly, by concomitant inhibition of pathways or proteins positively regulating MCL1 expression such as the PI3K/AKT and Ras/MAPK pathways and cyclin-dependent kinases (CDKs). Inhibitors of the PI3K/AKT and Ras/MAPK pathways and CDKs have been shown to effectively downregulate MCL1 protein levels and promising results were observed when directly combining these inhibitors with venetoclax (21, 22). Implementing such combination strategies in neuroblastoma treatment might be an effective strategy to overcome MCL1-mediated resistance to venetoclax.

The second strategy enacted to overcome MCL1-mediated resistance to venetoclax is by combination treatment with compounds directly inhibiting MCL1 by occupying its BH3 domain. In the current thesis, we report moderate synergistic and strong additive effects between venetoclax and MCL1 inhibitor A-1210477 across the BCL2 high-expressing cell lines. Additional studies need to be performed to validate the *in vitro* obtained results with this combination in *in vivo* model systems.

In **chapter 5**, we studied the re-sensitization of venetoclax-resistant BCL2 high-expressing cell lines to venetoclax by targeted and chemotherapeutic compounds. High-throughput drug screening of venetoclax-resistant cells and their corresponding motherlines with over 200 compounds revealed a select number of targeted and chemotherapeutic compounds capable of re-sensitizing venetoclax-resistant cell lines to venetoclax. Besides the above discussed P13K/mTOR and CDK inhibitors, histone deacetylase (HDAC) inhibitors and the MDM2 inhibitor idasanutlin were identified as promising targeted compounds for combination treatment with venetoclax, of which idasanutlin was the most promising re-sensitizing compound. P53-mediated BAX activation of apoptosis in venetoclax-resistant BCL2 high-expressing cell lines might be an attractive strategy to overcome resistance in these cells. At the mechanistic level, re-sensitization of the venetoclax-resistant neuroblastoma cell lines to venetoclax

by idasanutlin could be attributed to the potent upregulation of the pro-apoptotic protein BAX. Additional studies need to be performed in order to elucidate the exact mechanistic contribution of idasanutlin in activating the intrinsic apoptotic pathway in venetoclax-resistant BCL2 high-expressing cell lines.

Combined treatment with BCL2 and MDM2 inhibitors venetoclax and idasanutlin led to partial responses *in vivo*, with clear tumor regression and a strong upregulation of BAX. However, no complete regression was obtained and tumors regrew upon withdrawal of both compounds in mice. Several approaches could be explored to improve the efficacy of this combination. We can test more intensive treatment regimens both concerning dosage as well as duration. This is in line with the treatment protocols that will be implemented in the clinical trial. An additional strategy might be the implementation of the venetoclax/idasanutlin combination treatment in regular treatment protocols.

Numerous other malignancies have a high expression of BCL2 and targeting this protein with BH3 mimetics has shown promising results in various adult malignancies. The BCL2-specific small molecule inhibitor venetoclax has recently been clinically validated in chronic lymphocytic leukemia (23). For further clinical development of this compound for pediatric patients with solid tumors, a systematic summary of the relevant literature addressing this subject was needed. In **chapter 6**, we performed a systematic review on the expression patterns and pre-clinical evaluation of small molecule BCL2 inhibitors in pediatric solid tumors.

Based on the literature review, we found overexpression of BCL2 present in 5 pediatric solid tumor types (i.e. neuroblastoma, synovial sarcoma, retinoblastoma, osteosarcoma and Ewing sarcoma), while a negative BCL2 target presence was noted in two of the tumor types (atypical teratoid rhabdoid and inflammatory myofibroblastic tumors) (15, 24-31). For the tumors whereby expression analysis was deemed inconclusive, additional studies are needed in order to validate target presence. BH3 mimetics were extensively pre-clinically tested in several tumor types (i.e. neuroblastoma, synovial sarcomas, retinoblastoma, osteosarcoma, Ewing Sarcoma, glioma and hepatoblastoma) and showed strong apoptotic responses with tumor regression and growth inhibition *in vivo* (15, 19, 32-39). Till date, clinical trials of venetoclax as a single agent have only been performed in adult lymphoid malignancies (23), but the first trials in neuroblastoma patients are in the pipeline. Results obtained from clinical trials in neuroblastoma patients might pave the way for the future implementation in neuroblastoma patients as well as pediatric patients with other solid tumor types expressing high levels of BCL2.

FUTURE DIRECTIONS

1. Organoid systems in neuroblastoma

One of the most challenging aspects of isolating and maintaining neuroblastoma TIC lines is the determination of an adequate culture condition to improve the growth of these cell lines. Affymetrix profiling of the primary tumors from which the TIC lines are derived should pinpoint which growth factors are highly expressed in primary tumors. Subsequent addition of these growth factors to the culture medium of TIC lines might improve the efficiency of spheroid growth in this system. The TIC lines are currently grown without a supporting matrix. Methods to grow the TIC lines in a 3D matrix should also be explored. Additionally, studies need to be carried out to determine the advantages of using TIC lines for *in vitro* pre-clinical studies over classical neuroblastoma cell lines. Great emphasis should also be placed on the development of neuroblastoma PDX models, as they represent *in vivo* models that are phenotypically and genetically more identical to the primary tumors than the xenograft models from classic cell lines. Results obtained from pre-clinical studies in TIC lines and PDX models might improve the efficacy of testing of diverse therapeutic agents and the ease of translation of the results in a clinically relevant setting.

2. Hypothesis on the functional role of EZH2 in neuroblastoma

EZH2 is aberrantly expressed in neuroblastoma and despite widespread evidence of its tumor-promoting role due to its histone methyltransferase activity, a histone methyltransferase-independent function of the protein seems involved in neuroblastoma. This calls into question the relevance of targeting the histone methyltransferase function of EZH2 with small molecule inhibitors in neuroblastoma. Additional studies are needed to elucidate the non-canonical functions of this protein. We observed that *in vitro* targeted depletion of EZH2 results in an apoptotic phenotype and consequently hypothesize that EZH2 might exist upstream of neuroblastoma survival pathways. These could then be inhibited by small molecule inhibitors specifically targeting the complete EZH2 protein. Previous attempts to specifically target EZH2 non-canonical functions with the first generation EZH2 inhibitor DZNeP did not prove successful due to off-target effects and *in vivo* toxicity caused by the concomitant downregulation of other histone methyltransferases (40, 41). The recently discovered stabilized- α -helix of EZH2 peptide (SAH-EZH2) downregulates EZH2 protein by disrupting the PRC2 complex and has shown great promise in CLL cells (42). Pre-clinical evaluation of this peptide

in neuroblastoma might shed light on the therapeutic implication and feasibility of targeting the EZH2 protein in neuroblastoma.

3. Effective targeting of BCL2 in neuroblastoma

BCL2 mRNA, BCL2 protein and BIM/BCL2 complex levels have extensively been validated as predictive biomarkers for sensitivity to venetoclax in neuroblastoma. A phase I/II clinical trial to determine PK and PD in neuroblastoma patients is planned. However, based on *in vitro* and *in vivo* evidence of MCL1 upregulation and the occurrence of resistance to venetoclax, treatment of neuroblastoma patients with venetoclax as a single agent might not be an effective therapeutic strategy. Combination strategies of venetoclax with chemotherapeutic agents, MCL1 inhibitors and targeted therapies with known synergistic effects might be more effective than single treatment with the compound. Targeted MDM2 inhibitor idasanutlin has been identified as an excellent candidate re-sensitizing agent, with good partial responses obtained in mice with BCL2 high-expressing neuroblastoma xenografts. A clinical trial with venetoclax in combination with idasanutlin might be an effective therapeutic strategy to prevent resistance to venetoclax in neuroblastoma patients. Additional studies still need to be carried out to identify other candidate re-sensitizing agents as well as other routes through which neuroblastoma resistance to venetoclax can occur.

REFERENCES

1. Clevers H. Modeling Development and Disease with Organoids. *Cell* 2016;165(7):1586-97.
2. Lee J, Kotliarova S, Kotliarov Y, Li A, Su Q, Donin NM, et al. Tumor stem cells derived from glioblastomas cultured in bFGF and EGF more closely mirror the phenotype and genotype of primary tumors than do serum-cultured cell lines. *Cancer Cell* 2006;9(5):391-403.
3. Bate-Eya LT, Ebus ME, Koster J, den Hartog IJ, Zwijnenburg DA, Schild L, et al. Newly-derived neuroblastoma cell lines propagated in serum-free media recapitulate the genotype and phenotype of primary neuroblastoma tumours. *Eur J Cancer* 2014;50(3):628-37.
4. Eleveld TF, Oldridge DA, Bernard V, Koster J, Daage LC, Diskin SJ, et al. Relapsed neuroblastomas show frequent RAS-MAPK pathway mutations. *Nat Genet* 2015;47(8):864-71.
5. Howes AL, Richardson RD, Finlay D, Vuori K. 3-Dimensional culture systems for anti-cancer compound profiling and high-throughput screening reveal increases in EGFR inhibitor-mediated cytotoxicity compared to monolayer culture systems. *PLoS One* 2014;9(9):e108283.
6. Kunz-Schughart LA, Freyer JP, Hofstaedter F, Ebner R. The use of 3-D cultures for high-throughput screening: the multicellular spheroid model. *J Biomol Screen* 2004;9(4):273-85.
7. Molenaar JJ, Koster J, Zwijnenburg DA, van Sluis P, Valentijn LJ, van der Ploeg I, et al. Sequencing of neuroblastoma identifies chromothripsis and defects in neuritogenesis genes. *Nature* 2012;483(7391):589-93.
8. Bird A. Perceptions of epigenetics. *Nature* 2007;447(7143):396-8.
9. Wang C, Liu Z, Woo CW, Li Z, Wang L, Wei JS, et al. EZH2 Mediates epigenetic silencing of neuroblastoma suppressor genes CASZ1, CLU, RUNX3, and NGFR. *Cancer Res* 2012;72(1):315-24.
10. Henrich KO, Bender S, Saadati M, Dreidax D, Gartlgruber M, Shao C, et al. Integrative Genome-Scale Analysis Identifies Epigenetic Mechanisms of Transcriptional Deregulation in Unfavorable Neuroblastomas. *Cancer Res* 2016;76(18):5523-37.
11. Shen JK, Cote GM, Gao Y, Choy E, Mankin HJ, Hornicek FJ, et al. Targeting EZH2-mediated methylation of H3K27 inhibits proliferation and migration of Synovial Sarcoma in vitro. *Sci Rep* 2016;6:25239.
12. Bate-Eya LT, Gierman HJ, Ebus ME, Koster J, Caron HN, Versteeg R, et al. Enhancer of zeste homologue 2 plays an important role in neuroblastoma cell survival independent of its histone methyltransferase activity. *Eur J Cancer* 2017;75:63-72.
13. Wu ZL, Zheng SS, Li ZM, Qiao YY, Aau MY, Yu Q. Polycomb protein EZH2 regulates E2F1-dependent apoptosis through epigenetically modulating Bim expression. *Cell Death Differ* 2010;17(5):801-10.
14. Fulda S, Poremba C, Berwanger B, Hacker S, Eilers M, Christiansen H, et al. Loss of caspase-8 expression does not correlate with MYCN amplification, aggressive disease, or prognosis in neuroblastoma. *Cancer Res* 2006;66(20):10016-23.

15. Lamers F, Schild L, den Hartog IJ, Ebus ME, Westerhout EM, Ora I, et al. Targeted BCL2 inhibition effectively inhibits neuroblastoma tumour growth. *Eur J Cancer* 2012;48(16):3093-103.
16. Lamers F, van der Ploeg I, Schild L, Ebus ME, Koster J, Hansen BR, et al. Knockdown of survivin (BIRC5) causes apoptosis in neuroblastoma via mitotic catastrophe. *Endocr Relat Cancer* 2011;18(6):657-68.
17. Roberts AW, Seymour JF, Brown JR, Wierda WG, Kipps TJ, Khaw SL, et al. Substantial susceptibility of chronic lymphocytic leukemia to BCL2 inhibition: results of a phase I study of navitoclax in patients with relapsed or refractory disease. *J Clin Oncol* 2012;30(5):488-96.
18. Souers AJ, Levenson JD, Boghaert ER, Ackler SL, Catron ND, Chen J, et al. ABT-199, a potent and selective BCL-2 inhibitor, achieves antitumor activity while sparing platelets. *Nat Med* 2013;19(2):202-8.
19. Bate-Eya LT, den Hartog IJ, van der Ploeg I, Schild L, Koster J, Santo EE, et al. High efficacy of the BCL-2 inhibitor ABT199 (venetoclax) in BCL-2 high-expressing neuroblastoma cell lines and xenografts and rational for combination with MCL-1 inhibition. *Oncotarget* 2016;7(19):27946-58.
20. Ham J, Costa C, Sano R, Lochmann TL, Sennott EM, Patel NU, et al. Exploitation of the Apoptosis-Primed State of MYCN-Amplified Neuroblastoma to Develop a Potent and Specific Targeted Therapy Combination. *Cancer Cell* 2016;29(2):159-72.
21. Choudhary GS, Al-Harbi S, Mazumder S, Hill BT, Smith MR, Bodo J, et al. MCL-1 and BCL-xL-dependent resistance to the BCL-2 inhibitor ABT-199 can be overcome by preventing PI3K/AKT/mTOR activation in lymphoid malignancies. *Cell Death Dis* 2015;6:e1593.
22. Gores GJ, Kaufmann SH. Selectively targeting Mcl-1 for the treatment of acute myelogenous leukemia and solid tumors. *Genes Dev* 2012;26(4):305-11.
23. Roberts AW, Davids MS, Pagel JM, Kahl BS, Puvvada SD, Gerecitano JF, et al. Targeting BCL2 with Venetoclax in Relapsed Chronic Lymphocytic Leukemia. *N Engl J Med* 2016;374(4):311-22.
24. Lestini BJ, Goldsmith KC, Fluchel MN, Liu X, Chen NL, Goyal B, et al. Mcl1 downregulation sensitizes neuroblastoma to cytotoxic chemotherapy and small molecule Bcl2-family antagonists. *Cancer Biol Ther* 2009;8(16):1587-95.
25. Goldsmith KC, Lestini BJ, Gross M, Ip L, Bhumbra A, Zhang X, et al. BH3 response profiles from neuroblastoma mitochondria predict activity of small molecule Bcl-2 family antagonists. *Cell Death Differ* 2010;17(5):872-82.
26. Krskova L, Kalinova M, Brizova H, Mrhalova M, Sumerauer D, Kodet R. Molecular and immunohistochemical analyses of BCL2, KI-67, and cyclin D1 expression in synovial sarcoma. *Cancer Genet Cytogenet* 2009;193(1):1-8.
27. Nedelcu T, Kubista B, Koller A, Sulzbacher I, Mosberger I, Arrich F, et al. Livin and Bcl-2 expression in high-grade osteosarcoma. *J Cancer Res Clin Oncol* 2008;134(2):237-44.

28. Trieb K, Sulzbacher I, Kubista B. Bcl-2 correlates with localization but not outcome in human osteosarcoma. *Oncol Lett* 2013;6(2):559-561.
29. Fu T, Xia C, Li Z, Wu H. Lack of association between bcl-2 expression and prognosis of osteosarcoma: a meta-analysis. *Int J Clin Exp Med* 2015;8(6):9093-9.
30. Kavalari R, Pohar Marinsek Z, Jereb B, Cagran B, Golouh R. Prognostic value of immunohistochemistry in the Ewing's sarcoma family of tumors. *Med Sci Monit* 2009;15(8):Cr442-52.
31. Singh L, Pushker N, Saini N, Sen S, Sharma A, Bakhshi S, et al. Expression of pro-apoptotic Bax and anti-apoptotic Bcl-2 proteins in human retinoblastoma. *Clin Exp Ophthalmol* 2015;43(3):259-67.
32. Tanos R, Karmali D, Nalluri S, Goldsmith KC. Select Bcl-2 antagonism restores chemotherapy sensitivity in high-risk neuroblastoma. *BMC Cancer* 2016;16:97.
33. Joyner DE, Albritton KH, Bastar JD, Randall RL. G3139 antisense oligonucleotide directed against antiapoptotic Bcl-2 enhances doxorubicin cytotoxicity in the FU-SY-1 synovial sarcoma cell line. *J Orthop Res* 2006;24(3):474-80.
34. Olsen RR, Mary-Sinclair MN, Yin Z, Freeman KW. Antagonizing Bcl-2 family members sensitizes neuroblastoma and Ewing's sarcoma to an inhibitor of glutamine metabolism. *PLoS One* 2015;10(1):e0116998.
35. Li Z, Yu Y, Sun S, Qi B, Wang W, Yu A. Niclosamide inhibits the proliferation of human osteosarcoma cell lines by inducing apoptosis and cell cycle arrest. *Oncol Rep* 2015;33(4):1763-8.
36. Allaman-Pillet N, Oberson A, Munier F, Schorderet DF. The Bcl-2/Bcl-XL inhibitor ABT-737 promotes death of retinoblastoma cancer cells. *Ophthalmic Genet* 2013;34(1-2):1-13.
37. Allaman-Pillet N, Oberson A, Schorderet DF. BIRO1, a cell-permeable BH3 peptide, promotes mitochondrial fragmentation and death of retinoblastoma cells. *Mol Cancer Res* 2015;13(1):86-97.
38. Lieber J, Ellerkamp V, Vogt F, Wenz J, Warmann SW, Fuchs J, et al. BH3-mimetic drugs prevent tumour onset in an orthotopic mouse model of hepatoblastoma. *Exp Cell Res* 2014;322(1):217-25.
39. Tagscherer KE, Fassl A, Campos B, Farhadi M, Kraemer A, Bock BC, et al. Apoptosis-based treatment of glioblastomas with ABT-737, a novel small molecule inhibitor of Bcl-2 family proteins. *Oncogene* 2008;27(52):6646-56.
40. Girard N, Bazille C, Lhuissier E, Benateau H, Llombart-Bosch A, Boumediene K, et al. 3-Deazaneplanocin A (DZNep), an inhibitor of the histone methyltransferase EZH2, induces apoptosis and reduces cell migration in chondrosarcoma cells. *PLoS One* 2014;9(5):e98176.
41. Miranda TB, Cortez CC, Yoo CB, Liang G, Abe M, Kelly TK, et al. DZNep is a global histone methylation inhibitor that reactivates developmental genes not silenced by DNA methylation. *Mol Cancer Ther* 2009;8(6):1579-88.

42. Hibino S, Saito Y, Muramatsu T, Otani A, Kasai Y, Kimura M, et al. Inhibitors of enhancer of zeste homolog 2 (EZH2) activate tumor-suppressor microRNAs in human cancer cells. *Oncogenesis* 2014;3:e104.



APPENDICES

ENGLISH SUMMARY

NEDERLANDSE SAMENVATTING

ACKNOWLEDGEMENTS

CURRICULUM VITAE

PORTFOLIO

PUBLICATION LIST

ENGLISH SUMMARY

Neuroblastoma is a childhood cancer that arises from the sympathetic nervous system and accounts for about 6% of all pediatric tumors. An overall survival rate of about 30% is observed in infants less than one year of age and only about 15% in older children. Classification of neuroblastoma is based on the INSS system with local disease observed in stage 1-3 and distal metastatic patterns observed in stage 4 patients. MYCN amplification is a strong predictor of aggressive disease and poor survival. The treatment regimen of neuroblastoma is based on the DCOG 2009 protocol using myeloablative chemotherapeutics, autologous stem cell transplantation and MIBG treatment. However, due to a low success rate and recurrence of the disease after conventional chemotherapeutic treatment, a more precise therapy based on the molecular and genomic profile of the patients is needed.

Most often, *in vitro* pre-clinical evaluation of targeted therapies involves the use of 2D-cultured classical cell lines. However, spontaneous genomic mutations in 2D-cultured cells might arise due to the long-term culture of these cells. These cells thus fail to recapitulate the phenotype and genotype of primary tumors from which they are derived from. Adequate *in vitro* model systems that best represent primary tumors are thus needed. In **chapter 2**, we described the isolation and characterization of neuroblastoma TIC lines or organoids. We show that TIC lines recapitulate the phenotype and genotype of primary tumors from which they are derived from. However, the success rate of isolating and maintaining such organoid systems remains low due to sub-optimal culture conditions. Tumor cells co-exist in a 3D architecture consisting of extracellular matrix and stromal derived cells. The secretion of paracrine and growth factors by these stromal cells is necessary for the maintenance and growth of the tumor cell niche. Thus, identification of tumor stromal cell-derived growth factors is imperative. Supplementing TIC medium with such growth factors might improve the efficacy of the *in vitro* growth conditions of such cells. Additionally, co-culturing TIC lines directly with tumor-derived stromal cells might be another strategy to improve the maintenance of such cells *ex vivo*.

Several somatic and germline genomic events have been observed in neuroblastoma. MYCN amplification, 17q gain and loss of 11q and LOH 1p are key genomic events in neuroblastoma. A local gain of the 7q36 locus harboring the *EZH2* gene has previously been reported in neuroblastoma. *EZH2*, a histone methyltransferase is overexpressed in neuroblastoma. In **chapter 3**, we described the pre-clinical evaluation of the *EZH2*-

specific histone methyltransferase inhibitors EPZ6438 and GSK126. Targeted inhibition of the histone methyltransferase function of EZH2 with the small molecule inhibitors surprisingly led to only a slight G1 arrest in EZH2 high-expressing neuroblastoma cell lines. Inhibition of the histone methyltransferase function of EZH2 with EZH2 specific inhibitors in neuroblastoma cells might lead to molecular changes within these cells rendering them susceptible to other small molecule inhibitors. An effective strategy to improve the efficacy of EZH2 small molecule inhibitors was based on the enhanced phenotypic effect observed upon combining DNA demethylating agents with EZH2 specific histone methyltransferase inhibitors. Based on these results, combining EZH2 specific inhibitors and DNA demethylating agents might be an effective strategy in the treatment of neuroblastoma.

A second effective strategy might be by targeting the non-canonical functions of EZH2. A strong apoptotic response was indeed observed upon targeted downregulation of the EZH2 protein with shRNA. These results clearly demonstrate the need for compounds that specifically target the histone methyltransferase independent functions of EZH2 in neuroblastoma.

Uncontrolled proliferation of tumor cells most often occurs as a result of resistance to apoptotic cues in these cells. Overexpression of members of the extrinsic and intrinsic apoptotic pathway has frequently been observed in numerous malignancies. The *BCL2* gene, an important member of the intrinsic apoptotic pathway is overexpressed in neuroblastoma. Thus, targeting this protein with small molecule inhibitors might prove an effective strategy for the treatment of neuroblastoma. In **chapter 4**, we described the *in vitro* and *in vivo* pre-clinical evaluation of the BCL2-specific small molecule inhibitor venetoclax in neuroblastoma. Sensitivity to venetoclax was strongly correlated to *BCL2* mRNA, protein and BIM/BCL2 complex levels. Despite the promising results obtained from the *in vitro* and *in vivo* evaluation of the compound, resistance to venetoclax was observed. Resistance to the compound could be attributed to the upregulation of the anti-apoptotic protein MCL1. Upregulated MCL1 sequestered BIM displaced from BCL2 by venetoclax, preventing further activation of the intrinsic apoptotic pathway. Several strategies to overcome MCL1-mediated resistance to venetoclax were studied. Targeted downregulation of MCL1 in combination with BCL2 inhibition proved an effective strategy in overcoming resistance. BIM displacement from MCL1 by MCL1-specific small molecule inhibitors in combination with BCL2 inhibition by venetoclax proved an effective strategy as well. It is thus crucial to validate such results in *in vivo* systems.

In **chapter 5**, we studied strategies to resensitize venetoclax-resistant BCL2-high expressing cell lines to the compound by targeted therapy and chemotherapeutic compounds. High-throughput screening of these resistant cell lines with compound libraries identified the MDM2 inhibitor idasanutlin as the most promising candidate resensitizing agent in the panel of compounds. Resensitization of these cells to venetoclax could be attributed to p53-mediated upregulation of BAX by idasanutlin and activation of apoptosis. At the *in vivo* level, a partial response was observed upon combined inhibition of MDM2 by idasanutlin and BCL2 by venetoclax. However, complete regression was not observed and tumors regrew upon redrawal of both compounds. Several strategies could be explored in order to improve the efficacy of this combination. Increasing the dosage as well as the duration of treatment with both compounds might be an effective strategy. An additional approach might be by implementation of the idasanutlin/venetoclax combination in the neuroblastoma treatment protocol.

Numerous malignancies have high expression of BCL2. Pre-clinical evaluation of BH3 mimetics has shown promising results in various adult tumors. The BCL2-specific inhibitor venetoclax has recently been validated in lymphoid malignancies. In order to determine the relevance of targeting BCL2 with this small molecule inhibitor, in **chapter 6**, we performed a systematic review on the expression patterns and pre-clinical evaluation of BH3 mimetics in pediatric solid tumors. Based on the systematic review, BCL2 was reported to be highly expressed in five pediatric solid tumors (neuroblastoma, osteosarcoma, synovial sarcoma, Ewing sarcoma and retinoblastoma) while a negative expression was observed in two tumors (atypical teratoid rhabdoid and inflammatory myofibroblastic tumors). Extensive studies on the pre-clinical validation of BH3 mimetics was reported in several tumor types (i.e. neuroblastoma, synovial sarcomas, retinoblastoma, osteosarcoma, Ewing Sarcoma, glioma and hepatoblastoma) with a strong apoptotic response and tumor regression being observed *in vivo*. Till date, clinical trials with venetoclax as a single agent have only been performed in adult lymphoid malignancies. A clinical trial with venetoclax as a single agent in neuroblastoma is in the pipeline. Results obtained from the clinical trials in neuroblastoma might pave the way for future implementations in other pediatric solid tumors with high BCL2 expression.

NEDERLANDSE SAMENVATTING

Neuroblastoom is een vorm van kinderkanker die ontstaat uit het sympathisch zenuwstelsel en ongeveer 6% van alle kindertumoren uitmaakt. Neuroblastoma patiënten met hoog risicoziekte hebben slechts een overleving kans van 40% of minder. Neuroblastoom tumoren worden ingedeeld in verschillende stadia op basis van het zogenoemde "International Neuroblastoma Staging System (INSS)". Bij stadium 1, 2 en 3 neuroblastoom tumoren gaat het om lokale tumoren, terwijl stadium 4 tumoren worden gekenmerkt door de aanwezigheid van metastasen naar andere plaatsen in het lichaam. Amplificatie van het MYCN gen, heeft een sterke negatieve invloed op de prognose van neuroblastoom patiënten. De huidige behandeling van neuroblastoom patiënten in Nederland is gebaseerd op een protocol dat in 2009 is opgesteld door de zogenoemde "Dutch Childhood Oncology Group (DCOG)". Volgens dit protocol worden neuroblastoom patiënten behandeld met een combinatie van radiotherapie, chemotherapie (al dan niet gevolgd door autologe stamceltransplantatie) en chirurgie. Maar deze zware behandeling is in een groot aantal van de patiënten niet curatief en daarom is er een nauwkeurigere therapie op basis van de genomische afwijkingen in de tumor van de patiënten nodig.

Meestal impliceert de *in vitro* preklinische evaluatie van deze nieuwe therapieën, het gebruik van 2D-gekweekte klassieke cellijnen. Het nadeel is echter dat dat deze kweek modellen niet representatief zijn voor de tumoren waar ze van zijn afgeleid. Zowel fenotypisch als genotypisch kunnen er significante verschillen ontstaan. *In vitro* modelsystemen die meer overeenkomen met de primaire tumoren zijn dus nodig. In **hoofdstuk 2** beschrijven we het isoleren en karakteriseren van neuroblastoom Tumor Initiërende Cellijnen (TICs) of organoids. We laten zien dat deze organoids zowel wat fenotype als genotype lijken op de primaire tumoren waarvan ze zijn afgeleid. Maar de succes frequentie waarmee organoids daadwerkelijk kunnen worden gekweekt uit primaire tumoren is nog laag door suboptimale kweekomstandigheden. Tumorcellen, groeien normaal in een 3D architectuur omringd door een extracellulaire matrix en stromale cellen. Excretie van groeifactoren door die stromale cellen is essentieel voor de groei van neuroblastoma cellen. Supplementeren van het organoid groeimedium met deze groeifactoren zou de efficiëntie en slagingspercentage van het groeien van organoids uit primaire tumoren kunnen verbeteren. Daarnaast zou het co-kweken van neuroblastoma tumorcellen, met stromale cellen een andere methode kunnen zijn om de groei van organoiden te verbeteren.

In neuroblastoma worden diverse genomische afwijkingen regelmatig gezien. Amplificatie van het MYCN oncogen, gain van de 17q, verlies van 1p en 11q zijn zulke typische neuroblastoma afwijkingen. Daarnaast wordt gain van chromosoom 7 regelmatig gezien. In een tumor zagen wij een lokale gain van het 7q36 locus met het EZH2 gen. Dit gen komt ook erg hoog tot expressie in neuroblastoma hetgeen bij elkaar suggereert dat dit een drijvend oncogen is in neuroblastoma. In Hoofdstuk 3 beschrijven wij de preklinische evaluatie van de EZH2 specifieke methyltransferase remmers EPZ6438 en GSK126. Volledige remming van de histon methyltransferase activiteit van EZH2 met deze remmers resulteerde in slechts een geringe remming van de celcyclus in neuroblastoma cellen met hoge expressie van EZH2. Als mono behandeling zijn deze EZH2 specifieke remmers dus niet geschikt voor het remmen van neuroblastoma groei, maar het is wel mogelijk dat deze EZH2 remmers, neuroblastoma cellen gevoelig maken voor andere remmers. Dit is bijvoorbeeld aangetoond voor DNA demethylerende middelen in combinatie met EZH2 remmers. Dit zou dus een potentiële nieuwe behandeling voor neuroblastoma kunnen zijn. Naast deze benadering is de non-canonische functie van EZH2 een potentiële manier om neuroblastoma groei te remmen. Wij lieten zien dat het remmen van de expressie van EZH2 eiwit een sterke apoptotische reactie gaf. Remmers die werken op de methyltransferase onafhankelijke functies van EZH2 moeten dus evident verder ontwikkeld worden voor neuroblastoma.

Een van de cruciale eigenschappen van tumorcellen is het feit dat deze cellen de geprogrammeerde celdood (apoptose) geïnactiveerd hebben. Over-expressie van genen die zowel de intrinsieke als excentrieke apoptose remmen wordt frequent gezien in diverse soorten kanker. Het BCL2 gen is een belangrijke speler in de intrinsieke apoptotische route en dit gen komt sterk tot over expressie in neuroblastoma. Het remmen van dit genproduct met chemische inhibitors zou dus een strategie kunnen zijn voor het behandelen van neuroblastoma. In hoofdstuk 4 beschrijven we de in vitro en in vivo evaluatie van de BCL2 remmer Venetoclax. Gevoeligheid voor de remmer bleek sterk gecorreleerd met over expressie van het BCL2 gen en BCL2/BIM complex niveaus. Ondanks de veelbelovende in vitro en in vivo resultaten werd er ook resistentie tegen de remmer gezien. Resistentie tegen de BCL2 remmer werd met name veroorzaakt door over expressie van een ander lid uit de BCL2 familie; MCL1. MCL1 sekwestreert BIM als dat van BCL2 loskomt bij behandeling met de Venetoclax waardoor apoptotische activatie wordt voorkomen. We hebben diverse methodes getest om deze MCL1 gemedieerde resistentie tegen Venetoclax te voorkomen. Remmen van MCL1 met antisense RNA liet

zien dat de cellen weer gevoelig werden voor BCL2 remming. Chemische remmers van MCL1 lieten een soortgelijk effect zien. Het is cruciaal om dit verder in vivo te valideren.

In hoofdstuk 5 hebben we de bekeken hoe we de Venetoclax resistente neuroblastoma cellen met hoge BCL2 expressie weer gevoelig konden maken voor BCL2 remming. Screening met een groot aantal potentiële medicijnen liet zien dat de MDM2 remmer Idasanutlin de beste re-sensitizer was. Deze re-sensitatie werd met name veroorzaakt door P53 gemedieerde op regulatie van BAX en diens gevolg re-activatie van de apoptose. In vivo werd een VGPR (zeer goede partiële response) gezien maar er bleven resttumoren aanwezig. Diverse strategieën worden nu getest om dit effect nog verder te optimaliseren. De dosering kan verder verhoogd worden, de behandelduur uitgebreid of beiden. Daarnaast kan overwogen worden om deze behandeling combinatie in de bestaande protocollen in te passen.

Verschillende andere tumoren laten over expressie van BCL2 zien en pre-klinische evaluatie van BCL2 remmers hebben positieve resultaten gegeven in diverse trials. Om te kunnen bepalen in welke andere kindertumoren de BCL2 remmer Venetoclax mogelijk effectief is, hebben we een systematisch literatuuronderzoek gedaan hetgeen beschreven staat in hoofdstuk 6. Uit dit onderzoek bleek dat er vijf soorten kindertumoren zijn waar het testen van de BCL2 remmers mogelijk effect zou kunnen hebben (neuroblastoma, osteosarcoma, synovial sarcoma, Ewing Sarcoma en Retinoblastoma). In een aantal andere tumoren leek er genoeg bewijs te zijn om BCL2 remming verder niet te testen (ATRT en myofibroblastische tumoren). Tot op heden is Venetoclax alleen getest in tumoren bij volwassenen. Een trial met Venetoclax in neuroblastoma is in de planning. Resultaten in neuroblastoma zouden mogelijk kunnen leiden tot het verder testen van Venetoclax in andere kindertumoren met hoge BCL2 expressie.

ACKNOWLEDGMENTS

Finally the acknowledgments. The most difficult section of the thesis to write and no matter how hard I try not everyone can be mentioned. The work presented in this thesis was due to the contribution of many people whose love, guidance, leadership and prayers made it all possible and worthwhile.

Huib, without you it will not have been possible to get to the end of my journey as a PhD student. Thank you for your support and mentoring and for having the faith and confidence in me to promote me as your student.

Jan, what a journey we travelled together!!! Even though I was not originally your PhD student, we bonded over our shared disagreement on the existence of cancer stem cells in neuroblastoma and decided to rename them “Tumour-initiating cells”. Thank you so much for letting me join your group. I am so blessed to have had you stand in as my supervisor and mentor for all these years. I admire your analytical way of thinking and your problem-solving skills. You taught me how to think in an independent manner, discover my weak and strong points and finally made me become the scientist that I am today. A big thank you to you!!!! **Emmy (Emmytje)**, where do I start. Our journey together began with our BCL2 project. We started off as supervisor/student and eventually became mates over the years we worked together. I learned so much from you that I cannot even begin to list all that I learned. You were so patient with me and painstakingly taught me how to work efficiently. Your sense of precision and organization was legendary. Most importantly, your patience and perseverance paid off with me being your first graduating PhD student. I hope I can one day teach my future students what I learned from you. **Linda S.**, you were so much fun with your straight talking and no nonsense attitude. Thank you for teaching me how to work in the ML2 and all the other technics on DNA isolation and sequencing. **Marli**, I remember when we first started at the oncogenomics department you took us out I and Maria and made us feel welcome within the group. That was so lovely on your part. With your wealth of experience I learned so much from you **Thomas**. Thank you for the valuable laboratory skills you taught me which I know will help me build up a fantastic scientific career. **Ida**, I did not only work side-by-side with you in the laboratory but I also had the pleasure of calling you my friend. You were the person who introduced me to my first “stampot”. Het was heerlijk!! Thank you for helping me start our BCL2 project and with your help we finally made it!! **Ilona**, you taught me everything on *in vivo* experimentation thank you for your patience and guidance. Your teaching paid off because I became an expert at

“oral gavage”. **Bianca**, you were so much fun to be around. You taught me how to work efficiency at the CSC with our million and one experiments which we had going at the same time. I also had fun at our “Fun during lunch” time with all the mateys in our small group which was a great initiative by the way. **Lindy A.** Although we knew ourselves only for a relatively short time I am happy I had the pleasure of knowing you. You were the fun and life of the party. Thank you for the great and successful work on our first *in vivo* combination studies. It was a job well done. To the rest of my colleagues from our group and the Prinses Maxima centrum whom I have not mentioned but not forgotten. Thank you very much.

To all my colleagues at the **AMC** in the department of Oncogenomics a big thank you. Special thanks to my colleagues at the Bioinformatics groups whom we collectively referred to as the “nerds”. **Jan K.** whom I refer to as mister Jan. You were my office buddy for more than 5 years. You took the time to teach me the ins and out of R2 but specifically you always knew how to bring out the fun side of me. Thank you for making me laugh every day. **Richard, Danny** and **Piet.** I remember the way you teased me during the “making fun of Laurel” days. I had a blast by the way. **Peter S.** whom we all called “Stroekey” I had so much fun working alongside you and the pleasure of calling you my friend. I learned so much from you and I hope I can teach my future students all that I learned from you. Also thanks to **Jennemiek, Marloes** and **Nurdan.** You girls were so kind and nice and played a great role in shaping the lab to what it is today. You will surely be missed. **Mohammed, Ellen** and **Evan.** I was fortunate to get to know you not only as colleagues but as friends as well. You guys were so kind and patient. I learned a lot from you and I hope that you all succeed in your future endeavours. Have faith!!!!

Anne and **Maria**, thank you for agreeing to be there for me as my paranymphs. Maria, we went through so much together. Through all the many trials we faced, we never gave up on each other. I admire your strength, your brilliant mind and most importantly your honesty. I am doing this defense for both you and I. I pray that in the future I will be seeing you standing up and defending your thesis. Never give up on your dreams. Anne, you are still discovering who you are as a research scientist. It’s not going to be an easy road but trust me the satisfaction you will get when you are finished with your thesis will be worth every failed experiment (laughs) you performed. Keep up the good work.

To my dearest family in Cameroon, where do I begin? I want to express my most profound gratitude to you all. We have a saying that “it takes a whole village to bring up a child”. Well I am what I am today because of a multitude of people. My dearest **Papa**

and **Mama**, you raised me to always follow my dreams and reach for the stars. From an early age, I always knew I wanted to do a PhD and you always encouraged me. Well, today my dream came true. Thank you for all the support you gave me throughout this period of my life. My dearest and almost twin sister **Becky**, you are the one I always looked up to. You always made everything possible for me and you were my most fervent supporter always cheering me up from the sidelines. Thank you. To the rest of my brothers and sisters **Rose, Clarice, Ayuk, James** and **Agbor**. I have come this far because of the contributions you all made in shaping who I am today. Special thanks to **Joseph** (Agbor) for the support you gave me when I first started my journey in Finland and ultimately ending in the Netherlands. You are the best. **Jennifer** and **Prof. Ako-Njang**, thank you for encouraging and supporting me all the way from Germany. I did you guys proud.

To my dearest family in Rotterdam. You guys were so awesome. You were the best support system here ever. My darling second mom (**Ma Eli**), you have a heart of gold. Where do I start. You opened your home and your heart to me and I learned a lot from you. Thank you for your encouragement all these years. To my sisters **Petrina, Ladi, Karen and Aletia**. We have gone through a lot together and come out stronger on the other side. We are still going places together and I know we shall succeed in whatever we set our hearts to. To **Valerie** and **Divine** my PhD brothers. Keep up the good work. You are almost there. Thank you **Mr. and Mrs. Wenfua, Mr. and Mrs. Elombo, Armstrong, Dieudonné** and **Manyang Emilia Ebai** for your support.

To my darling fiancé, **Remi**, what a journey we have had together. Thank you for your support. I cannot wait for our next adventures. The best is yet to come.

CURRICULUM VITAE

The author of this thesis was born on the 29th of July 1983 in Yaounde, the Republic of Cameroon. Her primary and secondary education was completed in 2001 after which she enrolled at the University of Yaounde I to study a BSc. in Animal Biology and Physiology which was completed in 2005. She spent 2 years working as a volunteer in the African Indigenous Women's Organization in Yaounde Cameroon and subsequently enrolled for a Post graduate certificate in International Project Management at the Rovaniemi University of Applied Sciences in Lapland, Finland which was completed in 2008. She started a Masters in Biosciences at the Åbo Akademi University in Turku, Finland. During this time, she did her thesis at the department of Biosciences under the supervision of Dr. Cecilia Sahlgren. In November 2010, she started her PhD in the group of Prof. Dr. Rogier Versteeg at the department of Oncogenomics under the supervision of Dr. Jan Molenaar, Dr. Emmy Dolman and Prof. Dr. Huib Caron. In 2016, she moved to the Princess Maxima Centre for Pediatric Oncology where her PhD studies were completed at the department of Translational Medicine under the supervision of Dr Jan Molenaar and Dr. Emmy Dolman. The data presented in this thesis is a summary of the main research subjects undertaken during her PhD.

PORTFOLIO

Name PhD student: Laurel T. Bate-Eya
 PhD period: November 2010-March 2017
 Name PhD supervisor: Prof. Huib N. Caron
 Name PhD co-supervisor (s): Dr. Jan J. Molenaar
 Dr. Emmy Dolman

PhD training	Year	Workload (Hours/ECTS)
General courses		
• Project management	2016	0.6
• Clinical data management	2016	0.3
• Ebrok	2016	1.0
• Gene targeting	2014	0.4
• Bioinformatics	2013	1.1
• Biostatistics	2013	0.3
Presentations		
<ul style="list-style-type: none"> • The histone methyl transferase activity of EZH2 in neuroblastoma: Friend or Foe, Advances in Neuroblastoma Research. • EZH2 is highly expressed in neuroblastoma and plays an important role in neuroblastoma cell survival independent of its histone methyltransferase activity, Advances in Neuroblastoma Research. • High efficacy of BCL-2 inhibitor venetoclax (ABT-199) in neuroblastoma and rationale for combination therapy, Advances in Neuroblastoma Research. 		
(Inter)national conferences		
• Advances in Neuroblastoma Research (Cairns, Australia).	2016	0.5
• Advances in Neuroblastoma Research (Cologne, Germany).	2014	0.5
• Annual oncology Graduate School (OOA) PhD retreat (Texel, NL, Poster).	2014	0.5
• Annual oncology Graduate School (OOA) PhD retreat (Texel, NL, Poster).	2011	0.5

PUBLICATION LIST

Publications	Year
<p>Peer reviewed Publication in thesis</p> <ul style="list-style-type: none"> • Bate-Eya LT, Gierman HJ, Ebus ME <i>et al.</i> EZH2 is highly expressed in neuroblastoma and plays an important role in neuroblastoma cell survival independent of its histone methyltransferase activity. <i>European Journal of Cancer</i> • Bate-Eya LT, Den Hartog IJM, Van der Ploeg I <i>et al.</i> High efficacy of the BCL-2 inhibitor ABT199 in neuroblastoma and rational for combination with MCL-1 inhibition. <i>Oncotarget</i>. 2016; 7: 27946-27958. • Bate-Eya LT, Ebus ME, Koster J <i>et al.</i> Newly-derived cell lines propagated in serum-free media recapitulate the genotype and phenotype of primary neuroblastoma tumours. <i>European Journal of Cancer</i>. 2014; 50: 628-637. • Bate-Eya LT, Schubert NA, Alles LK <i>et al.</i> High-throughput screening identifies idasanutlin as a re-sensitizing drug for venetoclax-resistant neuroblastoma cells. Submitted. • Bate-Eya LT, Schubert NA, Caron HN, <i>et al.</i> A systematic review on targeting BCL2 in pediatric solid tumors. Manuscript in preparation. 	<p>2017</p> <p>2016</p> <p>2014</p>
<p>Other Publications</p> <ul style="list-style-type: none"> • M.Emmy.M Dolman, Van Der Ploeg I, Koster J, Bate-Eya LT <i>et al.</i> DNA-dependent protein kinase as molecular target for radiosensitization of neuroblastoma cells. <i>Plosone</i>; 10: 1-18 • Mamaeva V, Rosenholm JM, Bate-Eya LT <i>et al.</i> Mesoporous Silica Particles as Drug Delivery Systems for Targeted Inhibition of Notch Signalling in Cancer <i>Mol Ther</i>. 2011; 19: 1538-46. • Rosenholm JM, Pehu E, Bate-Eya LT <i>et al.</i> Cancer-Cell-Specific Induction of Apoptosis using Mesoporous Silica Nanoparticles as Drug Delivery Systems. <i>Small</i> 2010; 6: 1234-41 	<p>2015</p> <p>2011</p> <p>2010</p>